Regolith-Landforms and regolith geochemistry of the 'Tomahawk' Au-in-calcrete anomaly: Tunkillia, Gawler Craton, South Australia.

Laura Lillian Klingberg

Geology & Geophysics
School of Earth and Environmental Sciences
The University of Adelaide

The University of Adelaide, SA, 5005 Australia
Email: laura.klingberg@student.adelaide.edu.au
Tel: +61 (08) 8303 4041
Mob: +61 0403 446 003

Manuscript Submitted as fulfilment of the requirements for the
Honours Degree of Bachelor of Science,
University of Adelaide

26th October 2009

Supervisors: Dr. Steven M. Hill & Assoc. Prof. David Chittleborough

TABLE OF CONTENTS

ABSTRACT **3**

1.0 INTRODUCTION **5**

1.1 Source of calcium in regolith carbonates: their association with Au-in-calcrete anomalies 7

2.0 SETTING **11**

2.1 Location and land use 11

2.2 Climate 12

2.3 Regional Geology of the Tunkillia Prospect 12

2.4 Previous Geological Studies 14

2.5 Regolith-landforms and vegetation of the 'Tomahawk' area 14

3.0 METHODS **16**

3.1 Calcrete sampling 16

3.2 Regolith-landform mapping 17

3.3 Regolith profile logging 17

3.4 Sample preparation and analysis 17

3.4.1 QA/QC 19

3.5 Calcrete geochemistry mapping 19

4.0 RESULTS **21**

4.1 Regolith Setting 21

4.1.1 REGOLITH-LANDFORM MAP OF THE 'TOMAHAWK' AREA. 21

4.1.2 REGOLITH PROFILE LOGS 21

4.2 Calcrete Geochemistry 23

4.2.1 % OF ELEMENTS CONSISTENTLY BELOW OR APPROACHING DETECTION LIMIT 23

4.2.2 QA/QC 23

4.2.3 BROAD ELEMENT ASSOCIATIONS 24

4.2.3.1 Correlation Matrices 24

4.2.4 SELECTION OF 12 KEY ELEMENTS 25

4.2.5 SUMMARY STATISTICS 25

4.2.6 X AND Y SCATTER PLOTS 26

4.2.7 NORMAL PROBABILITY PLOTS 27

4.2.8 SPATIAL PLOTS OF THE 12 KEY ELEMENTS 27

5.0 DISCUSSION: Landscape controls on biogeochemical expressions of mineralisation **29**

5.1 Regolith-landscape setting and palaeolandscape reconstruction 29

5.1.1 REGOLITH LANDFORM HISTORY: PALAEO- VS CONTEMPORARY LANDSCAPE 30

5.1.1.1 Contemporary Landscape 30

5.1.1.2 Palaeolandscape and Palaeodrainage 31

5.1.2 BEDROCK / MINERALISATION 34

5.2 Expression of Mineralisation: Controls on Geochemistry 35

5.3 Implications for Mineral Exploration Under Cover 40

6.0 CONCLUSION **42**

7.0 ACKNOWLEDGEMENTS **44**

8.0 REFERENCES **45**

9.0 FIGURE CAPTIONS **50**

10.0 TABLES **53**

APPENDIX 1 ..... **60**

APPENDIX 2 ..... **68**

APPENDIX 3 ..... **82**

APPENDIX 4 ..... **96**

APPENDIX 5 ..... **120**

11.0 FIGURES **122**

Regolith-Landforms and regolith geochemistry of the 'Tomahawk' Au-in-calcrete anomaly: Tunkillia, Gawler Craton, South Australia.

Laura Lillian Klingberg

Department of Geology & Geophysics
School of Earth and Environmental Sciences
The University of Adelaide, SA, 5005 Australia

ABSTRACT

The 'Tomahawk' Au-in-calcrete anomaly is a zone of peak Au-in-calcrete content within the Tunkillia prospect of the central Gawler Craton, South Australia. Exploration drilling of this area has failed to intersect significant underlying mineralisation, making this an important setting to investigate controls on linkages between Au-in-calcrete expression and possible mineralisation sources. This study is the first to consider the multi-element geochemical characteristics of calcretes at 'Tomahawk' rather than using the Au-only approach of previous geochemical exploration. This investigation also considers the potential for laterally dispersed geochemical signatures across the landscape recorded at the surface of Au and associated elements, and suggests that Au was, and may still be physically mobilised along old and contemporary alluvial drainage depressions. There is a low relief, but locally significant drainage divide to the south of 'Tomahawk', so the anomaly area is associated with a point of low, broad confluence of several north flowing palaeodrainage depressions. The interpretation of these palaeolandscape controls further builds on palaeodrainage channel identification from previous studies and supports hypotheses that 'Tomahawk' is in an upper catchment setting, relative to the 'Area 191' Au-in-calcrete anomaly. Primary Au mineralisation at Tunkillia is associated with pyrite, minor galena and sphalerite within quartz-sulphide veins, and has a geochemical association with Au, Ag, Pb and Zn. Supergene Au enrichment has been recognised within ferruginised saprock overlying mineralised bedrock, and this is

largely considered Au-only mineralisation. The calcrete geochemistry here shows some distinction between possible primary and secondary Au occurrences based in the trace element characteristics. The Au-in-calcrete concentrations obtained in this study are up to 194 ppb within CHep and $ISps_2$ regolith-landforms in the north of the study area, corresponding to the lower margins of topography and areas interpreted to be within palaeodrainage systems. Silver concentrations above detection were found in association with many of the elevated Au results, therefore identifying areas of interest and possible alteration halos surrounding primary Au mineralisation. Furthermore small exposures of weathered *in situ* quartz veins support a possible source for the 'Tomahawk' Au-in-calcrete anomaly to the south, which is immediately upslope of the palaeodrainage system.

KEY WORDS: central Gawler Craton, Tunkillia, 'Tomahawk', regolith, mineral exploration, calcrete geochemistry, gold.

Element abbreviations after (Reimann et al. 1998)

1.0 INTRODUCTION

Aeolian dunefields are a prominent transported regolith-landform type in Australia, and account for over 40 % of the continent's land surface (Taylor & Eggleton 2001). They are a major impediment to surficial mineral exploration techniques that target underlying substrates because the geochemistry of the aeolian sediments is largely exotic to the underlying substrate (Lowrey 2007). Mineral exploration however, is shifting towards more challenging exploration settings, with further discoveries in the future likely to occur under greater depths of transported overburden, such as aeolian dunefields (Mayo & Hill 2005).

A geochemical exploration technique that has been widely applied in aeolian landscapes is the sampling of regolith carbonates (e.g. 'calcrete'). Approximately $1.6x10^6$ km^2 (21 %) of the Australian land surface is covered by pedogenic carbonates forming in soils, sediments, saprolite and other regolith materials (Chen *et al.* 2002; Dart *et al.* 2005) and concentrated along a west-east trending broad belt inland from the Great Australian Bight (Dart 2009). Carbonates in Australia are abundant in the semi-arid and arid regions (Lintern *et al.* 2006) and can be a significant geochemical sampling medium for Au exploration. Successful application of regolith carbonate sampling has occurred in the Yilgarn Craton, Western Australia and more recently the Gawler Craton, South Australia (McQueen *et al.* 1999). Systematically sampling surficial calcrete has exposed economically important deposits such as Challenger in 1995 of 0.75 Moz Au and the prospect of interest, Tunkillia. The >20 km^2 Tunkillia gold prospect on EL 3403, Lake Everard (Wilson & Savcin 2004) hosts the world's largest >10 ppb (spatially) Au-in-calcrete anomaly discovered to date in the Gawler Craton (Ferris & Wilson 2004; Dart 2009).

The association between calcrete at or near the land surface within transported cover, such as aeolian sediments, and the underlying mineralised substrate has been enigmatic (Dart 2009). An understanding of the mechanisms for Au-in-calcrete anomaly formation and multi-element geochemical characteristics of calcretes is yet to be fully constrained within previous research. Previous research has largely failed (with the exceptions of Hill et al., 1999; McQueen et al., 2000; Chen *et al.*, 2002; Dart, 2009) to

consider Au-in-calcrete geochemical anomalies within contemporary and palaeo-landscape settings, particularly for distinguishing between transported and *in situ* geochemical characteristics within calcretes. Previous geochemical exploration has been largely based on Au-only geochemical results. There has been limited consideration of multi-element expressions of mineralisation, such as the use of accessory and pathfinder elements for mineralisation. There has also been limited inclusion of major element secondary mineral host geochemical analyses, including the amount of Ca within samples as well as the significance of other element hosts, such as Fe-oxides and clays within the calcrete samples. Further calcrete geochemical research is therefore required to link the potential of regolith carbonate sampling to mineral exploration under cover. There is also limit to its effectiveness in expressing buried substrates, based on the extensive nature and thickness of the transported cover (aeolian dunefields), hence sampling is restricted in areas of dune cover (Lowrey 2007).

The 'Tomahawk' Au-in-calcrete anomaly is within the larger Tunkillia Au-in-calcrete anomaly and conforms to a zone of some of the highest Au concentrations (up to 250 ppb Au) within the Tunkillia anomaly area (Martin & Wilson 2005). Previous exploration drilling programs, including reverse circulation (RC), rotary air blast (RAB) and diamond drilling (DD) have failed to identify significant, underlying mineralisation. This therefore makes for an ideal setting to try to better constrain possible linkages between Au-in-calcrete and adjacent mineralisation sources, as well as to consider the multi-element geochemical characteristics of the calcretes rather than using the Au-only geochemical approach of previous geochemical exploration here. A previous study by Dart (2009) has shown that significant variations in regolith-landform setting can relate to variations in landscape history, therefore different characteristics for geochemical exploration programs within the Tunkillia area and may include the contemporary landscape setting and processes as well as palaeodrainage networks. This study therefore considers the geochemical characteristics of calcretes at 'Tomahawk' in the context of a locally developed regolith-landform map and local landscape evolution model, constructed in this study.

1.1 Source of calcium in regolith carbonates: their association with Au-in-calcrete anomalies

Determining the possible associations between Au and Ca means identifying the source of Ca in regolith carbonates (Dart 2009). Crocker (1946) initially hypothesised that calcrete formation was the result of an aeolian source of Ca in southern Australia. He suggested exposure of the southern Australian carbonate-rich continental shelf during low sea levels (such as in glacial periods) facilitated cool dry conditions, leading to wind erosion and the reworking of coastal calcareous aeolianites (Crocker 1946; Dart *et al.* 2005). This provided a source for the calcareous material over much of South Australia to consolidate into coastal dunes during interglacial periods (Dart *et al.* 2005; Lintern *et al.* 2006; Dart *et al.* 2007). A large part of the aeolian dust deposited is later removed further by fluvial activity giving rise to the variability in deposit thickness over a region (Dart *et al.* 2005). Through this process, regolith carbonates in the Australian landscape, which can be potential CO_2 sinks, do not capture any additional CO_2 and instead, simply remobilise it from a marine to a terrestrial setting (Dart *et al.* 2007).

Strontium isotope signatures of the bedrock in this region typically have consistent $^{87}Sr/^{86}Sr$ ratios, and vary due to the decay of ^{87}Rb which over time, increases the Sr ratio (Dart 2009). Numerous Sr- isotope determinations have been widely used to demonstrate the predominantly windblown and less common bedrock origin (~10 %) of pedogenic carbonates in southern Australia (Dart *et al.* 2005; Lintern *et al.* 2006). Samples have been analysed from the Tunkillia region and show dominant marine/windblown input with typical Sr-isotope ratios for the ocean (Dart *et al.* 2005). Here, stable old rocks such as the Achaean bedrock in the Gawler Craton would consist of pedogenic carbonates with abundance in radiogenic ^{87}Sr isotopes due to radioactive decay. They would have high $^{87}Sr/^{86}Sr$ ratios, as opposed to marine/windblown low $^{87}Sr/^{86}Sr$ ratios with low radiogenic isotope signatures (Lintern *et al.* 2006).

Pedogenic carbonates generally precipitate in vadose soil horizons where the average annual rainfall ranges from ~100-500 mm (Lintern 1997; McQueen *et al.* 1999) and precipitation is less than evapotranspiration (Goudie 1983). Regolith carbonate development in southern and central Australia have been attributed with trends towards

more arid conditions and increased aeolian activity since the late Miocene (Hou *et al.* 2008). Regolith carbonates can be subdivided into morphological facies including duricrusts/hardpan, nodules, pisoliths, coated grains, rhizomorphs, powder, laminae and within a regolith host matrix (McQueen *et al.* 1999; Lintern *et al.* 2006). The availability of carbonates in the soil are the result of a number of conditions including the weathering of Ca-rich minerals, the onset of aridity, tectonic stability and impeded drainage (Lintern *et al.* 2006). Understanding the carbonates is imperative to their applications in mineral exploration (Hill *et al.* 1999).

Rainfall chemistry can also exhibit important controls on the distribution of regolith carbonates. Pedogenic carbonates in southern Australia are widely recognised south of the 'Menzies Line' in Western Australia with equivalent extensions eastward into South Australia and New South Wales (McQueen *et al.* 1999; Chen *et al.* 2002). The Ca- and Mg-rich winter rain derived from the Indian and Southern Oceans approximately extends to 30 S latitude which also corresponds to the extent of pedogenic carbonates. Further northwards, pedogenic carbonates become sparse and groundwater valley carbonates dominate (Hill *et al.* 1999; McQueen *et al.* 1999; Chen *et al.* 2002). Marked changes in soil type, vegetation, groundwater chemistry and climate also correspond with this transition and this refutes previous models of regolith carbonate development that are primarily associated with aridity (Hill *et al.* 1999).

Carbonates form in the regolith via interactions of Ca^{2+} and Mg^{2+} derived from either bedrock: *in situ* weathering of rocks and minerals (intrinsic) or external aerosols and laterally moving soil waters, deposition and erosion (extrinsic) (Anand *et al.* 1997; Dart 2009); and bicarbonate (HCO^{3-}) derived from CO_2 gas produced by root and microbial respiration, where CO_2 dissolves readily in water dissociating to HCO^{3-} that in turn reacts with free Ca^{2+} in soil water (Lintern 1997). After reaching saturation, this results in the precipitation of calcite ($CaCO_3$) and dolomite ($MgCO_3$) from solution and can be redissolved/remobilised under varying chemical conditions (Chen *et al.* 2002). Saturation is largely controlled by evaporation/evapotranspiration, which removes water or can be enhanced in areas where source rocks are rich in carbonates (Lintern 1997; Hill *et al.* 1999). Figure 1 outlines the numerous principal sources of pedogenic

carbonates. Gold deposition has been suggested to occur via similar processes concentrating the highly soluble Au complexes in near surface regolith profiles and then saturation is reached through removal of water via plant uptake in root systems (McQueen *et al.* 1999). Calcite is the most abundant carbonate mineral in the upper profiles with dolomite concentration typically increasing with depth. This has been attributed to near surface dissolutions of carbonate through the percolation downwards of rainwater and re-precipitation of calcite before dolomite due to pH and pCO_2 change (Hill *et al.* 1999; McQueen *et al.* 1999). Regolith carbonate accumulations with morphologies reflecting an origin of pedogenesis and with high Ca/Mg ratios have the strongest associations with gold (Hill *et al.* 1999).

Calcrete is the term appropriate for indurated regolith carbonates dominated by calcium carbonates (Hill *et al.* 1999). They develop in soil profiles, colluvial and alluvial sediments, weathering profiles, or directly over and within bedrock (Anand *et al.* 1997). Nodular carbonate facies and coated grains are strong and weakly indurated carbonate rich bodies of >2 mm diameter and typically occur above hardpans (Hill *et al.* 1999). Multiple stages of carbonate precipitation can also give rise to concentrically zoned cemented and coalesced nodules (McQueen *et al.* 1999) with centres of undifferentiated micritic carbonate accumulations or detrital clasts of bedrock and quartz suggesting detrital reworking (Hill *et al.* 1999). Hardpan facies are hard impervious indurated layers. Internal morphology is complex and generally consists of coalesced nodules, coated grains and other fragments of indurated carbonates (Hill *et al.* 1999). The distribution of calcrete and their associated soils in Australia is represented in Figure 2.

Gold was first demonstrated to be closely correlated with Ca and regolith carbonates with studies published in 1984 by Smith and Keele, where Au values were recognised to be highest within the top 1 m of profiles containing 5–30 % carbonate mineral and overlying mineralisation at Norseman, Western Australia. This study however, did not associate Au with a carbonate increase, and instead related it back to vegetation (Smith & Keele 1984). Gold is well known as a relatively immobile element in the superficial environment and therefore the geochemical signature of an occurrence is limited and difficult to interpret (Reis *et al.* 2001). Under certain conditions however, epigenetic

gold can become mobile and disperse from its source to form geochemical Au-anomalies at the surface (Reis *et al.* 2001). A study based at Mt Hope, Western Australia in 1989 by M.J. Lintern was one of the first published references of a recognised carbonate and Au relationship. Here it was suggested that similar to Ca, Au is soluble and mobile in soils (Lintern 1997).

Instead of acting as a dilutent to Au, as it does for many elements in soils such as Fe, calcrete horizons actually concentrate the Au (Lintern 1997). Gold complexes associated with calcrete are soluble in water and mobilised in soil solution as an organic complex (Lintern 1997). As a result, Au within carbonate horizons should be depleted rather than enriched. It has been suggested that the carbonate horizon is an evaporative zone where solutions carrying mobile elements including both Au and Ca (-Mg) carbonates will precipitate, adding to the carbonates, therefore concentrating Au in this horizon (Lintern 1997; Gray & Lintern 1998; Butt *et al.* 2000). Lintern *et al*. (2006) further suggest that the associations between Au and regolith carbonates are due to hydromorphic processes and associated environmental factors that result in the dissolution and re-precipitation of Ca and Au within the soil profile. This therefore demonstrates high solubility of Au within the carbonate horizon which also matches Ca solubility, therefore both elements will dissolve and co-precipitate under similar conditions (Lintern *et al*. 2006; Dart 2009). Gold anomalies range from 5–300 ppb against an ~2 ppb background (Butt *et al.* 2000).

Regional Au anomalies around mineralisation appear to be associated to lateral transport of Au via groundwater movement down slope or by mechanical dispersion of Au-bearing regolith such as ferruginous lag (McQueen *et al.* 1999) (lag: a residual accumulation of coarse, usually hard rock fragments remaining on a surface after the fine material has been blown away by winds (Carver *et al.* 1987)). In some circumstances high concentrations of an element do not necessarily mean that mineral deposits of economic value will be found (Levinson 1974). Dispersion is the process causing distribution or re-distribution of elements by physical and chemical agents, and processes can occur either in the primary or secondary environment (Levinson 1974). Minerals formed under primary conditions are often unstable in the secondary

environment and will weather allowing elements contained within to be released, transported and re-distributed (Levinson 1974). So called, 'false anomalies' identify high Au content in carbonates however there is no underlying source of mineralisation, 'blind deposits' do not identify a strong Au expression within the surficial carbonates for an underlying mineral deposit (Hill *et al.* 1999). Explanations for these may be due to previously poorly recognised landscape controls and lateral dispersion down slope (Hill *et al.* 1999).

The specific aims of this research project are to:

1. Produce a detailed regolith-landform map and associated landscape history for the 'Tomahawk' area, Tunkillia, to constrain the influences of regolith material and landscape setting on possible associations between calcrete geochemistry and mineralisation;
2. Provide a profile morphological and landscape multi-element geochemical study of calcretes from the 'Tomahawk' area, including samples from transects across the mapped regolith-landforms;
3. Consider the implications of the previous aims for developing a better understanding of processes and mechanisms for Au-in-calcrete anomaly formation and the implications of this for further mineral exploration under cover.

2.0 SETTING

2.1 Location and land use

The Tunkillia Prospect (Figure 3) is ~660 km northwest of Adelaide (Ferris & Wilson 2004), ~70 km south-southeast of Tarcoola (Wilson & Savcin 2004; Lowrey 2007) and on the eastern margin of the Great Victoria Desert (GVD) in the central Gawler Craton (CGC) (Dart 2009). Access is via the Stuart Highway to Glendambo, 280 km north of Port Augusta (Martin & Wilson 2005), and then to Kingoonya (40 km) via the old Stuart Highway, followed by ~60 km along station tracks to the southwest (Wilson & Savcin 2004; Martin & Wilson 2005). Moderate access is possible throughout majority of the area via station tracks and gridlines cleared for previous exploration (Wilson &

Savcin 2004; Lowrey 2007), however four-wheel drive vehicles are essential. Much of the tenement is covered by well vegetated Pleistocene sand dunes except for the northern margin where Pleistocene soils and clays dominate (Martin & Wilson 2005). Much of the tenement is within Pastoral Lease and this remains ungrazed due to lack of portable water and moderately vegetated sand dunes (Wilson & Savcin 2004).

2.2 Climate

Tunkillia has a semi-arid climate, with Tarcoola the closest weather monitoring station, ~70 km to the north-northwest. It has a mean annual rainfall of ~174 mm consistently falling throughout the seasons, with an average of ~14 mm/month excluding a maximum in February of 21.1 mm {Meteorology, 2009 #75}. Average maximum and minimum temperatures for summer are 35.0^{o}C and 17.9^{o}C respectively in January, while average maximum and minimum temperatures for winter are 18.2^{o}C and 4.2^{o}C respectively in July {Meteorology, 2009 #75}. Data collection at Tarcoola occurred between 1922 and 1999 for temperature and rainfall between 1904 and 1999. Since 1997 however, Tarcoola Aero monitoring station, 1 km further east has commenced data collection and continues to the present day. Mean annual rainfall there is 179.8 mm, with maximum mean monthly rainfall in December of 29.2 mm, and a minimum of 5.9 mm in May, with a range of ~10-19 mm/month {Meteorology, 2009 #76}. Average maximum and minimum temperatures for summer are 36.6^{o}C and 19.6^{o}C respectively in January, while average maximum and minimum temperatures for winter are 18.9^{o}C and 4.5^{o}C respectively in July {Meteorology, 2009 #76}.

2.3 Regional Geology of the Tunkillia Prospect

The Gawler Craton underlies a large part of South Australia (Dart 2009). The bedrock consists of crystalline, Achaean to Palaeoproterozoic granite/granite gneiss, intruded by Mesoproterozoic granites, that are possibly members of the anorogenic Hiltaba Suite granites (Lane & Worrall 2002). This basement has been relatively stable with only minor deformation since 1450 Ma (Rogers & Zang 2006; Hand *et al.* 2007). Bedrock exposures are scarce, due to a veneer of deep weathering and extensive Mesozoic to Quaternary sediments including sand, calcrete and silcrete (Wilson & Savcin 2004; Lintern *et al.* 2006).

The Tunkillia Prospect is part of a large hydrothermal system in the CGC, and associated with the northern termination and rotation of the Yarlbrinda Shear Zone (YSZ) which is a ductile-brittle north-south trending structure extending approximately 150 km and up to 12 km wide (Figure 4) (Ferris & Wilson 2004). It is believed to have formed during the Palaeoproterozoic Kimban Orogeny (Flint 2005) and was reactivated in the Mesoproterozoic (Lane & Worrall 2002). It separates the western edge of the Gawler Range Volcanics (GRV) (~1595 to 1575 million years) from the Palaeoproterozoic Tunkillia Suite (~1690 to 1670 million years); and Saint Peter Suite granitoids (~1630 to 1608 million years) (Ferris & Wilson 2004). Closer to the northern end of the structure it trends towards the northwest where it intersects the Koonibba Thrust Fault and the Yerda Shear Zone (Lane & Worrall 2002; Wilson & Savcin 2004; Dart 2009).

Host rocks of the Tunkillia Prospect are the medium to coarse-grained Tunkillia Suite granitoids, (granodioritic gneiss and quartzite) (Mayo & Hill 2005) which intruded the crust during the Kararan Orogeny (~1690 to 1670 million years) and have been intensively sheared and brecciated associated with the YSZ (Ferris & Wilson 2004; Ferris & Schwarz 2004). They represent I-type intrusive plutons and rhyolitic and mafic dykes with poor outcrop mainly in the south and west of Tunkillia (Ferris & Wilson 2004; Ferris & Schwarz 2004). The Au is associated with pyrite and minor galena, hosted in striking 325^{o}/steep west dipping quartz-sulphide veins (lode-Au-style) within zones of chlorite-sericite alteration (Ferris & Wilson 2004; Ferris & Schwarz 2004).

Mineralisation and demagnetisation in this area is syn-deformational with respect to the main shearing and foliation-forming event (Ferris & Wilson 2004) and most likely associated with a fluid influx from syn-tectonic emplacement of the Hiltaba Suite granites (~1590 to 1575 million years), within an active YSZ during the widespread Mesoproterozoic anorogenic magmatism of the GRV across the CGC. Fluids derived from the granite were possibly mixed with metamorphic fluids of low salinity at depth, and were trapped at sites of fault intersections within the shear zone, thereby providing the dominant structural control on mineralisation (Ferris & Wilson 2004).

Mineralisation is the same age as at Olympic Dam, Prominent Hill and the Tarcoola Gold Field (Martin & Wilson 2005), and occurs beneath a thick sequence ~60 m of weathered rock with only background levels of Au (Gibbons 1997).

2.4 Previous Geological Studies

Previous exploration at Tunkillia has focused on geophysical properties (Lane & Worrall 2002); hydrogeochemistry (Gray & Pirlo 2004, 2005); biogeochemical surveys (not including Au analysis) (Thomas 2004) and geochemistry and mineralogy of mineralisation (Ferris & Wilson 2004). Regolith studies have involved biogeochemistry and the recognition and mapping of the variation in dune types over mineralisation (Lowrey & Hill 2006; Lowrey 2007). Further regolith research on regolith carbonates and their association with Au mineralisation by Dart (2009), identified Au-in-calcrete anomalies include contributions from Au and associated elements laterally transported from mineralised areas by physical and chemical landscape processes.

Mineralisation at Tunkillia was discovered by Helix Resources Ltd. in 1996 following an extensive calcrete sampling program (Ferris & Wilson 2004). Three prospects with higher zones of Au-in-calcrete content were identified at Tunkillia: 'Area 191', 'Area 223' and 'Tomahawk'; of which 'Area 223' is the largest potential resource (Ferris & Wilson 2004). In 2005 Helix Resources Ltd. entered into joint venture with Minotaur Exploration Ltd. in confirming the mineralisation extent and exploring into surrounding areas (Belperio 2006).

2.5 Regolith-landforms and vegetation of the 'Tomahawk' area

The south of the area is covered by densely vegetated longitudinal sand dunes of the eastern margin of the GVD, which are generally migrating eastwards over erosional plains that dominate the central area (Wilson & Savcin 2004; Lowrey & Hill 2006; Dart 2009). They are dominated by linear dune ridges and swales that trend west to east, may be up to ~10 m high, spaced at ~250 m between dune crests and composed of red-brown quartzose sands (Lowrey & Hill 2006). Lowrey (2007) constrained the aeolian dunes of the Tunkillia area into three phases of dunefield evolution and these have distinctive soils and vegetation assemblages (Figure 5). From this, Phase I dunes form

the core of majority of the dunes in the study area, with phase II and III dunes building up predominantly on the western side (stoss side) of the dune ridge. Phase III includes contemporary aeolian sand migration and typically buries growing vegetation.

Interdunal swales and areas of higher elevation associated with aeolian dunes are broad and flat, and surficial regolith consists of red-brown, poorly to moderately sorted, sub-rounded, fine to medium grained quartzose sand and silts with minor regolith-carbonate nodules and hardpan; quartz and lithic fragments and Fe-oxide cutans (Lowrey & Hill 2006; Lowrey 2007; Dart 2009). Dune swale vegetation is typically open woodlands of the Great Victoria Desert (GVD) mallee (*Eucalyptus concinnia*), umbrella wattle (*Acacia ligulata*) and black oak (*Casuarina pauper*). The black oaks typically have an understorey of pearl bluebush (*Maireana sedifolia*), particularly where calcrete is within the top 60 cm of the regolith (Lowrey 2007), and walker's pea (*Bossiaea walkeri*) (Dart 2009). When dune swales are broad, surface lag becomes more predominant and is composed of calcrete/silcrete (Dart 2009). These additionally reveal windows of the pre-dune surface features including palaeodrainage gravels, erosional plains and drainage depressions (Dart 2009).

Erosional plains dominate the northern part of the study area. Surficial regolith generally consists of brown-red moderately to well sorted, fine to medium grained quartzose sand and silts with varying quantities of regolith-carbonate nodules, silcrete fragments, quartz and Fe-oxide gravels of size from 0.5-10 cm. Vegetation consists of open woodlands dominated by black oak, GVD mallee, occasional mulga thickets *(Acacia aneura)* with understorey of pearl bluebush, bluebush daisy *(Cratystylis conocephala)*, and cassia (*Senna artesmesioides).*

Depositional plains dominate the north-eastern part of the study area with surficial regolith consisting of light brown-red, moderate to well sorted, very-fine to fine grained quartzose sand with highly rounded quartz, iron-oxide, lithic and carbonate lag. Strong cryptogram crust occurs on the soil surface with open woodland vegetation dominated by either black oak, or GVD mallee*;* and also umbrella wattle, occasional red mallee *(Eucalyptus socialis)* and pearl bluebush.

Drainage depressions and ephemeral swamps are small discrete and low-lying within the study area. Generally they consist of red-brown very-fine to fine grained, well sorted consolidated clayey/silty soils with dense cryptogram crusts. Drainage depressions have minor medium grained quartz and occasional silcrete and calcrete nodules, with open woodland of dense mulga thickets, occasional black oak, and understorey of pearl bluebush and umbrella wattle. Swamplands conversely have chenopod shrubland of black oak, umbrella wattle, mulga thickets, and pearl bluebush.

3.0 METHODS

3.1 Calcrete sampling

Regolith carbonates (RCs) were collected from the surface on an opportunistic basis, including within small drainage depressions, excavations associated with previous drilling and exposures assisted by natural processes, such as overturned trees exposing RCs from depth. Contamination is a major concern when collecting samples for analysis, i.e. gold, the element of most interest is generally in low concentrations. Avoiding contamination is essential but can arise through factors such as previous anthropogenic activity in the area or sample methodology inadequacies. To reduce contamination from external sources, site selection occurred away from obvious source for contamination, such as remnants of drill spoil. Personal jewellery items were removed and hands were washed clean of sunscreen and other oils.

Sampling transects were centred along previously cleared drilling and geophysical transects. Approximately 500-800 g of sample was placed into a snap-lock bag, and where possible, a further large sample was collected for hand sample examination. RC samples were labelled with GPS coordinates using the GDA 94 datum and Universal Transverse Mercator (UTM) projection. Additional regolith and landform observations were recorded at each site, along with morphological form of RCs.

In total, 98 RCs were collected in the forms of nodular and hardpan morphologies. The RCs were sufficiently abundant for them to be used as a regional sampling medium and

can be useful in providing a regional chemical context particularly for Au and other trace metals (Gibbons & Hill 2005).

3.2 Regolith-landform mapping

Regolith-landform (R-L) mapping of the study area was conducted at a 1:10,000 scale to provide a context for the sampling and to help interpret the surficial transport pathways. Distinct regolith-landform units (RLUs) were observed in detail within an area of ~9.5 km^2 and a total of 11 RLUs were defined. Examples of each unit were recorded by a Garmin 72 Global Positioning System (GPS) with ~5-10 m horizontal accuracy; and outlined on the R-L map.

A 1:10,000 scale SPOT-5 image obtained from Google Earth assisted the compilation of the map to identify RLU boundaries. This was then scanned and edited using Adobe Photoshop CS2 9.0 and Adobe Illustrator CS 11.0 and georectified using ArcMAP to produce a R-L map of the area of interest, which conformed to the Australian Map Grid (AMG) GDA 1994, zone 53.

3.3 Regolith profile logging

Surficial remnants of rock chips from 11 previous RAB drill holes were logged over the 'Tomahawk' Au-in-calcrete anomaly along the sampling transects. The overall log of drill chips was initially labelled with GPS coordinates and log number and then photographed for later reference and visual aid. Lithology, colour, grain-size, sorting, rounding, minerals present, and mottling were recorded. These logs were then compiled in Microsoft Excel 2007.

3.4 Sample preparation and analysis

Each calcrete sample was transported to the University of Adelaide where they could be rehandled under clean working conditions. A representative sample (smaller nodules with greater surface area were preferred) from each location of ~300 g was collected and re-bagged to ensure any remaining loose detritus soil inclusions still attached to the

calcrete was removed. Bags were re-labelled appropriately to represent the original site of sampling and the remainder of the samples were retained for reference materials.

In addition to the 98 samples, a further ten split duplicate samples were taken from approximately one in ten samples for QA/QC purposes. The samples were then submitted to Genalysis Laboratory Services in Adelaide, where further sample preparation could be conducted including drying (code: DR), crushing (code: CR) and single stage mix and grind (code: SSMG). Conventional jaw crushing was to a nominal -10 mm. Pulverising is aimed to achieve 85 % at -75 µm and 'Low-chrome' steel pulveriser bowls are used, which typically add a few tens of ppm chromium to the sample.

The pre-analysis Aqua Regia sample digestion consisted of a 10 g sample being digested and leached. After cooling, the solution was vacuum filtered and accurately diluted to volume. Sample analysis for 59 elements was conducted by the following methods on the digested solutions (detection limit for each element is in the parentheses):

Elements analysed by ICP/OES – Inductively Coupled Plasma Optical (Atomic) Emission Spectrometry:
Al (20 ppm), Ca (0.01 %), Cr (2 ppm), Cu (1 ppm), Fe (0.01 %), K (20 ppm), Mg (0.01 %), Mn (1 ppm), Ni (1 ppm), P (20 ppm), Sc (1 ppm), Ti (5 ppm), V (2 ppm), Zn (1 ppm).

Elements analysed by ICP/MS – Inductively Coupled Plasma Mass Spectrometry:
Ag (0.05 ppm), As (1 ppm), Au (1 ppb), Ba (1 ppm), Be (0.05 ppm), Bi (0.01 ppm), Cd (0.05 ppm), Ce (0.01 ppm), Co (0.1 ppm), Cs (0.002 ppm), Dy (0.01 ppm), Er (0.01 ppm), Eu (0.01 ppm), Ga (0.05 ppm), Gd (0.01 ppm), Hf (0.01 ppm), Ho (0.01 ppm), In (0.01 ppm), La (0.01 ppm), Li (0.1 ppm), Mo (0.1 ppm), Nb (0.02 ppm), Nd (0.01 ppm), Pb (1 ppm), Pd (10 ppb), Pr (0.005 ppm), Pt (5 ppb), Rb (0.02 ppm), Re (0.01 ppm), Sb (0.02 ppm), Se (1 ppm), Sm (0.01 ppm), Sn (0.05 ppm), Sr (0.02 ppm), Ta (0.01 ppm), Tb (0.005 ppm), Te (0.05 ppm),

Th (0.01 ppm), Tl (0.01 ppm), Tm (0.01 ppm), U (0.01 ppm), W (0.05 ppm), Y (0.02 ppm), Yb (0.01 ppm), Zr (0.1 ppm).

Elements analysed by ETA – solvent extraction and graphite furnace atomic absorption spectrometry: Au (1 ppb).

3.4.1 QA/QC

A routinely adopted Quality Control Procedure has been described by Genalysis Laboratory Services where sample duplicates and control blanks were used for quality assurance/quality control purposes. Standards and blanks were inserted randomly with a total of two control blanks; and four standards: CMM-01, BSL9, NGL-21, BSL9, where 'nominal' values of all elements are in-house reference materials used primarily as QC monitors for the aqua regia process. Samples are selected where possible to suit the element suite required, the range expected for element concentrations, and the expected matrix of the samples. Additionally, six samples were subject to check analysis, while eight samples were repeated for Au using the ETA method. One in ten samples were split and duplicated as previously mentioned within the sample stream to provide a total of ten samples.

3.5 Calcrete geochemistry mapping

Results for all 59 elements were analysed for statistical trends and known element associations, using Microsoft Excel and IoGAS. This helped to reduce the total suite of 59 elements to elements which best represented the known mineralisation associations. Initially, a Pearson's correlation coefficient was conducted on all elements to determine elemental associations. The correlation coefficient value measured the strength to which two measurement variables were associated and obtained a value between +/- 1. Large values of one variable associated with large values of another were given a positive correlation; small values of one variable associated with large values of another were given a negative correlation; when values of both variables were unrelated, correlation was near zero and a perfect correlation equated to one. A correlation coefficient (r) of +/- 0.75 was chosen as the value of significance for discerning elemental associations, further concentrating to elements which best represented

associations with mineralisation. This value was chosen based on the allocation that 0.7–0.9 is termed strongly correlated (Dart 2009).

Twelve key elements were then selected for this study based on mineralisation characteristics including known element associations, pathfinder and host elements and prospective commodities. Statistics for each element were summarised in Microsoft Excel to give a basic set of parameters that can be reported for elements in the geochemical data set. X-Y plots were produced using IoGAS to further illustrate broad elemental associations as well as the correlations between the specific 12 elements selected. This additionally identifies other important relationships between the variables, where the correlation coefficient only equates all of the variance to a single linear relationship.

Normal probability plots were produced using IoGAS to further summarise the data and provide a visual estimate. The data is plotted as a scatterplot against the values expected from a normal distribution and the data is then ranked. From this ranking, values are calculated based on the assumption that the data came from a normal distribution. For all elements, four assay level ranges were established to use in geochemical mapping. The breaks in the total data set were identified so one category represented samples below or approaching analytical detection limit and the three remaining were separated through breaks in population subsets. Figure 6 shows an example for Au and how the probability plot is used for identifying the four population subsets.

The elemental population subsets produced with normal probability plots could then be graphed spatially against their easting and northing coordinates, in the ‘Tomahawk’ area using IoGAS and ArcMAP where results were plotted on the study produced regolith-landform map. This allowed analysis of correlations, clusters and discrete ‘hits’ to find association possibly to geological structures, landforms and associated features. Au in Figure 7 identifies the different population subsets along transects in the ‘Tomahawk’ area.

Geochemical results from the ‘Tomahawk’ sampling area can be summarised into four main sub-populations relating to analytical concentrations:

1. High Locally;
2. Medium to High Locally;
3. Low Locally; and,
4. Below or Approaching Detection Limit.

4.0 RESULTS

4.1 Regolith Setting

4.1.1 REGOLITH-LANDFORM MAP OF THE ‘TOMAHAWK’ AREA.

The regolith-landform map of the ‘Tomahawk’ area completed in this study is shown in Figure 8, compiled from interpretation of aerial photographs and observations when in the field. A full description of the regolith and landform codes as well as example location (GPS) points of these units with photo example reference are also shown in Appendix 1a. The four major regolith-landform types are represented as images in Appendix 1b and outlined below:

1. Dune Fields: ISu $_{1,2,3}$ and Isps $_{1,2}$
2. Alluvial Drainage: Aed and Aaw
3. Erosional Plain: CHep $_{1,2,3}$
4. Depositional Plain: CHpd $_{1,2}$

4.1.2 REGOLITH PROFILE LOGS

Detailed regolith profiles logged along the ‘Tomahawk’ Au-in-calcrete anomaly transects were recorded to establish a typical weathering profile of the ‘Tomahawk’ area, and subsequentially the Tunkillia region. Location of where the logs were taken is found in Appendix 2a. These regolith profile logs were compiled from the remains of previous RAB drilling samples and illustrate that the weathering profile of the study area varies with both depth and composition. They were produced to identify if variance between profiles occurs between aeolian sand dunes versus palaeo- and current

drainage channels, and also whether the drilling reached fresh basement or only tested the supergene enrichment zone (depleted zones). Observations from this analysis are however, subject to error due to the disintegration and degradation of the rock chips available from susceptibility to weathering and climate controls over time. Several metres can be missing due to wind or water erosion, and on occasion the samples were disregarded due to contamination and deemed an incorrect representation of the profile characteristics.

Given the long history of subaerial weathering in many regions of Australia, polygenetic weathering profiles are likely to be dominant (Pillans 2005). All regolith profiles are illustrated in Appendix 2b, with image representation of what the regolith profiles looked like in the field in Appendix 2c. Figure 9 illustrates the typical weathering profile established for the 'Tomahawk' area from the top of the weathering profile, and consists of the following intervals: red-brown sediment cover of sands to fine grained soils and clays, followed by an interval variable in composition and also spatially of indurated hardpan or nodular regolith carbonates, silcrete or ferricrete. A cementation front is then passed as the plasmic/pallid zone of powdery white kaolin clays where all or majority of the primary fabric has been destroyed. This overlies kaolinised saprolite (>20 % weatherable minerals altered) (Eggleton 2001), where primary fabric is preserved. This overlies saprock (<20 % weatherable minerals altered) (Eggleton 2001), again with primary fabric preserved however less leaching/bleaching has occurred and thus original colour is more effectively retained. A weathering front is passed as the zone of fresh rock is entered: the underlying basement material, which in the case of 'Tomahawk' corresponds to undifferentiated granitoids of the Tunkillia Suite.

Zones of deeper weathering may coincide with palaeo- and contemporary drainage systems. This is because for majority of profiles logged in CHep landforms, basement was not reached, and in some cases saprock was not reached at >40 m (e.g. regolith profiles two and nine). It must be taken into account however that over time these intervals of rock chips may have been lost on the surface, due to weathering and erosion

in their location, but aside this suggestion, of the total 11 holes logged, four holes did reach basement, therefore ~64 % did not.

4.2 Calcrete Geochemistry

Location of calcrete sampling sites in the field is found in Appendix 3a, while full spreadsheets of analytical results are found in Appendix 3b.

4.2.1 % OF ELEMENTS CONSISTENTLY BELOW OR APPROACHING DETECTION LIMIT

Any elements that produced values below detection limit (DL) returned the value X in the original output table. For analysis purposes, elements that produced these values were given values of half their individual DL. Elements wholly below analytical DL in the original output table were disregarded on first instance as insignificant elements for this study. Summarised in Table 1, are the percentage number found below DL, for all 59 elements. The following elements were disregarded for this study because all or majority of the samples were consistently below DL: Re (100 %), Se (100 %), Ta (100 %), Pd (99.07 %) and Pt (99.07 %).

4.2.2 QA/QC

Inserted standard reference materials (sample duplicates and control blanks) used by Genalysis in the analytical stream for QA/QC purposes returned sufficient results to support the accuracy of the data and the methods used for analysis. For more details on the standard values used, please refer to Appendix 3c.

Field duplicates, check analyses and repeat Au analyses, were compared for randomly selected elements to their original field value. This was conducted using GraphPad Prism 5, plotting original vs. duplicate value; conducting a linear regression and then applying 95 % confidence intervals on the line of best fit. The percentage of values which lay within this interval indicated the level of confidence that could be applied to the original data values. Linear regression and confidence interval data analysis can be found in Appendix 3d and can be summarised that the field samples collected and the analysis conducted was of high quality and accuracy, due to the high percentage of values that occurred within the 95 % confidence interval, illustrated in Tables 2 to 4.

Averaging data points with field duplicates, check analyses and Au repeats was not necessary to obtain a more accurate elemental concentration.

4.2.3 BROAD ELEMENT ASSOCIATIONS

4.2.3.1 Correlation Matrices

The overall correlation matrix is shown in Appendix 4a. Three particular elemental associations found of interest in the correlation were that of Fe, Al and REEs. As previously mentioned, a correlation coefficient (r) of +/- 0.75 was chosen, and any values higher were deemed significant. Table 5 summarises the broad elemental associations established through the procedure of a Pearson's correlation. Pearson's correlation was used instead of Spearman's rank correlation coefficient because it characterises the degree of linear dependence between two normal random variables of normal distribution where extreme outliers are not present i.e. 'Tomahawk' is wholly within mineralisation as opposed to comparing with background concentrations in the sampling area, and the data is of reasonable normal distribution. Spearman's correlation however takes the variable ranks instead of the values and characterises a degree of arbitrary non-linear dependence.

Select X-Y scatterplots were produced using IoGAS to further visually illustrate strong correlations, and are found in Appendix 4b. REE relationships are very similar, with all analysed returning high correlations with other REEs. Typically r values are >0.95 except for Ce which increases the overall correlation ranges of other REEs when it is included. Moderate correlations also exist with REEs and Co with correlation coefficient range of 0.774-0.828. This high correlation coefficient applies for all REE elements analysed, as well as for Mn (0.753), highest correlation with Ce (0.828), followed by Gd (0.809). Correlation also occurs with REEs and Cd with high correlation ranges from Tb (0.751) to Tm (0.791), correlation however only occurs with REE elements: Dy, Er, Ho, Tb, Tm, Y and Yb. The correlation coefficients for Fe ranged from 0.788 for Pb, to 0.948 for Cr, while correlations with Al ranged from 0.814 for Sn, to 0.947 for Cs. The highest correlation coefficient for Au was with Ga (0.521).

4.2.4 SELECTION OF 12 KEY ELEMENTS

An element measured to detect mineralisation is generally termed an indicator element and in many situations this element is also an economically valuable component of the mineralisation (Rose *et al.* 1979). These can be difficult to analyse; be immobile; or yield data difficult to interpret, and therefore alternative elements, known as pathfinder elements associated with the mineralisation are subsequentially analysed (Rose *et al.* 1979). Reasoning for associations between pathfinder elements and mineralisation, and the geochemical environments in which the associations occur should be studied. These generally occur due to the similarities in relative mobility and stability during geological processes (Rose *et al.* 1979).

The results here are described for a selected 12 element suite. These were established to specifically relate to chosen settings for the Tunkillia area, including the elements:

1. Associated with mineralisation and known indicator elements (Au, Ag, Pb, Zn, Sb and La);
2. Secondary trace element host minerals (Ca, Fe and Al);
3. Traditional pathfinder elements for Au from previous studies (As); and,
4. Other commodities that could be prospective in the area (Cu and U).

Further justification for selection of the 12 elements is found in Table 6.

4.2.5 SUMMARY STATISTICS

Summary statistics report the basic parameters for the 12 selected key elements in the data set. This allows a brief, but informative way to illustrate the variable characteristics of individual elements for the data set. The summary statistics for selected elements are found in Table 7. It highlights values of interest such as high variance for Au (1055) and Al (5661981), low variance of Ag (0.00), Fe (0.268) and Sb (0.001) while still gauging the reliability of the data with % below DL i.e. Ag 89.8 % below DL and As 53.7 % below DL. The range of the element concentrations identifies the consistency of the data, and this must take into account the overall values of significance (i.e. in relation to analytical DL in the data set such as range of 193 ppb for Au where maximum is 194 ppb and minimum is 1 ppb). Whether these values are related to outliers in the data population or whether there is a consistent spread of the

data between these two values then lies with the mean and median (i.e. for Au the mean is 36.8 ppb, median is 27 ppb, therefore suggesting the maximum values are more strongly related to population outliers).

A correlation matrix (Table 8) of the elements of interest constructed from the main correlation matrix (Appendix 4a) further summarises the relationships between these elements. Significant correlations (>0.75) are observed only between Fe and As (0.840) and Pb and Fe (0.788), while correlations >0.50 are summarized below:

- U and Au (0.517), Al (0.521), As (0.630), Fe (0.507);
- Zn and Al: 0.585;
- Pb and As: 0.663; and,
- La and Ca: 0.528.

4.2.6 X AND Y SCATTER PLOTS

Scatter plots were produced to illustrate key examples established above. Based on the correlation matrix values, the only elements with significant linear correlations are Fe and As (0.840) and Pb and Fe (0.788) illustrated in Figures 10 and 11 respectively. A full set of the X-Y scatter plots can be found in Appendix 4c.1 to 4c.12.

An X-Y scatter plot also of interest is Ca and Au, with a weak negative linear relationship of r= -0.132, which is a weak negative linear relationship. Majority of medium to high Au values however, occur within a range of Ca %. This can be seen in Figure 12, with a mean and median value (Table 7) of ~20 %, a range where most data occur between ~16 and 25 %.

The X-Y scatter plot of Ag and Au (Figure 13) is of interest with known association of these elements in the Tunkillia Au prospect, of 4:1 ratio of Ag:Au reported in primary mineralisation. This has a correlation coefficient of r= -0.306, and is generally reasonable in comparison to correlations with other elements, even though it is still only a weak linear relationship. The spatial distribution of both high values of Au and Ag will be discussed later.

4.2.7 NORMAL PROBABILITY PLOTS

Normal probability plots were created to establish population subsets used later in spatial plotting of elements and can be viewed in Appendix 4d.

4.2.8 SPATIAL PLOTS OF THE 12 KEY ELEMENTS

Please refer to Figures 14.1 to 14.12 for element concentrations plotted spatially on the 'Tomahawk' Regolith-landform map, Appendix 1a for regolith landform codes and Appendix 4e for IoGAS spatial plots.

The Au spatial plot identifies clustering of high Au content (>75 ppb) locally, particularly in the central area of transects one and two. Medium to high concentrations (25-75 ppb) surround these values and are in the central and southwest of the study area. Of particular interest are the high Au values in transect four. Low Au values (<10 ppb) are in the northeast end of transect two, and south from this location in transects three to five.

A majority of Ag values were below analytical DL (<0.05 ppm), however a small region in the central area of transect three, recorded values of Ag two times the DL (>0.10 ppm) at 479710E, 6546212N, which also correspond to high Au values. This is further surrounded by medium to high values of Ag (0.08-0.09 ppm) to the southwest, however these correspond to low values of Au.

High values of Al (>9600 ppm) were identified in transects one, two and four and some values generally increase to the north. As with Au, medium to high (7600-9500 ppm) values surround high values, again, identifying a large region in the central area of transects one and two, and transect four. At 479553E, 6545649N high Pb, Fe, Al and Sb values were also recorded. The north-eastern end of transect one includes two high values of Al, and 480461E, 6545970N in transect six corresponds to high La values. Overall, concentrations generally increase to the north, and cluster in the central parts of transects one and two.

The results for As include a large number of values at or below analytical DL (>1 ppm). A majority of these are in the southern transects, as part of an overall trend of increasing

concentrations to the north. One value is classified as high (>6 ppm) at 479571E, 6546361N, which corresponds to a sample that also has high values of Al and Au. Medium to high (4-5 ppm) values follow an irregular distribution pattern, however, they relate to high values also in Al and medium to high in Au concentration.

All values of Ca were found to be significantly higher than analytical DL (0.01 %). The high values conform to an irregular trend, however, at the eastern ends of transects five to seven and in the central area of transects one to three, an approximate southeast to northwest trend is followed. At 479537E, 6546345N, high Ca concentration corresponds to a sample with high Au content. There is also a cluster of high values around 479258E, 6546166N.

A small percentage (1.85 %) of Cu results are at or below analytical DL, and concentrations are up to a maximum of 17 times DL. These values were irregularly distributed in transects one and three, however, in transect three, at 479710E, 6546212N, high Ag concentration (0.11 ppm) is also detected, while high concentrations at the northeast end of transect one, correspond to high concentrations in Al (>9600 ppm). A slight increase in concentration occurs towards the north, with medium to high values (6-8 ppm) on the south-western ends of the transects. Low Cu values are focussed in the central southern area.

Iron concentrations are greatest to the north, with a majority of medium and high values recorded in transects one and two. High concentration at 479553E, 6545649N coincides with highs in Pb, Al and Sb, while the central area of medium to high concentrations corresponds with highs in Al.

High La (>14 ppm) concentrations in the central region of a majority of the transects generally coincide with high Ca concentrations. There is an irregular distribution of high and low values, with only one high value at 480461E, 6545970N corresponding to abundant Al.

Medium to high concentrations of Pb are correlated generally in a north-south orientation, with high Pb values in the south in transects four and five corresponding to high concentrations of Fe, and similarly in the north in transect one. A majority of Pb concentrations approach DL (2-4 ppm) with high values up to ~22 ppm.

The Sb concentrations follow similar trends to that of Fe and Al, where medium to high values are concentrated in the central area. Sample site 479553E, 6545649N has locally high (>0.10 ppm) Sb concentration, at over five times the DL (0.02 ppm) and corresponds to highs in Pb, Fe and Al. The eastern end of transects five to seven identify an approximate northwest to southeast trend in medium to high concentrations of Sb. High Sb concentrations in transect two coincide with high Al and Au concentrations.

The U concentrations follow similar spatial trends to Al, Au and Ca. High readings in transects one and two are associated with high Al, and high Au and Sb concentrations respectively, while both corresponded to high Ca values. Overall, the concentrations of U are greater towards the north, and in the central region of transects one and two.

Locally high Zn concentrations in transect four correspond to high (>10 ppm) concentrations of Al, Au and Pb. High concentrations occur on the north-eastern end of transect one. These also correlate with high Al and Pb concentrations. Concentration of Zn is generally greater towards the north, with a majority of low concentrations in the central parts of transects three to six.

5.0 DISCUSSION: Landscape controls on biogeochemical expressions of mineralisation

5.1 Regolith-landscape setting and palaeolandscape reconstruction

Dart (2009) recognised that known bedrock-hosted mineralisation at Tunkillia occurs on the northern side of a regional drainage divide, Figure 15. In relation to the ‘Tomahawk’ Au-in-calcrete anomaly, elevation change from the drainage divide in the south is from approximately 220 m to 190 m in the north at ‘Tomahawk’. Even a gentle

gradient change, such as this, can be a major influence on the landscape processes and drainage patterns (Dart 2009). The region is strongly influenced by aeolian activity, therefore any palaeo- and contemporary drainage systems will be, over time overlain by dune fields with past drainage patterns visible in current landscape dune swales, and low lying areas.

Dart (2009) was successful in producing a symbolic overview of the drainage pathways at the Tunkillia prospect using the topographic map and regolith-landform descriptions (Appendix 5a). 'Tunkillia Central' palaeodrainage extended across 'Area 223', and closely followed the Au-in-calcrete anomaly. 'Tomahawk' may be a possible result of a slight saddle in the minor north-south interfluve ridge which has redirected palaeo-flow from the 'Tunkillia East' drainage, towards the 'Tunkillia Central' drainage (Dart 2009).

5.1.1 REGOLITH LANDFORM HISTORY: PALAEO- VS CONTEMPORARY LANDSCAPE

5.1.1.1 Contemporary Landscape

Tunkillia and adjacent parts of the CGC experience a semi arid climate of low frequency/high intensity rainfall. The area hosts minor tectonic activity (neotectonic deformation) and extensive weathering over a low relief landscape. Variations in geochemical characteristics can be associated with differences in the landform processes currently active, including:

1. Aeolian dunefields and sand-plain development with subsequent migration of aeolian sediments to the northeast via dominant westerly winds within frontal systems (Hesse & McTainsh 2003). This results in burial of erosional plains and blockage of drainage channels preventing further movement of alluvial sediments and forcing migration channels (Dart 2009). This modifies the dispersion pathways of the elements associated with mineralisation.

   Dunefield development described by (Lowrey 2007), includes phase I dunes, that are dominant in the north and are relatively stable landforms that should

have the strongest accumulation of geochemical signatures due to their extended time for element cycling, dispersion and accumulation. Phase II dunes are the most widespread and are predominantly in the south of the study area. They are relatively stable, however have had shorter time for geochemical signature cycling than for Phase I dunes. Phase III dunes, the youngest, have mobile crests, are the current migrating phase and should have the weakest geochemical signatures through chemical development, influenced more so by physical transport. Sandy dune swale (ISps) landforms have thinner aeolian cover than dune systems, therefore have a stronger chemical development than a physically transported geochemical signature, hence stronger expression of buried mineralisation.

2. Surficial sediment migration across low relief landscape to the north via colluvial sheetflow from prevailing winds, broad meandering and braided alluvial channels. This occurs when high intensity rainfall events exceed the infiltration capacity of aeolian sediment and soils (Dart 2009). With scattered surface lag, erosional plains (CHep) are the result of numerous sheetflow events. Geochemical characteristics are a window to the older surface of underlying saprolite, and offer stronger geochemical cycling and accumulation due to the closer vertical proximity to the saprolite, compared to dunefields.

3. Deposition and accumulation of colluvial and alluvial sediments in low lying areas in the north (Dart 2009) with landforms CHpd, Aed and Aaw in the 'Tomahawk' study area. Dart, (2009) proposed contemporary drainage lies along the western edge of the Au-in-calcrete anomaly through the central area of the Tunkillia prospect and this drainage mis-alignment is the result of migration of drainage channels (Dart 2009).

5.1.1.2 Palaeolandscape and Palaeodrainage

Australia is considered a stable, ancient continent of intraplate tectonic setting. It is however, not totally excluded from tectonic activity with deformation occurring since the major rifting of Australia and Antarctica ~43 Ma ago producing ongoing change to landscape processes (Sandiford *et al.* 2008). As a consequence of the low erosion rates,

weathering products of previous climatic regimes are often preserved (Carver *et al.* 1987). Regolith profiles are therefore the result of a long, complex history of weathering and landscape processes (Pillans 2005), a mixture of ancient and contemporary, either superimposed in a vertical sequence over original parent-rock materials, or laterally displaced by local erosional processes (Carver *et al.* 1987). Understanding these processes and the climates associated help to explain the extent of the Au-in-calcrete anomaly.

Prior to partial masking of the palaeolandscape, Dart (2009) described the landscape as 'a series of drainage depressions overall flowing towards the north derived from exposed east-west drainage divide'. Masked by contemporary processes palaeodrainage patterns are disrupted, and therefore elemental dispersion patterns, including those associated with mineralisation (Dart 2009).

The deep weathering regolith profile observed is typical of wet/dry tropical climates, or conversely colder and drier conditions given enough time and inadequate surface erosion (Dart 2009). Climate controls the availability of water and the provision of winds and temperatures that ultimately drive many regolith and landscape processes (Hill *et al.* 2008).

An initial climatic impact on the landscape in the central Gawler Province, thus Tunkillia area, was the cool climate in the Permian. Widespread glaciations scoured bedrock and deep weathering profiles (Sheard *et al.* 2008). Wetter climates then during the Triassic and Jurassic promoted renewal of deep weathering which provided the source materials for late Jurassic and early Cretaceous deposition of sediments (Hill *et al.* 2008). Extensive deep weathering that commenced during the Mesozoic and may have continued until early Tertiary left behind extensive pallid saprolite zones from strong oxidation conditions (Benbow *et al.* 1995).

The Pliocene is associated with a warm climate and development of aridity where ferricrete and extensive silcrete formed inland of this area during the late Pliocene (Benbow *et al.* 1995). Aridity in the Pliocene waned many river systems, becoming

silty or ceasing in flow (Rogers & Zang 2006; Dart 2009). Quaternary times were marked by climatic oscillations of temperature, evaporation and rainfall on a global scale. The peak of the last glacial maximum 20-18 ka resulted in marine recession exposing the continental shelf, and maximum intensity of aeolian activity with continuous and/or cyclicity for at least the last 100 ka (Dart 2009). Erosion during the Pliocene to Quaternary cut into landscape and persistent strong winds in Pleistocene caused extensive dune fields (Sheard *et al* 2008). Prolonged tectonic stability and proposed weathering and erosion rates has given rise to the survival of ancient landforms and weathering profiles in the modern Australian landscape (Pillans 2007).

The palaeodrainage systems on a regional scale initiated possibly during the Cretaceous are continuing throughout the Cenozoic. At Tunkillia, spatial coincidence between the Au-in-calcrete anomaly and palaeochannels that drain the northern flanks of the Tunkillia divide was found by Airborne Electromagnetic (AEM) data (Lane & Worrall 2002). This suggested that geochemical signatures of the calcrete sampled at surface in this area would highlight this transported and dispersed anomaly. Furthermore, through a derivative map of drainage over 'Tomahawk', in association with Dart's symbolic drainage pathways overall over Tunkillia, the source area for this drainage could be shown hence providing a dispersion course for elements strongly associated with mineralisation (Dart 2009).

Using the RTP image, regolith-landform map, SPOT-5 Google Earth image, and topography, Figure 16 illustrates a revised derivative map of 'Tomahawk' as established by palaeo- and contemporary drainage identification. Furthermore in Figure 17, superimposed on Dart 2009's Tunkillia drainage map, the constraints of the palaeodrainage in this prospect can be further recognised. 'Tomahawk' is associated with a low lying area, and point of low, broad mixing zone from a number of palaeodrainage channels with origin from the southern drainage divide. This further supports the previous hypotheses made by Dart (2009), that the 'Tomahawk' study area, southeast of 'Area 191', is also potentially up-palaeo slope. This can be seen in Figures 15 and 16 where due to major and minor drainage divides, palaeodrainage is guided by topography in passing through both 'Tomahawk' and 'Area 191'.

5.1.2 BEDROCK / MINERALISATION

Rocks within the YSZ are associated with a geophysical gravity low (Lane & Worrall 2002). Magnetics of the YSZ define its margins, with zones of low magnetic response known as the Western Demagnetised Zone (WDZ) and Eastern Demagnetised Zone (EDZ) (Figure 18) (Martin & Wilson 2005).

Interpreted to be due to alteration by fluids travelling through the shear zones, work by Ferris and Wilson (in press) confirmed mineralisation at Tunkillia is most probably related to the fluid influx from syn-tectonic Hiltaba Suite granite emplacement within a reactivated YSZ. Structure appears to be the dominant control on mineralisation with the shear zone focusing the fluids and fault intersections and as a result these points act as trap sites or dilation zones (Martin & Wilson 2005).

The 'Tomahawk' anomaly resides in the EDZ of the Northern YSZ, where linear northwest to southeast bands of demagnetisation and assumed high deformation and mylonitisation are evident in TMI and RTP imagery (Flint 2005). Mylonite zones range from ~100-250 m wide, and splay towards the southeast (Flint 2005). To the east of the YSZ, highly magnetic lithologies are enigmatic, and may consist of Tunkillia Suite granitoids, Hiltaba Suite granitoids, or GRV (Flint 2005). 'Tomahawk' (and 'Area 191') occur between two mylonitic splays with demagnetisation of host deformed granitoids.

Within the 'Tomahawk' study area, southwest of the magnetic low denotes a region of locally higher magnetics and previously mentioned northwest to southeast bands of high deformation, as can be seen in Figure 19: a Reduction to Pole (RTP) magnetic image of the 'Tomahawk' study area. The previously determined 100 ppb contour Au-in-calcrete anomaly at intersection points along calcrete sampling transect one and two (note the 100 ppb contour does not intersect transect two) is plotted, and furthermore the high Au assay values (>75 ppb) returned from sampling occur within these contours. It may be possible to reconstruct the 100 ppb anomaly contours, based on the present results, so it extends further to the south where it would intersect transect two particularly. High values of Au (black dot) also occur in the margins of high deformation zones i.e. from

low (blue/purple) to medium (green) magnetic response. These high Au values also occur in the margins of the linear trends in the locally high magnetic zone (Figure 19).

Because the entire study area is within the YSZ which has undergone melt emplacement and fluid movement, the comparisons of mineralisation to various bedrock lithologies was not possible. Au was the only element of those of interest that show any real variation to structural controls over mineralisation.

The palaeodrainage channels roughly follow northwest to southeast structural trends as seen in Figure 20. The main demagnetised zone (EDZ) corresponds with palaeodrainage identified from interpretation of the SPOT-5 Google Earth image. The palaeodrainage is denoted by darker shading due to denser vegetation cover, and this is further supported in the south and southwest corner of the study area, where a magnetic low zone further corresponds with palaeodrainage. Additionally, these areas correlate to topographic low points, where in some cases the topographic contour follows the structural variations in magnetic response, while palaeodrainage follows topography as illustrated by the derivative map previous. Field mapping found silicified (silcreted) quartzose sediments in many of these areas, further supporting the palaeodrainage interpretation here. Because dispersion patterns of elements of interest are largely constrained along both palaeo- and contemporary drainage pathways (Dart 2009), this will also control placer mineralisation expressions, such as those corresponding to the setting of the ‘Tomahawk’ anomaly. In this case, the palaeolandscape suggests that a transported deposit/false anomaly within the palaeodrainage system has been produced from northerly dispersion down palaeoslope.

5.2 Expression of Mineralisation: Controls on Geochemistry

The primary Au-Ag mineralisation at Tunkillia is associated with pyrite, minor galena and sphalerite within quartz-sulphide veins in zones of chlorite-sericite alteration. Some supergene Au enrichment (Au only with low Ag contents) has been recognised by Minotaur Exploration within ferruginised saprock overlying mineralised bedrock. Overlying the mineralised zone is a secondary Au-depleted zone within saprock and saprolite, which is further overlain by a calcium carbonate indurated regolith layer that

is Au-enriched in parts of the ‘Tomahawk’ and wider Tunkillia area. The mechanisms for vertical Au depletion and enrichment within the profile are beyond the scope of this study, however they are worthy of further research. This study has however shown that the prevalence of palaeodrainage systems in the ‘Tomahawk’ area provide a mechanism for the geochemical signatures at the surface (i.e. Au-in-calcrete). The palaeo-drainage channels that have been identified in this study are therefore a major control on trace element dispersion and residence at ‘Tomahawk’.

The use of alternative geochemical mapping such as multi-element halos can prove to be effective in the definition of Au secondary geochemical signatures (Reis *et al.* 2001) and to interpret associations with possible mineralisation sources. Less influenced by effects of random errors, they consequently exhibit a closer relationship to the structural features associated with mineralisation (Reis *et al.* 2001).

The best indicator of Au mineralisation lies with elemental Au. With values ranging from 1-194 ppb, the majority of the higher values were from within CHep and $ISps_2$ regolith-landforms in the north of the study area. This also corresponds to lower margins of topography in the study area, and areas interpreted to be within palaeodrainage systems. The highest Au concentrations are from an $ISps_2$ unit surrounded by CHep landforms in transects one and two. This could potentially be a more recently formed landform, still revealing the remnant underlying landform. Even though Au is a relatively immobile element, it can be mobilised in the secondary environment and redeposited, perhaps due to changes in availability of complexing agents such as chlorides, thiosulphate and organic compounds, accumulation of clay minerals, evapotranspiration of water, and conditions involving a reducing environment i.e. high carbonate regions and low pH. Gold exhibits extremely high variance in the data (1055.044) and data have a positive skew (20.94). With moderate kurtosis compared to other elements in the study, this means that more of the variance is due to infrequent extreme deviations, which suggest a heterogeneous (i.e. ‘nuggety’) association of Au in the samples. This is further supported through the high standard deviation of 32.48 ppb compared to <5 for majority of other elements, excluding Al (2379.5 ppm).

Silver is also associated with primary mineralisation, and returned a majority of values below analytical DL. It was however detected at or near DL in samples collected in the $ISps_2$ unit which returned high Au values. In unit $CHep_1$, high Ag (0.091–0.11 ppm) and high Au was found in sample THKLK045 (479710E 6546212N), and is of particular interest. Flanking this high reading to the southwest are two consecutive readings of medium to high Ag content, in unit ISu_2, which may be an alteration halo associated with, and surrounding Au mineralisation. Silver has a variance of 0 and identifies that measured data does not vary from the average value for Ag. It has positive skew, however a much larger kurtosis (13.51) compared to Au, suggesting any variance that does occur is due to extreme deviations. This may be caused by the percentage of values below DL (89.82 %). Generally, the lack of Ag in regolith carbonate samples and the secondary mineralised oxide zone is consistent with preferential leaching of Ag from the primary mineralisation. This suggests that Ag has most likely been mobilised further north via palaeodrainage channels. Furthermore the small exposures of weathered *in situ* quartz veins (Figure 8, regolith map), particularly at 479833E 6546084N, could be associated with a source for the immediately downslope high values of Au and Ag detected in the samples.

Aluminium showed similar responses to Au, Cu and Fe, with high readings, however these were not specific to any regolith-landform unit. Aluminium is generally of low mobility in most regolith conditions, however it is mostly physically mobilised in the secondary environment as Al oxides (clay minerals). Variance is extremely high at 5661981.18 which combined with kurtosis, identifies that irregular extreme variations occur, further supported by a standard deviation of 2379.49 ppm with mean 6574.41 ppm. Higher values are concentrated in the central regions of transects with the exception of transect one where high values were returned at the north-eastern end. This could be possibly due to palaeodrainage channels in relation to weathering of parent materials. This provides clay minerals to move downslope and concentrate in the channels.

Previously studied As and Au associations in the environment have not been repeated in this particular study area. Over half of the assay results for As are below analytical DL

(<1 ppm) therefore keeping the variance low (1.39) and kurtosis reasonably high for the data set (5.44). This identifies that there are infrequent extreme deviations from the mean of 1.324 ppm, supported by the standard deviation of 1.18 ppm. This is further supported with one value classified as locally high in As at THKLK032 (479571E 6546361N), corresponding to a high value of Au within an $ISps_2$ unit. No association with landform is identifiable and this may reflect an absence of the mineral arsenopyrite, which generally relates to associations of As and Au.

Calcium abundance is high with maximum values of ~27 %. A majority of these high values (i.e. >23 %) are from CHep units, with only a small number in landforms $ISps_2$ and ISu_2. This corresponds to the sample medium being calcrete, which have high calcium content, and also identifies an association with palaeochannels because Ca is highly mobile under all conditions in the environment. Calcium returned the only negatively skewed data of the 12 element suite (-1.261). A low kurtosis of 2.8 suggests that the variance, which is relatively high for the dataset (20.60), is only partially due to infrequent extreme deviations, reflected in the reasonable spread, mean (19.94 %) and standard deviation of the data (4.54 %).

Copper abundance was generally high, with relatively patchy distribution of high values and no real trends in relation to palaeodrainage and/or landform. With a positive skew, Cu assays were up to 17 times the DL (1 ppm) and majority at least 2 times the DL. Kurtosis is relatively high (8.36) compared to majority of the other elements suggesting that with a variance of 4.30, extreme variations in the data exist, further supported by a standard deviation of 2.075 ppm even though the mean is only 5.49 ppm. Copper is considered reasonably immobile, and this is supported by the lack in focusing of concentrations within palaeodrainage channels, however overall reasonably elevated values still supporting the findings that the area is in close proximity to mineralisation. The previously mentioned sample THKLK045 in $CHep_1$, with high Au and Ag, also had a high Cu assay result (8.01–20 ppm).

Dispersion patterns for the main elements associated with mineralisation including Pb (galena PbS), Zn (sphalerite (Zn,Fe)S) and Fe (pyrite Fe_2S), have poor relationships

with the mineralised areas. They, as was found for Au, return higher local values in ISps and CHep units: topographically lower areas in the study area, and in the linear features of low magnetic response of the YSZ in the RTP image. All three elements have an association within the entire data set, particularly Pb and Fe, which could be due to a Fe-oxide hosted halo to the northeast of a possible mineralisation source, where Pb is less mobile and therefore more proximal to a sulphide source and Zn is more mobile and therefore occurs further from source.

Lead, Zn and Fe are all considered relatively immobile (Reimann *et al.* 1998), however, due to their dispersion patterns are mobile within the environment, where they can be incorporated within or bound to clay minerals during weathering (Dart 2009). High sorption properties of stable and mobile clay and Al/Fe oxide/hydroxide minerals are a major control on dispersion of many trace elements (Dart 2009), reflected in the number of elements closely correlated with Al_2O_3 and Fe_2O_3. Statistical data for Pb, Zn and Fe reveal all are positively skewed and almost all of the analytical results are above DL (Zn, 1.852 % below DL). Lead, with lowest kurtosis of the three (2.48), exhibits the highest variance (16.52) therefore suggesting that variance is not due to irregular extreme deviations. Evenly spread data is further supported by a standard deviation of 4.07 ppm with median of 8.315 ppm. Zn had the highest kurtosis and second highest for the 12 element spread of 11.18. This suggests variance at 10.554 was possibly due to extreme outliers of the dataset. Finally, Fe had the medium kurtosis (3.263) with low variance of 0.268, therefore indicating a relatively even spread of the values in the study area.

Lanthanum exhibits low mobility and this may explain the low concentrations in palaeodrainage channels and instead a reasonably patchy placement of high results relative to the regolith-landform setting. The low kurtosis (2.27) and variance (3.0) indicate a broad spread of results supported by a mean of 3.5 ppm and standard deviation of 1.7 ppm. Structurally however, La does not appear to associate with the main edges of the YSZ, and instead is closely associated with moderate magnetic responses in the central region of the shear zone. The element dispersion patterns in the Tunkillia area suggest weathering and transportation of material towards the north,

particularly along the palaeo- and contemporary drainage. Element dispersion in this area is therefore largely controlled by the landscape.

Uranium results suggest that this prospect has low potential for U mineralisation associations. High U values occur where there is a high and moderate-high value of Au, but is poorly constrained by landform assemblages, or structural trends. Uranium had low kurtosis (1.2) and variance (0.012) due to the low range of data obtained in the study area. Antinomy has a close association with Fe in returning high values, and therefore also similar relationships to the other elements associated with mineralisation Zn and Pb. Like these, Sb is generally of low mobility in most environments, but higher values concentrate within the central zone of transects two to four, which could be a confluence of upstream tributaries of palaeochannels. Sb, like U had low variance (0.001) and kurtosis (1.07).

5.3 Implications for Mineral Exploration Under Cover

The discovery of mineralisation at the Tunkillia Au prospect, along with other discoveries in regolith-dominated terrain, such as Challenger, demonstrates that regolith carbonates are an important mineral exploration sampling medium. Valuable characteristics include their widespread and abundant distribution, ease of field identification and their proven ability to provide at least an Au geochemical expression of buried mineralisation. A limitation, however, is the typically poor resolution and distinction between mineralised and ‘background’ settings at the prospect-scale, with comparatively homogenous geochemical expressions across large areas at Tunkillia and more specifically within the immediate vicinity of the ‘Tomahawk’ Au-in-calcrete anomaly (Lowrey 2007). When this occurs, however, it is possible to standardise results based on landforms or lithologies, and therefore relate the results to dispersion pathways in the contemporary landscape and the palaeolandscape and associated landscape processes.

It has been suggested that regolith carbonate sampling becomes less useful at sample spacings of less than approximately 200 m (Lowrey 2007). Instead it is more appropriate for reconnaissance surveys for locating areas of interest, then followed up

with more detailed surveys as mentioned above (Carver et al. 1987). Results from surface lag samples do, however, provide a broad spread of anomalous values compared to other geochemical techniques such as soils, and are more sensitive to minor mineralisation in bedrock providing a better anomaly contrast (Carver et al. 1987).

One implication for mineral exploration using regolith carbonates as a sample medium, is establishing that the medium being sampled is, in fact regolith carbonates. Past sampling projects have been less successful in testing an anomaly because calcrete was not sampled. Poorly constrained sampling projects have included sampling Tertiary calcareous sediment, variable carbonate morphological facies, or medium with only a thin coating of carbonates on other indurated regolith materials such as silcrete and ferricrete. Effervescence from hydrochloric (HCL) acid is used in the field to determine if the sample is truly a calcrete. This does not however determine the amount or type of calcrete, instead just whether carbonates are present in the sample, and numerous other materials can effervesce when HCl is added. If calcrete is consistently sampled however, it can provide a successful medium for sampling and identification of mineralisation.

In the vicinity of the ‘Tomahawk’ Au-in-calcrete anomaly, the previous mineral exploration techniques need to be further evaluated for their ability to have successfully tested for the presence of mineralisation. Regolith profiles from previous drilling, and re-logged in this study, suggest that previous RAB drilling conducted in this area may not have sufficiently tested the anomaly. Numerous ‘end of hole’ depths finished short of fresh bedrock ceasing in saprock or in some instances only saprolite, which is typically Au-depleted zone, even above Au-mineralisation. A further limitation of previous exploration is that calcrete sampling can only be conducted where calcrete is readily available, and hence areas where aeolian dunes are predominant have typically not been effectively or at least consistently sampled (e.g. if variable calcrete horizons within the dune sequence have instead been sampled) and require further supporting geochemical techniques such as soil and vegetation sampling to sufficiently test an area.

The Tunkillia prospect spatially provides a large mineralisation footprint, associated with smaller discrete areas of Au-mineralisation. The YSZ is a large structure, and may host other Au-mineralisation pockets within the Tunkillia prospect and tenement. This includes the area to the south of Tunkillia where the YSZ has so far not been thoroughly explored and offers potential for targets for Au exploration (Flint 2005). Mineralisation occurrences have been discovered in this area, including Myall, Sheoak and Bimba (Flint 2005) so there is the potential, even though much of the YSZ is covered by extensive dune systems, to explore using calcretes due to their extensive nature in the landscape. As the first wave of exploration in the Gawler Craton has passed and the major Au-in-calcrete anomalies have been drilled, the interpretation of the lower order anomalies and understanding the regolith processes will become much more important (Lintern *et al.* 1997).

6.0 CONCLUSION

The results from this study have major implications for mineral exploration in areas dominated extensively by aeolian cover. Regolith-landform mapping along with geochemical signatures from regolith carbonate sampling and regolith profile logging have assisted in the re-construction of the 'Tomahawk' palaeo- and contemporary landscape evolution particularly in relation to drainage pathways and the various dune phase development. In doing so, a means for lateral dispersion of Au from mineralised zones was established and hence the reasoning related to the 'spatially large' Au-in-calcrete anomaly.

In previous exploration in this area, Au was the only element analysed for samples in drilling and soil/calcrete sampling programs, and therefore the full geochemical potential of these samples was not optimised. By analysing a multi-element assay suite for regolith carbonates in this study, it is shown that Au and its associated mineralisation elements, particularly Ag, Pb, Zn, and Fe were once mobile within the secondary environment, and over time have been preferentially concentrated in indurated materials such as regolith carbonates. The highest Au concentration returned in the sampling area was 194 ppb roughly correlating with palaeodrainage channels.

Silver associated with primary mineralisation returned a majority of values below analytical DL, however was detected at or near detection limits in samples that returned high Au values. This further identifies particular areas of interest, some of which contain saprock exposures at surface, and possible alteration halos in relation to Au.

Through identification of landform controls, such as the southern drainage divide and associated minor divides, 'Tomahawk' is shown to be associated with a low lying area and point of low, broad mixing and confluence of several palaeovalleys (drainage depressions), with a provenance northwards from the southern drainage divide. From this study, the original Au-in-calcrete anomaly's association with palaeodrainage can be established, however further exploration needs to be conducted between the main southern drainage divide and 'Tomahawk' study area (i.e. further southeast) to further test the anomaly, and possibly locate a source of mineralisation.

Further questions do arise from this study and include the following:

- Was the calcrete enriched with Au and then eroded/transported down palaeochannels, or transported and later enriched with Au in solution via palaeochannels; i.e. how has Au come to be associated with the upper stages of the regolith; are Au and other elements still being added at the surface?
- Many of the nodules have coalesced to form discontinuous hardpan layers. Carbonate nodules have multiple stages of carbonate precipitation, which give rise to the concentrically zoned nodules which have then been cemented and coalesced. Is there textural evidence to indicate carbonate accumulations undergoing dissolution and re-deposition?

Should further drilling programs with new knowledge be successful in defining economic grade mineralisation, the significance of prioritising calcrete anomalies in other covered areas of the Gawler Craton will increase, while concentration of Au in regolith carbonates may mean that Au will prove to be a useful pathfinder element for other base metal deposits (McQueen et al. 1999).

7.0 ACKNOWLEDGEMENTS

I would like to sincerely thank my honours supervisor, Steve Hill, for his enthusiasm and support. It has given me the opportunity to develop a project that involves application of an alternative angle to mineral exploration, a field that I intend to undertake in the near future. Robert Dart has also been fantastic with his assistance to the workings of ArcGIS, and his expertise on calcrete.

This honours project would not have been possible without the initial interest and suggestion from Minotaur Exploration Ltd, in particular Richard Flint and Barry van der Stelt, for their assistance with data collection and project organisation. Also, thank you to Amy Lockheed and Iain Hutchesson for their support in the field, and to Minotaur for the provision of their Tunkillia camp, supplies, vehicles and funds for processing samples.

A big thanks to the other 'Tunkillia group' members; Amanda, Ben and Adam, and 'Steve's honours group', even though our projects were different, sharing ideas, assistance in interpreting new programs; and support; has been outstanding, as well as the fun we have had with extra-curricular activities keeping us sane! The 2009 honours group have been fantastic; we have all shared the experience of Geology at Uni Adelaide and without them, I probably wouldn't have made it to honours!

Finally a huge thanks to my family and friends for their support, and for showing interest in my studies, it has been a frantic year and degree, and their support is sincerely appreciated.

8.0 REFERENCES

ANAND R. R., PHANG C., WILDMAN J. E. & LINTERN M. J. 1997. Genesis of some calcretes in the southern Yilgarn Craton, Western Australia: implications for mineral exploration. *Australian Journal of Earth Sciences* **44**, 87-103.

BELPERIO A. 2006. Advancing Tunkillia. Paper presented at Paydirt's Gold Conference, Perth, Western Australia (unpubl.).

BENBOW M. C., ALLEY N. F., CALLEN R. A. & GREENWOOD C. R. 1995. Tertiary: Geological History and Palaeoclimate. *In:* Drexel J. F. & Preiss W. V. eds. *The Geology of South Australia. Volume 2, The Phanerozoic*, pp. 208-218. **54** Geological Survey. Bulletin, South Australia.

BUTT C. R. M., LINTERN M. J. & ANAND R. R. 2000. Evolution of regoliths and landscapes in deeply weathered terrain - implications for geochemical exploration. *Ore Geology Reviews* **16**, 167-183.

CARVER R. N., CHENOWETH L. M., MAZZUCCHELLI R. H., OATES C. J. & ROBBINS T. W. 1987. "Lag" - A Geochemical Sampling Medium for Arid Regions *Journal of Geochemical Exploration* **28**, 183-199.

CHEN X. Y., LINTERN M. J. & ROACH I. C. 2002. Calcrete: characteristics, Distribution and Use in Mineral Exploration. *Cooperative Research Centre for Landscape Environments and Mineral Exploration (CRC LEME), Canberra, Australia*, 170.

CROCKER R. L. 1946. *Post-Miocene climatic and geologic history and its significance in relation to the genesis of the major soil types of South Australia*. CSIRO (Commonwealth Scientific and Industrial Research Organization), Melbourne, Victoria, Australia.

DART R. 2009. Gold-in-calcrete: A continental to profile scale study of regolith carbonates and their association with gold mineralisation. PHD Thesis, University of Adelaide (unpublished) South Australia.

DART R. C., BAROVICH K. M. & CHITTLEBOROUGH D. 2005. Pedogenic carbonates, strontium isotopes and their relationship with Australian dust processes. *In:* Roach I. C. ed. *Regolith 2005 - Ten Years of CRC LEME.* CRC LEME, pp. 64-66.

DART R. C., BAROVICH K. M., CHITTLEBOROUGH D. J. & HILL S. M. 2007. Calcium in regolith carbonates of central and southern Australia: Its source and implications for the global carbon cycle. *Palaeogeography, Palaeoclimatology, Palaeoecology* **249**, 322-334.

EGGLETON R. A. ed. 2001. *The Regolith Glossary: surficial geology, soils and landscapes*. CRC LEME, Perth.

FERRIS G. & WILSON M. 2004. Tunkillia Project - Proterozoic shear-zone-hosted gold mineralisation within the Yarlbrinda Shear Zone. *MESA Journal* **35**, 6-12.

FERRIS G. M. & SCHWARZ M. 2004. Definition of the Tunkillia Suite, western Gawler Craton. *MESA Journal* **34**, 32-41.

FLINT R. B. 2005. Tunkillia joint venture opportunity for Minotaur / Oxiana into tenements ELs 2697 & 2854, ELA 2994/180 held by Helix Resources. Minotaur Exploration Adelaide, SA.

GIBBONS L. 1997. Regolith study of the Old Well gold prospect, Tarcoola District, Gawler Craton. The University of Adelaide, Adelaide (unpubl.).

GIBBONS S. & HILL S. M. 2005. Regolith carbonates of the Tibooburra/Milparinka Inliers, northwest NSW: characteristics, regional geochemistry and minerals exploration implications. *In:* Roach I. C. ed. *Regolith 2005 - Ten years of CRC LEME* CRC LEME, pp.107-111.

GOUDIE A. S. 1983. Calcrete. *In:* Goudie A. S. & Pye K. eds. *Chemical sediments and geomorphology; precipitates and residua in the near-surface environment*, pp. 93-131. Academic Press, London.

GRAY D. & PIRLO M. 2004. Geochemistry of Groundwaters at Tunkillia: Similarities and differences to Yilgarn Craton Groundwaters. *In:* Roach I. C. ed. *Regolith 2004*. CRC LEME, pp. 103-106.

GRAY D. & PIRLO M. 2005. Hydrogeochemistry of the Tunkillia Gold Prospect, South Australia. CRC LEME open file report 194, CRC LEME, Bentley.

GRAY D. J. & LINTERN M. J. 1998. Chemistry of gold in soils from the Yilgarn Craton, Western Australia, pp 209-221. *In:* Eggleton R. A. ed. *The state of the regolith. Proceedings of the second Australian conference on landscape evolution and mineral exploration* Geological Society of Australia Special Publication, Brisbane.

HAND M., REID A. & JAGODZINISKI L. 2007. Tectonic Framework and Evolution of the Gawler Craton, Southern Australia. *Economic Geology* **102**, 1377-1395.

HESSE P. P. & MCTAINSH G. H. 2003. Australian dust deposits: modern processes and the Quaternary record. *Quaternary Science Reviews* **118-119**, 87-102.

HILL S. M., GREENFIELD J. E., GILMORE P. G. & REID W. J. 2008. Guide for mineral exploration through and within the regolith in the southwestern Thomson Orogen, New South Wales.

HILL S. M., MCQUEEN K. G. & FOSTER K. A. 1999. Regolith carbonate accumulations in Western and Central NSW: characteristics and potential as an exploration sampling medium. *In:* Taylor G. M. & Pain C. F. eds. *State of the Regolith. Proc. Regolith 98*, pp. 191-208.

HOU B., FRAKES L. A., SANDIFORD M., WORRALL L., KEELING J. L. & ALLEY N. F. 2008. Cenozoic Eucla Basin and associated palaeovalleys, southern Australia - Climatic and tectonic influences on landscape evolution, sedimentation and heavy mineral accumulation. *Sedimentary Geology* **203**, 112-130.

JARVIS A., REUTER H. I., NELSON E. & GUEVARA E. 2006. Hole-filled seamless SRTM data V3. Online <http://srtm.csi.cgiar.org>

LANE R. & WORRALL L. 2002. Gawler Craton mineral promotion project: Interpretation of Airborne Electromagnetic Data Summary report on The Tunkillia Workshop.

LEVINSON A. A. 1974. *Introduction to Exploration Geochemistry*. Applied publishing, Ltd., Calgary, Alberta, Canada.

LINTERN M. J. 1997. Calcrete sampling for gold exploration. *MESA Journal* **5**, 5-8.

LINTERN M. J., BUTT C. R. M. & SCOTT K. M. 1997. Gold in vegetation and soil - three case studies from the goldfields of southern Western Australia. *Journal of Geochemical Exploration* **58**, 1-14.

LINTERN M. J., SHEARD M. J. & CHIVAS A. R. 2006. The source of pedogenic carbonate associated with gold-calcrete anomalies in the western Gawler Craton, South Australia. *Chemical Geology* **235**, 299-324.

LOWREY J. R. 2007. Plant Biogeochemical expression of Au-Mineralisation buried by an aeolian dunefield: Tunkillia, South Australia. Honours Thesis, University of Adelaide, Adelaide (unpublished.).

LOWREY J. R. & HILL S. M. 2006. Plant biogeochemistry of Au-mineralisation buried by an aeolian dunefield: Tunkillia, SA. *In:* Fitzpatrick R. W. & Shand P. eds. *Regolith 2006 - Consolidation and Dispersion of Ideas* CRC LEME, pp. 217-220.

MARTIN A. R. & WILSON M. H. 2005. Project Proposal: Lake Everard collaborative drilling program, drill testing of IP anomalies. Helix Resources Limited, Perth, WA.

MAYO A. M. & HILL S. M. 2005. Mineral exploration through an aeolian dunefield near Wudinna, Gawler Craton, South Australia: a framework of plant biogeochemistry and geobotany. *In:* Roach I. C. ed. *Regolith 2005 - Ten Years of CRC LEME.* CRC LEME, pp. 223-228.

MCQUEEN K. G., HILL S. M. & FOSTER K. A. 1999. The nature and distribution of regolith carbonate accumulations in southeastern Australia and their potential as a sampling medium in geochemical exploration. *Journal of Geochemical Exploration* **67**, 67-82.

METEOROLOGY B. O. 2009a. Climate statistics for Australian locations: Summary statistics for Tarcoola. Online <http://www.bom.gov.au/climate/averages/tables/cw_016044.shtml>

METEOROLOGY B. O. 2009b. Climate statistics for Australian locations: Summary statistics for Tarcoola Aero. Online <http://www.bom.gov.au/climate/averages/tables/cw_016098.shtml>

PILLANS B. 2005. Geochronology of the Australian Regolith. *In:* Anand R. R. & De Broekert P. eds. *Regolith landscape evolution across Australia*, pp. 41-52. CRC LEME, Perth.

PILLANS B. 2007. Pre-Quaternary landscape inheritance in Australia. *Journal of Quaternary Science* **22**, 439-447.

REIMANN C., AYRAS M., CHEKUSHIN V., BOGATYREV I., BOYD R., CARITAT P., DE DUTTER R., FINNE T. E., HALLERAKER J. H., JAEGER O., KASHULINA G., LEHTO O., NISKAVAARA H., PAVLOV V., RAISANEN M. L., STRAND T. & VOLDEN T. 1998. *Environmental Geochemical Atlas of the Central Barents Region* Norges Geologiske Undersokelse, Geological Survey of Norway, Trondheim, Norway.

REIS A. P., SOUSA A. J. & CARDOSO FONSECA E. 2001. Soil geochemical prospecting for gold at Marrancos (Northern Portugal). *Journal of Geochemical Exploration* **73**, 1-10.

ROGERS P. A. & ZANG W. 2006. Guide to the sedimentary cover of the Central Gawler Craton, South Australia (with special emphasis on the Harris Greenstone Belt region). Government of South Australia, Primary Industries and Resources SA, Report Book, 2006/01, South Australia.

ROSE A. W., HAWKES H. E. & WEBB J. S. 1979. *Geochemistry in Mineral Exploration* (Second edition). Academic Press Inc, London Ltd.

SANDIFORD M., QUIGLEY M., DE BROEKERT P. & JAKICA S. 2008. Tectonic framework for the Cainozoic cratonic basins of Australia. Online <http://jaeger.earthsci.unimelb.edu.au/msandifo/Publications/Manuscripts/Manuscripts/2008_IASV.pdf>

SHEARD M. J., KEELING J. L., LINTERN M. J., HOU B., MCQUEEN K. G. & HILL S. M. 2008. A guide for mineral exploration through the regolith of the Central Gawler Craton, South Australia.

SMITH B. H. & KEELE R. A. 1984. Some observations on the geochemistry of gold mineralisation in the weathered zone at Norseman, Western Australia. *Journal of Geochemical Exploration* **22**, 1-20.

TAYLOR G. & EGGLETON R. A. 2001. *Regolith geology and geomorphology*. John Wiley & Sons Ltd, West Sussex.

THOMAS M. 2004. Biogeochemical data ranges from Tunkillia prospect, central Gawler Craton, South Australia. *In:* Roach I. C. ed. *Regolith 2004* CRC LEME, pp. 362-364.

WILSON M. & SAVCIN S. 2004. Lake Everard - South Australia EL 2697 Annual Report, for the period 14/02/2003 to 13/02/2004, Helix Resources Limited (unpublished).

9.0 FIGURE CAPTIONS

Figure 1: The principal sources of pedogenic carbonate generation: its origin lies with a combination of geological, geomorphological and environmental conditions such as the presence of remnant outcropping Ca- and Mg-rich rocks, aridity and imperfect drainage (Lintern 1997).

Figure 2: The distribution of calcrete (red) and associated soils in Australia particularly noting abundance in Southern Australia (Lintern 1997).

Figure 3: Location map of the Tunkillia Au-Prospect, in relation to surrounding mines and towns, South Australia (Lowrey 2007).

Figure 4: Total Magnetic Intensity (TMI) image of the Tunkillia Au-Prospect tenement with the >10 ppb calcrete anomalies superimposed. Note the 'Tomahawk' prospect in relation to this calcrete anomaly and the Yarlbrinda Shear Zone (Ferris & Wilson 2004).

Figure 5: Various aged dune phases identified at the Tunkillia Au-prospect (Lowrey 2007).

Figure 6: Au normal probability plot for identifying the population subsets for localised low to high values.

Figure 7: Spatial distribution (easting vs. northing) plot of Au values based on the normal probability plot population subsets that can be used to associate 'hits' with landform and geological structures.

Figure 8: Regolith landform map of the 'Tomahawk' study area, Tunkillia.

Figure 9: Generalised typical regolith profile compiled from regolith logs taken in the field, found in Appendix 2b.

Figure 10: X-Y Scatter plot of Fe (%) and As (ppm), correlation r=0.840.

Figure 11: X-Y Scatter plot of Pb (ppm) and Fe (%), correlation r=0.788.

Figure 12: X-Y Scatter plot of Ca (%) and Au (ppb), correlation r=-0.132, highlighting the Ca % range in which majority of high Au values occur.

Figure 13: X-Y Scatter plot of Ag (ppm) and Au (ppb), correlation r=-0.306.

Figure 14.1: Spatial geochemical map of Au superimposed over regolith-landform map of 'Tomahawk'.

Figure 14.2: Spatial geochemical map of Ag superimposed over regolith-landform map of 'Tomahawk'.

Figure 14.3: Spatial geochemical map of Al superimposed over regolith-landform map of 'Tomahawk'.

Figure 14.4: Spatial geochemical map of As superimposed over regolith-landform map of 'Tomahawk'.

Figure 14.5: Spatial geochemical map of Ca superimposed over regolith-landform map of 'Tomahawk'.

Figure 14.6: Spatial geochemical map of Cu superimposed over regolith-landform map of 'Tomahawk'.

Figure 14.7: Spatial geochemical map of Fe superimposed over regolith-landform map of 'Tomahawk'.

Figure 14.8: Spatial geochemical map of La superimposed over regolith-landform map of 'Tomahawk'.

Figure 14.9: Spatial geochemical map of Pb superimposed over regolith-landform map of 'Tomahawk'.

Figure 14.10: Spatial geochemical map of Sb superimposed over regolith-landform map of 'Tomahawk'.

Figure 14.11: Spatial geochemical map of U superimposed over regolith-landform map of ‘Tomahawk’.

Figure 14.12: Spatial geochemical map of Zn superimposed over regolith-landform map of ‘Tomahawk’.

Figure 15: Topographic map of the Tunkillia prospect area, outlining the extent of the ‘Tomahawk’ Au-in-calcrete study area (black box); the position of the >10 ppb Au-in-calcrete anomaly (white) the locations of known mineralisation areas ‘223’ and ‘191’, and the general area of the drainage divide (contours with red = high). Data sourced from (Dart 2009), who obtained from (Jarvis *et al.* 2006).

Figure 16: Symbolic derivative map of the drainage pathways at ‘Tomahawk’ Au-in-calcrete anomaly, Tunkillia.

Figure 17: Symbolic derivative map of the drainage pathways at ‘Tomahawk’ Au-in-calcrete anomaly, Tunkillia, superimposed on the (Dart 2009) Tunkillia Drainage map.

Figure 18: Tunkillia calcrete anomaly on a detailed Reduction To Pole (RTP) magnetics image, also outlining the Western and Eastern Demagnetised Zones (WDZ & EDZ respectively) (Martin & Wilson 2005).

Figure 19: RTP image of the ‘Tomahawk’ study area identifying, the Eastern Demagnetised Zone (EDZ) the YSZ eastern boundary, linear deformation zones, previously identified contour intersections along study sampling transects, and subsequent Au assay results.

Figure 20: RTP image (colours) of the ‘Tomahawk’ study area with SPOT-5 Google Earth image, and topography (black lines) superimposed to identify the associations of structure and palaeo- and contemporary landforms.

10.0 TABLES

Table 1: Summary of the percentage of samples for each element that were below their respective detection limits, with percentage below detection given in the parentheses.

% below DL	**Elements** (% in parentheses)
0%	Au, Al, Ba, Be, Bi, Ca, Ce, Co, Cr, Cs, Dy, Er, Eu, Fe, Ga, Gd, Ho, K, La, Li, Mg, Mn, Nb, Nd, Ni, Pb, Pr, Rb, Sm, Sn, Sr, Tb, Th, Ti, Tl, Tm, U, Y, Yb, Zr.
1-5%	Cu (1.85), Hf (2.78), P (2.78), Sb (4.63), Zn (1.85).
6-25%	Cd (7.41), Mo (20.37), V (25.0).
26-50%	Sc (27.78).
51-75%	As (53.70), In (74.07), W (62.96).
76-99%	Ag (89.81), Pd (99.07), Pt (99.07), Te (81.48).
100%	Re, Se, Ta.

Table 2: QA/QC Summary of original field value vs. field duplicates.

Element	# within 95 % CI	Total Duplicates	% within 95 % CI
Al	8	10	80
Au	6	10	60
Ca	8	10	80
Ce	8	10	80
La	8	10	80
U	8	10	80
Th	9	10	90
Pb	8	10	80
Zn	6	10	60
Sb	7	10	70
Cu	6	10	60
Fe	8	10	80
TOTAL	90	120	**75 %**

Table 3: QA/QC Summary of original Au field value vs. Au lab repeats.

Element	# within 95 % CI	Total Duplicates	% within 95 % CI
Al	5	6	83
Au	6	6	100
Ca	5	6	83
Ce	6	6	100
La	6	6	100
U	6	6	100
Th	6	6	100
Pb	6	6	100
Zn	6	6	100
Sb	6	6	100
Cu	5	6	83
Fe	6	6	100
TOTAL	69	72	**96 %**

Table 4: QA/QC Summary of original field value vs. lab duplicates.

Element	# within 95 % CI	Total Duplicates	% within 95 % CI
Al	6	8	75
TOTAL	6	8	**75 %**

Table 5: Significant correlations (-0.75>r>0.75) identified between elements in the 59 element analysis suite with values for elemental correlation associations denoted in the parentheses. In the case of REEs the range associated with correlations to other REEs is within the parentheses.

Element of Interest	Significant r correlations with elements
Fe (%)	As (0.840), Bi (0.921), Cr (0.948), Ga (0.809), Hf (0.794), In (0.900), Mo (0.791), Pb (0.788), Th (0.894), V (0.939), Zr (0.805).
Al (ppm)	Cs (0.947), K (0.878), Li (0.819), Rb (0.924), Sn (0.814).
REEs	Ce (0.897-0.952), Dy (0.945-0.999), Er (0.940-0.996), Eu (0.930-0.997), Gd (0.926-998), Ho (0.939-0.997), La (0.897-0.993), Nd (0.920-0.998), Pr (0.925-0.996), Sm (0.931-0.994), Tb (0.940-0.994), Tm (0.942-0.994), Y (0.917-0.995), Yb (0.952-0.994)

Table 6: Justification for selection of the 12 key elements.

Element	Crustal Abundance (ppm) (Levinson 1974)	Main Geological Occurrence in rock and mineral (Reimann *et al.* 1998)	Previous Tunkillia Prospect Significance
Au	0.004	Native Gold	Found hosted in quartz-sulphide veins (Ferris & Wilson 2004).
Ag	0.07	Mineral, argentite, native Host Mineral: galena, sphalerite, chalcopyrite, aresnites Rock: gabbro, basalt, shale, schist, granite, granodiorite, coal	Associated with main alteration zone with a 4:1 Ag:Au ratio (Dart 2009).
Pb	12.5	Mineral: galena, anglesite Host Mineral: K-feldspar, plagioclase, mica, zircon, magnetite Rock: shale, schist, granite, granodiorite,	Associated with Mineralisation (galena mineral) (Lane & Worrall 2002)
Zn	70	Mineral: sphalerite, smithonite, wurtzite Host mineral: pyroxenes, amphiboles, mica, garnet, magnetite Rock: Shale, schist, gabbro, basalt, greywacke, ultramafic rock.	Associated with Mineralisation (Lane & Worrall 2002)
Sb	0.2	Mineral: stibnite, kermesite, valentinite Host Mineral: ilmenite, Mg-olivine, galena, sphalerite, pyrite Rock: Coal, Shale, schist, granite, granodiorite.	Small amounts present in Tunkillia suite host rock
La	30	Mineral: monazite, bastnaesite Host rock: Biotite, apatite, pyroxenes, feldspars, zircon Rock: Granite, granodiorite, schale schist, greywacke	Available in large quantities in the earth's crust
Ca	33 000 (Rose *et al.* 1979)	Mineral: calcite, gypsum, fluorite, feldspars, amphiboles, Rock: Limestone, Gabbro, basalt, Ultramafic rock, Shale, schist	World's largest >10 ppb (spatially) Au-in-calcrete anomaly
Fe	46 500 (Rose *et al.* 1979)	Minerals: Magnetite, Hematite, goethite/limonite, pyrite Host Minerals: olivine, pyroxenes, amphiboles, micas, garnets	Associated with Mineralisation (pyrite mineral) (Dart 2009).
Al	81 000 (Rose *et al.* 1979)	Mineral: Feldspars, Mica, clays – kaolinite Rock: Shale, schist, Gabbro, basalt, Granite, granodiorite.	Present through plagioclase feldspar within the granitoids of the Tunkillia Suite
As	1.8	Mineral: Arsenopyrite, Realgar, orpiment, Host minerals: feldspars, magnetite, ilmenite, pyrite, galena, sphalerite, apatite Rock: Granite, granodiorite, Schale, schist, coal	Small amounts present in Tunkillia suite host rock, no real known significance.
Cu	55	Mineral: chalcopyrite, bornite, chalcosite, malachite, covellite, digenite, native Cu Host mineral: Mica (biotite), pyroxene, amphibole, magnetite Rock: Gabbro, basalt, shale, schist, ultramafic rock	No known significance
U	2.7	Mineral: Uraninite/pitchblende, brannerite, carnotite Host mineral: Zircon, apatite, allanie, monazite Rock: Granite, granodiorite, schale schist, sandstone	No known significance

Table 7: Summary statistics for selected elements from the 'Tomahawk' Tunkillia calcrete geochemistry data set.

	Au (ppb)	Ag (ppm)	Al (ppm)	As (ppm)	Ca (%)	Cu (ppm)	Fe (%)	La (ppm)	Pb (ppm)	Sb (ppm)	U (ppm)	Zn (ppm)
Counts	108	108 (97<DL)	108	108 (57<DL)	108	108 (2<DL)	108	108	108	108 (5<DL)	108	108 (2<DL)
Minimum	1	0.025	2474	0.5	0.78	0.5	0.24	2.75	1	0.01	0.1	0.5
Maximum	194	0.11	19361	7	27.06	17	2.81	22.92	9	0.15	0.64	23
Range	193	0.085	16887	6.5	26.28	16.5	2.57	20.17	8	0.14	0.54	22.5
Mean	36.824	0.029	6574.417	1.324	19.943	5.491	0.769	8.670	3.528	0.059	0.270	4.241
Median	27	0.025	6358	1	20.36	5	0.59	8.315	3	0.06	0.25	3.5
Variance	1055.044	0.000	5661981.180	1.394	20.604	4.304	0.268	16.524	2.999	0.001	0.012	10.554
Standard Deviation	32.481	0.014	2379.492	1.181	4.539	2.075	0.518	4.065	1.732	0.025	0.108	3.249
Skewness	2.094	3.600	1.674	2.089	-1.261	1.618	1.835	1.369	1.465	0.474	1.003	2.740
Kurtosis	5.647	13.512	6.795	5.439	2.800	8.361	3.263	2.480	2.272	1.074	1.200	11.175
Analytical Detection Limit	1.0	0.05	20	1	0.01	1	0.01	1	0.01	0.02	0.01	1
% Below DL	0.000	89.815	0.000	53.704	0.000	1.852	0.000	0.000	0.000	4.630	0.000	1.852

Table 8: Correlation matrix for the 12 elements examined in table 7, with bold numbers identifying correlations of >0.5.

	Au (ppb)	Ag (ppm)	Al (ppm)	As (ppm)	Ca (%)	Cu (ppm)	Fe (%)	La (ppm)	Pb (ppm)	Sb (ppm)	U (ppm)	Zn (ppm)
Au (ppb)	1.000											
Ag (ppm)	0.306	1.000										
Al (ppm)	0.458	0.031	1.000									
As (ppm)	0.371	0.161	0.366	1.000								
Ca (%)	-0.132	0.179	-0.072	-0.170	1.000							
Cu (ppm)	0.088	0.243	0.303	0.324	0.232	1.000						
Fe (%)	0.367	0.089	0.483	**0.840**	-0.404	0.259	1.000					
La (ppm)	-0.031	0.176	0.236	0.157	**0.528**	0.326	0.048	1.000				
Pb (ppm)	0.258	0.007	0.442	**0.663**	-0.448	0.155	**0.788**	0.149	1.000			
Sb (ppm)	0.142	0.244	0.137	0.208	0.042	0.110	0.286	0.082	0.096	1.000		
U (ppm)	**0.517**	0.048	**0.521**	**0.630**	0.091	0.163	**0.507**	0.262	0.362	0.245	1.000	
Zn (ppm)	0.127	-0.077	**0.585**	0.288	-0.444	0.272	0.469	-0.076	0.498	-0.040	0.120	1.000

APPENDIX 1

Regolith-Landform Map of ‘Tomahawk’, Tunkillia, S.A.

Appendix 1a: Enlarged regolith-landform legend, with codes, photo and GPS reference of each unit.

Aeolian Sediments

ISu_1	Red-brown, well sorted, fine to medium-grained quartzose sands with iron-oxide and clay cutans on a low relief, longitudinal dune. Open woodland dominated by *Acacia anuera, Eucalyptus socialis, Acacia ramulosa* and *Acacia ligulata*. Occasional *Eucalyptus concinnia* and *Casuarina pauper* with extensive, well developed surficial cryptogram crust on the soil surface.

Map Location (GPS): Easting: 478990, Northing: 6545596 Photo Example: Appendix 1b.1

ISu_2	Light red-brown, well sorted, fine to medium-grained, quartzose sands with iron-oxide and clay cutans on a moderate relief, longitudinal dune. Open woodland dominated by *Eucalyptus socialis, Triodia irritans, Acacia ramulosa, Bossiaea walkeri* and *Triodia scariosa, Acacia ligulata* and *Acacia burkittii.* Moderate cover of surficial cryptogram crust on the soil surface.

Map Location (GPS): Easting: 480493, Northing: 6546692 Photo Example: Appendix 1b.2,3

ISu_3	Brown to light red-brown, well sorted, fine to medium-grained quartzose sand with iron-oxide and clay cutans on a high relief, longitudinal dune. Mobile crests impinge on older ISu_1 and ISu_2 landforms, and therefore vegetation is partially covered by sand and characterises older landforms: Open woodland dominated by *Acacia ramulosa, Casuarina pauper, Bossiaea walkeri, Acacia aneura* and *herbs and tussock grasses.*

Map Location (GPS): Easting: 478121, Northing: 6545894 Photo Example: Appendix 1b.4,5

$ISps_1$	Red-brown, moderate to poorly-sorted, fine to medium-grained, quartzose sand with iron-oxide cutans on a low-relief sand plain/dune swale. Well developed cover of cryptogram crust on the soil surface. Open woodland dominated by *Eucalyptus concinnia, Maireana sedifolia* and *Cratystylis conocephala*. Occasional *Casuarina pauper*, *Acacia anuera* and *Acacia ligulata*.

Map Location (GPS): Easting: 481025, Northing: 6544680 Photo Example: Appendix 1b.6

$ISps_2$	Red-brown, moderately to well-sorted, fine to medium-grained, quartzose sand with iron-oxide cutans on a low-relief sand plain/dune swale. Iron-oxide, lithic and quartz lag of <0.2cm. Open woodland dominated by *Casuarina pauper, Maireana sedifolia and Cratystylis conocephala.* Occasional *Eucalyptus concinnia, Acacia birkittii* and *Acacia ligulata.*

Map Location (GPS): Easting: 479060, Northing: 6546056 Photo Example: Appendix 1b.7

Aed	Red-brown, very fine to fine-grained, well sorted and well rounded consolidated clayey/silty soils, on a flat lying erosional drainage area. Minor medium-grained quartz and very high cover of cryptogram crust on the soil surface. Occasional minor calcrete and silcrete nodules, well rounded-sub rounded <2.0cm. Open woodland of dense thickets of *Acacia aneura* with occasional *Casuarina pauper*. Chenopod understorey of *Maireana sedifolia,* and *Acacia ligulata*.

Map Location (GPS): Easting: 480169, Northing: 6546029 Photo Example: Appendix 1b.8

Aaw	Red-brown, very fine to fine-grained, well sorted consolidated clayey soils with very well developed cryptogram crust on the soil surface. Occasional rounded to sub-rounded calcrete and silcrete nodules <3.0cm. Chenopod shrubland of *Casuarina pauper* and *Acacia ligulata*, occasional *Acacia anuera*, *Maireana sedifolia* and well developed cover of cryptogram crust on the soil surface.

Map Location (GPS): Easting: 480169, Northing: 6546029 Photo Example: Appendix 1b.9

Appendix 1a: Enlarged regolith-landform legend, with codes, photo and GPS reference of each unit.

Sheetflow Sediments

CHep$_1$	Light brown to red, moderately sorted, fine to medium-grained quartzose sand with medium-grained sub-rounded quartz, iron-oxide <1.0cm and silcrete <2.0cm. High occurrence of sub-rounded to rounded 0.5-8.0cm nodular calcrete lag on a low relief landform dominated by sheetflow sedimentary transport and well developed cover of cryptogram crust on the soil surface. Open woodland dominated by *Casuarina pauper* and occasional *Eucalyptus concinnia* and *Acacia aneura* thickets, with chenopod shrubland understorey dominated by *Maireana sedifolia*, *Cratystylis conocephala* and *Senna artesmesioides*.
	Map Location (GPS): Easting: 479564, Northing: 6545659 Photo Example: Appendix 1b.10
CHep$_2$	Red-brown to brown, moderately sorted, fine to medium-grained quartzose sand with angular to rounded silcrete lag <8.0cm on a low relief landform dominated by sheetflow sedimentary transport. Sub-rounded to rounded nodular calcrete lag <5.0cm, iron-oxides <2.0cm and a moderate cover of cryptogram crust on the soil surface. Chenopod shrubland dominated by *Maireana sedifolia*, *Cratystylis conocephala* and occasional *Casuarina pauper, Senna artesmesioides* and *Acacia anuera.*
	Map Location (GPS): Easting: 479845, Northing: 6546737 Photo Example: Appendix 1b.11
CHep$_3$	Brown-red, well sorted, fine to medium-grained quartzose sand. Low relief landform dominated by sheetflow sedimentary transport with a well developed cover of cryptogram crust on the soil surface. Angular to sub-angular calcrete <5.0cm and shallow <50cm hardpan carbonates. Rounded iron-oxide and sub-angular to sub-rounded silcrete grains <1.0 to 6.0cm cm and sub-angular to sub-rounded vein quartz <3.0cm. Chenopod shrubland dominated by *Maireana sedifolia*, *Cratystylis conocephala*, *Casuarina pauper*, *Senna artesmesioides* and *Acacia anuera*.
	Map Location (GPS): Easting: 479703, Northing: 6546685 Photo Example: Appendix 1b.12, 13
CHpd$_1$	Brown-red, well sorted, very fine to fine-grained, quartzose sand with coarse sand sized grains of sub-angular to rounded quartz, iron-oxide, lithic and carbonates on a colluvial sheetflow depositional plain. Occasional angular to sub-rounded carbonates from 1-5cm. Very well developed cover of cryptogram crust on the soil surface. Open woodland dominated by *Casuarina pauper* with occasional *Eucalyptus concinnia*. Chenopod understorey of *Maireana sedifolia*, *Cratystylis conocephala*, *Acacia ligulata* and *Senna artesmesioides*.
	Map Location (GPS): Easting: 480654, Northing: 6547223 Photo Example: Appendix 1b.14,15
CHpd$_2$	Light brown to red, moderate to well sorted, very fine to fine-grained quartzose sand with medium sized grains of iron-oxide, quartz and sub-angular carbonates on a colluvial sheetflow depositional plain. Medium cover of cryptogram crust on the soil surface. Open woodland dominated by *Eucalyptus concinnia*, *Acacia ligulata*, *Senna artesmesioides* and *Cratystylis conocephala*. Occasional *Eucalyptus socialis*, *Casuarina pauper* and *Maireana sedifolia*. More dense low lying vegetation than CHpd$_1$.
	Map Location (GPS): Easting: 480862, Northing: 6546925 Photo Example: Appendix 1b.16

Saprolith

SMep	Small exposures of moderately weathered, *in situ* Quartz vein.
	Map Location (GPS): Easting: 479833, Northing: 6546084

Appendix 1b: Image representation of regolith-landform units in the 'Tomahawk' study area, identifying characteristic properties.

Photo 1b.1: **ISu_1**

Photo 1b.2, 3: **ISu_2**

Photo 1b.4, 5: **ISu_3**

Appendix 1b: Image representation of regolith-landform units in the 'Tomahawk' study area, identifying characteristic properties.

Photo 1b.6: **$ISps_1$**

Photo 1b.7: **$ISps_2$**

Appendix 1b: Image representation of regolith-landform units in the 'Tomahawk' study area, identifying characteristic properties.

Photo 1b.8: **Aed**

Photo 1b.9: **Aaw**

Appendix 1b: Image representation of regolith-landform units in the 'Tomahawk' study area, identifying characteristic properties.

Photo 1b.10: **$CHep_1$**

Photo 1b.11: **$CHep_2$**

Photo 1b.12, 13: **$CHep_3$**

Appendix 1b: Image representation of regolith-landform units in the 'Tomahawk' study area, identifying characteristic properties.

Photo 1b.14,15: **CHpd$_1$**

Photo 1b.16 **CHpd$_2$**

APPENDIX 2

Regolith Profile Logs

Appendix 2a: Location of regolith profile logs in the 'Tomahawk' study area.

2a.1 Location of regolith profile logs (red dots) on regolith-landform map of the 'Tomahawk' study area (numbering next to location corresponds to log number, Appendix 2b).

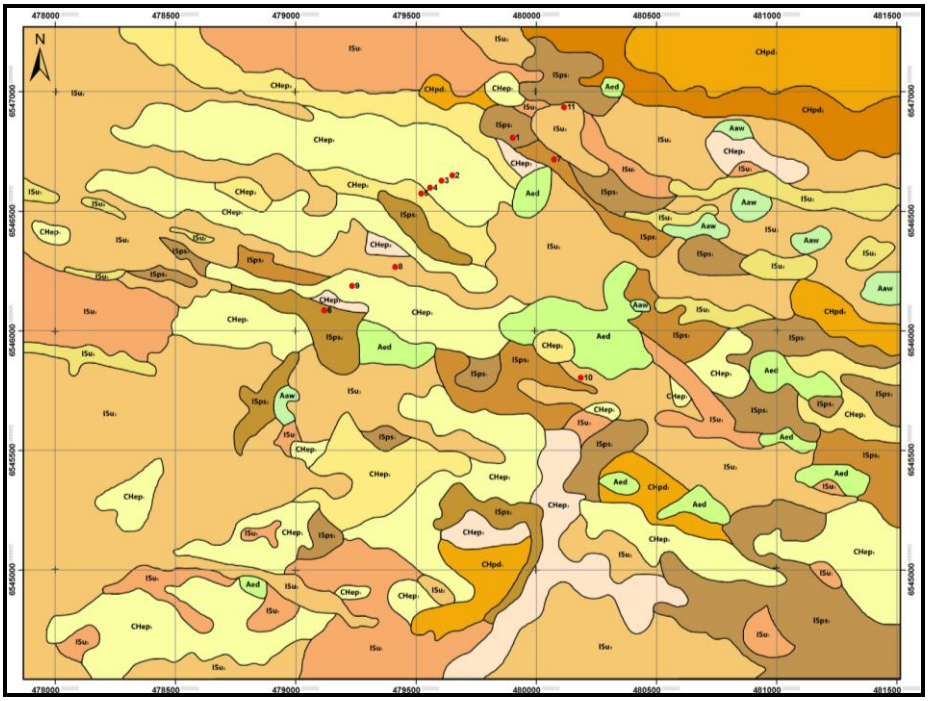

2a.2 Location of regolith profile logs on SPOT-5 Google Earth base map image of the 'Tomahawk' study area.

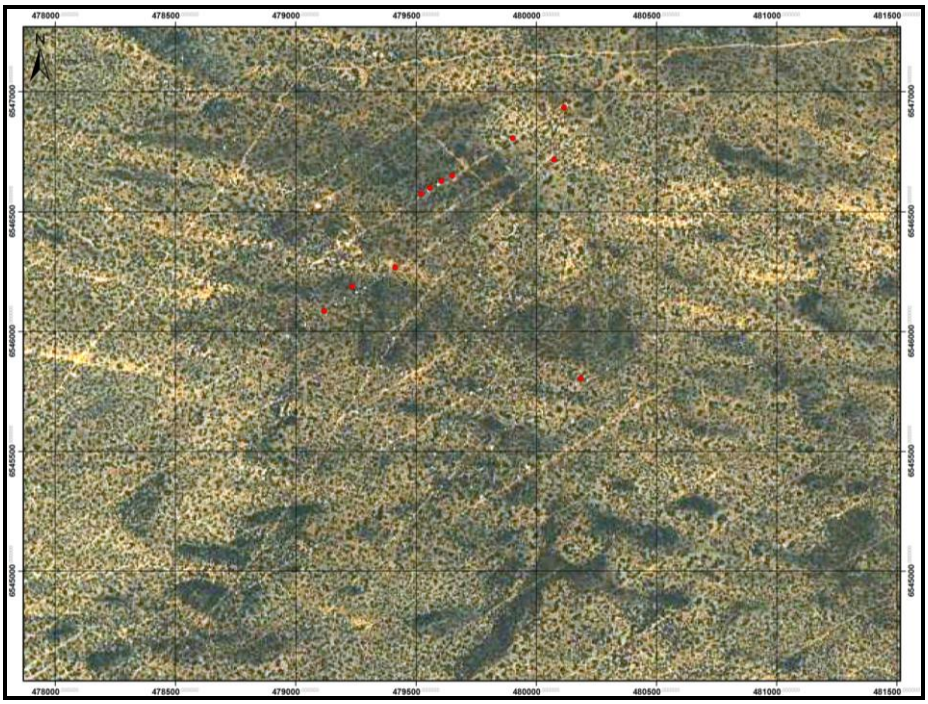

Appendix 2b: Regolith profile logs in the 'Tomahawk' study area.

Regolith Profile 1 Easting: 479902 Northing: 6546807

Depth (m)	Lithology	Colour	Description
1–3	Sediment Cover	Brown	Brown, well-rounded and well-sorted, fine-grained quartzose sand matrix with minor medium-grained sub-round quartz grains.
4–19	Saprolite	White	White, kaolinitic zone with very fine-grained, well sorted matrix of powder/clay texture. Minor medium-grained sub-angular quartz and plagioclase feldspar. Increasing down profile was the amount of sub-angular to sub-rounded underlying saprock grains up to 1cm size.
20–27	Saprolite	Pink-Orange	Matrix has been lost to erosion and weathering. Remaining, is pink-orange coarse sand to gravel sized sub-angular K-feldspar, plagioclase feldspar, quartz, goethite and minor micas. Weathering has occurred due to the presence of goethite.
28–34	Saprock	Brown-Grey	Brown-grey, coarse sand to gravel sized sub-angular to sub-round k-feldspar, quartz and plagioclase feldspar. Chlorite alteration visible, and rock is overall increasingly fresher (no goethite).
35–52	Saprock	Brown-Grey	Brown-grey, gravel sized sub-angular to sub-round k-feldspar, quartz, plagioclase feldspar. Chlorite alteration still present, and goethite alteration returns.
53–54	Fresh Bedrock	Grey	Grey, gravel sized sub-angular to sub-round fresh bedrock with visible gneissic fabric and mineralogy of mica, k-feldspar, quartz, plagioclase feldspar. No chlorite alteration visible.

Regolith Profile 2 Easting: 479651 Northing: 6546649

Depth (m)	Lithology	Colour	Description
1	Silcrete ?	Dark Brown-Red	Soil matrix has been lost to erosion and weathering. Any remaining is very fine-grained brown-red. Gravel to cobble sized sub-angular to sub-round calcite, silcrete grains with goethite weathering.
2			
3			
4			
5	Saprolite	White	White, kaolinitic zone with very fine-grained, well-sorted matrix of clay/powder texture. Medium-grained, sub-round quartz and minor plagioclase feldspar grains.
6			
7			
8			
9			
10			
11			
12			
13			
14			
15			
16			
17			
18			
19			
20			
21			
22			
23			
24			
25			
26			
27			
28			
29			
30			
31			
32		Cream	Cream, very fine-grained, well-rounded clay/powder texture matrix, with mineralogy of sub-round feldspars, quartz and weathering mineral of goethite.
33			
34			
35			
36			
37			
38			
39			
40			
41			
42			
43			
44			
45			
46			
47			
48			
49			
50			
51			
52	Saprock	Brown-Cream	Brown-cream, gravel sized, sub-angular to sub-round k-feldspar, quartz and plagioclase feldspar grains, with notable chlorite alteration; minor weathering of goethite, and down profile strength in weathering decreases. Approaching fresh rock at base of hole, however has not been fully reached.
53			
54			
55			
56			
57			
58			
59			
60			
61			
62			
63			
64			
65-67			

Regolith Profile 3 Easting: 479607 Northing: 6546627

Depth (m)	Lithology	Colour	Description
1	Silcrete ?	Dark Brown-Red	Soil matrix has been lost to erosion and weathering. Any remaining is very fine-grained brown-red. Gravel to cobble sized sub-angular to sub-round calcrete, goethite and silcrete grains.
2			
3			
4	Saprolite	White	White, kaolinitic zone with very fine-grained, well-sorted matrix of clay/powder texture. Medium-grained, sub-round quartz and minor plagioclase feldspar grains.
5			
6			
7			
8			
9			
10			
11			
12			
13			
14			
15			
16			
17			
18			
19			
20			
21			
22			
23			
24			
25			
26			
27		Cream-Brown	Any finer grained matrix has been lost. Cream-brown, 0.5-1cm sized gravel, sub-angular to sub-round white plagioclase feldspar and quartz. Highly weathered, all colour has been leached.
28			
29			
30		Olive-Brown	Olive-brown, 0.5-1cm sized gravel, sub-angular to sub-rounded white plagioclase feldspar and quartz with minor k-feldspar. Highly weathered all colour has been leached, with minor chlorite alteration visible.
31			
32			
33			
34			
35			
36			
37			
38	Saprock	Orange-Brown	Orange-brown, gravel sized sub-angular to sub-round quartz, k-feldspar, plagioclase feldspar and micas. Chlorite alteration and goethite weathering visible. Down profile, rock increases in fresh nature with content of k-feldspar increasing till rock is almost all dark-pink in colour.
39			
40			
41			
42			
43			
44	Fresh Bedrock	Grey	Grey, gravel sized sub-angular to sub-round fresh bedrock with visible gneissic fabric and mineralogy of mica, k-feldspar, quartz, plagioclase feldspar. No chlorite alteration visible.
45			

Regolith Profile 4 Easting: 479559 Northing: 6546598

Depth (m)	Lithology	Colour	Description
1	Calcrete ?	Cream	Cream, 0.5-2.0cm sized well rounded nodular and minor sub-angular silcrete. If matrix was present, it has now been lost to weathering and erosion.
2			
3			
4	Saprolite	Yellow	Yellow, very fine-grained matrix well-sorted and well-rounded. 0.5-1cm sized gravels, sub-rounded mineralogy of quartz, and plagioclase? High goethite weathering giving the yellow colour.
5			
6			
7		White	White, kaolinitic zone with very fine-grained, well-sorted matrix of clay/powder texture. Medium-grained, sub-round quartz and minor plagioclase feldspar grains.
8			
9			
10			
11			
12			
13			
14			
15			
16			
17			
18			
19			
20			
21		Brown-Grey	Brown-grey, coarse sand to gravel sized sub-angular to sub-round k-feldspar, quartz and plagioclase feldspar. Chlorite alteration visible, and rock is overall increasingly fresher (no goethite).
22			
23			
24			
25			
26			
27			
28			
29	Saprock	Orange-Brown	Orange-brown, gravel sized sub-angular to sub-round quartz, k-feldspar, plagioclase feldspar and micas. Chlorite alteration and goethite weathering visible.
30			
31			
32			
33			
34			
35			
36		Orange-Brown / Grey	Orange-brown with increasing quantity of grains of Brown-grey colour, gravel sized sub-angular to sub-round quartz, k-feldspar, plagioclase feldspar and micas. Chlorite alteration and goethite weathering visible. Approaching fresh basement at end of hole, however has not been fully reached.
37			
38			
39			
40			
41			
42			
43			
44			
45			
46			
47			
48			

Regolith Profile 5 Easting: 479522 Northing: 6546574

Depth (m)	Lithology	Colour	Description
1–3	Sediment Cover	Brown	Brown, well-rounded and well-sorted, fine-grained quartzose sand matrix with minor medium-grained sub-round quartz grains.
4–12	Saprolite	Yellow	Yellow, very fine-grained matrix well-sorted and well-rounded. 0.5-1cm sized gravels, sub-rounded mineralogy of quartz, and plagioclase? High goethite weathering giving the yellow colour.
13–26	Saprolite	White	White, kaolinitic zone with very fine-grained, well-sorted matrix of clay/powder texture. Medium-grained, sub-round quartz and minor plagioclase feldspar grains.
27–36	Saprolite	Cream-Brown	Any finer grained matrix has been lost. Cream-brown, 0.5-1cm sized gravel, sub-angular to sub-round white plagioclase feldspar and quartz. Highly weathered all colour has been leached.
37–40	Saprock	Brown-Grey	Brown-grey, gravel sized sub-angular to sub-round k-feldspar, quartz, plagioclase feldspar. Chlorite alteration still present, and goethite alteration returns. Basement has not been reached.

Regolith Profile 6 Easting: 479119 Northing: 6546085

Depth (m)	Lithology	Colour	Description
1	Sediment Cover	Dark Brown-Red	Dark brown-red, fine to medium-grained sub-rounded and well-sorted quartzose sand matrix with fine-grain sub-rounded quartz and calcrete.
2			
3	Silcrete ?	Orange-Yellow	Orange-yellow, sub-round to sub-angular gravel sized silcrete, with quartz grains within the silcrete, and goethite weathering visible.
4	Saprolite	Cream	Cream, very fine-grained, well-rounded, well-sorted clayey matrix with mineralogy of sub-angular quartz and minor silcrete possibly from contamination.
5			
6		Yellow	Yellow, very fine-grained, well-rounded, well-sorted clayey matrix with mineralogy of sub angular quartz. Goethite staining visible.
7			
8			
9			
10		White	White, kaolinitic zone with very fine-grained, well-sorted matrix of clay/powder texture. Medium-grained, sub-round quartz and minor plagioclase feldspar grains.
11			
12			
13			
14			
15			
16			
17			
18			
19			
20			
21			
22			
23			
24			
25			
26			
27			
28			
29			
30			
31			
32			
33			
34			
35	Saprock	Brown-Grey	Brown-grey, gravel sized sub-angular to sub-round k-feldspar, quartz, plagioclase feldspar. Chlorite alteration still present, and overall rock appears increasingly fresh, however, fresh basement has not been reached.
36			
37			
38			
39			
40			
41			
42			
43			
44			
45			
46			
47			
48			
49			
50-54			
55		Olive-Brown	Brown-green, coarse sand to gravel sized sub-angular to sub-rounded k-feldspar plagioclase feldspar with increased quartz content from saprock above. Chlorite alteration is also stronger and rock is increasingly fresh but does not reach fresh rock.
56			
57			
58			
59			
60			

Regolith Profile 7 Easting: 479902 Northing: 6546807

Depth (m)	Lithology	Colour	Description
1	Nodular Calcrete	Cream	Cream, very fine-grained well-sorted and well-rounded matrix with 0.2-1.5cm calcrete nodules.
2	Sediment Cover	Dark-Brown Red and Cream	Light-brown matrix of fine-grained, well-sorted and well-rounded quartzose sands, with strong dark-brown red textures of sub-angular to sub-rounded 0.2-4cm size silcrete, calcrete, quartz vein and Fe-oxides.
3			
4	Saprolite	Yellow	Yellow, very fine-grained, well-sorted and well-rounded matrix, with sub-angular <2cm sized silcrete and quartz grains. Goethite weathering visible.
5			
6			
7			
8		White	White, kaolinitic zone with very fine-grained, well-sorted matrix of clay/powder texture. Medium-grained, sub-round quartz and minor plagioclase feldspar grains.
9			
10			
11			
12			
13			
14			
15			
16			
17		Brown-Cream	Brown-cream, fine-grained, well-sorted and well-rounded matrix with sub-angular, gravel sized quartz, k-feldspar, and plagioclase feldspar. Strong goethite weathering and minor chlorite alteration.
18			
19			
20			
21			
22			
23			
24			
25			
26		Light-Brown	Light-brown, >1.5cm sized sub-angular gravels of k-feldspar, and quartz. Goethite weathering less from above saprolite, and chlorite alteration present.
27			
28			

Regolith Profile 8 Easting: 479414 Northing: 6546267

Depth (m)	Lithology	Colour	Description
1	Sediment Cover	Dark Brown-Red	Lost over time
2	Silcrete?	Light Brown	Light-brown, very fine-grained, well-rounded and moderately-sorted matrix, with sub-rounded gravel sized silcrete, calcrete and quartz chips. Goethite weathering visible.
3			
4			
5	Saprolite	Yellow	Yellow, very fine-grained, well-sorted and well-rounded matrix, with sub-angular <2cm sized silcrete and quartz grains. Goethite weathering visible
6			
7		Cream	Cream, very fine-grained, well-sorted and well-rounded matrix of sub-round quartz grains.
8			
9			
10		White	White, kaolinitic zone with very fine-grained, well-sorted matrix of clay/powder texture. Medium-grained, sub-round quartz and minor plagioclase feldspar grains.
11			
12			
13			
14			
15			
16			
17			
18			
19			
20			
21			
22		White-Green	White-green, kaolinitic zone with very fine-grained, well-sorted matrix of clay/powder texture. Sub-rounded quartz and minor plagioclase feldspar with chlorite alteration visible.
23			
24			
25			
26		White	White, kaolinitic zone with very fine-grained, well-sorted matrix of clay/powder texture. Medium-grained, sub-round quartz and minor plagioclase feldspar grains.
27			
28			
29			
30			
31	Saprock	Cream-Brown / White-Green	Pink-cream and green-white sub-angular to sub-round <2cm in size quartz, k-feldspar (dark pink coloured) plagioclase feldspar with high chlorite alteration and minor goethite weathering.
32			
33			
34			
35			
36			
37			
38			
39			
40			

Regolith Profile 9 Easting: 479235 Northing: 6546187

Depth (m)	Lithology	Colour	Description
1–4	Sediment Cover	Dark Brown-Red	Brown-red matrix of very-fine to fine-grained, well-sorted and well-rounded quartzose sands, with strong dark-brown red textures of sub-angular to sub-rounded silcrete, quartz and minor calcrete, all which have undergone substantial goethite weathering.
5–30	Saprolite	White	White, kaolinitic zone with very fine-grained, well-sorted matrix of clay/powder texture. Medium-grained, sub-round quartz and minor plagioclase feldspar grains.
31–37	Saprolite	Cream	Cream, kaolinitic zone with very fine-grained, well-sorted matrix of clay/powder texture. Mineralogy includes sub-round quartz and minor plagioclase feldspar.
38–45	Saprolite	Brown-Cream	Brown-cream, 0.1-1cm sized rounded, poorly sorted grains of k-feldspar, quartz, plagioclase feldspar and occasional mica which have undergone minor goethite weathering.

Regolith Profile 10 Easting: 480185 Northing: 6545803

Depth (m)	Lithology	Colour	Description
1	Sediment Cover	Light Brown	Light-brown, fine to medium-grained, well-rounded and well-sorted quartzose sand matrix.
2			
3			
4	Silcrete	Orange-Brown	Orange-brown, sub-rounded to sub-angular 0.2-1cm sized silcrete grains, with quartz grains within the silcrete, and goethite weathering visible.
5			
6	Saprolite	White	White, kaolinitic zone with very fine-grained, well-sorted matrix of clay/powder texture. Medium-grained, sub-round quartz and minor plagioclase feldspar grains.
7			
8			
9			
10			
11			
12			
13			
14			
15			
16			
17			
18			
19			
20			
21			
22			
23		Cream	Cream, kaolinitic zone with very fine-grained, well-sorted matrix of clay/powder texture. Mineralogy includes sub-round quartz and minor plagioclase feldspar. Minor goethite weathering.
24			
25			
26		Light Grey	Light-grey, 0.5cm sized, moderately sorted, sub-angular grains of plagioclase feldspar and quartz.
27			
28			
29			
30			
31			
32			
33			
34			
35			
36	Saprock	Brown-Cream	Brown-cream gravel sized, sub-angular to sub-round k-feldspar, quartz and plagioclase feldspar grains, with chlorite alteration, minor goethite weathering, and down profile the strength in weathering decreases.
37			
38			
39			
40			
41			
42			
43			
44			
45			
46			
47			
48			
49			
50-55			
56	Fresh Bedrock	Grey-Pink	Grey-pink, gravel sized sub-angular to sub-round fresh bedrock with visible gneissic fabric and mineralogy of mica, k-feldspar, quartz, plagioclase feldspar. Very minor chlorite alteration visible.
57			
58			
59			
60			
61			

Regolith Profile 11 Easting: 480116 Northing: 6546935

Depth (m)	Lithology	Colour	Description
1–4	Sediment Cover	Light-Brown	Light-brown, fine-grained, well-rounded and well-sorted quartzose sand matrix.
5–16	Saprolite	White	White, kaolinitic zone with very fine-grained, well-sorted matrix of clay/powder texture. Medium-grained, sub-round quartz and minor plagioclase feldspar grains.
17–20	Saprolite	Light-Grey	Light-grey kaolinitic zone with very fine-grained, well-sorted matrix of clay/powder texture. Mineralogy includes sub-round quartz and minor plagioclase feldspar.
21–26	Saprock	Grey-Pink	Grey-pink, fine-grained, sub-round quartz and lithic fragments of the saprock interval below. All matrix if previously present has been lost to weathering and erosion.
27–36	Saprock	Orange-Brown	Orange-brown, gravel sized sub-angular to sub-round quartz, k-feldspar, plagioclase feldspar and micas. Chlorite alteration and goethite weathering visible.
37–40	Fresh Bedrock	Grey	Grey, gravel sized sub-angular to sub-round fresh bedrock with visible gneissic fabric and mineralogy of mica, k-feldspar, quartz, plagioclase feldspar. No chlorite alteration visible.

Legend

	Brown
	Dark Brown-Red
	White
	Cream
	Yellow
	Brown-Cream
	Cream-Brown
	Pink Orange

	White-Green
	Olive Brown
	Orange Brown
	Light Brown
	Brown Grey
	Light Grey
	Grey
	Erosive Unconformity

Appendix 2c: Image representation examples of regolith profiles in the field.

Photo 2c.1: Regolith profile 2: Easting: 479651, Northing: 6546649

Photo 2c.2: Regolith profile 4: Easting: 479559, Northing: 6546598

Photo 2c.3: Regolith profile 10: Easting: 480185, Northing: 6545803

APPENDIX 3

Calcrete Geochemical Assay Results

Appendix 3a: Location of calcrete sample sites in the 'Tomahawk' study area.

3a.1 Location of calcrete sample sites (yellow dots) on regolith-landform map of the 'Tomahawk' study area (numbering in table adjacent refers to sample numbering along each transect. This corresponds to sample number in geochemical analysis, Appendix 3b).

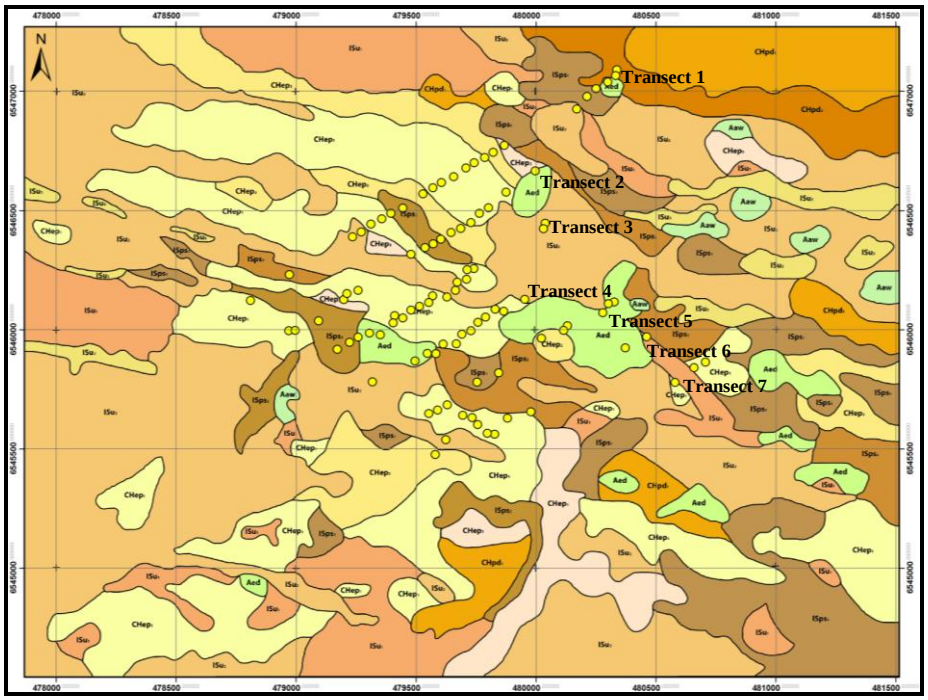

Transect	Southwest to Northeast along the transect	
1	23	1
2	24	40
3	60	41
4	73	61
5	84	74
6	85	95
7	98	96

3a.2 Location of calcrete sample sites on SPOT-5 Google Earth base map image of the 'Tomahawk' study area.

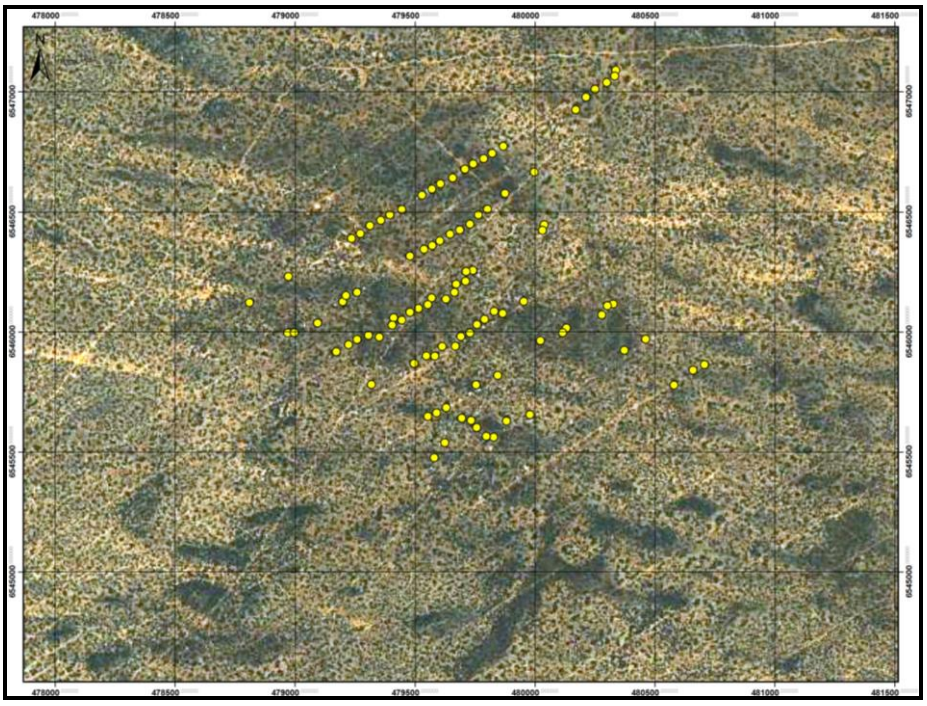

Appendix 3b: Geochemical Assay Results 001-098: Au-Ga

Easting GDA	Northing GDA	Sample Morphology	Sample No.	Au (ppb)	Au-Rp1 (ppb)	Ag (ppm)	Al (ppm)	As (ppm)	Ba (ppm)	Be (ppm)	Bi (ppm)	Ca (%)	Cd (ppm)	Ce (ppm)	Co (ppm)	Cr (ppm)	Cs (ppm)	Cu (ppm)	Dy (ppm)	Er (ppm)	Eu (ppm)	Fe (%)	Ga (ppm)
480337	6547091	powder	THK LK 001	20		0.025	8943	0.5	106	0.21	0.04	12.69	0.025	5.27	2.6	8	0.476	3	0.39	0.2	0.12	0.71	2.21
480332	6547066	hardpan	THK LK 002	16		0.025	19361	2	93	0.48	0.07	9.44	0.025	13.23	6.7	26	1.176	11	1.13	0.59	0.33	2.05	5.25
480299	6547040	nodular	THK LK 003	17		0.025	9112	2	132	0.38	0.09	15.99	0.08	11.79	4.3	15	0.515	5	1.8	0.94	0.52	1.41	2.94
480250	6547012	hardpan	THK LK 004	20		0.025	9592	2	145	0.4	0.05	19.64	0.09	12.45	6.7	16	0.598	9	1.37	0.71	0.39	1.19	3.11
480212	6546978	nodular	THK LK 005	28		0.025	6630	2	202	0.28	0.03	19.97	0.1	13.79	6.8	7	0.436	7	1.82	0.94	0.52	0.53	1.97
480169	6546926	nodular	THK LK 006	31		0.025	5924	0.5	126	0.32	0.03	19.65	0.11	12.81	6.6	8	0.379	6	1.83	0.93	0.52	0.58	1.92
479867	6546774	nodular	THK LK 007	22		0.025	5006	3	299	0.27	0.07	9.88	0.05	9.88	4.8	17	0.253	5	1.39	0.78	0.38	1.67	2.62
479821	6546744	nodular	THK LK 008	14		0.025	5539	4	181	0.33	0.09	11.99	0.07	11.47	8.1	27	0.291	8	1.59	0.85	0.43	2.17	3.34
479786	6546723	nodular	THK LK 009	16		0.025	5195	5	132	0.28	0.09	6.87	0.025	6.57	2.9	22	0.182	4	0.86	0.44	0.25	2.47	3.26
479742	6546701	hardpan	THK LK 010	69		0.025	7186	4	191	0.4	0.05	18.96	0.08	13.04	7.7	17	0.422	9	1.4	0.73	0.38	1.45	2.94
479742	6546701	hardpan	THK LK 010a	52		0.025	5976	2	151	0.33	0.05	15.9	0.08	10.44	5.2	14	0.353	6	1.14	0.62	0.32	1.12	2.37
479708	6546679	hardpan	THK LK 011	86		0.05	7261	2	188	0.35	0.05	22.49	0.15	17.46	8.7	14	0.473	6	3.03	1.58	0.92	1.12	2.71
479656	6546642	hardpan	THK LK 012	63		0.025	5968	3	234	0.28	0.03	16.84	0.06	10.69	5.8	9	0.342	5	1.6	0.83	0.47	0.89	2.29
479605	6546618	hardpan	THK LK 013	46		0.025	8740	2	541	0.33	0.03	20.28	0.09	15	6.8	8	0.55	7	2.08	1.06	0.6	0.68	2.5
479570	6546596	hardpan	THK LK 014	49		0.025	6063	2	208	0.33	0.03	21.66	0.1	14.26	7.8	6	0.404	6	1.99	1.03	0.55	0.49	1.78
479529	6546570	hardpan	THK LK 015	53		0.025	9232	2	234	0.39	0.04	22.33	0.09	10.92	6.5	10	0.614	7	1.4	0.73	0.4	0.89	2.7
479444	6546510	nodular	THK LK 016	78	74	0.025	8799	1	721	0.39	0.04	20.97	0.1	13.55	6.9	10	0.462	5	1.83	0.98	0.53	0.82	2.66
479394	6546489	hardpan	THK LK 017	90		0.06	6247	2	812	0.29	0.04	15.93	0.07	9.06	5.8	9	0.293	5	1.12	0.58	0.35	0.75	2.57
479356	6546465	hardpan	THK LK 018	43		0.025	7919	2	686	0.41	0.03	26.83	0.1	14.7	7.4	7	0.503	7	1.92	0.98	0.54	0.54	2.13
479312	6546444	hardpan	THK LK 019	56		0.05	7356	2	195	0.38	0.03	22.29	0.09	11.7	6.4	8	0.469	7	1.25	0.68	0.34	0.6	2.27
479271	6546410	nodular	THK LK 020	61		0.025	9817	2	492	0.4	0.04	23.14	0.1	15.01	6	7	0.632	5	1.84	0.98	0.54	0.69	2.72
479271	6546410	nodular	THK LK 020a	47		0.025	10489	2	711	0.4	0.04	22.36	0.09	16.91	6.2	8	0.642	5	1.93	0.99	0.56	0.74	2.91
479235	6546390	nodular	THK LK 021	48		0.07	8346	1	213	0.43	0.03	24.43	0.15	20.03	10.1	7	0.512	8	2.88	1.53	0.79	0.57	2.32
478972	6546231	nodular	THK LK 022	69		0.025	9414	3	165	0.43	0.05	17.69	0.1	11.81	5.2	15	0.563	7	1.36	0.74	0.37	1.55	2.83
478809	6546123	nodular	THK LK 023	9		0.025	4880	0.5	133	0.27	0.02	18.94	0.11	10.13	3.3	5	0.303	5	1.31	0.71	0.35	0.39	1.39
478969	6545996	nodular	THK LK 024	14		0.025	7281	0.5	144	0.4	0.03	23.22	0.2	15.17	6.5	8	0.421	6	2.1	1.13	0.58	0.6	2.05
478996	6545997	hardpan	THK LK 025	28		0.025	5800	1	158	0.35	0.02	23.05	0.14	12	5.8	5	0.36	7	1.69	0.91	0.48	0.42	1.62
479093	6546038	hardpan	THK LK 026	17		0.025	5365	1	138	0.25	0.02	20.9	0.13	8.86	5.1	7	0.338	7	1.21	0.65	0.35	0.45	1.51
479198	6546127	nodular	THK LK 027	27		0.025	7035	1	156	0.46	0.03	26.43	0.19	16.75	8.3	8	0.443	7	2.49	1.35	0.67	0.58	1.98
479211	6546152	nodular	THK LK 028	29		0.025	6365	1	150	0.44	0.03	25.45	0.16	15.46	7.3	10	0.405	7	1.96	1.05	0.5	0.74	2
479258	6546166	nodular	THK LK 029	11		0.025	6828	1	187	0.42	0.03	25.89	0.16	15.18	6.7	7	0.428	6	1.85	1.01	0.48	0.52	1.88
479478	6546317	hardpan	THK LK 030	40		0.025	7889	2	198	0.61	0.04	19.58	0.14	22.37	10.3	16	0.453	6	3.8	1.95	1.05	1.27	3.95
479478	6546317	hardpan	THK LK 030a	35		0.025	10313	2	221	0.69	0.06	23.48	0.17	25.52	10.7	13	0.592	6	4.14	2.21	1.16	1.42	3.62
479537	6546345	hardpan	THK LK 031	133	105	0.06	9432	3	369	0.5	0.04	24.45	0.1	14.33	7.9	13	0.546	8	2.03	1.08	0.56	1.16	2.93
479571	6546361	hardpan	THK LK 032	137	119	0.06	9486	7	225	0.66	0.11	17.65	0.09	13.23	4.2	32	0.418	6	1.73	0.95	0.46	2.81	8.03
479603	6546380	nodular	THK LK 033	194	199	0.025	12262	1	135	0.59	0.05	16.2	0.06	9.22	5.8	15	0.722	4	0.83	0.45	0.22	1.12	3.22
479646	6546408	nodular	THK LK 034	125	155	0.025	8881	1	184	0.44	0.05	18.45	0.06	8.09	4.5	10	0.543	3	0.71	0.39	0.19	0.81	2.39
479686	6546425	nodular	THK LK 035	50		0.025	9423	3	170	0.55	0.05	23.18	0.15	12.85	5.3	13	0.498	8	1.62	0.91	0.41	1.99	2.76
479728	6546450	nodular	THK LK 036	10		0.025	3239	0.5	116	0.24	0.02	20.17	0.09	5.77	3.1	4	0.232	4	0.82	0.45	0.23	0.28	0.91
479764	6546488	nodular	THK LK 037	5		0.025	4262	0.5	121	0.26	0.02	21.79	0.13	11.17	4.1	5	0.301	4	1.69	0.92	0.44	0.37	1.25
479802	6546512	hardpan	THK LK 038	11		0.025	4507	0.5	186	0.18	0.01	24.8	0.07	9.73	4.4	3	0.284	4	1.15	0.68	0.33	0.33	1.27
479875	6546577	hardpan	THK LK 039	1		0.025	2474	0.5	94	0.18	0.01	15.88	0.07	6.58	3.7	3	0.164	3	0.89	0.48	0.24	0.24	0.76
479997	6546666	hardpan	THK LK 040	7		0.025	6875	1	170	0.37	0.03	22.12	0.13	11.14	4.2	5	0.457	5	1.66	0.9	0.45	0.49	1.84
479997	6546666	hardpan	THK LK 040a	11		0.025	6838	1	301	0.28	0.03	25.85	0.12	9.99	3.7	6	0.439	6	1.38	0.77	0.38	0.52	1.91
480038	6546447	nodular	THK LK 041	17		0.025	4700	0.5	229	0.27	0.03	21.98	0.11	9.17	4.1	5	0.306	3	1.43	0.78	0.4	0.44	1.32
480030	6546424	hardpan	THK LK 042	10		0.025	2914	0.5	127	0.16	0.01	17.98	0.07	6.07	3.8	3	0.19	5	0.75	0.42	0.21	0.26	0.81
479741	6546257	nodular?	THK LK 043	30		0.025	3599	0.5	144	0.23	0.02	20.76	0.09	8.02	4.8	4	0.237	4	1.26	0.69	0.33	0.31	1.06
479713	6546252	nodular	THK LK 044	22		0.025	5177	1	892	0.35	0.02	23.68	0.12	12.34	5	5	0.326	4	2.2	1.19	0.61	0.49	1.62
479710	6546212	nodular	THK LK 045	118	96	0.11	6382	1	185	0.43	0.03	23.02	0.12	12.69	7	8	0.404	10	1.96	1.01	0.56	0.65	1.88
479671	6546200	nodular	THK LK 046	20		0.09	3298	1	116	0.32	0.02	19.68	0.11	8.86	4.6	6	0.201	5	1.45	0.78	0.38	0.58	1.18
479664	6546165	nodular	THK LK 047	21		0.08	7874	2	223	0.46	0.04	27.06	0.22	22.39	11.8	11	0.499	7	3.89	2.04	1.08	1.05	2.63
479628	6546137	nodular	THK LK 048	22		0.07	5556	1	187	0.33	0.03	25.06	0.14	10.81	5.8	10	0.348	6	1.74	0.96	0.48	0.86	2.21
479569	6546143	hardpan	THK LK 049	13		0.025	3988	0.5	136	0.28	0.01	19.64	0.11	8.37	4.6	3	0.256	4	1.22	0.67	0.34	0.29	1.06
479553	6546115	hardpan	THK LK 050	71		0.025	7188	5	246	0.4	0.06	19.7	0.09	8.26	4.2	16	0.364	6	1.14	0.62	0.33	2.17	3.45

Appendix 3b: Geochemical Assay Results 001-098: Au-Ga

Easting GDA	Northing GDA	Sample Morphology	Sample No.	Au (ppb)	Au-Rp1 (ppb)	Ag (ppm)	Al (ppm)	As (ppm)	Ba (ppm)	Be (ppm)	Bi (ppm)	Ca (%)	Cd (ppm)	Ce (ppm)	Co (ppm)	Cr (ppm)	Cs (ppm)	Cu (ppm)	Dy (ppm)	Er (ppm)	Eu (ppm)	Fe (%)	Ga (ppm)
479553	6546115	hardpan	THK LK 050a	43		0.025	7322	2	334	0.37	0.04	23.37	0.12	10.25	3.9	7	0.449	5	1.41	0.78	0.39	1	2.48
479514	6546098	hardpan	THK LK 051	32		0.025	6717	0.5	208	0.35	0.04	20.44	0.09	11.3	4.4	10	0.419	7	1.32	0.69	0.37	0.8	1.96
479479	6546083	hardpan	THK LK 052	39		0.05	6950	2	184	0.46	0.03	24.56	0.14	14.45	8.3	6	0.47	8	1.99	1.06	0.53	0.51	1.9
479444	6546050	hardpan	THK LK 053	37		0.025	7563	2	231	0.41	0.03	24.55	0.12	16.83	8.5	8	0.486	8	2.49	1.31	0.73	0.62	2.14
479410	6546059	nodular	THK LK 054	21		0.025	4252	0.5	127	0.27	0.02	18.77	0.09	8.3	4.1	4	0.267	5	1	0.55	0.28	0.31	1.19
479404	6546029	nodular	THK LK 055	11		0.025	4109	0.5	143	0.25	0.02	18.28	0.1	10.53	6.1	4	0.269	5	1.5	0.8	0.42	0.32	1.22
479350	6545979	nodular	THK LK 056	13		0.025	5955	0.5	177	0.26	0.02	22.7	0.1	12.46	5.3	4	0.38	4	1.48	0.89	0.42	0.41	1.7
479305	6545986	nodular	THK LK 057	10		0.025	3739	0.5	166	0.22	0.01	16.22	0.07	5.89	2.8	4	0.242	3	0.66	0.37	0.18	0.31	1.04
479258	6545969	nodular	THK LK 058	15		0.025	5326	0.5	211	0.34	0.02	20.56	0.1	9.86	2.9	6	0.345	5	1.12	0.63	0.28	0.44	1.42
479222	6545947	nodular	THK LK 059	33		0.025	5114	1	159	0.31	0.02	21.44	0.12	8.78	6.2	7	0.317	17	1.34	0.72	0.39	0.49	1.5
479222	6545947	nodular	THK LK 059a	18		0.025	3636	0.5	121	0.24	0.02	18.34	0.09	6.08	4.2	4	0.23	6	0.82	0.46	0.22	0.31	1.01
479171	6545918	nodular	THK LK 060	17		0.025	5992	0.5	196	0.36	0.02	23.2	0.15	13.37	5.2	6	0.399	6	1.91	1.06	0.54	0.43	1.7
479952	6546128	nodular	THK LK 061	10		0.025	4856	1	131	0.33	0.02	18.07	0.13	11.67	4.3	5	0.3	4	1.59	0.88	0.44	0.5	1.52
479865	6546078	nodular	THK LK 062	18		0.025	3614	1	138	0.24	0.02	17.79	0.1	8.67	5.2	5	0.23	4	1.19	0.67	0.33	0.49	1.21
479830	6546086	nodular	THK LK 063	44		0.025	4880	1	145	0.39	0.03	19.63	0.11	10.49	5	6	0.308	4	1.39	0.78	0.38	0.65	1.46
479789	6546054	nodular	THK LK 064	15		0.025	5215	0.5	222	0.31	0.02	19.94	0.11	15.45	5.4	5	0.315	5	2.03	1.07	0.59	0.44	1.53
479757	6546031	nodular	THK LK 065	11		0.025	2944	0.5	90	0.23	0.01	16.28	0.08	8.21	4.2	3	0.193	4	1.17	0.64	0.32	0.25	0.88
479728	6545996	hardpan	THK LK 066	33		0.025	6939	0.5	155	0.43	0.03	22	0.13	18.34	8.8	6	0.438	5	2.38	1.27	0.66	0.54	1.97
479690	6545981	hardpan	THK LK 067	30		0.025	6351	2	197	0.32	0.06	13.56	0.07	9.15	3.4	16	0.278	4	1.36	0.71	0.41	1.45	2.79
479667	6545941	hardpan	THK LK 068	27		0.025	3974	1	171	0.17	0.06	6.89	0.025	6.02	3	23	0.138	6	0.72	0.4	0.19	1.61	2.03
479613	6545940	nodular	THK LK 069	106	135	0.025	4412	0.5	356	0.21	0.03	13.36	0.025	5.58	3.6	12	0.191	4	0.64	0.34	0.18	0.98	2.49
479582	6545900	hardpan	THK LK 070	71		0.025	5910	2	222	0.34	0.04	16.48	0.08	9.22	5.4	15	0.312	6	1.52	0.8	0.46	1.22	2.67
479582	6545900	hardpan	THK LK 070a	59		0.025	8226	2	283	0.38	0.03	23.78	0.11	13.17	8	8	0.474	6	2.43	1.29	0.76	0.66	2.37
479547	6545901	hardpan/nodular	THK LK 071	44		0.025	9385	4	247	0.53	0.06	21.9	0.14	17.32	7.7	16	0.454	6	2.63	1.47	0.74	1.29	4.64
479496	6545869	nodular	THK LK 072	102	114	0.025	12631	0.5	54	0.11	0.03	0.78	0.025	3.67	0.6	6	0.607	4	0.18	0.09	0.06	0.63	5.12
479317	6545782	nodular	THK LK 073	14		0.025	4134	0.5	112	0.23	0.02	18.74	0.12	11.62	6.2	4	0.266	5	2.02	1.07	0.6	0.32	1.23
480325	6546117	nodular	THK LK 074	10		0.025	5859	0.5	189	0.33	0.02	24.46	0.11	10.09	7.6	4	0.373	5	1.41	1.15	0.54	0.37	1.58
480301	6546110	nodular	THK LK 075	43		0.025	7749	0.5	210	0.41	0.03	21.85	0.1	13.19	6.8	8	0.494	5	1.45	0.81	0.39	0.6	2.2
480278	6546072	nodular	THK LK 076	11		0.025	6477	0.5	196	0.37	0.02	21.44	0.13	13.58	6.2	6	0.452	6	1.85	1.04	0.48	0.46	1.82
480130	6546017	nodular	THK LK 077	10		0.025	3641	0.5	228	0.18	0.02	17.18	0.08	7.61	4.3	5	0.217	4	0.99	0.56	0.27	0.37	1.1
480115	6545997	nodular	THK LK 078	16		0.025	4597	0.5	336	0.26	0.02	17.29	0.09	8.02	5.3	6	0.283	5	1.09	0.59	0.3	0.45	1.48
480022	6545964	nodular	THK LK 079	41		0.025	6848	0.5	615	0.35	0.03	14.42	0.07	6.41	3.8	9	0.405	0.5	0.57	0.32	0.16	0.89	2.07
479844	6545819	hardpan	THK LK 080	22		0.025	5411	0.5	172	0.34	0.02	19.03	0.11	11.48	3.7	5	0.333	3	1.8	1.04	0.48	0.4	1.4
479844	6545819	hardpan	THK LK 080a	15		0.025	5169	0.5	188	0.29	0.02	21.67	0.1	10.51	3.6	6	0.328	4	1.59	0.91	0.43	0.42	1.4
479754	6545780	nodular	THK LK 081	19		0.025	5928	0.5	202	0.4	0.03	21.79	0.09	9.95	3	6	0.362	2	1.06	0.6	0.29	0.47	1.54
479629	6545685	nodular/hardpan	THK LK 082	65		0.025	7844	1	194	0.46	0.03	21.32	0.1	10.69	4.1	10	0.479	6	1.19	0.67	0.32	0.71	2.12
479589	6545664	nodular/hardpan	THK LK 083	22		0.025	4867	0.5	142	0.32	0.02	19.67	0.12	11.65	6.5	6	0.272	4	1.66	0.93	0.44	0.45	1.58
479553	6545649	nodular/hardpan	THK LK 084	38		0.025	9039	4	205	0.42	0.07	13.44	0.05	9.48	5.4	23	0.346	8	1.01	0.54	0.27	2.2	4.74
479756	6545603	hardpan/nodular	THK LK 085	21		0.025	6441	0.5	179	0.31	0.03	19.41	0.11	13.93	6.3	6	0.364	5	1.9	1.02	0.52	0.47	1.65
479733	6545632	nodular	THK LK 086	68		0.025	8023	0.5	160	0.3	0.03	19.24	0.07	8.97	4.5	10	0.48	5	0.85	0.46	0.24	0.75	2.22
479694	6545642	nodular	THK LK 087	34		0.025	5917	0.5	209	0.29	0.03	15.75	0.08	6.91	2.6	4	0.352	0.5	0.69	0.38	0.19	0.47	1.52
479624	6545539	hardpan	THK LK 088	11		0.025	4384	0.5	120	0.33	0.02	19.69	0.1	12.61	4.9	5	0.262	5	1.44	0.81	0.39	0.37	1.32
479580	6545477	nodular	THK LK 089	7		0.025	5371	1	188	0.35	0.02	25.23	0.16	15.45	7.5	5	0.34	7	2.32	1.26	0.67	0.47	1.61
479827	6545562	hardpan	THK LK 090	15		0.025	4609	0.5	169	0.37	0.02	23.15	0.15	12.53	6.1	5	0.28	5	2.04	1.13	0.56	0.37	1.32
479827	6545562	hardpan	THK LK 090a	50		0.025	4906	0.5	192	0.38	0.02	26.81	0.16	14.85	8.2	5	0.299	5	2.36	1.29	0.66	0.35	1.31
479796	6545566	nodular/hardpan	THK LK 091	14		0.025	5144	0.5	200	0.38	0.03	21.99	0.12	11.99	4.2	7	0.339	6	1.45	0.86	0.36	0.48	1.45
479881	6545629	nodular/hardpan	THK LK 092	10		0.025	6956	0.5	158	0.36	0.02	23.6	0.14	12.77	5.9	5	0.339	5	1.91	1.04	0.52	0.56	1.44
479978	6545656	hardpan	THK LK 093	52		0.025	6578	0.5	121	0.29	0.03	17.88	0.06	6.76	5	12	0.392	4	0.6	0.32	0.16	0.85	1.87
480372	6545924	nodular/hardpan	THK LK 094	39		0.025	8338	2	1317	0.42	0.04	22.16	0.07	10.77	3.8	9	0.54	4	1.35	0.73	0.41	0.66	2.16
480461	6545970	nodular/hardpan	THK LK 095	14		0.025	8810	0.5	246	0.58	0.04	26.32	0.16	21.45	6.1	9	0.576	7	3.61	1.94	1.03	0.67	2.36
480706	6545865	nodular/hardpan	THK LK 096	9		0.025	6474	0.5	164	0.44	0.03	25.19	0.18	16.56	6.4	6	0.409	6	2.32	1.29	0.62	0.61	1.81
480658	6545841	nodular/hardpan	THK LK 097	26		0.025	5604	0.5	199	0.33	0.02	25.16	0.16	11.19	5	6	0.355	6	1.63	0.92	0.46	0.45	1.48
480579	6545779	nodular	THK LK 098	50		0.025	8185	0.5	168	0.39	0.04	16.7	0.025	7.6	3.5	7	0.459	2	0.67	0.37	0.19	0.7	1.99
480579	6545779	nodular	THK LK 098a	40		0.025	6496	0.5	163	0.27	0.03	16.12	0.025	6.78	3.8	10	0.393	3	0.65	0.35	0.18	0.79	1.77

Appendix 3b: Geochemical Assay Results 001-098: Gd-Re

Easting GDA	Northing GDA	Sample Morphology	Sample No.	Gd (ppm)	Hf (ppm)	Ho (ppm)	In (ppm)	K (ppm)	La (ppm)	Li (ppm)	Mg (%)	Mn (ppm)	Mo (ppm)	Nb (ppm)	Nd (ppm)	Ni (ppm)	P (ppm)	Pb (ppm)	Pd (ppb)	Pr (ppm)	Pt (ppb)	Rb (ppm)	Re (ppm)
480337	6547091	powder	THK LK 001	0.52	0.07	0.08	0.005	1847	2.75	4.3	0.8	39	0.1	0.07	2.79	6	22	3	5	0.663	2.5	6.85	0.005
480332	6547066	hardpan	THK LK 002	1.37	0.21	0.23	0.02	4569	6.67	10.2	0.67	95	0.6	0.08	7.06	17	54	5	5	1.716	2.5	19.95	0.005
480299	6547040	nodular	THK LK 003	2.33	0.17	0.38	0.02	1473	11.63	5	0.39	88	0.3	0.09	11.36	6	33	7	5	2.615	2.5	8.56	0.005
480250	6547012	hardpan	THK LK 004	1.79	0.08	0.28	0.01	1762	8.25	5	0.38	72	0.5	0.12	8.51	11	74	4	5	1.955	2.5	9.87	0.005
480212	6546978	nodular	THK LK 005	2.38	0.03	0.37	0.005	1349	9.9	3.3	0.46	103	0.1	0.1	10.97	7	77	3	5	2.469	2.5	7.26	0.005
480169	6546926	nodular	THK LK 006	2.37	0.01	0.37	0.005	1256	9.92	2.4	0.35	154	0.1	0.1	10.9	8	77	3	5	2.486	2.5	6.31	0.005
479867	6546774	nodular	THK LK 007	1.73	0.17	0.3	0.02	747	7.33	2.8	0.17	114	0.2	0.05	7.84	5	28	9	18	1.813	2.5	4.11	0.005
479821	6546744	nodular	THK LK 008	1.95	0.23	0.33	0.03	811	8.82	3.2	0.19	143	0.4	0.05	9.06	10	32	9	5	2.107	2.5	4.69	0.005
479786	6546723	nodular	THK LK 009	1.06	0.2	0.18	0.03	487	4.66	2.7	0.12	59	0.3	0.03	5.27	4	31	9	5	1.218	2.5	2.86	0.005
479742	6546701	hardpan	THK LK 010	1.75	0.02	0.29	0.02	1182	7.35	3.9	0.37	76	0.4	0.12	8.06	8	88	6	5	1.868	2.5	6.64	0.005
479742	6546701	hardpan	THK LK 010a	1.41	0.01	0.24	0.01	966	6.21	3.4	0.27	69	0.3	0.14	6.68	4	79	6	5	1.557	2.5	5.51	0.005
479708	6546679	hardpan	THK LK 011	4.22	0.09	0.63	0.01	1365	17.99	3.1	0.43	128	0.2	0.08	19.29	9	85	6	5	4.293	2.5	7.59	0.005
479656	6546642	hardpan	THK LK 012	2.12	0.04	0.33	0.01	1147	8.38	3.4	0.46	66	0.2	0.1	9.66	7	64	3	5	2.165	2.5	5.69	0.005
479605	6546618	hardpan	THK LK 013	2.71	0.05	0.42	0.005	1426	11.79	4.4	0.57	103	0.1	0.09	12.71	8	58	3	5	2.856	2.5	8.37	0.005
479570	6546596	hardpan	THK LK 014	2.55	0.03	0.41	0.005	1314	10.83	3	0.53	104	0.05	0.11	11.38	7	64	3	5	2.624	2.5	6.52	0.005
479529	6546570	hardpan	THK LK 015	1.83	0.04	0.28	0.01	1263	8.43	4.9	0.49	44	0.2	0.1	8.57	9	52	3	5	1.987	2.5	9.01	0.005
479444	6546510	nodular	THK LK 016	2.47	0.06	0.38	0.01	1567	11.28	3.8	0.58	106	0.1	0.07	11.53	9	46	3	5	2.665	2.5	7.67	0.005
479394	6546489	hardpan	THK LK 017	1.47	0.03	0.23	0.005	917	6.69	2.6	0.44	78	0.3	0.07	6.9	7	63	4	5	1.606	2.5	4.66	0.005
479356	6546465	hardpan	THK LK 018	2.56	0.03	0.39	0.005	1307	11.89	4.2	0.61	63	0.2	0.14	11.77	7	68	3	5	2.74	5	7.71	0.005
479312	6546444	hardpan	THK LK 019	1.52	0.03	0.26	0.005	1255	6.45	3.7	0.7	68	0.2	0.15	6.81	8	80	3	5	1.6	2.5	7.21	0.005
479271	6546410	nodular	THK LK 020	2.36	0.14	0.38	0.005	1741	10.11	5.5	2.11	62	0.1	0.13	10.84	8	44	3	5	2.502	2.5	9.6	0.005
479271	6546410	nodular	THK LK 020a	2.51	0.08	0.39	0.01	1707	10.86	5.8	1.71	66	0.2	0.16	11.64	8	41	3	5	2.671	2.5	9.76	0.005
479235	6546390	nodular	THK LK 021	3.65	0.08	0.58	0.005	1520	14.1	4.4	1.31	215	0.2	0.15	15.78	11	85	3	5	3.582	2.5	8.33	0.005
478972	6546231	nodular	THK LK 022	1.7	0.07	0.29	0.01	1610	7.91	5.1	1.19	79	0.3	0.08	7.62	9	37	5	5	1.796	2.5	8.55	0.005
478809	6546123	nodular	THK LK 023	1.63	0.04	0.28	0.005	959	6.97	2.3	0.48	71	0.05	0.08	7.37	5	49	3	5	1.682	2.5	5.21	0.005
478969	6545996	nodular	THK LK 024	2.65	0.03	0.44	0.005	1427	10.99	3.5	0.44	177	0.1	0.11	11.78	7	92	4	5	2.659	2.5	7.14	0.005
478996	6545997	hardpan	THK LK 025	2.23	0.03	0.36	0.005	1188	9.4	2.7	0.43	103	0.1	0.12	10.12	6	82	2	5	2.275	2.5	5.95	0.005
479093	6546038	hardpan	THK LK 026	1.56	0.02	0.25	0.005	1021	7.1	2.3	0.55	82	0.1	0.13	7.18	7	57	2	5	1.633	2.5	5.93	0.005
479198	6546127	nodular	THK LK 027	3.22	0.04	0.53	0.005	1330	13.13	3.2	0.52	200	0.1	0.16	13.89	8	120	3	5	3.111	2.5	7.66	0.005
479211	6546152	nodular	THK LK 028	2.38	0.03	0.41	0.005	1385	8.53	3	0.47	186	0.2	0.13	9.71	7	145	3	5	2.185	2.5	6.65	0.005
479258	6546166	nodular	THK LK 029	2.24	0.02	0.39	0.005	1409	8.41	3.4	0.53	145	0.1	0.15	9.36	6	124	4	5	2.118	2.5	7.28	0.005
479478	6546317	hardpan	THK LK 030	5	0.11	0.78	0.02	1505	21.69	4.2	0.45	160	0.3	0.08	22.73	11	57	5	5	5.129	2.5	7.56	0.005
479478	6546317	hardpan	THK LK 030a	5.49	0.07	0.88	0.02	1916	22.92	5.6	0.54	174	0.3	0.12	24.47	11	71	6	5	5.536	2.5	9.6	0.005
479537	6546345	hardpan	THK LK 031	2.71	0.04	0.42	0.01	1688	10.79	4.8	0.82	75	0.3	0.16	11.72	9	86	4	5	2.644	2.5	8.84	0.005
479571	6546361	hardpan	THK LK 032	2.09	0.18	0.37	0.04	1354	8.48	4.6	0.58	59	0.4	0.08	9.17	6	57	7	5	2.134	2.5	6.63	0.005
479603	6546380	nodular	THK LK 033	1.01	0.15	0.17	0.01	2618	4.78	6.9	2.04	60	0.2	0.06	4.84	9	31	4	5	1.156	2.5	12.36	0.005
479646	6546408	nodular	THK LK 034	0.89	0.06	0.15	0.005	1738	4.21	6.2	1.69	59	0.2	0.11	4.18	5	24	4	5	0.994	2.5	8.42	0.005
479686	6546425	nodular	THK LK 035	1.97	0.13	0.34	0.01	1357	7.66	6.3	0.57	72	0.2	0.09	8.25	7	82	6	5	1.887	2.5	7.55	0.005
479728	6546450	nodular	THK LK 036	1.08	0.01	0.18	0.005	674	4.26	1.7	0.33	41	0.05	0.09	4.62	4	43	1	5	1.046	2.5	3.72	0.005
479764	6546488	nodular	THK LK 037	2.14	0.03	0.35	0.005	898	8.85	2.5	0.49	63	0.05	0.11	9.32	4	53	2	5	2.093	2.5	5.02	0.005
479802	6546512	hardpan	THK LK 038	1.45	0.01	0.24	0.005	927	5.98	2	0.63	50	0.05	0.1	6.67	4	57	1	5	1.534	2.5	5.36	0.005
479875	6546577	hardpan	THK LK 039	1.09	0.01	0.19	0.005	582	4.16	1.5	0.23	54	0.05	0.08	4.73	3	58	2	5	1.061	2.5	2.77	0.005
479997	6546666	hardpan	THK LK 040	2.16	0.02	0.35	0.005	1424	8.63	4	0.48	57	0.05	0.15	9.29	4	75	3	5	2.075	2.5	7.27	0.005
479997	6546666	hardpan	THK LK 040a	1.84	0.03	0.3	0.005	1352	7.46	4	0.48	41	0.1	0.16	8.02	5	69	3	5	1.803	2.5	6.91	0.005
480038	6546447	nodular	THK LK 041	1.9	0.02	0.3	0.005	863	8.63	3.2	0.55	42	0.1	0.14	8.62	4	60	2	5	1.934	2.5	4.95	0.005
480030	6546424	hardpan	THK LK 042	0.96	0.005	0.16	0.005	631	3.53	1.7	0.39	43	0.05	0.09	4.07	4	62	1	5	0.908	2.5	3.23	0.005
479741	6546257	nodular?	THK LK 043	1.62	0.01	0.27	0.005	792	6.4	2	0.43	74	0.05	0.11	6.73	4	45	2	5	1.494	2.5	4.14	0.005
479713	6546252	nodular	THK LK 044	2.93	0.02	0.47	0.005	962	12.71	3.1	0.38	78	0.1	0.14	12.65	5	63	2	5	2.773	2.5	5.33	0.005
479710	6546212	nodular	THK LK 045	2.63	0.03	0.41	0.005	1346	10.01	3.1	0.77	115	0.1	0.14	11.28	10	101	2	5	2.491	2.5	6.43	0.005
479671	6546200	nodular	THK LK 046	1.81	0.02	0.31	0.005	713	6.49	1.7	0.32	109	0.1	0.1	7.51	5	82	2	5	1.636	2.5	3.44	0.005
479664	6546165	nodular	THK LK 047	5.17	0.04	0.8	0.01	1335	20.95	4.1	0.42	315	0.2	0.16	21.97	11	82	5	5	4.93	2.5	7.67	0.005
479628	6546137	nodular	THK LK 048	2.26	0.02	0.37	0.005	924	9.11	2.9	0.5	116	0.2	0.14	9.58	7	93	3	5	2.129	2.5	5.45	0.005
479569	6546143	hardpan	THK LK 049	1.58	0.01	0.26	0.005	816	6.06	2	0.41	87	0.05	0.12	6.57	4	71	2	5	1.481	2.5	4.2	0.005
479553	6546115	hardpan	THK LK 050	1.47	0.03	0.24	0.03	1115	6.44	3.8	0.52	54	0.6	0.12	6.67	6	51	5	5	1.509	2.5	5.51	0.005

Appendix 3b: Geochemical Assay Results 001-098: Gd-Re

Easting GDA	Northing GDA	Sample Morphology	Sample No.	Gd (ppm)	Hf (ppm)	Ho (ppm)	In (ppm)	K (ppm)	La (ppm)	Li (ppm)	Mg (%)	Mn (ppm)	Mo (ppm)	Nb (ppm)	Nd (ppm)	Ni (ppm)	P (ppm)	Pb (ppm)	Pd (ppb)	Pr (ppm)	Pt (ppb)	Rb (ppm)	Re (ppm)
479553	6546115	hardpan	THK LK 050a	1.75	0.03	0.3	0.005	1389	7.37	3.7	0.79	51	0.1	0.12	7.86	4	68	3	5	1.753	2.5	6.75	0.005
479514	6546098	hardpan	THK LK 051	1.66	0.02	0.27	0.005	1105	7.17	3.9	0.95	60	0.3	0.14	7.79	7	62	3	5	1.824	2.5	6.11	0.005
479479	6546083	hardpan	THK LK 052	2.47	0.04	0.41	0.005	1312	9.13	3.5	0.55	196	0.05	0.13	10.11	8	105	4	5	2.291	2.5	6.89	0.005
479444	6546050	hardpan	THK LK 053	3.36	0.04	0.51	0.005	1085	16.89	3.7	0.57	140	0.2	0.17	16.42	9	81	4	5	3.704	2.5	7.02	0.005
479410	6546059	nodular	THK LK 054	1.23	0.02	0.21	0.005	792	5.05	1.9	0.36	80	0.05	0.13	5.5	4	77	2	5	1.241	2.5	4.57	0.005
479404	6546029	nodular	THK LK 055	1.87	0.01	0.31	0.005	731	8.23	1.9	0.31	92	0.1	0.12	8.72	5	73	2	5	1.919	2.5	4.45	0.005
479350	6545979	nodular	THK LK 056	1.81	0.01	0.32	0.005	1031	8.42	2.6	0.42	125	0.05	0.12	8.81	4	83	2	5	2.049	2.5	6.76	0.005
479305	6545986	nodular	THK LK 057	0.78	0.02	0.14	0.005	787	3.33	2.1	0.61	61	0.1	0.11	3.52	3	51	2	5	0.814	2.5	4.22	0.005
479258	6545969	nodular	THK LK 058	1.28	0.04	0.23	0.005	1271	5.27	3	1.16	69	0.2	0.15	5.78	4	65	2	5	1.278	2.5	6.09	0.005
479222	6545947	nodular	THK LK 059	1.77	0.02	0.28	0.005	1126	8.15	2.4	1.4	84	0.2	0.11	8.25	11	76	2	5	1.808	2.5	5.73	0.005
479222	6545947	nodular	THK LK 059a	1.03	0.01	0.17	0.005	848	4.42	2	0.8	67	0.05	0.11	4.63	6	64	1	5	1.012	2.5	4.15	0.005
479171	6545918	nodular	THK LK 060	2.44	0.03	0.4	0.005	1224	11.1	3.1	0.55	90	0.1	0.15	11.03	6	70	3	5	2.441	2.5	7.05	0.005
479952	6546128	nodular	THK LK 061	1.99	0.03	0.33	0.005	880	8.45	2.5	0.26	121	0.2	0.14	8.97	4	71	3	5	1.989	2.5	5.5	0.005
479865	6546078	nodular	THK LK 062	1.47	0.02	0.25	0.005	732	6.09	2	0.33	118	0.2	0.11	6.64	6	59	2	5	1.481	2.5	4.12	0.005
479830	6546086	nodular	THK LK 063	1.7	0.02	0.3	0.005	1025	6.85	2.8	0.76	118	0.1	0.13	7.62	5	72	3	5	1.683	2.5	5.35	0.005
479789	6546054	nodular	THK LK 064	2.59	0.02	0.42	0.005	974	11.25	2.5	0.57	119	0.1	0.12	12.09	6	71	3	5	2.64	2.5	5.57	0.005
479757	6546031	nodular	THK LK 065	1.5	0.005	0.24	0.005	659	6.14	1.5	0.3	78	0.05	0.09	6.63	4	62	2	5	1.475	2.5	3.51	0.005
479728	6545996	hardpan	THK LK 066	2.95	0.05	0.48	0.005	1287	12.45	3.3	0.42	227	0.1	0.17	13.79	9	65	4	5	3.105	2.5	7.11	0.005
479690	6545981	hardpan	THK LK 067	1.71	0.1	0.28	0.02	659	9.09	3.6	0.25	72	0.3	0.08	8.95	5	32	5	5	2.044	2.5	4.1	0.005
479667	6545941	hardpan	THK LK 068	0.83	0.13	0.15	0.01	416	3.88	1.9	0.17	56	0.6	0.05	4.06	8	10	6	5	0.951	2.5	2.24	0.005
479613	6545940	nodular	THK LK 069	0.76	0.07	0.13	0.01	620	3.47	2.6	0.34	59	0.3	0.12	3.65	4	26	3	5	0.844	2.5	3.26	0.005
479582	6545900	hardpan	THK LK 070	2.04	0.05	0.31	0.01	799	10.46	3.8	0.46	71	0.5	0.12	10.27	8	39	4	5	2.281	2.5	4.76	0.005
479582	6545900	hardpan	THK LK 070a	3.41	0.02	0.51	0.005	1202	17.52	5.2	0.66	76	0.2	0.17	16.88	7	55	3	5	3.759	2.5	7.46	0.005
479547	6545901	hardpan/nodular	THK LK 071	3.34	0.07	0.55	0.02	1348	14.9	7.2	0.48	109	0.4	0.16	15.36	8	59	6	5	3.432	2.5	6.83	0.005
479496	6545869	nodular	THK LK 072	0.23	0.05	0.04	0.005	1342	3.65	1.1	0.08	58	0.2	0.03	1.45	2	10	9	5	0.385	2.5	9.4	0.005
479317	6545782	nodular	THK LK 073	2.74	0.02	0.41	0.005	863	12.88	1.9	0.37	68	0.2	0.1	13.3	6	61	2	5	2.922	2.5	4.56	0.005
480325	6546117	nodular	THK LK 074	2.44	0.01	0.29	0.005	1070	10.05	2.2	0.3	126	0.05	0.12	11.28	4	69	2	5	1.723	2.5	4.67	0.005
480301	6546110	nodular	THK LK 075	1.73	0.03	0.3	0.005	1469	7.55	4.5	0.92	100	0.2	0.17	8.01	7	44	3	5	1.826	2.5	7.9	0.005
480278	6546072	nodular	THK LK 076	2.21	0.03	0.38	0.005	1221	9.3	3.2	0.44	99	0.05	0.16	9.94	5	44	4	5	2.238	2.5	7.43	0.005
480130	6546017	nodular	THK LK 077	1.21	0.04	0.21	0.005	720	5.02	2.2	0.35	76	0.1	0.13	5.43	4	61	2	5	1.193	2.5	3.93	0.005
480115	6545997	nodular	THK LK 078	1.34	0.01	0.22	0.005	826	5.05	2.3	0.34	63	0.05	0.13	5.95	4	61	2	5	1.298	2.5	4.65	0.005
480022	6545964	nodular	THK LK 079	0.69	0.12	0.12	0.005	1112	3.66	5.3	3.5	83	0.3	0.12	3.6	6	10	3	5	0.847	2.5	6.3	0.005
479844	6545819	hardpan	THK LK 080	2.14	0.02	0.39	0.005	1016	9.42	3.4	1.51	52	0.05	0.15	9.69	4	65	3	5	2.114	2.5	5.36	0.005
479844	6545819	hardpan	THK LK 080a	1.97	0.02	0.34	0.005	1036	8.62	3.2	1.03	52	0.1	0.13	8.99	5	72	2	5	1.967	2.5	5.46	0.005
479754	6545780	nodular	THK LK 081	1.27	0.04	0.22	0.005	1397	5.46	4.5	2.12	72	0.1	0.14	5.91	5	46	5	5	1.311	2.5	6.4	0.005
479629	6545685	nodular/hardpan	THK LK 082	1.39	0.03	0.25	0.005	1717	6.13	4.8	1.31	47	0.2	0.15	6.48	7	59	4	5	1.478	2.5	7.65	0.005
479589	6545664	nodular/hardpan	THK LK 083	1.98	0.005	0.34	0.005	903	7.68	2.8	0.4	129	0.1	0.12	8.69	6	72	4	5	1.902	2.5	4.41	0.005
479553	6545649	nodular/hardpan	THK LK 084	1.19	0.15	0.2	0.03	1081	5.21	4.7	0.93	59	0.7	0.12	5.62	9	32	8	5	1.287	2.5	5.42	0.005
479756	6545603	hardpan/nodular	THK LK 085	2.36	0.02	0.39	0.005	1194	10.1	3.1	0.71	100	0.1	0.16	10.93	6	85	3	5	2.393	2.5	5.97	0.005
479733	6545632	nodular	THK LK 086	1.05	0.07	0.18	0.005	1715	4.94	4.9	1.95	49	0.2	0.13	5.1	7	43	3	5	1.162	2.5	7.84	0.005
479694	6545642	nodular	THK LK 087	0.81	0.06	0.14	0.005	1193	3.73	5	3.3	38	0.05	0.12	3.97	4	34	4	5	0.892	2.5	5.6	0.005
479624	6545539	hardpan	THK LK 088	1.73	0.01	0.3	0.005	885	6.89	2.4	0.36	117	0.05	0.12	7.7	5	89	3	5	1.705	2.5	4.47	0.005
479580	6545477	nodular	THK LK 089	2.87	0.02	0.48	0.005	1121	12.51	2.8	0.57	118	0.1	0.16	13.34	7	84	3	5	2.895	2.5	5.8	0.005
479827	6545562	hardpan	THK LK 090	2.53	0.01	0.42	0.005	1038	10.76	2.8	0.48	106	0.1	0.13	11.57	6	98	3	5	2.494	2.5	5.02	0.005
479827	6545562	hardpan	THK LK 090a	3.02	0.02	0.5	0.005	1133	12.55	3.2	0.57	135	0.05	0.13	13.59	8	110	3	5	2.919	2.5	5.32	0.005
479796	6545566	nodular/hardpan	THK LK 091	1.66	0.02	0.31	0.005	1227	6.02	3.3	0.65	60	0.1	0.12	6.92	6	82	3	5	1.494	2.5	5.85	0.005
479881	6545629	nodular/hardpan	THK LK 092	2.33	0.02	0.4	0.005	1003	9.63	2.4	0.35	118	0.1	0.12	10.59	5	88	3	5	2.3	2.5	5.59	0.005
479978	6545656	hardpan	THK LK 093	0.75	0.04	0.12	0.005	1351	3.54	4.8	1.83	92	0.4	0.16	3.62	8	33	2	5	0.843	2.5	6.46	0.005
480372	6545924	nodular/hardpan	THK LK 094	1.66	0.09	0.28	0.005	1614	7.33	6.6	2.09	41	0.2	0.15	7.92	6	38	4	5	1.757	2.5	8.61	0.005
480461	6545970	nodular/hardpan	THK LK 095	4.72	0.05	0.75	0.005	1639	21.48	4.6	0.68	82	0.2	0.16	21.98	7	74	4	5	4.885	2.5	9.15	0.005
480706	6545865	nodular/hardpan	THK LK 096	2.78	0.02	0.48	0.005	1471	11.08	3.6	0.5	165	0.1	0.15	12.31	6	107	4	5	2.702	2.5	6.87	0.005
480658	6545841	nodular/hardpan	THK LK 097	2.06	0.02	0.35	0.005	1150	8.56	3.5	0.63	88	0.2	0.18	9.21	6	53	3	5	1.99	2.5	6.15	0.005
480579	6545779	nodular	THK LK 098	0.82	0.04	0.14	0.005	1568	4	5.8	2.1	42	0.2	0.16	4.09	6	27	3	5	0.956	2.5	7.5	0.005
480579	6545779	nodular	THK LK 098a	0.77	0.03	0.13	0.005	1370	3.59	5.5	2.51	39	0.3	0.11	3.78	8	32	2	5	0.889	2.5	6.41	0.005

Appendix 3b: Geochemical Assay Results 001-098: Sb-Zr

Easting GDA	Northing GDA	Sample Morphology	Sample No.	Sb (ppm)	Sc (ppm)	Se (ppm)	Sm (ppm)	Sn (ppm)	Sr (ppm)	Ta (ppm)	Tb (ppm)	Te (ppm)	Th (ppm)	Ti (ppm)	Tl (ppm)	Tm (ppm)	U (ppm)	V (ppm)	W (ppm)	Y (ppm)	Yb (ppm)	Zn (ppm)	Zr (ppm)
480337	6547091	powder	THK LK 001	0.04	0.5	0.5	0.53	0.24	479.45	0.005	0.073	0.025	0.92	78	0.06	0.03	0.19	9	0.11	2.23	0.19	7	2.9
480332	6547066	hardpan	THK LK 002	0.1	3	0.5	1.44	0.75	312.12	0.005	0.206	0.025	3.01	147	0.12	0.08	0.21	25	0.25	6.09	0.53	23	8.2
480299	6547040	nodular	THK LK 003	0.07	2	0.5	2.15	0.39	273.73	0.005	0.319	0.025	4.04	109	0.1	0.14	0.27	30	0.16	12.19	0.79	16	7.7
480250	6547012	hardpan	THK LK 004	0.05	2	0.5	1.69	0.48	415.93	0.005	0.242	0.025	2.27	78	0.1	0.1	0.29	15	0.1	9.01	0.61	11	3.8
480212	6546978	nodular	THK LK 005	0.02	1	0.5	2.22	0.26	514.14	0.005	0.324	0.025	1.18	31	0.09	0.13	0.41	6	0.07	11.54	0.78	6	1.2
480169	6546926	nodular	THK LK 006	0.03	1	0.5	2.17	0.23	359.09	0.005	0.329	0.025	1.08	35	0.08	0.13	0.24	5	0.06	11.58	0.76	3	0.5
479867	6546774	nodular	THK LK 007	0.03	1	0.5	1.58	0.28	146.42	0.005	0.242	0.025	5.22	75	0.08	0.11	0.26	50	0.08	9.2	0.66	6	8
479821	6546744	nodular	THK LK 008	0.04	2	0.5	1.81	0.46	150.4	0.005	0.28	0.025	7.82	92	0.11	0.12	0.31	69	0.06	10.31	0.76	13	10.3
479786	6546723	nodular	THK LK 009	0.02	2	0.5	1.05	0.23	97.88	0.005	0.15	0.025	6.24	69	0.05	0.06	0.29	80	0.025	5.15	0.4	7	8
479742	6546701	hardpan	THK LK 010	0.05	2	0.5	1.61	0.36	385.69	0.005	0.241	0.025	3	50	0.09	0.1	0.38	29	0.08	8.73	0.65	10	1.1
479742	6546701	hardpan	THK LK 010a	0.07	1	0.5	1.34	0.3	278.29	0.005	0.2	0.025	2.09	58	0.07	0.09	0.32	22	0.025	7.34	0.56	9	0.7
479708	6546679	hardpan	THK LK 011	0.06	2	0.5	3.86	0.17	430.21	0.005	0.543	0.025	2.42	31	0.09	0.21	0.3	15	0.06	20.99	1.21	4	3.2
479656	6546642	hardpan	THK LK 012	0.04	1	0.5	2	0.21	479.56	0.005	0.287	0.025	2	30	0.06	0.11	0.29	16	0.025	10.42	0.65	3	1.4
479605	6546618	hardpan	THK LK 013	0.01	2	0.5	2.47	0.3	558.31	0.005	0.368	0.025	1.42	35	0.09	0.14	0.41	8	0.025	13.7	0.85	10	1.9
479570	6546596	hardpan	THK LK 014	0.03	1	0.5	2.27	0.22	618.98	0.005	0.344	0.025	1.06	19	0.07	0.15	0.39	4	0.025	13.26	0.86	7	1
479529	6546570	hardpan	THK LK 015	0.03	2	0.5	1.68	0.37	464.96	0.005	0.248	0.025	1.44	27	0.09	0.1	0.34	9	0.025	9.49	0.6	10	1.8
479444	6546510	nodular	THK LK 016	0.01	2	0.5	2.24	0.32	623.06	0.005	0.33	0.025	2.05	30	0.09	0.13	0.36	11	0.06	13.03	0.76	7	2.6
479394	6546489	hardpan	THK LK 017	0.02	0.5	0.5	1.33	0.22	429.9	0.005	0.196	0.09	1.78	28	0.2	0.08	0.26	14	0.06	7.54	0.46	5	1.6
479356	6546465	hardpan	THK LK 018	0.04	2	0.5	2.33	0.27	699.62	0.005	0.338	0.05	1.13	41	0.11	0.13	0.37	4	0.22	13.7	0.79	2	1.4
479312	6546444	hardpan	THK LK 019	0.06	1	0.5	1.39	0.27	691.58	0.005	0.216	0.025	1.37	55	0.11	0.1	0.37	7	0.16	8.1	0.59	4	1.2
479271	6546410	nodular	THK LK 020	0.05	2	0.5	2.18	0.34	1026.69	0.005	0.331	0.06	2.53	44	0.12	0.14	0.59	8	0.16	12.08	0.84	3	6.7
479271	6546410	nodular	THK LK 020a	0.07	2	0.5	2.32	0.36	988.99	0.005	0.343	0.025	1.74	67	0.11	0.14	0.61	10	0.025	12.44	0.84	3	3.6
479235	6546390	nodular	THK LK 021	0.06	2	0.5	3.24	0.27	772.29	0.005	0.507	0.025	2.31	43	0.11	0.21	0.38	3	0.21	19.09	1.22	3	2.9
478972	6546231	nodular	THK LK 022	0.04	2	0.5	1.53	0.4	575.28	0.005	0.235	0.025	2.79	67	0.11	0.11	0.35	23	0.09	9.22	0.66	4	3.5
478809	6546123	nodular	THK LK 023	0.02	1	0.5	1.51	0.16	549	0.005	0.229	0.025	1.25	26	0.07	0.1	0.25	1	0.025	8.64	0.61	2	1.9
478969	6545996	nodular	THK LK 024	0.01	1	0.5	2.39	0.24	419.7	0.005	0.374	0.025	1.44	43	0.08	0.16	0.2	4	0.06	13.98	0.95	6	1.2
478996	6545997	hardpan	THK LK 025	0.03	1	0.5	2.04	0.19	431.86	0.005	0.302	0.025	1.1	36	0.07	0.13	0.2	1	0.08	11.45	0.71	2	1.6
479093	6546038	hardpan	THK LK 026	0.04	0.5	0.5	1.46	0.21	429.15	0.005	0.209	0.025	1.01	43	0.06	0.09	0.17	1	0.06	8.43	0.53	2	1.2
479198	6546127	nodular	THK LK 027	0.05	2	0.5	2.82	0.23	474.24	0.005	0.431	0.025	1.42	52	0.09	0.18	0.21	3	0.08	17.66	1.06	3	1.6
479211	6546152	nodular	THK LK 028	0.03	2	0.5	2.03	0.25	513.2	0.005	0.335	0.025	1.68	42	0.07	0.15	0.21	5	0.07	12.57	0.91	4	1.6
479258	6546166	nodular	THK LK 029	0.05	1	0.5	1.94	0.24	590.06	0.005	0.316	0.025	1.35	46	0.07	0.15	0.32	3	0.05	12.46	0.88	4	1
479478	6546317	hardpan	THK LK 030	0.03	2	0.5	4.44	0.36	451.69	0.005	0.669	0.025	4.82	43	0.1	0.27	0.38	24	0.06	27.25	1.52	4	5.2
479478	6546317	hardpan	THK LK 030a	0.08	2	0.5	4.86	0.42	550.28	0.005	0.743	0.05	3.52	63	0.12	0.3	0.45	26	0.025	29.7	1.72	3	3.5
479537	6546345	hardpan	THK LK 031	0.12	2	0.5	2.41	0.33	620.33	0.005	0.364	0.06	2.32	55	0.1	0.14	0.5	19	0.06	14.2	0.88	2	1.8
479571	6546361	hardpan	THK LK 032	0.12	3	0.5	1.88	0.37	473.06	0.005	0.298	0.07	8.94	94	0.1	0.14	0.64	82	0.025	11.52	0.83	3	8.2
479603	6546380	nodular	THK LK 033	0.03	2	0.5	0.96	0.53	787.31	0.005	0.144	0.025	1.86	69	0.11	0.06	0.36	13	0.025	5.21	0.41	5	5.5
479646	6546408	nodular	THK LK 034	0.08	2	0.5	0.81	0.36	694.8	0.005	0.126	0.025	1.57	76	0.1	0.06	0.33	13	0.05	4.64	0.36	5	3.2
479686	6546425	nodular	THK LK 035	0.01	2	0.5	1.72	0.41	436.86	0.005	0.28	0.025	3.38	65	0.09	0.13	0.29	24	0.025	11.12	0.81	3	5.2
479728	6546450	nodular	THK LK 036	0.05	0.5	0.5	0.94	0.17	329.82	0.005	0.15	0.025	0.59	24	0.05	0.07	0.17	1	0.025	5.78	0.38	1	0.5
479764	6546488	nodular	THK LK 037	0.05	0.5	0.5	1.86	0.18	533.16	0.005	0.3	0.025	0.76	32	0.06	0.13	0.2	1	0.025	11.9	0.76	0.5	1
479802	6546512	hardpan	THK LK 038	0.05	0.5	0.5	1.38	0.13	684.1	0.005	0.197	0.025	0.98	26	0.04	0.06	0.44	1	0.025	7.58	0.51	0.5	1
479875	6546577	hardpan	THK LK 039	0.03	0.5	0.5	0.98	0.13	256.65	0.005	0.154	0.025	0.49	24	0.03	0.07	0.1	1	0.05	5.81	0.41	1	0.5
479997	6546666	hardpan	THK LK 040	0.06	1	0.5	1.88	0.26	391.98	0.005	0.293	0.025	0.88	47	0.07	0.12	0.23	4	0.025	11.47	0.74	5	0.9
479997	6546666	hardpan	THK LK 040a	0.06	1	0.5	1.58	0.28	459.88	0.005	0.248	0.025	0.89	48	0.07	0.1	0.3	5	0.07	9.74	0.64	4	1.2
480038	6546447	nodular	THK LK 041	0.07	0.5	0.5	1.66	0.21	481.85	0.005	0.25	0.025	0.82	37	0.06	0.11	0.24	3	0.06	10.43	0.61	2	0.9
480030	6546424	hardpan	THK LK 042	0.05	0.5	0.5	0.84	0.15	418.45	0.005	0.13	0.025	0.6	29	0.04	0.06	0.14	1	0.025	4.76	0.36	1	0.6
479741	6546257	nodular?	THK LK 043	0.07	0.5	0.5	1.36	0.16	433.09	0.005	0.22	0.025	0.7	27	0.05	0.1	0.18	1	0.05	9.22	0.57	1	0.6
479713	6546252	nodular	THK LK 044	0.06	1	0.5	2.46	0.22	423.68	0.005	0.392	0.025	0.93	45	0.06	0.16	0.25	3	0.05	16.81	0.94	1	0.8
479710	6546212	nodular	THK LK 045	0.09	1	0.5	2.27	0.23	475.61	0.005	0.346	0.05	0.93	36	0.07	0.14	0.2	5	0.06	12.91	0.8	6	0.9
479671	6546200	nodular	THK LK 046	0.06	0.5	0.5	1.54	0.18	290.43	0.005	0.254	0.025	1.22	31	0.05	0.11	0.15	7	0.05	10.15	0.67	2	1.1
479664	6546165	nodular	THK LK 047	0.09	2	0.5	4.36	0.28	392.3	0.005	0.682	0.025	2.15	50	0.1	0.28	0.21	12	0.025	26.93	1.59	2	1.7
479628	6546137	nodular	THK LK 048	0.09	1	0.5	1.96	0.34	409.66	0.005	0.299	0.06	1.88	46	0.08	0.13	0.2	13	0.06	12.39	0.77	1	1.2
479569	6546143	hardpan	THK LK 049	0.06	0.5	0.5	1.38	0.17	407.25	0.005	0.214	0.025	0.57	36	0.08	0.09	0.15	1	0.07	8.36	0.55	2	0.7
479553	6546115	hardpan	THK LK 050	0.1	2	0.5	1.33	0.34	442.65	0.005	0.202	0.06	2.53	57	0.08	0.09	0.42	47	0.05	7.66	0.53	5	1.7

Appendix 3b: Geochemical Assay Results 001-098: Sb-Zr

Easting GDA	Northing GDA	Sample Morphology	Sample No.	Sb (ppm)	Sc (ppm)	Se (ppm)	Sm (ppm)	Sn (ppm)	Sr (ppm)	Ta (ppm)	Tb (ppm)	Te (ppm)	Th (ppm)	Ti (ppm)	Tl (ppm)	Tm (ppm)	U (ppm)	V (ppm)	W (ppm)	Y (ppm)	Yb (ppm)	Zn (ppm)	Zr (ppm)
479553	6546115	hardpan	THK LK 050a	0.07	1	0.5	1.59	0.31	583.91	0.005	0.244	0.07	1.18	40	0.09	0.11	0.35	13	0.025	9.6	0.67	6	1
479514	6546098	hardpan	THK LK 051	0.1	1	0.5	1.55	0.37	564.83	0.005	0.227	0.06	1.31	61	0.08	0.1	0.31	9	0.05	8.5	0.61	4	0.8
479479	6546083	hardpan	THK LK 052	0.08	1	0.5	2.11	0.31	542.15	0.005	0.341	0.025	0.87	37	0.08	0.15	0.24	2	0.05	12.79	0.91	6	1.1
479444	6546050	hardpan	THK LK 053	0.07	1	0.5	3.11	0.3	662.27	0.005	0.433	0.07	0.87	53	0.1	0.17	0.38	5	0.07	17.49	1.03	2	1.7
479410	6546059	nodular	THK LK 054	0.05	0.5	0.5	1.15	0.16	436.6	0.005	0.169	0.025	0.62	42	0.05	0.08	0.15	1	0.06	6.49	0.47	2	0.6
479404	6546029	nodular	THK LK 055	0.05	0.5	0.5	1.74	0.18	367.1	0.005	0.252	0.025	0.65	34	0.05	0.11	0.13	1	0.025	9.89	0.64	1	0.6
479350	6545979	nodular	THK LK 056	0.05	0.5	0.5	1.77	0.24	489.6	0.005	0.251	0.025	0.91	37	0.05	0.09	0.2	1	0.025	10.06	0.73	4	0.5
479305	6545986	nodular	THK LK 057	0.04	0.5	0.5	0.75	0.19	413.53	0.005	0.113	0.025	0.64	37	0.05	0.05	0.14	1	0.025	4.36	0.35	4	0.9
479258	6545969	nodular	THK LK 058	0.07	1	0.5	1.19	0.2	807.87	0.005	0.188	0.12	1.12	50	0.1	0.09	0.21	1	0.025	7.27	0.57	6	2.7
479222	6545947	nodular	THK LK 059	0.06	1	0.5	1.63	0.23	665.04	0.005	0.235	0.05	0.89	29	0.06	0.1	0.25	1	0.025	9.48	0.57	2	1.5
479222	6545947	nodular	THK LK 059a	0.06	0.5	0.5	0.93	0.15	508.57	0.005	0.14	0.025	0.58	31	0.04	0.06	0.16	1	0.025	5.93	0.4	2	0.6
479171	6545918	nodular	THK LK 060	0.06	1	0.5	2.22	0.26	584.75	0.005	0.325	0.025	0.97	41	0.08	0.15	0.28	1	0.025	13.93	0.9	4	1.2
479952	6546128	nodular	THK LK 061	0.05	1	0.5	1.77	0.24	311.96	0.005	0.273	0.08	1.29	58	0.06	0.12	0.16	5	0.025	10.79	0.71	4	1.9
479865	6546078	nodular	THK LK 062	0.06	0.5	0.5	1.36	0.21	351.12	0.005	0.207	0.025	1	35	0.05	0.09	0.16	4	0.025	8.32	0.56	2	0.7
479830	6546086	nodular	THK LK 063	0.07	0.5	0.5	1.59	0.23	536.31	0.005	0.237	0.025	1.04	39	0.06	0.1	0.19	8	0.025	9.33	0.63	3	0.6
479789	6546054	nodular	THK LK 064	0.06	0.5	0.5	2.44	0.24	442.19	0.005	0.362	0.025	0.87	43	0.06	0.14	0.2	3	0.025	13.78	0.83	2	0.8
479757	6546031	nodular	THK LK 065	0.05	0.5	0.5	1.33	0.17	303.96	0.005	0.209	0.025	0.59	29	0.04	0.09	0.12	1	0.025	7.79	0.52	2	0.3
479728	6545996	hardpan	THK LK 066	0.07	1	0.5	2.78	0.26	500.11	0.005	0.41	0.025	1.11	69	0.09	0.17	0.24	2	0.025	14.92	1.02	4	2.1
479690	6545981	hardpan	THK LK 067	0.09	2	0.5	1.71	0.35	233.56	0.005	0.237	0.025	3.28	89	0.05	0.1	0.35	32	0.025	9.16	0.59	7	4.7
479667	6545941	hardpan	THK LK 068	0.1	1	0.5	0.82	0.45	142.32	0.005	0.124	0.025	2.74	123	0.03	0.06	0.22	34	0.025	4.33	0.37	7	5.6
479613	6545940	nodular	THK LK 069	0.08	1	0.5	0.74	0.22	370.68	0.005	0.106	0.025	2.49	72	0.04	0.05	0.4	23	0.025	4.01	0.31	5	3.9
479582	6545900	hardpan	THK LK 070	0.09	1	0.5	1.96	0.38	384.22	0.005	0.271	0.025	2.14	74	0.06	0.11	0.33	27	0.025	10.52	0.63	3	3.1
479582	6545900	hardpan	THK LK 070a	0.08	2	0.5	3.21	0.3	611.56	0.005	0.424	0.05	1.38	67	0.09	0.16	0.31	9	0.025	18.49	0.93	3	1.1
479547	6545901	hardpan/nodular	THK LK 071	0.1	2	0.5	3.03	0.36	529.24	0.005	0.458	0.06	3.93	69	0.08	0.2	0.46	32	0.025	18.26	1.18	3	3.3
479496	6545869	nodular	THK LK 072	0.01	0.5	0.5	0.25	0.46	20.35	0.005	0.031	0.025	1	14	0.05	0.01	0.2	5	0.025	0.94	0.08	12	1.5
479317	6545782	nodular	THK LK 073	0.09	0.5	0.5	2.58	0.19	346.91	0.005	0.358	0.025	0.66	36	0.05	0.13	0.19	1	0.025	13.96	0.78	3	0.6
480325	6546117	nodular	THK LK 074	0.04	0.5	0.5	1.59	0.16	488.34	0.005	0.323	0.025	0.61	38	0.04	0.1	0.14	1	0.025	12.86	0.84	3	0.4
480301	6546110	nodular	THK LK 075	0.08	2	0.5	1.67	0.3	798.71	0.005	0.242	0.025	1.19	67	0.09	0.11	0.29	5	0.025	9.27	0.7	4	1.5
480278	6546072	nodular	THK LK 076	0.06	1	0.5	2.04	0.23	458.24	0.005	0.316	0.025	1.09	52	0.07	0.15	0.16	3	0.025	12.51	0.85	3	1.8
480130	6546017	nodular	THK LK 077	0.05	0.5	0.5	1.1	0.17	372.13	0.005	0.169	0.025	0.75	46	0.04	0.08	0.11	2	0.025	6.59	0.47	2	1.7
480115	6545997	nodular	THK LK 078	0.07	0.5	0.5	1.24	0.16	391.86	0.005	0.185	0.025	0.83	43	0.04	0.08	0.14	4	0.025	7.24	0.5	3	0.6
480022	6545964	nodular	THK LK 079	0.07	1	0.5	0.7	0.33	1009.19	0.005	0.099	0.025	1.35	68	0.08	0.05	0.35	14	0.025	3.71	0.29	2	4.1
479844	6545819	hardpan	THK LK 080	0.06	0.5	0.5	1.97	0.2	586.69	0.005	0.306	0.025	0.85	50	0.06	0.14	0.25	3	0.025	12.82	0.88	2	0.9
479844	6545819	hardpan	THK LK 080a	0.05	1	0.5	1.8	0.2	582.67	0.005	0.272	0.05	0.79	37	0.06	0.12	0.29	1	0.025	11.08	0.75	2	0.7
479754	6545780	nodular	THK LK 081	0.06	1	0.5	1.15	0.21	980.44	0.005	0.177	0.025	1.07	58	0.08	0.09	0.29	4	0.025	6.93	0.56	3	2
479629	6545685	nodular/hardpan	THK LK 082	0.06	1	0.5	1.34	0.34	887.18	0.005	0.202	0.025	1.21	59	0.07	0.1	0.23	6	0.025	7.67	0.6	5	1.4
479589	6545664	nodular/hardpan	THK LK 083	0.05	0.5	0.5	1.84	0.24	393.05	0.005	0.285	0.025	0.84	39	0.06	0.13	0.15	4	0.025	10.84	0.8	5	0.3
479553	6545649	nodular/hardpan	THK LK 084	0.15	2	0.5	1.13	0.51	442.39	0.005	0.168	0.025	4.9	145	0.06	0.08	0.44	47	0.025	5.9	0.48	4	7
479756	6545603	hardpan/nodular	THK LK 085	0.06	1	0.5	2.2	0.25	536.16	0.005	0.322	0.025	1.04	59	0.06	0.13	0.23	3	0.025	12.36	0.81	4	0.9
479733	6545632	nodular	THK LK 086	0.06	1	0.5	1.03	0.35	902.14	0.005	0.145	0.025	1.27	78	0.07	0.06	0.25	7	0.025	5.23	0.42	3	2.7
479694	6545642	nodular	THK LK 087	0.06	1	0.5	0.78	0.23	939.13	0.005	0.118	0.025	1.04	55	0.06	0.06	0.21	5	0.025	4.25	0.35	2	2.8
479624	6545539	hardpan	THK LK 088	0.05	0.5	0.5	1.63	0.19	382.18	0.005	0.244	0.025	0.72	41	0.06	0.11	0.15	1	0.025	9.18	0.69	2	0.5
479580	6545477	nodular	THK LK 089	0.09	1	0.5	2.71	0.2	556.32	0.005	0.401	0.025	1.17	47	0.06	0.17	0.2	3	0.025	15.56	1.02	5	1
479827	6545562	hardpan	THK LK 090	0.05	0.5	0.5	2.34	0.18	504.36	0.005	0.344	0.025	0.82	42	0.06	0.15	0.17	1	0.025	14.07	0.88	3	0.4
479827	6545562	hardpan	THK LK 090a	0.05	1	0.5	2.77	0.17	557.45	0.005	0.409	0.025	0.78	36	0.07	0.18	0.2	1	0.025	15.94	1.03	3	0.5
479796	6545566	nodular/hardpan	THK LK 091	0.05	1	0.5	1.46	0.23	555.28	0.005	0.238	0.025	1.02	38	0.06	0.12	0.12	1	0.025	9.36	0.79	4	1.1
479881	6545629	nodular/hardpan	THK LK 092	0.05	1	0.5	2.16	0.19	366.69	0.005	0.326	0.025	1.05	31	0.06	0.14	0.16	3	0.025	15.78	0.86	4	1
479978	6545656	hardpan	THK LK 093	0.07	1	0.5	0.72	0.35	737.98	0.005	0.104	0.025	1.13	93	0.06	0.04	0.21	7	0.025	3.54	0.31	6	2.3
480372	6545924	nodular/hardpan	THK LK 094	0.07	2	0.5	1.55	0.32	1009.27	0.005	0.228	0.08	1.46	66	0.13	0.1	0.43	11	0.025	8.54	0.65	5	3.9
480461	6545970	nodular/hardpan	THK LK 095	0.08	2	0.5	4.4	0.32	618.21	0.005	0.634	0.06	1.56	55	0.1	0.26	0.29	4	0.025	25.26	1.49	3	2.4
480706	6545865	nodular/hardpan	THK LK 096	0.06	1	0.5	2.55	0.22	523.47	0.005	0.395	0.025	1.63	45	0.07	0.18	0.24	5	0.025	14.61	1.05	4	0.9
480658	6545841	nodular/hardpan	THK LK 097	0.06	1	0.5	1.84	0.22	680.73	0.005	0.28	0.025	1.1	62	0.07	0.13	0.25	1	0.025	11.56	0.75	1	0.9
480579	6545779	nodular	THK LK 098	0.09	1	0.5	0.83	0.29	864.58	0.005	0.116	0.025	1.17	97	0.07	0.05	0.29	9	0.025	3.97	0.34	4	2.1
480579	6545779	nodular	THK LK 098a	0.07	1	0.5	0.75	0.34	926.9	0.005	0.112	0.025	1.05	60	0.06	0.05	0.29	8	0.025	3.81	0.33	5	1.6

Appendix 3b: Geochemical Assay Results: Controls including checks, standards and blanks Au-Zr.

Sample No.	Au (ppb)	Ag (ppm)	Al (ppm)	As (ppm)	Ba (ppm)	Be (ppm)	Bi (ppm)	Ca (%)	Cd (ppm)	Ce (ppm)	Co (ppm)	Cr (ppm)	Cs (ppm)	Cu (ppm)	Dy (ppm)	Er (ppm)	Eu (ppm)	Fe (%)	Ga (ppm)	Gd (ppm)	Hf (ppm)	Ho (ppm)	In (ppm)	K (ppm)
CHECKS																								
THK LK 001	9	0.025	8081	0.5	131	0.19	0.04	12.86	0.025	5.72	3	9	0.472	4	0.48	0.25	0.14	0.84	2	0.58	0.06	0.1	0.005	1890
THK LK 020	71	0.025	10922	2	490	0.41	0.04	23.77	0.1	14.66	5.7	7	0.663	5	1.87	1.01	0.55	0.72	2.9	2.33	0.08	0.38	0.01	1829
THK LK 038	22	0.025	5546	1	207	0.2	0.02	27.06	0.11	9.33	4.8	5	0.346	7	1.23	0.65	0.33	0.37	1.48	1.49	0.02	0.25	0.005	1138
THK LK 056	20	0.025	7814	1	229	0.22	0.03	28.19	0.16	13.74	6.5	7	0.511	6	1.82	1.02	0.5	0.53	2.12	2.19	0.03	0.38	0.005	1426
THK LK 074	12	0.025	5530	0.5	197	0.34	0.02	24.82	0.16	12.8	7.3	5	0.358	6	1.86	1.05	0.51	0.38	1.53	2.34	0.01	0.39	0.005	1105
THK LK 092	9	0.025	6309	1	154	0.41	0.03	26.08	0.17	14.21	6.7	6	0.404	6	2.18	1.18	0.58	0.64	1.77	2.67	0.02	0.45	0.005	1177
STANDARDS																								
CMM-07	57	0.86	10708	109	10	0.2	8.68	9.25	0.89	6.92	37.5	309	0.14	88	0.55	0.5	0.15	5.8	10.47	0.91	0.76	0.33	0.06	517
BSL9	5	0.28	9848	13	51	0.07	2.27	1.12	0.25	2.24	10.3	159	0.045	28	0.15	0.08	0.04	4.31	3.82	0.41	0.33	0.27	0.02	6357
NGL-21	20	0.39	7666	17	92	0.06	2.93	0.94	0.29	2.55	9.1	348	0.026	111	0.12	0.06	0.03	4.61	6.93	0.14	0.45	0.02	0.04	818
BSL9	7	0.26	9239	16	49	0.07	2.42	1.16	0.24	2.39	11	165	0.045	28	0.15	0.08	0.04	4.45	4.53	0.41	0.34	0.27	0.02	6500
BLANKS																								
Control Blank	0.5	0.025	10	0.5	0.5	0.025	0.005	0.02	0.025	0.01	0.05	1	0.001	0.05	0.005	0.005	0.005	0.005	0.025	0.005	0.005	0.005	0.005	10
Control Blank	2	0.025	38	0.5	2	0.025	0.005	0.03	0.025	0.03	0.1	1	0.003	0.05	0.02	0.005	0.005	0.01	0.025	0.02	0.005	0.005	0.005	25

continued:

Sample No.	La (ppm)	Li (ppm)	Mg (%)	Mn (ppm)	Mo (ppm)	Nb (ppm)	Nd (ppm)	Ni (ppm)	P (ppm)	Pb (ppm)	Pd (ppb)	Pr (ppm)	Pt (ppb)	Rb (ppm)	Re (ppm)	Sb (ppm)	Sc (ppm)	Se (ppm)	Sm (ppm)	Sn (ppm)	Sr (ppm)	Ta (ppm)	Tb (ppm)	Te (ppm)
CHECKS																								
THK LK 001	3.04	5.7	0.98	47	0.2	0.1	3.15	6	10	3	5	0.75	2.5	7.75	0.005	0.09	1	0.5	0.62	0.31	487.37	0.005	0.085	0.025
THK LK 020	9.95	6.6	2.17	66	0.1	0.17	11.05	8	46	4	5	2.464	2.5	9.58	0.005	0.1	2	0.5	2.24	0.38	982.89	0.005	0.322	0.025
THK LK 038	6.02	2.2	0.67	37	0.05	0.16	6.6	6	65	2	5	1.447	2.5	5.86	0.005	0.08	1	0.5	1.37	0.19	708.66	0.005	0.206	0.07
THK LK 056	9.74	2.6	0.53	139	0.1	0.17	10.28	6	92	3	5	2.257	2.5	8.07	0.005	0.07	2	0.5	2.08	0.28	583.19	0.005	0.318	0.025
THK LK 074	9.15	3.2	0.39	110	0.05	0.15	10.2	5	100	2	5	2.225	2.5	5.94	0.005	0.05	1	0.5	2.11	0.22	471.71	0.005	0.32	0.025
THK LK 092	10.74	3.4	0.4	135	0.1	0.14	11.86	6	81	3	5	2.587	2.5	6.73	0.005	0.06	2	0.5	2.41	0.23	414.58	0.005	0.368	0.06
STANDARDS																								
CMM-07	11.8	1.9	3.28	536	20.2	0.05	3.21	91	101	46	122	0.781	232	1.88	0.005	4.35	7	0.5	0.68	1.3	107.18	0.005	0.099	6.28
BSL9	5.04	0.7	0.42	159	8	0.12	0.9	28	116	14	20	0.227	9	0.82	0.005	1.74	2	0.5	0.18	6.53	17.61	0.005	0.027	8.64
NGL-21	0.87	0.5	0.38	130	7.5	0.08	0.74	24	224	12	197	0.187	215	0.4	0.005	1.52	5	9	0.16	0.84	19.24	0.005	0.021	5.08
BSL9	5.68	0.8	0.43	169	7.8	0.12	0.93	29	105	13	22	0.231	14	0.86	0.005	1.48	2	0.5	0.21	6.52	14.25	0.005	0.028	8.65
BLANKS																								
Control Blank	0.005	0.05	0.005	0.5	0.05	0.01	0.02	1	10	0.5	5	0.0025	2.5	0.04	0.005	0.01	0.5	0.5	0.005	0.025	0.01	0.005	0.0025	0.025
Control Blank	0.02	0.05	0.005	2	0.05	0.01	0.03	0.5	10	0.5	5	0.018	2.5	0.06	0.005	0.01	0.5	0.5	0.02	0.025	0.11	0.005	0.0025	0.11

continued:

Sample No.	Th (ppm)	Ti (ppm)	Tl (ppm)	Tm (ppm)	U (ppm)	V (ppm)	W (ppm)	Y (ppm)	Yb (ppm)	Zn (ppm)	Zr (ppm)
CHECKS											
THK LK 001	1.26	89	0.06	0.04	0.23	11	0.025	2.64	0.23	8	2.8
THK LK 020	1.63	75	0.1	0.14	0.62	9	0.025	11.58	0.82	4	2.9
THK LK 038	1.02	45	0.07	0.09	0.39	1	0.025	7.82	0.56	0.5	1.3
THK LK 056	1.14	49	0.08	0.15	0.24	1	0.025	12.02	0.88	6	1.2
THK LK 074	0.81	41	0.06	0.14	0.19	1	0.025	12.41	0.86	4	0.5
THK LK 092	1.19	46	0.07	0.16	0.18	4	0.025	14.1	0.96	4	1.2
STANDARDS											
CMM-07	7.78	1060	8.81	0.04	9.69	299	0.06	3.22	0.24	76	31
BSL9	2.55	533	10.58	0.01	5.05	100	0.69	0.83	0.08	27	10
NGL-21	5.09	1082	1.81	0.01	9.17	152	0.14	0.52	0.07	22	16.2
BSL9	2.81	565	11.46	0.01	5.09	104	0.52	0.74	0.08	27	9.7
BLANKS											
Control Blank	0.005	2.5	0.005	0.005	0.005	1	0.07	0.01	0.005	1	0.2
Control Blank	0.08	6	0.03	0.005	0.01	1	0.025	0.09	0.005	0.5	0.3

NOTE: All data values returned from analysis with a value below detection limit and denoted by 'X' were given the value of half the detection limit (X/2) to average and reduce the skew of the data.

Appendix 3c: Information on standards used Au-Zr – provided by Genalysis.

Element		Au	Ag	Al	As	Ba	Be	Bi	Ca	Cd	Ce	Co	Cr	Cs	Cu	Dy	Er	Eu	Fe	Ga	Gd	Hf	Ho	In	K	La	Li
Method		**B/MS**	**B/MS**	**B/OES**	**B/MS**	**B/MS**	**B/MS**	**B/MS**	**B/OES**	**B/MS**	**B/MS**	**B/MS**	**B/OES**	**B/MS**	**B/OES**	**B/MS**	**B/MS**	**B/MS**	**B/OES**	**B/MS**	**B/MS**	**B/MS**	**B/MS**	**B/MS**	**B/OES**	**B/MS**	**B/MS**
Detection		**1**	**0.05**	**20**	**1**	**1**	**0.05**	**0.01**	**0.01**	**0.05**	**0.01**	**0.1**	**2**	**0.002**	**1**	**0.01**	**0.01**	**0.01**	**0.01**	**0.05**	**0.01**	**0.01**	**0.01**	**0.01**	**20**	**0.01**	**0.1**
Units		**ppb**	**ppm**	**ppm**	**ppm**	**ppm**	**ppm**	**ppm**	**%**	**ppm**	**ppm**	**ppm**	**ppm**	**ppm**	**ppm**	**ppm**	**ppm**	**ppm**	**%**	**ppm**	**ppm**	**ppm**	**ppm**	**ppm**	**ppm**	**ppm**	**ppm**
Duplicates																											
Tube	**Sample Name**																										
19	CMM-07 (Res)	57	0.86	10708	109	10	0.2	8.68	9.25	0.89	6.92	37.5	309	0.14	88	0.55	0.5	0.15	5.8	10.47	0.91	0.76	0.33	0.06	517	11.8	1.9
	CMM-07 (Nom)	**42**	**0.91**	**9930**	**116**	**7**		**8.3**	**6.75**	**0.83**		**35.8**	**293**		**90**				**5.95**						**350**		
54	BSL9 (Res)	5	0.28	9848	13	51	0.07	2.27	1.12	0.25	2.24	10.3	159	0.045	28	0.15	0.08	0.04	4.31	3.82	0.41	0.33	0.27	0.02	6357	5.04	0.7
	BSL9 (Nom)	**7**	**0.3**	**8760**	**14**	**49**	**0.08**	**2.46**	**1.1**	**0.29**	**2.27**	**10.8**	**154**	**0.04**	**27**	**0.14**	**0.07**	**0.04**	**4**	**4.18**	**0.38**	**0.35**	**0.27**	**0.03**	**6280**	**5.5**	**0.8**
66	NGL-21 (Res)	20	0.39	7666	17	92	0.06	2.93	0.94	0.29	2.55	9.1	348	0.026	111	0.12	0.06	0.03	4.61	6.93	0.14	0.45	0.02	0.04	818	0.87	0.5
	NGL-21 (Nom)	**18**	**0.42**	**7240**	**17**	**100**		**3**	**0.84**	**0.3**		**8.3**	**360**		**110**				**4.58**						**850**		
107	PL-15 (Res)	15	0.22	8488	13	19	0.19	2.01	0.22	0.19	3.74	9.3	256	0.038	26	0.2	0.12	0.09	10.33	7.11	0.16	0.53	0.06	0.04	220	1.73	0.7
	PL-15 (Nom)	**14**	**0.19**	**7710**	**15**	**15**		**2.06**	**0.2**	**0.2**	**3.2**	**9.2**	**266**	**0.035**	**27**	**0.16**	**0.09**	**0.05**	**10.15**	**6.9**	**0.17**	**0.62**	**0.03**	**0.05**	**139**	**0.94**	**0.6**
121	BSL9 (Res)	7	0.26	9239	16	49	0.07	2.42	1.16	0.24	2.39	11	165	0.045	28	0.15	0.08	0.04	4.45	4.53	0.41	0.34	0.27	0.02	6500	5.68	0.8
	BSL9 (Nom)	**7**	**0.3**	**8760**	**14**	**49**	**0.08**	**2.46**	**1.1**	**0.29**	**2.27**	**10.8**	**154**	**0.04**	**27**	**0.14**	**0.07**	**0.04**	**4**	**4.18**	**0.38**	**0.35**	**0.27**	**0.03**	**6280**	**5.5**	**0.8**

continued:

Element		Mg	Mn	Mo	Nb	Nd	Ni	P	Pb	Pd	Pr	Pt	Rb	Re	Sb	Sc	Se	Sm	Sn	Sr	Ta	Tb	Te	Th	Ti	Tl	Tm
Method		**B/OES**	**B/OES**	**B/MS**	**B/MS**	**B/MS**	**B/OES**	**B/OES**	**B/MS**	**B/MS**	**B/MS**	**B/MS**	**B/MS**	**B/MS**	**B/MS**	**B/OES**	**B/MS**	**B/MS**	**B/MS**	**B/MS**	**B/MS**	**B/MS**	**B/MS**	**B/MS**	**B/OES**	**B/MS**	**B/MS**
Detection		**0.01**	**1**	**0.1**	**0.02**	**0.01**	**1**	**20**	**1**	**10**	**0.005**	**5**	**0.02**	**0.01**	**0.02**	**1**	**1**	**0.01**	**0.05**	**0.02**	**0.01**	**0.005**	**0.05**	**0.01**	**5**	**0.01**	**0.01**
Units		**%**	**ppm**	**ppm**	**ppm**	**ppm**	**ppm**	**ppm**	**ppm**	**ppb**	**ppm**	**ppb**	**ppm**	**ppm**	**ppm**	**ppm**	**ppm**	**ppm**	**ppm**	**ppm**	**ppm**	**ppm**	**ppm**	**ppm**	**ppm**	**ppm**	**ppm**
Duplicates																											
Tube	**Sample Name**																										
19	CMM-07 (Res)	3.28	536	20.2	0.05	3.21	91	101	46	122	0.781	232	1.88	X	4.35	7	X	0.68	1.3	107.18	X	0.099	6.28	7.78	1060	8.81	0.04
	CMM-07 (Nom)	**3.38**	**517**	**23.7**			**88**		**46**						**8.2**				**1.2**				**7.8**	**6.9**		**8.1**	
54	BSL9 (Res)	0.42	159	8	0.12	0.9	28	116	14	20	0.227	9	0.82	X	1.74	2	X	0.18	6.53	17.61	X	0.027	8.64	2.55	533	10.58	0.01
	BSL9 (Nom)	**0.44**	**156**	**8.2**	**0.12**	**0.85**	**28**	**127**	**14**	**28**	**0.21**	**20**	**0.67**		**1.88**	**2**		**0.17**	**6.5**	**11.5**		**0.02**	**8**	**2.6**		**11**	
66	NGL-21 (Res)	0.38	130	7.5	0.08	0.74	24	224	12	197	0.187	215	0.4	X	1.52	5	9	0.16	0.84	19.24	X	0.021	5.08	5.09	1082	1.81	0.01
	NGL-21 (Nom)	**0.38**	**124**	**8.3**			**20**	**254**	**12**	**227**		**225**			**1.78**		**8**		**0.89**				**5.9**			**1.84**	
107	PL-15 (Res)	0.07	112	4.3	0.05	1.68	39	66	12	X	0.389	X	0.64	X	0.74	5	X	0.36	0.74	48.72	X	0.053	4.21	5.68	846	1.85	0.03
	PL-15 (Nom)	**0.02**	**100**	**4.3**	**0.06**	**0.87**	**36**	**94**	**12**		**0.23**		**0.26**		**0.92**	**5**		**0.19**	**0.75**	**16.4**		**0.026**	**4.5**			**2.14**	
121	BSL9 (Res)	0.43	169	7.8	0.12	0.93	29	105	13	22	0.231	14	0.86	X	1.48	2	X	0.21	6.52	14.25	X	0.028	8.65	2.81	565	11.46	0.01
	BSL9 (Nom)	**0.44**	**156**	**8.2**	**0.12**	**0.85**	**28**	**127**	**14**	**28**	**0.21**	**20**	**0.67**		**1.88**	**2**		**0.17**	**6.5**	**11.5**		**0.02**	**8**	**2.6**		**11**	

continued:

Element		U	V	W	Y	Yb	Zn	Zr
Method		**B/MS**	**B/OES**	**B/MS**	**B/MS**	**B/MS**	**B/OES**	**B/MS**
Detection		**0.01**	**2**	**0.05**	**0.02**	**0.01**	**1**	**0.1**
Units		**ppm**	**ppm**	**ppm**	**ppm**	**ppm**	**ppm**	**ppm**
Duplicates								
Tube	**Sample Name**							
19	CMM-07 (Res)	9.69	299	0.06	3.22	0.24	76	31
	CMM-07 (Nom)	**9.2**	**298**	**0.09**			**84**	**33**
54	BSL9 (Res)	5.05	100	0.69	0.83	0.08	27	10
	BSL9 (Nom)	**5.46**	**100**	**0.8**	**0.68**	**0.06**	**26**	**11.7**
66	NGL-21 (Res)	9.17	152	0.14	0.52	0.07	22	16.2
	NGL-21 (Nom)	**9.89**	**201**				**22**	**26.3**
107	PL-15 (Res)	1.94	143	X	1.68	0.15	21	18.4
	PL-15 (Nom)	**2**	**191**				**22**	**21.3**
121	BSL9 (Res)	5.09	104	0.52	0.74	0.08	27	9.7
	BSL9 (Nom)	**5.46**	**100**	**0.8**	**0.68**	**0.06**	**26**	**11.7**

Appendix 3d: QAQC Checks: Field Duplicates.

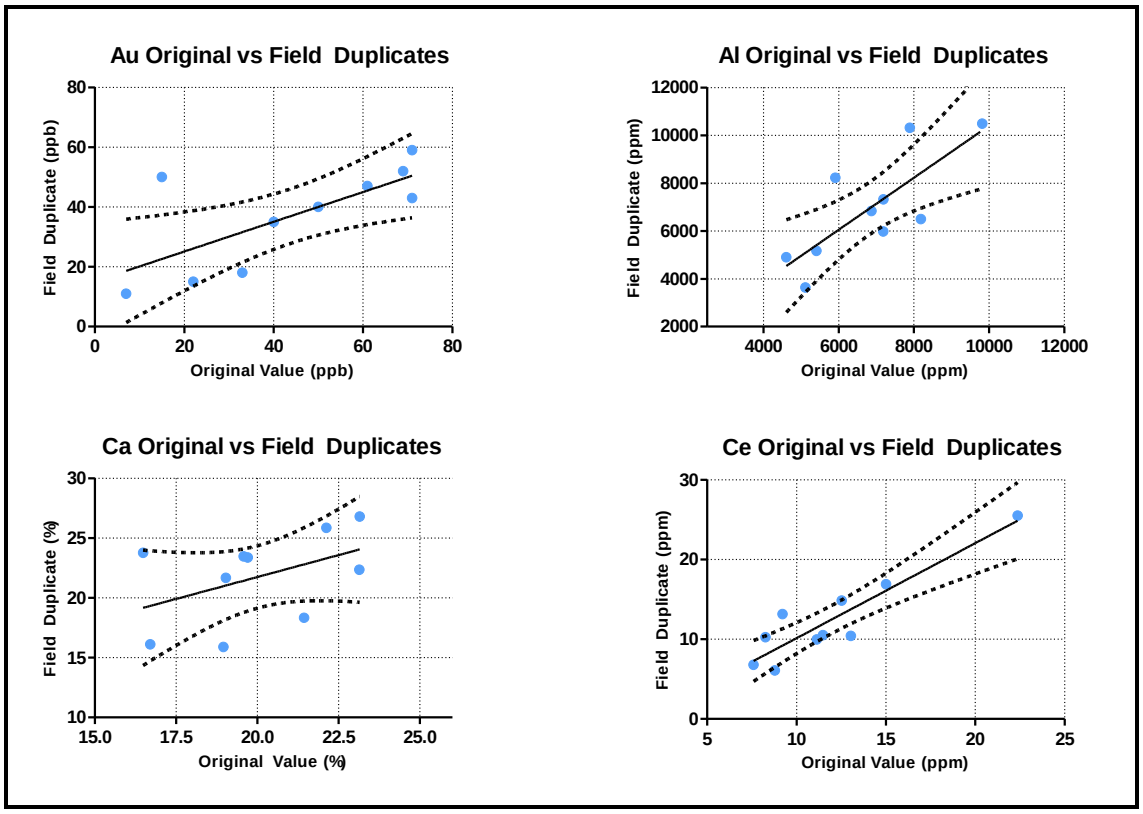

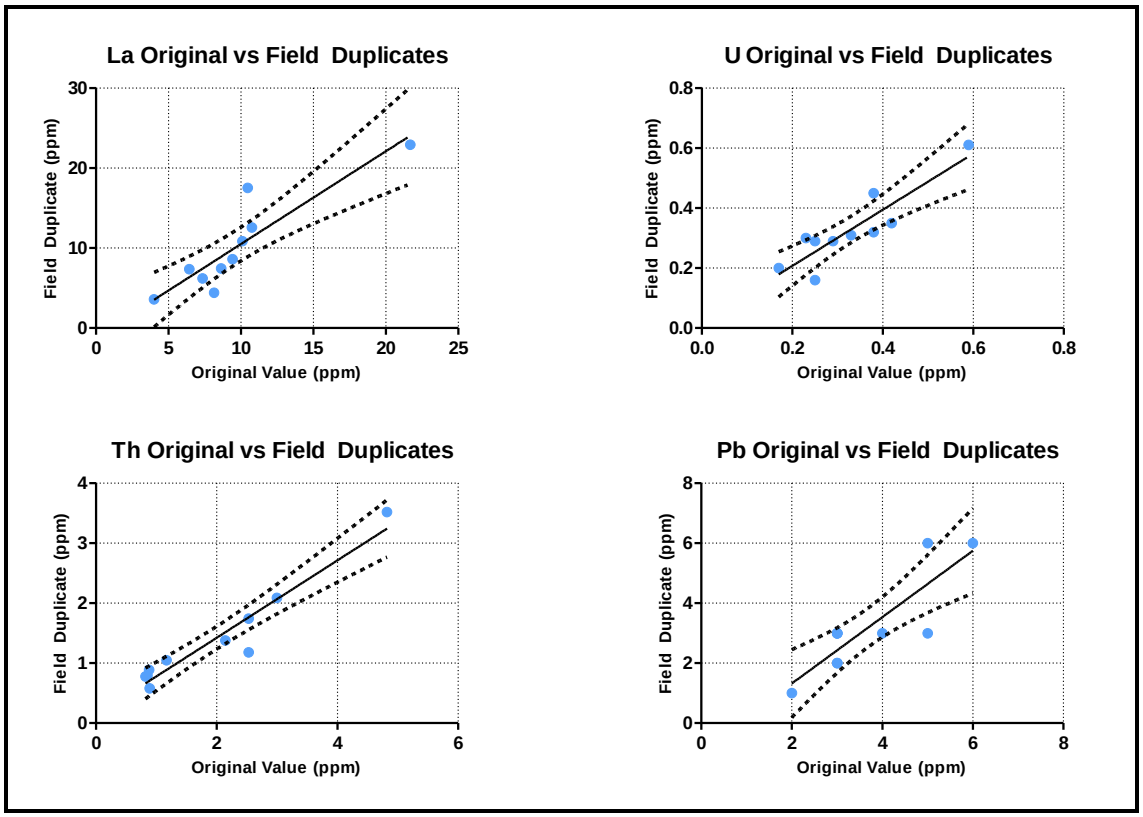

Appendix 3d: QAQC Checks: Field Duplicates.

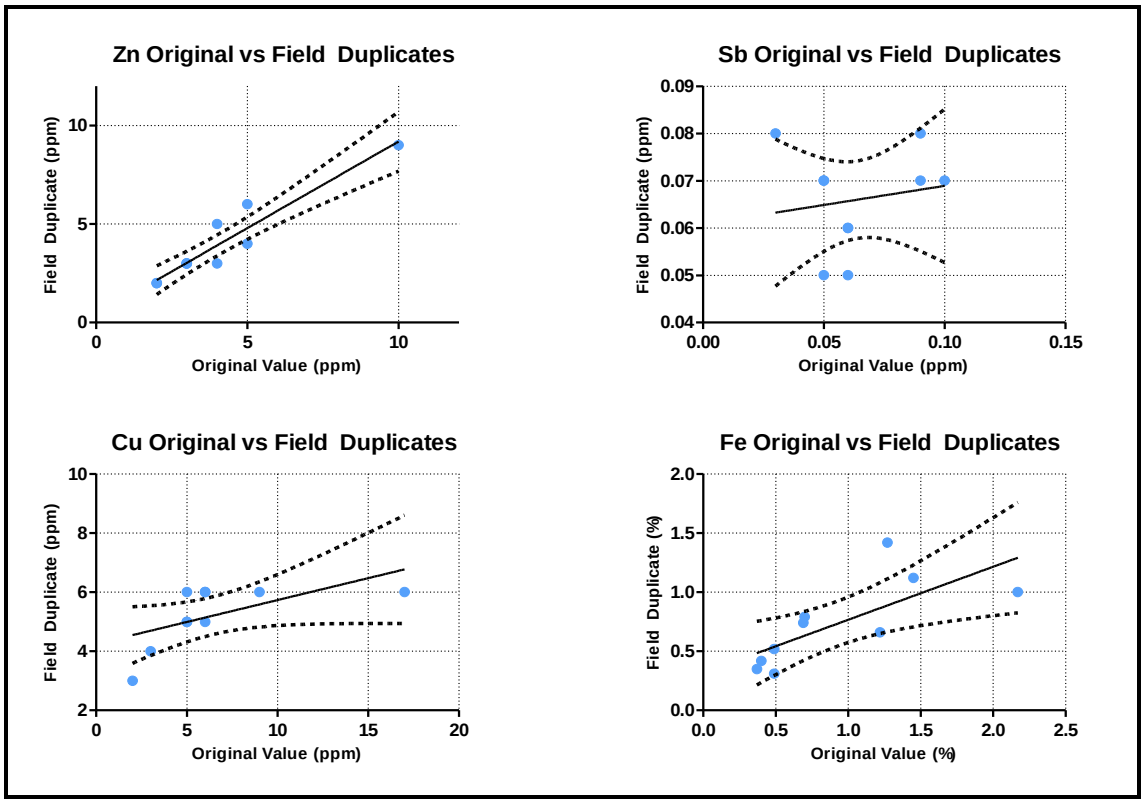

Appendix 3d: QAQC Checks: Lab Checks.

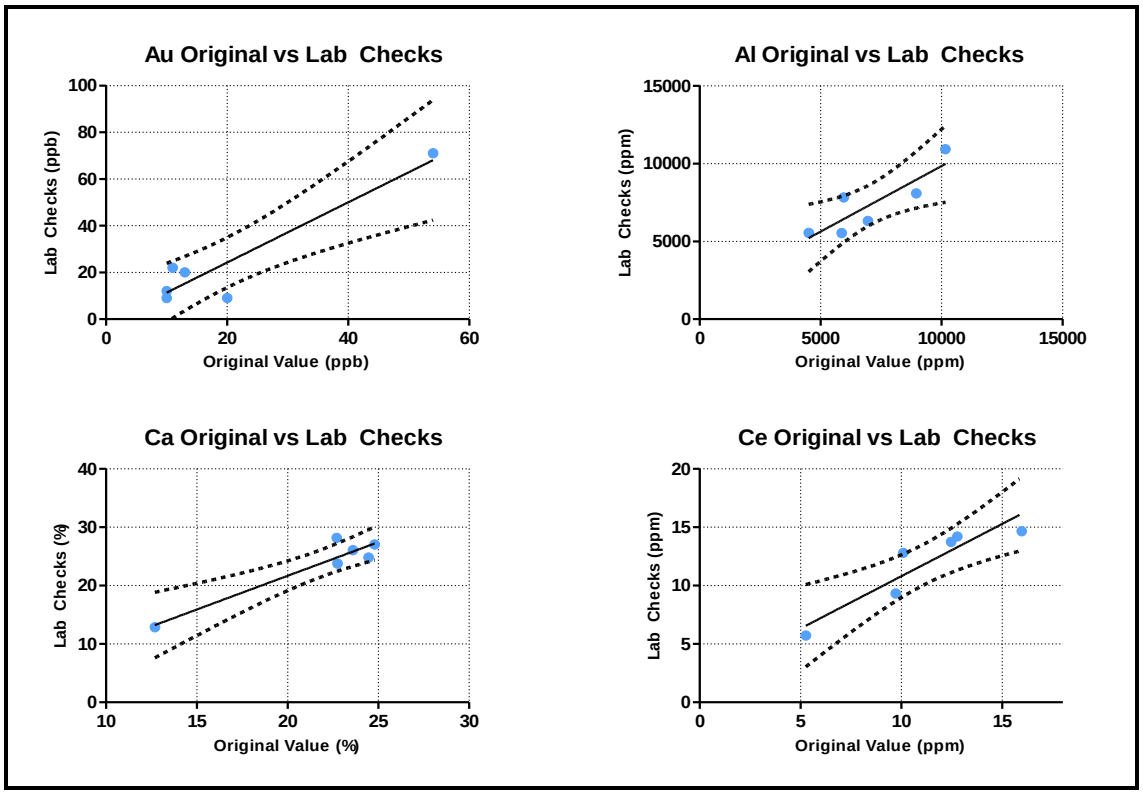

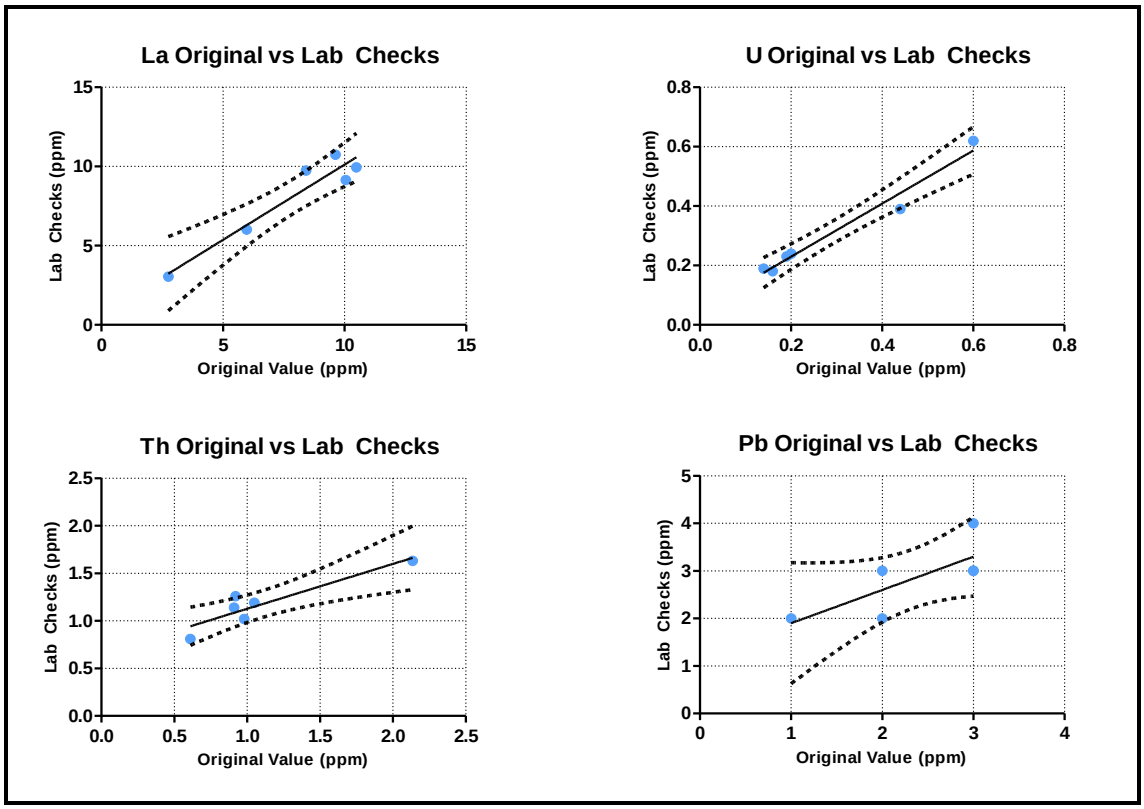

Appendix 3d: QAQC Checks: Lab Checks.

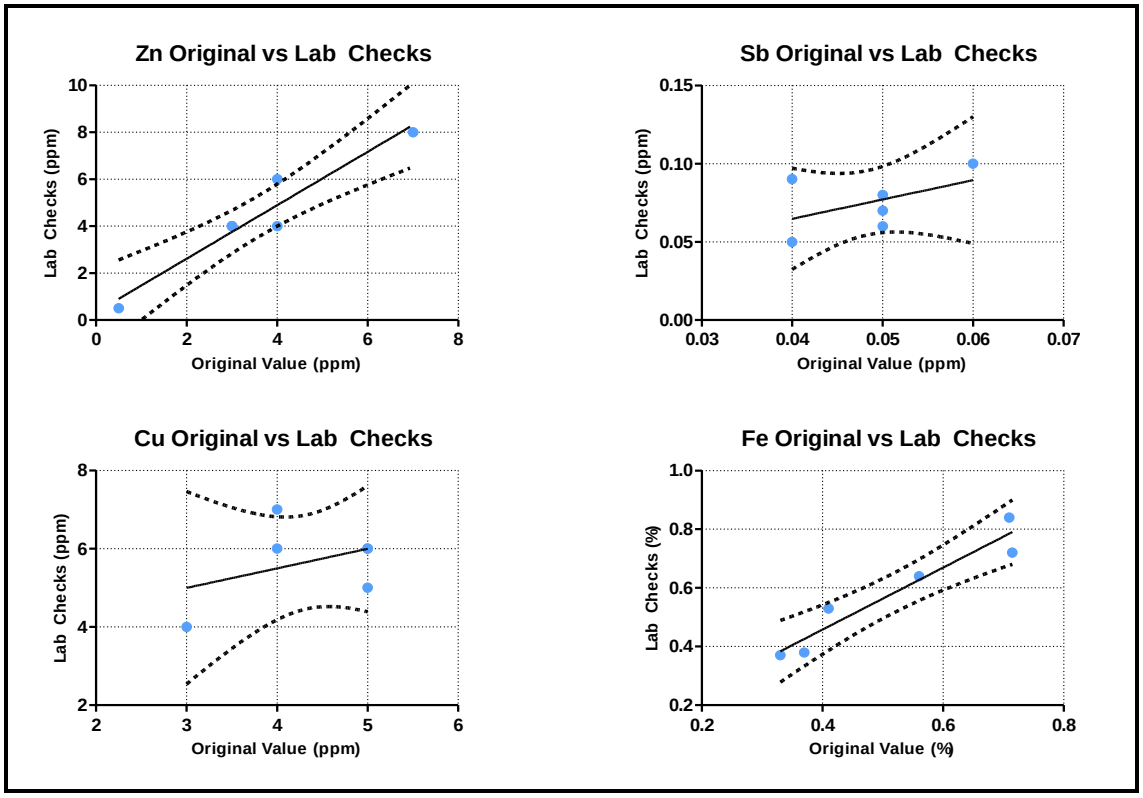

Appendix 3d: QAQC Checks: Au-Lab Repeats.

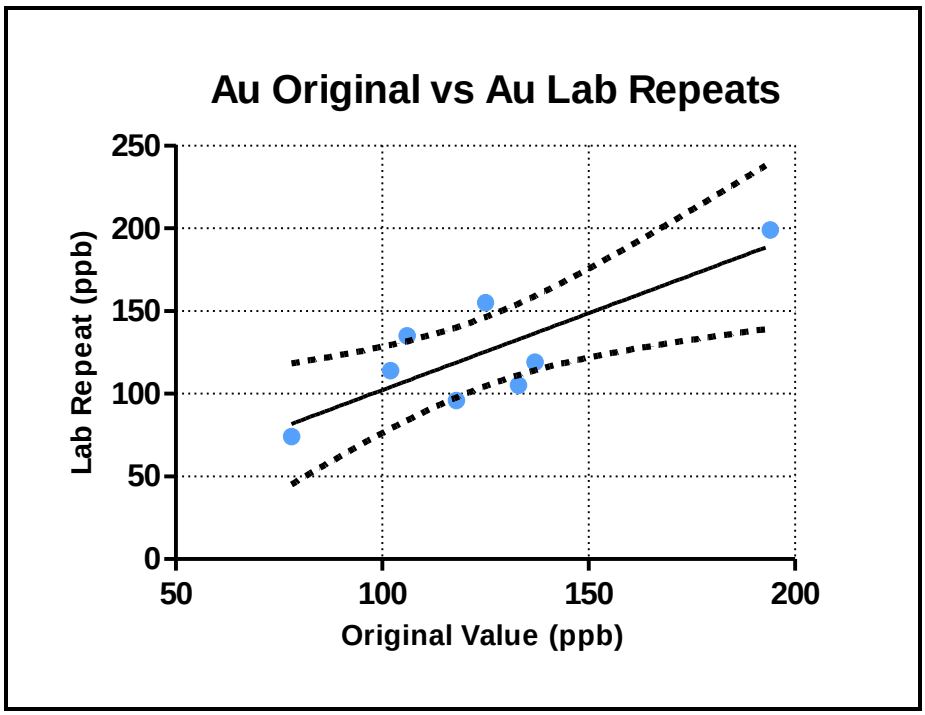

APPENDIX 4

Calcrete Geochemical Graphing and Mapping

Appendix 4a: Correlation Matrix Au-Ho

	Au (ppb)	*Au-Rp1 (ppb)*	*Ag (ppm)*	*Al (ppm)*	*As (ppm)*	*Ba (ppm)*	*Be (ppm)*	*Bi (ppm)*	*Ca (%)*	*Cd (ppm)*	*Ce (ppm)*	*Co (ppm)*	*Cr (ppm)*	*Cs (ppm)*	*Cu (ppm)*	*Dy (ppm)*	*Er (ppm)*	*Eu (ppm)*	*Fe (%)*	*Ga (ppm)*	*Gd (ppm)*	*Hf (ppm)*	*Ho (ppm)*
Au (ppb)	1.00000																						
Au-Rp1 (ppb)	**0.81745**	1.00000																					
Ag (ppm)	0.30648	-0.39678	1.00000																				
Al (ppm)	0.45833	0.30663	0.03085	1.00000																			
As (ppm)	0.37095	-0.12145	0.16073	0.36564	1.00000																		
Ba (ppm)	0.18214	-0.56148	0.02816	0.16537	0.15362	1.00000																	
Be (ppm)	0.37786	0.25589	0.19585	0.60115	0.42959	0.13895	1.00000																
Bi (ppm)	0.36251	0.13090	0.07682	0.52842	**0.78876**	0.06564	0.45847	1.00000															
Ca (%)	-0.13250	-0.20073	0.17852	-0.07169	-0.17004	0.15505	0.40507	-0.37803	1.00000														
Cd (ppm)	-0.25101	-0.48550	0.20029	-0.08914	-0.13614	-0.07324	0.42433	-0.26514	**0.78790**	1.00000													
Ce (ppm)	-0.01303	-0.41802	0.18835	0.35299	0.17806	0.11217	0.70460	0.13756	0.59544	0.70654	1.00000												
Co (ppm)	0.09860	-0.20275	0.28390	0.26484	0.20712	0.05160	0.55596	0.09295	0.51779	0.58238	**0.82829**	1.00000											
Cr (ppm)	0.38576	0.14150	0.09627	0.49698	**0.76660**	0.00839	0.42341	**0.91257**	-0.42151	-0.29792	0.09673	0.13226	1.00000										
Cs (ppm)	0.36225	0.41221	0.03117	**0.94739**	0.20645	0.17143	0.59687	0.34698	0.11825	0.03708	0.43154	0.33999	0.31097	1.00000									
Cu (ppm)	0.08819	-0.52915	0.24259	0.30288	0.32366	-0.08525	0.33304	0.19929	0.23222	0.28505	0.38277	0.50879	0.31604	0.32750	1.00000								
Dy (ppm)	-0.07628	-0.56307	0.23897	0.17541	0.14323	0.08911	0.59948	0.07133	0.59843	**0.76187**	**0.94334**	**0.80214**	0.02978	0.24634	0.33523	1.00000							
Er (ppm)	-0.10577	-0.55057	0.22287	0.15217	0.11855	0.07501	0.59571	0.04604	0.62565	**0.78232**	**0.93383**	**0.79317**	0.00225	0.22625	0.31613	**0.99215**	1.00000						
Eu (ppm)	-0.06252	-0.60221	0.23171	0.18796	0.14820	0.11524	0.57487	0.07465	0.58622	0.73157	**0.92738**	**0.80576**	0.02823	0.25714	0.33348	**0.99241**	**0.98837**	1.00000					
Fe (%)	0.36657	0.06604	0.08889	0.48267	**0.84036**	0.01263	0.43115	**0.92125**	-0.40449	-0.27085	0.07862	0.08374	**0.94809**	0.27755	0.25864	0.02579	0.00240	0.02362	1.00000				
Ga (ppm)	0.52179	-0.01383	0.13624	0.73410	**0.75061**	0.09913	0.54441	**0.80741**	-0.30078	-0.18333	0.24134	0.17389	**0.81518**	0.54583	0.26871	0.14687	0.12318	0.15253	**0.80919**	1.00000			
Gd (ppm)	-0.05879	-0.59411	0.24640	0.17852	0.14357	0.10173	0.57758	0.06620	0.59545	0.74243	**0.92418**	**0.80905**	0.02282	0.25058	0.33611	**0.99390**	**0.98910**	**0.99737**	0.01971	0.14483	1.00000		
Hf (ppm)	0.27075	0.50678	0.00434	0.52097	0.58204	0.10758	0.33047	**0.83156**	-0.48078	-0.34493	0.05743	0.02719	**0.80540**	0.36881	0.11490	-0.01767	-0.04339	-0.01552	**0.79390**	0.68114	-0.02562	1.00000	
Ho (ppm)	-0.08028	-0.56593	0.23803	0.16683	0.14246	0.08498	0.60016	0.07146	0.60305	**0.76953**	**0.93804**	**0.78966**	0.02680	0.23715	0.32811	**0.99893**	**0.99278**	**0.99032**	0.02556	0.14327	**0.99254**	-0.02171	1.00000
In (ppm)	0.23673	-0.03949	0.03362	0.32275	**0.84356**	-0.03203	0.36759	**0.85801**	-0.37833	-0.23113	0.09957	0.09709	**0.85933**	0.11608	0.19526	0.08402	0.06691	0.08241	**0.89992**	**0.76941**	0.07755	0.71275	0.08548
K (ppm)	0.31667	0.53638	0.00907	**0.87795**	0.11264	0.07853	0.56618	0.30260	0.07075	-0.00485	0.34789	0.26694	0.30665	**0.92636**	0.28716	0.15990	0.14457	0.16120	0.24967	0.47037	0.15564	0.36424	0.15379
La (ppm)	-0.03060	-0.69408	0.17624	0.23624	0.15742	0.12264	0.55747	0.10676	0.52787	0.67210	**0.89333**	**0.77408**	0.05849	0.29302	0.32558	**0.96928**	**0.96049**	**0.98437**	0.04783	0.19433	**0.98176**	0.01552	**0.96684**
Li (ppm)	0.37514	0.61289	-0.04058	**0.81891**	0.34527	0.26420	0.65555	0.50739	0.04667	-0.10844	0.29166	0.20468	0.47602	**0.80678**	0.13325	0.12721	0.10892	0.13042	0.45846	0.54663	0.11964	0.50948	0.12070
Mg (%)	0.26557	0.74589	-0.05296	0.24403	-0.13801	0.26366	0.16631	-0.00934	-0.00429	-0.23168	-0.14723	-0.20054	-0.04259	0.28141	-0.28296	-0.25280	-0.25899	-0.25102	-0.05007	-0.00547	-0.25872	0.15044	-0.25806
Mn (ppm)	-0.13928	-0.66467	0.31567	0.05025	-0.02188	-0.13099	0.35471	-0.01888	0.36791	0.65498	0.68569	0.75271	-0.01253	0.10178	0.27629	0.67408	0.67657	0.65187	-0.03064	0.01889	0.65717	-0.02531	0.66791
Mo (ppm)	0.31830	0.20962	0.01916	0.45517	0.60218	0.04564	0.28866	0.69465	-0.40697	-0.35009	-0.00333	0.07268	**0.83193**	0.27958	0.30290	-0.06561	-0.09520	-0.05449	**0.79116**	0.66923	-0.06359	0.57379	-0.07425
Nb (ppm)	-0.15062	-0.20363	0.06287	-0.03201	-0.25606	0.11932	0.26486	-0.36800	0.68152	0.48211	0.36310	0.27585	-0.37574	0.11381	0.06586	0.32370	0.34525	0.31058	-0.39733	-0.26880	0.30620	-0.46992	0.32289
Nd (ppm)	-0.05056	-0.60532	0.20234	0.20631	0.15187	0.11255	0.56934	0.09104	0.56078	0.69980	**0.91634**	**0.80003**	0.04569	0.27140	0.33097	**0.98490**	**0.97860**	**0.99648**	0.03679	0.16657	**0.99413**	0.00118	**0.98209**
Ni (ppm)	0.26853	-0.14029	0.25545	0.61378	0.31403	0.06173	0.56515	0.38295	0.13319	0.15539	0.54658	0.68265	0.50292	0.62714	0.65755	0.44331	0.40322	0.44684	0.40376	0.44478	0.44428	0.40257	0.42782
P (ppm)	-0.20491	-0.46636	0.27972	-0.15484	-0.10430	-0.15798	0.26535	-0.31471	0.67694	0.73148	0.51699	0.50000	-0.29355	-0.03055	0.39682	0.50881	0.52485	0.47703	-0.29329	-0.24295	0.48679	-0.45211	0.51487
Pb (ppm)	0.25835	0.04359	0.00727	0.44243	0.66288	-0.01807	0.34172	**0.81948**	-0.44815	-0.15605	0.17102	0.09963	**0.75627**	0.24492	0.15485	0.12091	0.10156	0.11510	**0.78755**	0.71749	0.10597	0.71210	0.12103
Pd (ppb)	-0.04433	#DIV/0!	-0.02980	-0.06402	0.13786	0.03726	-0.07582	0.19404	-0.21532	-0.13100	-0.04250	-0.03804	0.14338	-0.09588	-0.02298	-0.02631	-0.02028	-0.03010	0.16894	0.04546	-0.02921	0.24576	-0.01945
Pr (ppm)	-0.02757	-0.60139	0.20521	0.23680	0.17829	0.11981	0.58435	0.12356	0.54045	0.68234	**0.92532**	**0.79937**	0.07780	0.29826	0.34063	**0.98462**	**0.96857**	**0.99076**	0.06687	0.19775	**0.98906**	0.03268	**0.98154**
Pt (ppb)	0.01847	#DIV/0!	-0.02980	0.05488	0.05560	0.24538	0.05626	-0.01980	0.14736	-0.00776	0.07659	0.09384	-0.03319	0.07678	0.07066	0.04652	0.03175	0.04719	-0.04300	-0.00022	0.05570	-0.03714	0.04019
Rb (ppm)	0.33335	0.45649	0.01069	**0.92429**	0.15160	0.13461	0.58318	0.30852	0.11630	0.05333	0.43138	0.32949	0.29074	**0.98510**	0.33056	0.24367	0.22116	0.24775	0.24310	0.51022	0.24095	0.35976	0.23586
Re (ppm)	0.00000	#DIV/0!	0.00000	0.00000	0.00000	0.00000	0.00000	0.00000	0.00000	0.00000	0.00000	0.00000	0.00000	0.00000	0.00000	0.00000	0.00000	0.00000	0.00000	0.00000	0.00000	0.00000	0.00000
Sb (ppm)	0.14204	-0.05934	0.24422	0.13664	0.20832	-0.01557	0.25689	0.27213	0.04157	-0.05658	0.06325	0.05030	0.31866	0.07844	0.11047	0.07779	0.07715	0.08036	0.28598	0.27359	0.07115	0.10839	0.07647
Sc (ppm)	0.41629	0.13202	0.09488	0.72289	0.65421	0.24079	0.70590	0.71653	0.05277	0.04014	0.47084	0.40518	0.70632	0.65517	0.37530	0.35975	0.32659	0.35897	0.69487	0.73096	0.35517	0.64101	0.35319
Se (ppm)	#DIV/0!	#DIV/0!	#DIV/0!	#DIV/0!	#DIV/0!	#DIV/0!	#DIV/0!	#DIV/0!	#DIV/0!	#DIV/0!	#DIV/0!	#DIV/0!	#DIV/0!	#DIV/0!	#DIV/0!	#DIV/0!	#DIV/0!	#DIV/0!	#DIV/0!	#DIV/0!	#DIV/0!	#DIV/0!	#DIV/0!
Sm (ppm)	-0.05258	-0.59111	0.21503	0.19974	0.15027	0.09976	0.57815	0.08408	0.56973	0.71863	**0.93040**	**0.80021**	0.04326	0.26740	0.33931	**0.99288**	**0.98069**	**0.99567**	0.03466	0.16066	**0.99392**	-0.00341	**0.99059**
Sn (ppm)	0.40433	0.57570	-0.03056	**0.81444**	0.45536	0.07142	0.48269	0.67954	-0.32808	-0.28287	0.14692	0.13618	0.73954	0.70952	0.31818	-0.00182	-0.03220	-0.00158	0.69177	0.73857	-0.00767	0.66565	-0.00969
Sr (ppm)	0.22275	0.36100	-0.05306	0.23224	-0.16705	0.37199	0.30957	-0.17784	0.41334	0.04339	0.14327	0.04251	-0.21760	0.34314	-0.13731	0.00986	0.01449	0.01209	-0.23783	-0.08997	0.00252	-0.08046	0.00329
Ta (ppm)	0.00000	#DIV/0!	0.00000	0.00000	0.00000	0.00000	0.00000	0.00000	0.00000	0.00000	0.00000	0.00000	0.00000	0.00000	0.00000	0.00000	0.00000	0.00000	0.00000	0.00000	0.00000	0.00000	0.00000
Tb (ppm)	-0.07120	-0.57215	0.23970	0.18478	0.14636	0.09295	0.59506	0.07618	0.59363	**0.75104**	**0.93784**	**0.80820**	0.03246	0.25597	0.33591	**0.99715**	**0.99338**	**0.99586**	0.02973	0.15230	**0.99781**	-0.01195	**0.99586**
Te (ppm)	0.18443	-0.32375	0.19888	0.12413	0.25298	0.35170	0.25184	0.13544	0.15991	0.05618	0.12067	-0.01388	0.09823	0.10703	0.13788	0.12617	0.12410	0.13784	0.11541	0.20807	0.12762	0.02930	0.12773
Th (ppm)	0.27458	-0.03541	0.11157	0.33864	**0.81507**	0.03166	0.42321	**0.89172**	-0.34145	-0.16648	0.18964	0.16147	**0.88513**	0.14317	0.20724	0.16014	0.14075	0.15079	**0.89353**	**0.78032**	0.14622	**0.81935**	0.16134
Ti (ppm)	0.15354	0.53055	-0.09743	0.48467	0.36885	-0.00422	0.30448	0.68236	-0.38976	-0.37626	-0.03421	-0.05445	0.72810	0.34172	0.08473	-0.14170	-0.15326	-0.14016	0.66923	0.53503	-0.15532	0.68610	-0.14634
Tl (ppm)	0.38975	0.28603	0.22712	0.60930	0.39225	0.45918	0.60989	0.42179	0.20077	0.14119	0.48569	0.43116	0.34078	0.62945	0.27797	0.35789	0.32393	0.36233	0.32002	0.45899	0.35427	0.36598	0.35114
Tm (ppm)	-0.09068	-0.52799	0.23555	0.16152	0.14894	0.07295	0.62882	0.08894	0.60329	**0.79123**	**0.93815**	**0.77612**	0.04149	0.23113	0.32841	**0.99002**	**0.98507**	**0.97379**	0.03913	0.14867	**0.97661**	-0.00492	**0.99089**
U (ppm)	0.51739	0.03684	0.04807	0.52072	0.63031	0.42864	0.50112	0.53929	0.09094	-0.11404	0.33588	0.22698	0.48881	0.44282	0.16342	0.22470	0.19398	0.23615	0.50672	0.63499	0.22642	0.43734	0.21730
V (ppm)	0.29710	0.00192	0.07075	0.26817	**0.85035**	0.03345	0.28598	**0.90287**	-0.47082	-0.33173	-0.01590	0.00022	**0.89696**	0.04789	0.12923	-0.02589	-0.04519	-0.02481	**0.93908**	0.73481	-0.03143	**0.76958**	-0.02385
W (ppm)	0.03915	-0.56434	0.17858	0.43212	0.16342	0.08151	0.16322	0.23340	0.02033	-0.05210	0.19342	0.24378	0.20794	0.47420	0.32417	0.08855	0.06045	0.09165	0.16047	0.22432	0.09492	0.31328	0.08169
Y (ppm)	-0.08686	-0.58485	0.22633	0.14769	0.12168	0.09729	0.57865	0.04002	0.61371	**0.76703**	**0.91257**	**0.78272**	-0.00157	0.21591	0.31030	**0.99142**	**0.99139**	**0.98978**	0.00067	0.12088	**0.99338**	-0.04972	**0.99253**
Yb (ppm)	-0.10479	-0.48727	0.22244	0.17262	0.14611	0.07512	0.63521	0.08089	0.62940	**0.78952**	**0.94902**	**0.78870**	0.03626	0.24713	0.32704	**0.98714**	**0.99375**	**0.97472**	0.03516	0.14500	**0.97571**	-0.01145	**0.98820**
Zn (ppm)	0.12653	-0.16398	-0.07714	0.58476	0.28770	-0.04406	0.10872	0.54609	-0.44400	-0.34401	-0.00854	0.03073	0.53144	0.52678	0.27214	-0.12781	-0.15533	-0.11612	0.46866	0.47820	-0.13223	0.51966	-0.13677
Zr (ppm)	0.25192	0.44672	-0.01879	0.48236	0.59779	0.10768	0.32839	0.84158	-0.47445	-0.35485	0.04856	0.01174	**0.82058**	0.32318	0.12105	-0.02264	-0.04735	-0.02173	0.80517	0.68097	-0.03203	**0.98395**	-0.02623

Appendix 4a: Correlation Matrix In-Sr

	In (ppm)	*K (ppm)*	*La (ppm)*	*Li (ppm)*	*Mg (%)*	*Mn (ppm)*	*Mo (ppm)*	*Nb (ppm)*	*Nd (ppm)*	*Ni (ppm)*	*P (ppm)*	*Pb (ppm)*	*Pd (ppb)*	*Pr (ppm)*	*Pt (ppb)*	*Rb (ppm)*	*Re (ppm)*	*Sb (ppm)*	*Sc (ppm)*	*Se (ppm)*	*Sm (ppm)*	*Sn (ppm)*	*Sr (ppm)*
Au (ppb)																							
Au-Rp1 (ppb)																							
Ag (ppm)																							
Al (ppm)																							
As (ppm)																							
Ba (ppm)																							
Be (ppm)																							
Bi (ppm)																							
Ca (%)																							
Cd (ppm)																							
Ce (ppm)																							
Co (ppm)																							
Cr (ppm)																							
Cs (ppm)																							
Cu (ppm)																							
Dy (ppm)																							
Er (ppm)																							
Eu (ppm)																							
Fe (%)																							
Ga (ppm)																							
Gd (ppm)																							
Hf (ppm)																							
Ho (ppm)																							
In (ppm)	1.00000																						
K (ppm)	0.10859	1.00000																					
La (ppm)	0.09998	0.17345	1.00000																				
Li (ppm)	0.29164	**0.80007**	0.16000	1.00000																			
Mg (%)	-0.16829	0.32345	-0.23908	0.52563	1.00000																		
Mn (ppm)	-0.01522	0.07927	0.59122	-0.07181	-0.26241	1.00000																	
Mo (ppm)	0.67883	0.25893	-0.00344	0.46357	0.04836	-0.10245	1.00000																
Nb (ppm)	-0.38908	0.07099	0.27980	0.16546	0.21176	0.20202	-0.17209	1.00000															
Nd (ppm)	0.09405	0.16949	**0.99368**	0.14635	-0.24519	0.62442	-0.02912	0.29410	1.00000														
Ni (ppm)	0.28105	0.63160	0.45218	0.57538	0.10508	0.40591	0.49932	0.02778	0.45724	1.00000													
P (ppm)	-0.26281	-0.00342	0.38608	-0.22144	-0.34858	0.53464	-0.34012	0.39983	0.43765	0.12331	1.00000												
Pb (ppm)	0.73096	0.15962	0.14915	0.30358	-0.11721	0.12574	0.57448	-0.37767	0.12429	0.24153	-0.25894	1.00000											
Pd (ppb)	0.17158	-0.09323	-0.03203	-0.05168	-0.08759	0.04543	0.01306	-0.21147	-0.03040	-0.06290	-0.13920	0.30689	1.00000										
Pr (ppm)	0.11721	0.19221	**0.99151**	0.17559	-0.23578	0.61935	-0.00147	0.27851	**0.99539**	0.48502	0.41977	0.15063	-0.02513	1.00000									
Pt (ppb)	-0.04389	0.01975	0.07693	0.04235	-0.01905	-0.06137	0.01306	0.06042	0.05943	0.02149	0.01993	-0.02960	-0.00935	0.07026	1.00000								
Rb (ppm)	0.09712	**0.95228**	0.27885	0.78726	0.27708	0.11660	0.25892	0.11295	0.26037	0.63489	-0.00021	0.20953	-0.09847	0.29016	0.05887	1.00000							
Re (ppm)	0.00000	0.00000	0.00000	0.00000	0.00000	0.00000	0.00000	0.00000	0.00000	0.00000	0.00000	0.00000	0.00000	0.00000	0.00000	0.00000	1.00000						
Sb (ppm)	0.28801	0.09818	0.08208	0.28356	0.16421	-0.05444	0.48070	0.40871	0.08054	0.19280	-0.09497	0.09556	-0.11207	0.08280	-0.07328	0.06414	0.00000	1.00000					
Sc (ppm)	0.60954	0.56551	0.38208	0.71297	0.12428	0.14415	0.56841	-0.05056	0.37128	0.61747	-0.07040	0.52857	-0.02844	0.40568	0.12513	0.62957	0.00000	0.21085	1.00000				
Se (ppm)	#DIV/0!	#DIV/0!	#DIV/0!	#DIV/0!	#DIV/0!	#DIV/0!	#DIV/0!	#DIV/0!	#DIV/0!	#DIV/0!	#DIV/0!	#DIV/0!	#DIV/0!	#DIV/0!	#DIV/0!	#DIV/0!	#DIV/0!	#DIV/0!	#DIV/0!	1.00000			
Sm (ppm)	0.08908	0.17297	**0.98574**	0.14355	-0.24654	0.63615	-0.03770	0.30434	**0.99542**	0.46369	0.46574	0.12306	-0.02945	**0.99649**	0.05748	0.26349	0.00000	0.08477	0.37261	#DIV/0!	1.00000		
Sn (ppm)	0.50764	0.65062	0.06135	0.73269	0.19345	-0.04356	**0.75128**	-0.18398	0.02411	0.61858	-0.33350	0.58279	0.00680	0.06228	-0.00299	0.68745	0.00000	0.28880	0.67523	#DIV/0!	0.01864	1.00000	
Sr (ppm)	-0.31171	0.35780	0.00347	0.49585	**0.83109**	-0.14642	-0.11570	0.49143	0.00985	0.15686	-0.07655	-0.31029	-0.17865	0.01320	0.08836	0.33815	0.00000	0.13044	0.15091	#DIV/0!	0.01123	0.03672	1.00000
Ta (ppm)	0.00000	0.00000	0.00000	0.00000	0.00000	0.00000	0.00000	0.00000	0.00000	0.00000	0.00000	0.00000	0.00000	0.00000	0.00000	0.00000	**1.00000**	0.00000	0.00000	#DIV/0!	0.00000	0.00000	0.00000
Tb (ppm)	0.08840	0.16778	**0.97399**	0.12868	-0.25680	0.67053	-0.06301	0.30529	**0.98986**	0.44730	0.49569	0.11805	-0.02651	**0.98552**	0.04794	0.24868	0.00000	0.06836	0.36112	#DIV/0!	0.99240	0.00152	0.00319
Te (ppm)	0.08667	0.06243	0.14918	0.14101	0.09294	-0.09857	0.18836	0.18556	0.13717	0.03355	0.05848	0.02279	-0.04175	0.14224	0.09915	0.08467	0.00000	0.24996	0.18382	#DIV/0!	0.13174	0.08202	0.21161
Th (ppm)	**0.90939**	0.11224	0.16184	0.32054	-0.11221	0.07566	0.61633	-0.39976	0.15795	0.32556	-0.24459	**0.78467**	0.24385	0.18633	-0.03764	0.12180	0.00000	0.18258	0.65239	#DIV/0!	0.15834	0.51913	-0.24717
Ti (ppm)	0.54803	0.39240	-0.10131	0.60672	0.22757	-0.10275	0.73823	-0.01300	-0.11852	0.37990	-0.42591	0.51554	0.09472	-0.09699	-0.04457	0.33698	0.00000	0.53907	0.50609	#DIV/0!	-0.12589	0.70991	0.03379
Tl (ppm)	0.20494	0.53755	0.37485	0.57999	0.20624	0.19731	0.29236	0.06608	0.36398	0.54964	0.03622	0.31865	0.02115	0.39926	0.13534	0.60514	0.00000	-0.00975	0.60005	#DIV/0!	0.36718	0.46743	0.32473
Tm (ppm)	0.09742	0.15427	**0.94271**	0.13568	-0.23953	0.67451	-0.06680	0.33664	**0.96095**	0.42504	0.51494	0.14446	-0.01416	**0.96064**	0.02456	0.22818	0.00000	0.08540	0.36044	#DIV/0!	**0.97232**	-0.00209	0.01693
U (ppm)	0.47350	0.30907	0.26151	0.54587	0.27696	-0.11015	0.43183	0.03757	0.24949	0.35489	-0.20392	0.36217	-0.00880	0.28419	0.08982	0.39030	0.00000	0.24492	0.65662	#DIV/0!	0.24656	0.46397	0.39692
V (ppm)	**0.93093**	0.02225	-0.00441	0.27333	-0.11059	-0.07306	0.68864	-0.44356	-0.01309	0.21402	-0.34589	**0.78543**	0.24524	0.01193	-0.04374	0.01220	0.00000	0.24739	0.56658	#DIV/0!	-0.01770	0.50708	-0.30784
W (ppm)	0.10218	0.46774	0.10139	0.31997	-0.02002	0.10966	0.20056	-0.06052	0.09609	0.43886	0.07953	0.09872	0.07705	0.12445	0.40245	0.47413	0.00000	-0.04536	0.35735	#DIV/0!	0.09934	0.31306	0.00995
Y (ppm)	0.06506	0.12354	**0.97398**	0.09606	-0.26430	0.64455	-0.08876	0.32285	**0.98497**	0.39852	0.49485	0.08960	-0.02895	**0.97810**	0.05663	0.20931	0.00000	0.06824	0.32815	#DIV/0!	**0.98573**	-0.03474	-0.00109
Yb (ppm)	0.09146	0.16957	**0.93927**	0.14380	-0.23910	0.68390	-0.07962	0.35300	**0.96082**	0.41712	0.53772	0.13556	-0.01676	**0.95435**	0.02823	0.24267	0.00000	0.08022	0.35893	#DIV/0!	**0.96780**	-0.00060	0.03466
Zn (ppm)	0.38317	0.52242	-0.07650	0.40119	-0.10995	-0.01336	0.45829	-0.35211	-0.09793	0.38897	-0.19817	0.49798	0.05260	-0.07264	-0.06699	0.53054	0.00000	-0.04035	0.42844	#DIV/0!	-0.10631	0.64989	-0.26000
Zr (ppm)	0.74091	0.31780	0.01173	0.49354	0.13944	-0.04795	0.60702	-0.44407	-0.00400	0.38085	-0.47377	0.71150	0.27372	0.02802	-0.03597	0.31382	0.00000	0.14338	0.64481	#DIV/0!	-0.00952	0.65312	-0.07994

Appendix 4a: Correlation Matrix Ta-Zr

	Ta (ppm)	*Tb (ppm)*	*Te (ppm)*	*Th (ppm)*	*Ti (ppm)*	*Tl (ppm)*	*Tm (ppm)*	*U (ppm)*	*V (ppm)*	*W (ppm)*	*Y (ppm)*	*Yb (ppm)*	*Zn (ppm)*	*Zr (ppm)*
Au (ppb)														
Au-Rp1 (ppb)														
Ag (ppm)														
Al (ppm)														
As (ppm)														
Ba (ppm)														
Be (ppm)														
Bi (ppm)														
Ca (%)														
Cd (ppm)														
Ce (ppm)														
Co (ppm)														
Cr (ppm)														
Cs (ppm)														
Cu (ppm)														
Dy (ppm)														
Er (ppm)														
Eu (ppm)														
Fe (%)														
Ga (ppm)														
Gd (ppm)														
Hf (ppm)														
Ho (ppm)														
In (ppm)														
K (ppm)														
La (ppm)														
Li (ppm)														
Mg (%)														
Mn (ppm)														
Mo (ppm)														
Nb (ppm)														
Nd (ppm)														
Ni (ppm)														
P (ppm)														
Pb (ppm)														
Pd (ppb)														
Pr (ppm)														
Pt (ppb)														
Rb (ppm)														
Re (ppm)														
Sb (ppm)														
Sc (ppm)														
Se (ppm)														
Sm (ppm)														
Sn (ppm)														
Sr (ppm)														
Ta (ppm)	1.00000													
Tb (ppm)	0.00000	1.00000												
Te (ppm)	0.00000	0.12150	1.00000											
Th (ppm)	0.00000	0.16111	0.11700	1.00000										
Ti (ppm)	0.00000	-0.14421	0.01536	0.55073	1.00000									
Tl (ppm)	0.00000	0.35772	0.45898	0.32963	0.19988	1.00000								
Tm (ppm)	0.00000	**0.98473**	0.12700	0.17935	-0.12537	0.35983	1.00000							
U (ppm)	0.00000	0.22765	0.29435	0.52094	0.29605	0.53245	0.21313	1.00000						
V (ppm)	0.00000	-0.02249	0.11873	**0.93827**	0.58294	0.21838	-0.01182	0.47654	1.00000					
W (ppm)	0.00000	0.09990	0.01938	0.15567	0.21136	0.43792	0.08308	0.17133	0.06789	1.00000				
Y (ppm)	0.00000	**0.99291**	0.13061	0.13577	-0.17288	0.32804	**0.97972**	0.19982	-0.04522	0.06621	1.00000			
Yb (ppm)	0.00000	**0.98496**	0.12650	0.17428	-0.12377	0.35075	**0.98984**	0.21787	-0.01841	0.07233	**0.98007**	1.00000		
Zn (ppm)	0.00000	-0.12061	-0.05385	0.36247	0.45749	0.29589	-0.13677	0.11989	0.37216	0.38429	-0.16704	-0.12869	1.00000	
Zr (ppm)	0.00000	-0.01799	0.07616	**0.85108**	0.71229	0.36541	-0.00618	0.46014	**0.79497**	0.29528	-0.05221	-0.01418	0.49489	1.00000

Appendix 4b: X-Y Scatter Plots of Au vs. Ga using IoGAS.

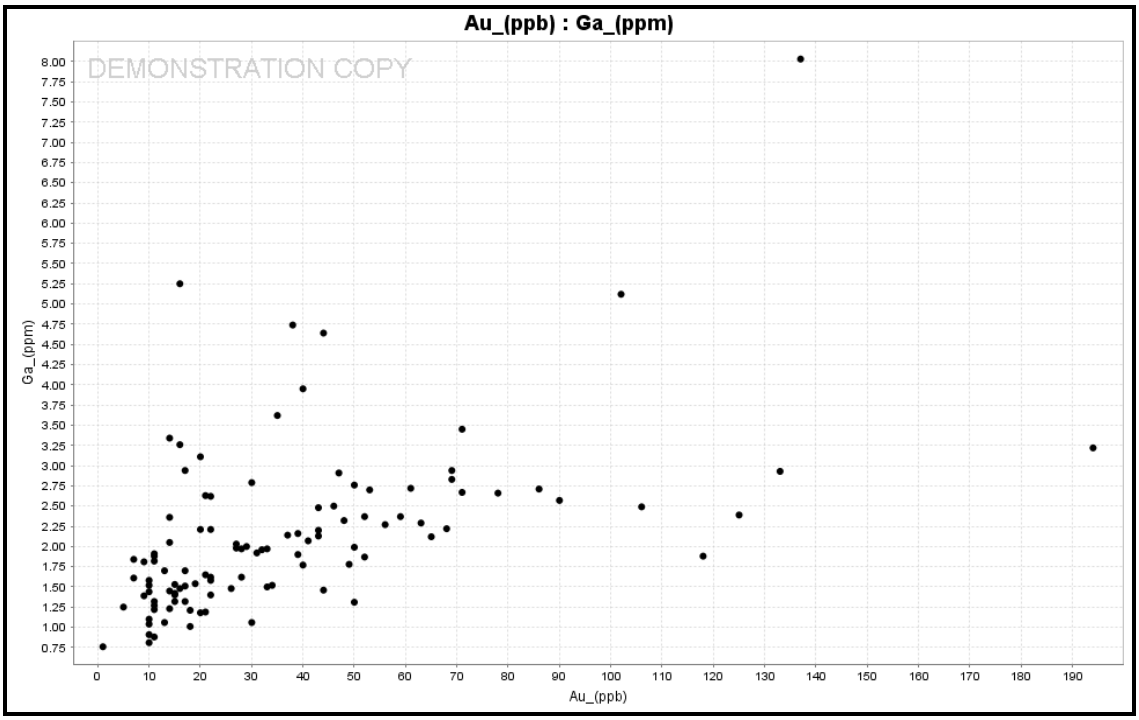

Appendix 4b: X-Y Scatter Plots of Iron and correlated elements using IoGAS.

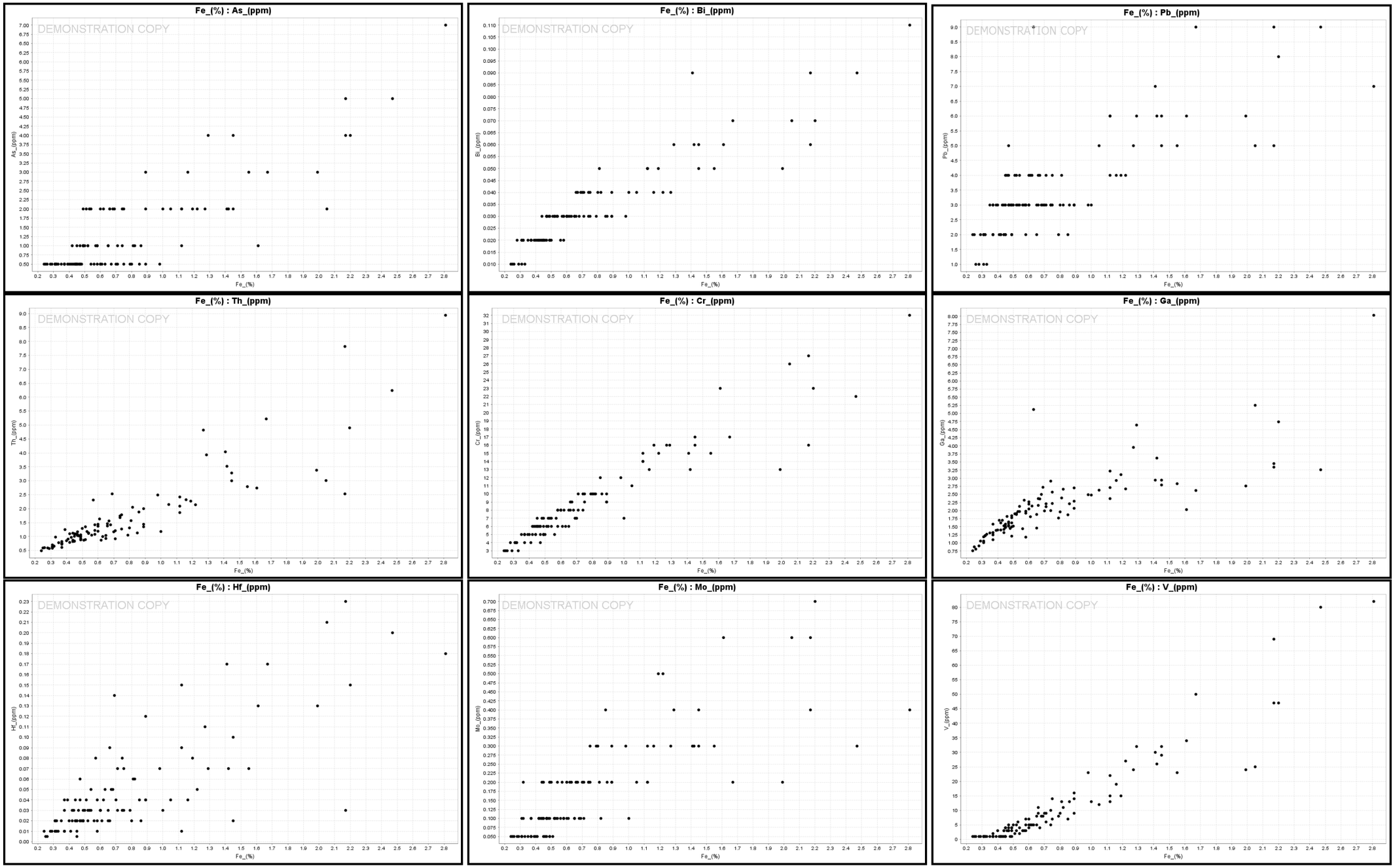

Appendix 4b: X-Y Scatter Plots of Iron and correlated elements using IoGAS.

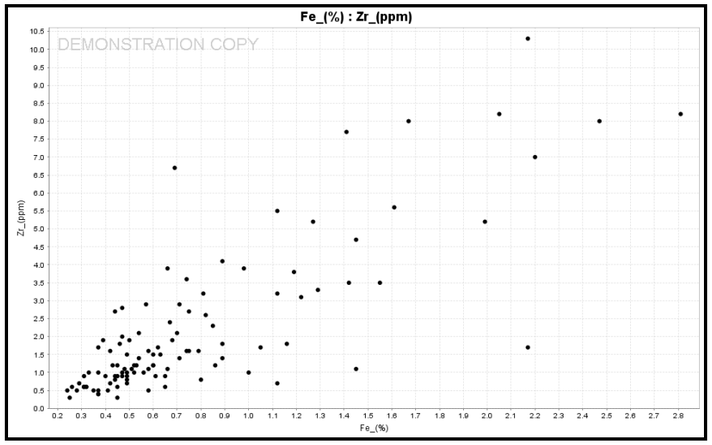

Appendix 4b: X-Y Scatter Plots of Aluminium and correlated elements using IoGAS.

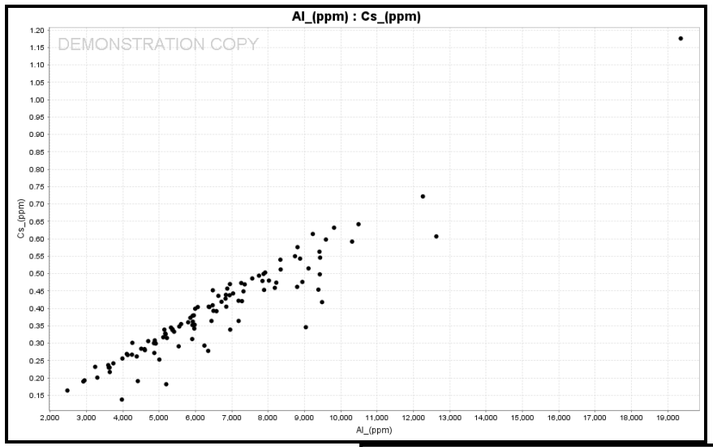

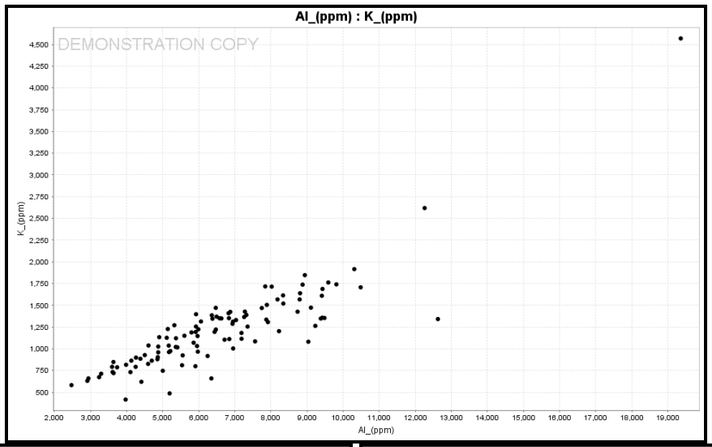

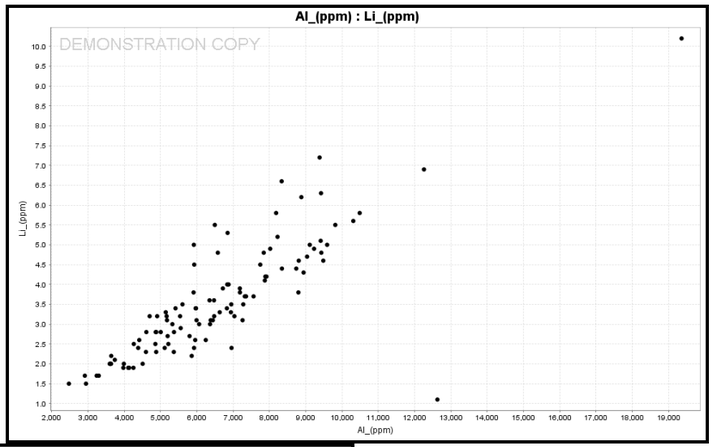

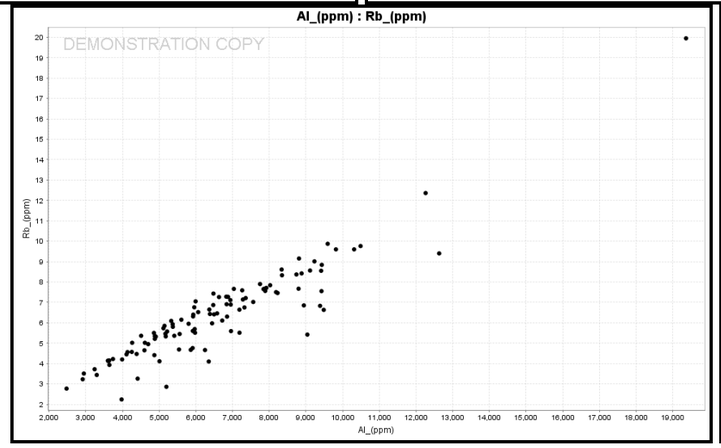

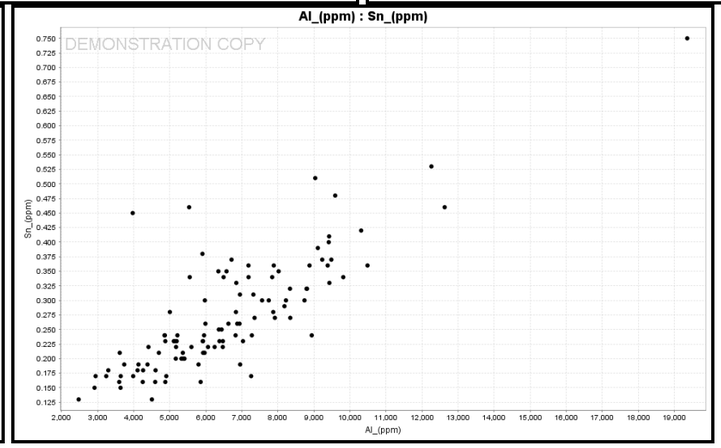

Appendix 4c.1: X-Y Scatter Plots of Au and correlated elements using IoGAS.

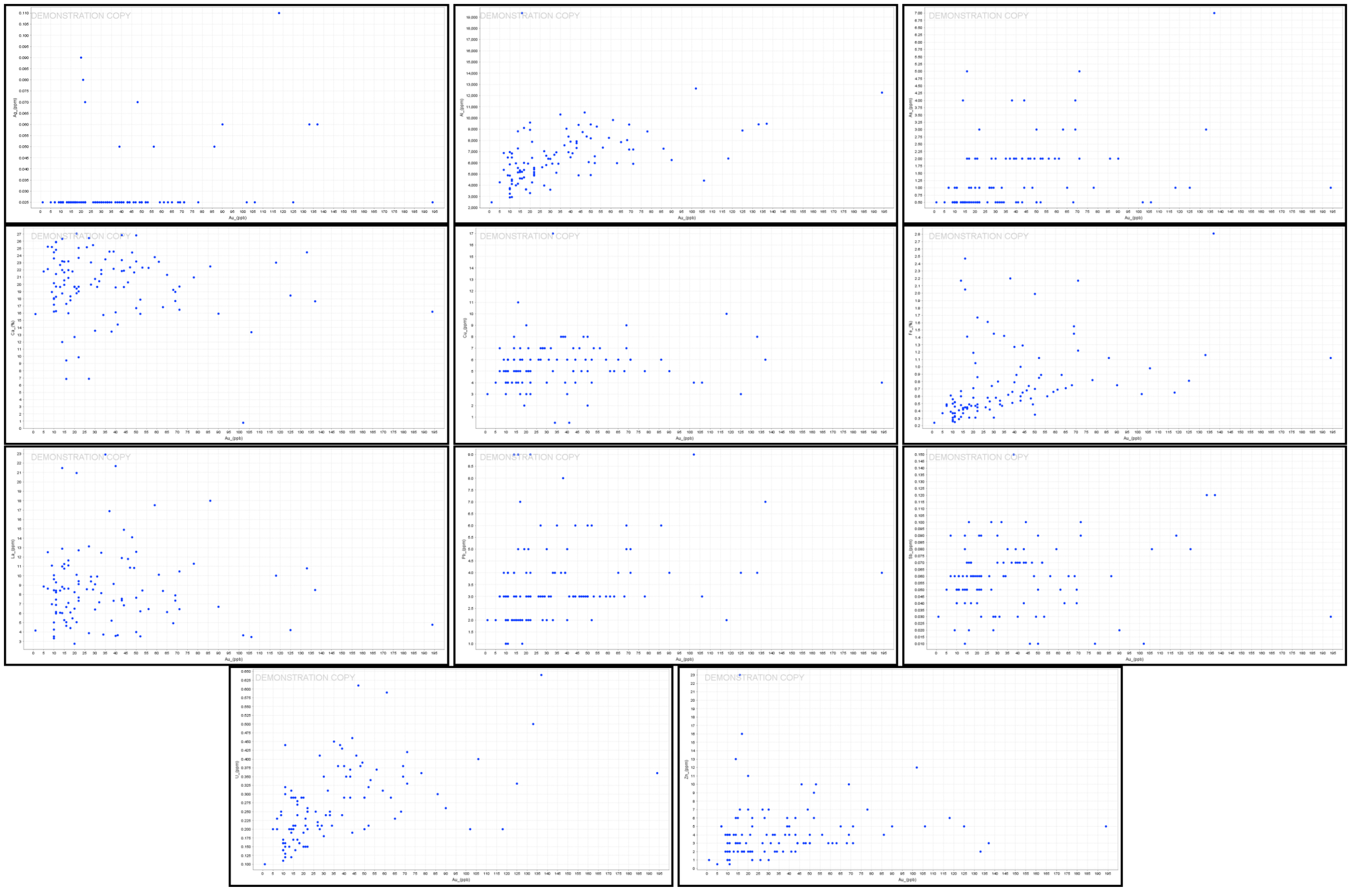

Appendix 4c.2: X-Y Scatter Plots of Ag and correlated elements using IoGAS.

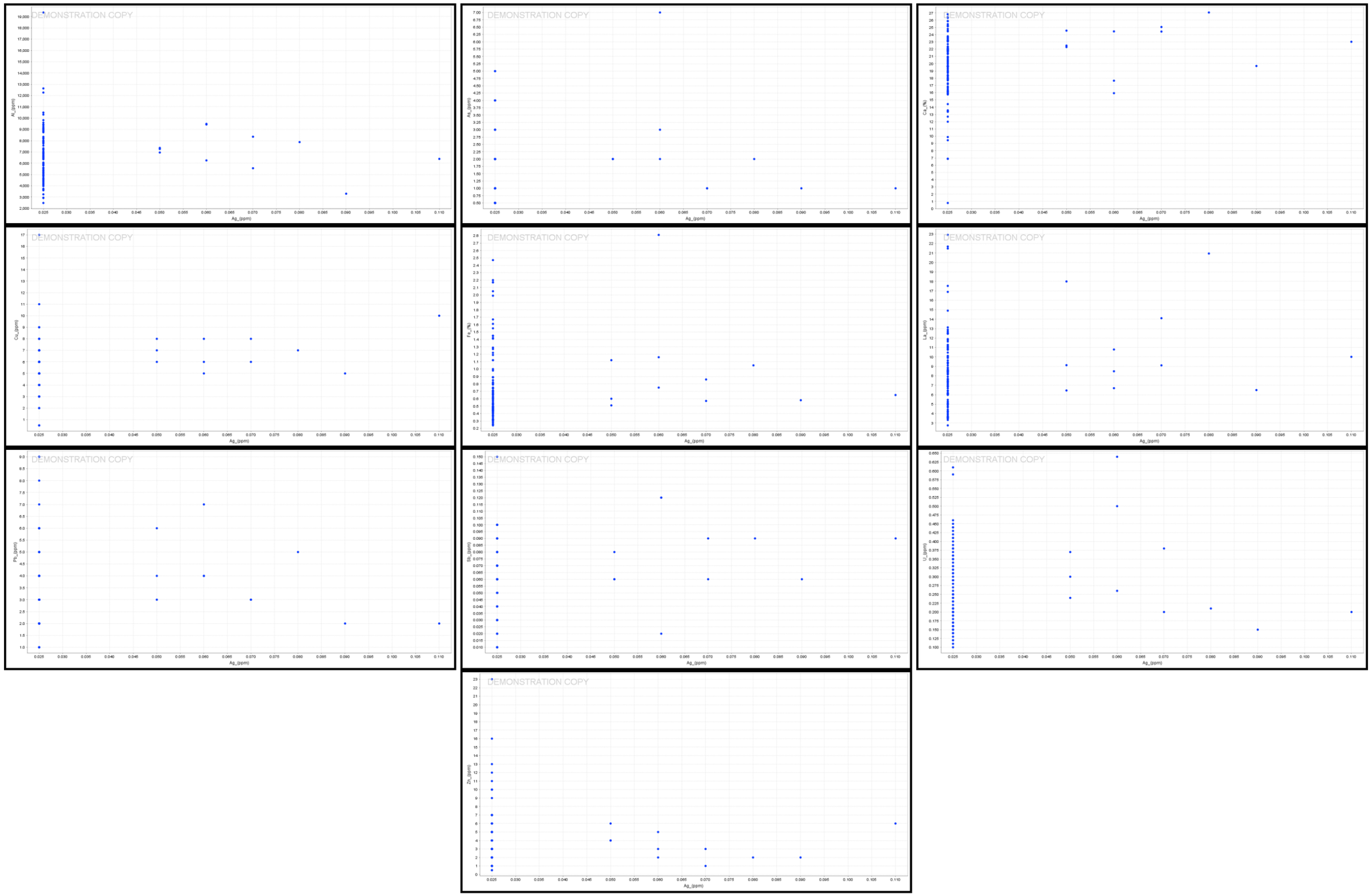

Appendix 4c.3: X-Y Scatter Plots of Al and correlated elements using IoGAS.

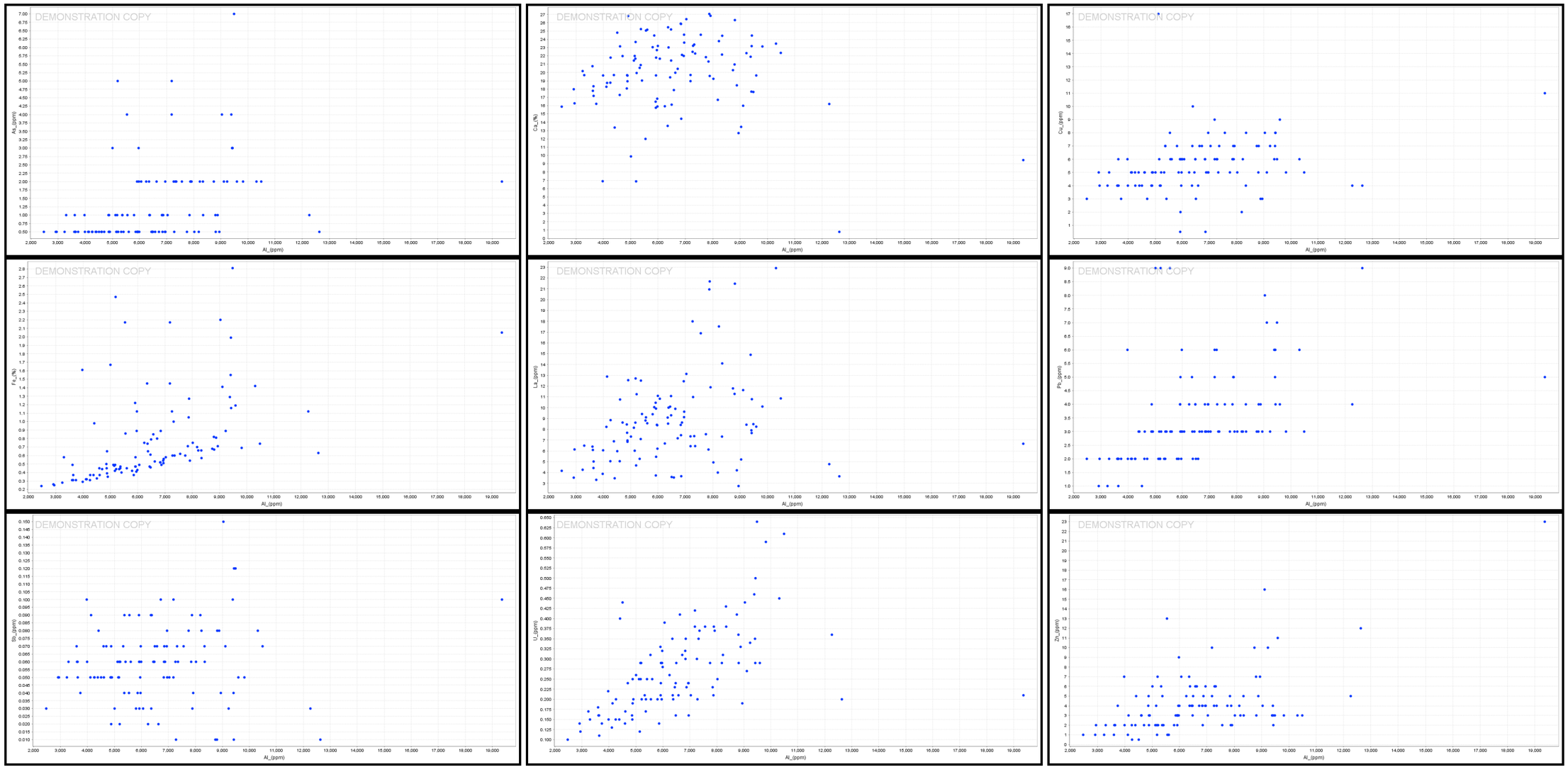

Appendix 4c.4: X-Y Scatter Plots of As and correlated elements using IoGAS.

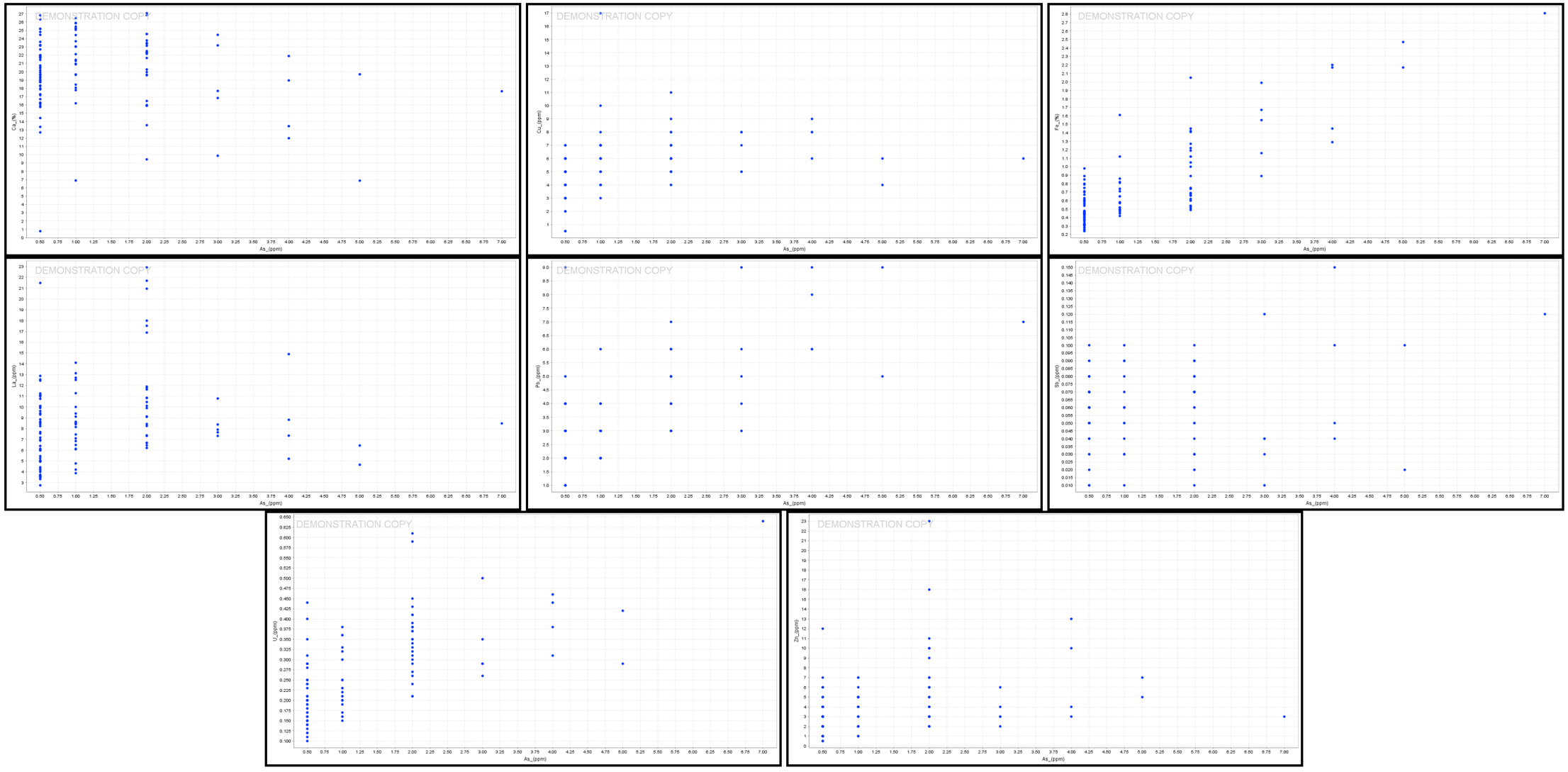

Appendix 4c.5: X-Y Scatter Plots of Ca and correlated elements using IoGAS.

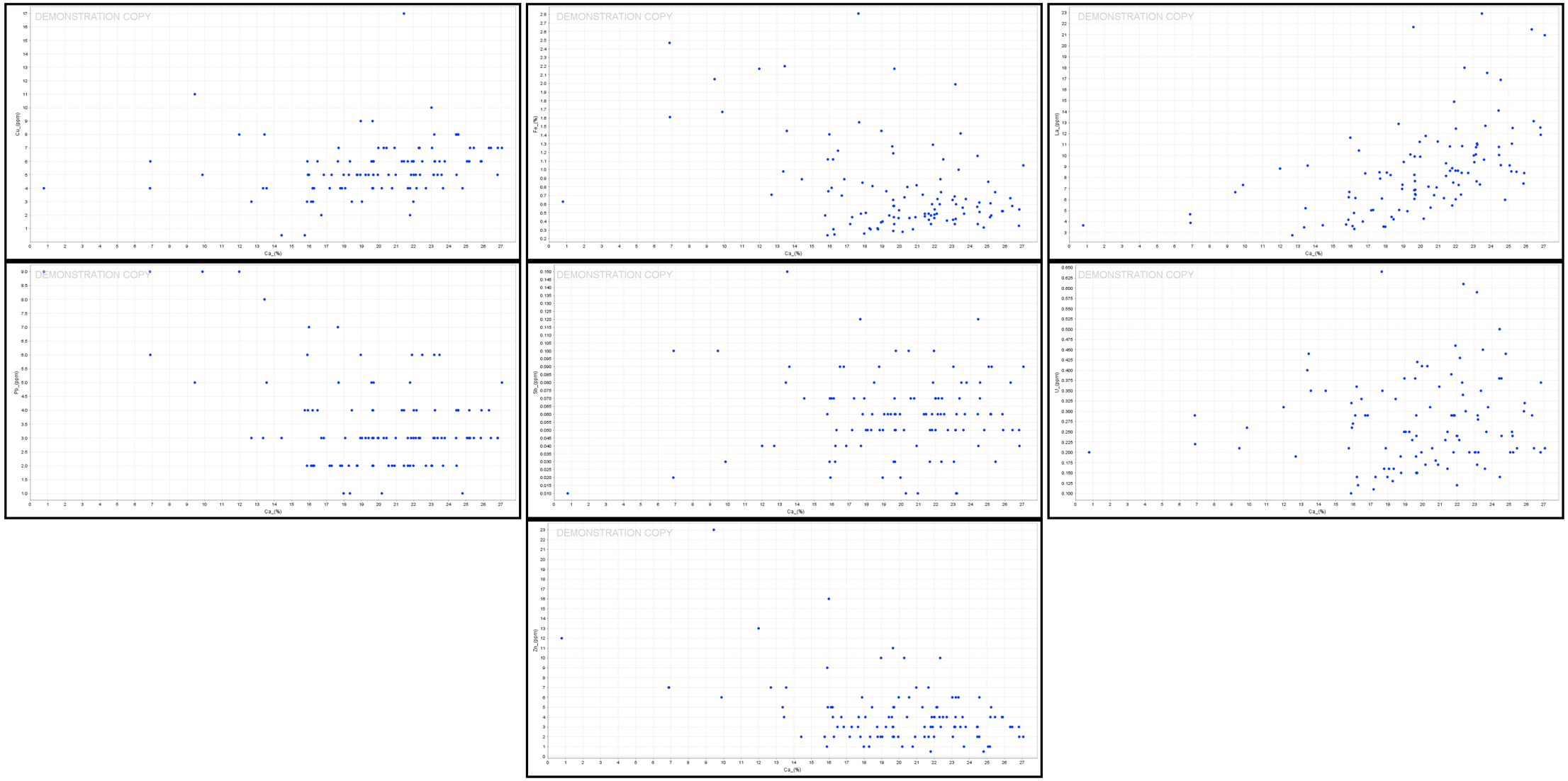

Appendix 4c.6: X-Y Scatter Plots of Cu and correlated elements using IoGAS.

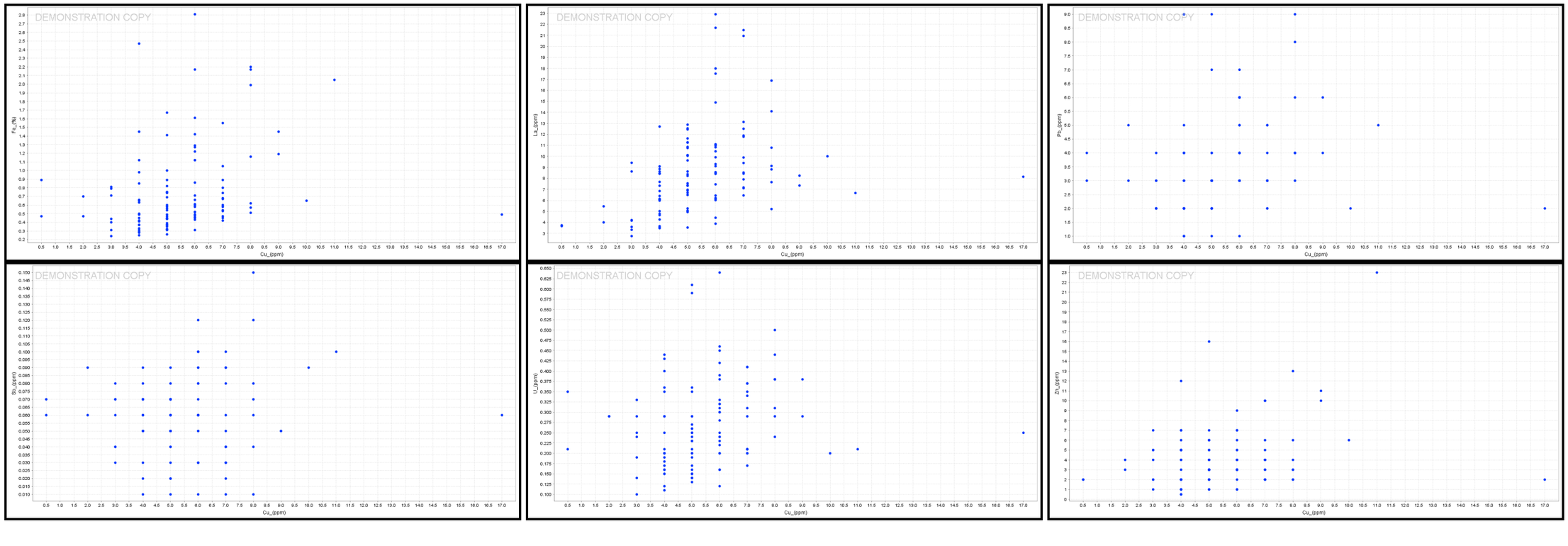

Appendix 4c.7: X-Y Scatter Plots of Fe and correlated elements using IoGAS.

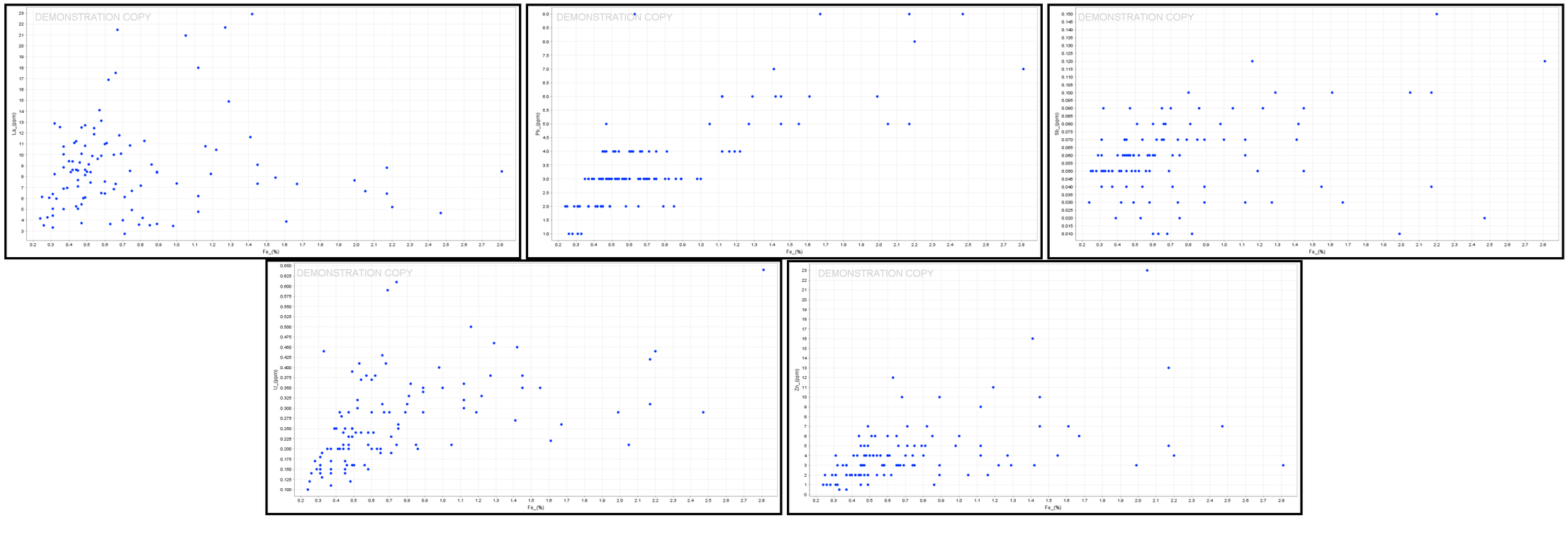

Appendix 4c.8: X-Y Scatter Plots of La and correlated elements using IoGAS.

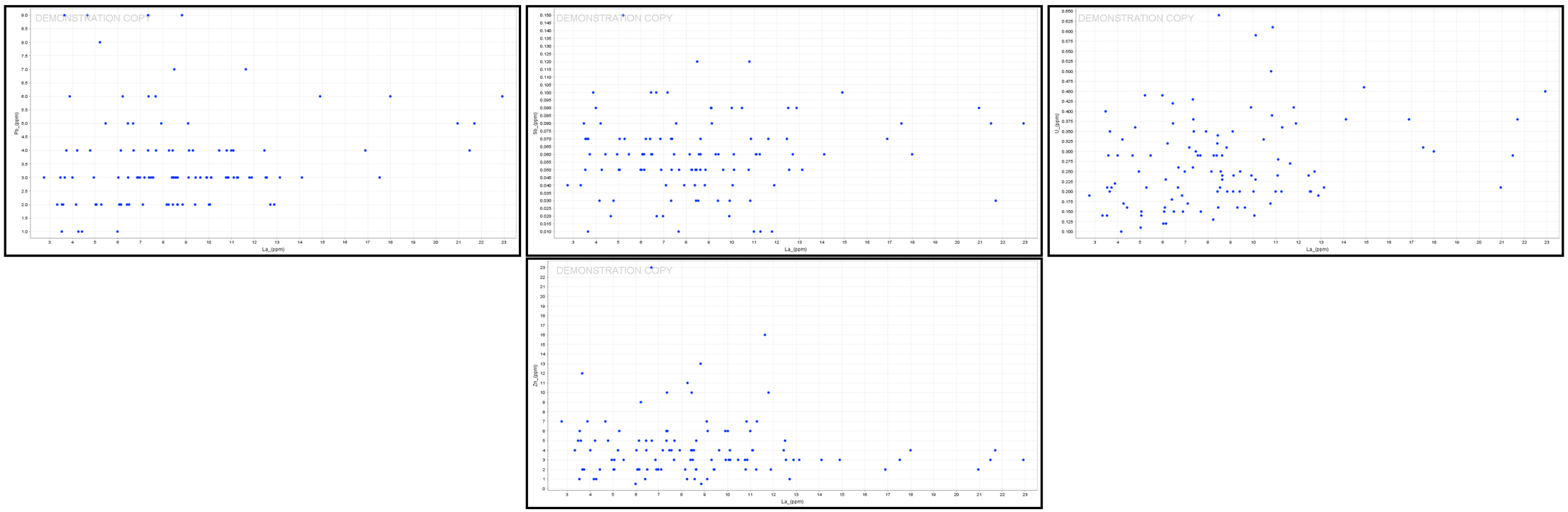

Appendix 4c.9: X-Y Scatter Plots of Pb and correlated elements using IoGAS.

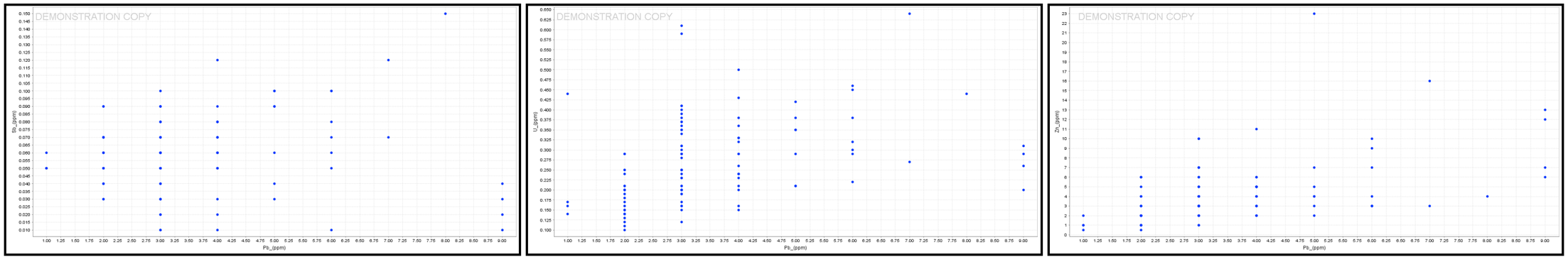

Appendix 4c.10: X-Y Scatter Plots of Sb and correlated elements using IoGAS.

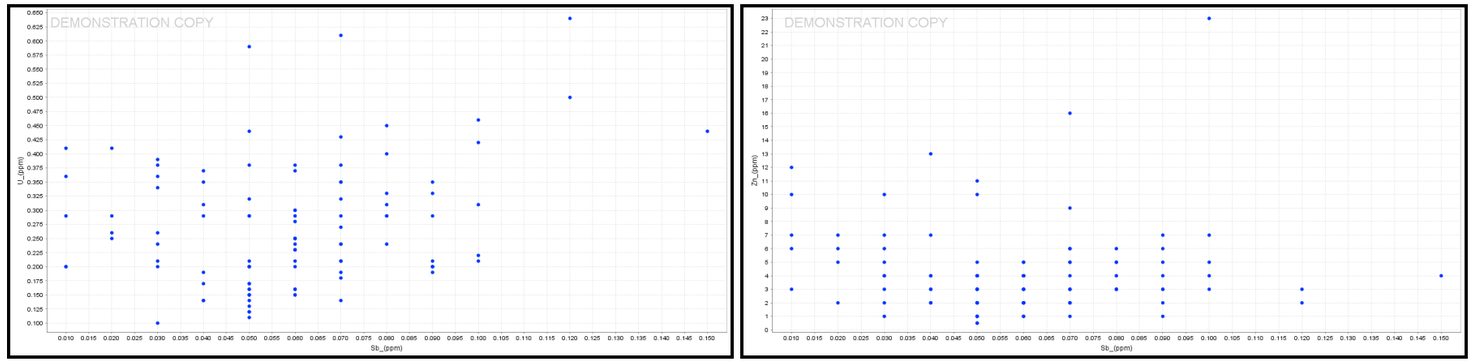

Appendix 4c.11 & 12: X-Y Scatter Plots of U & Zn and correlated elements using IoGAS.

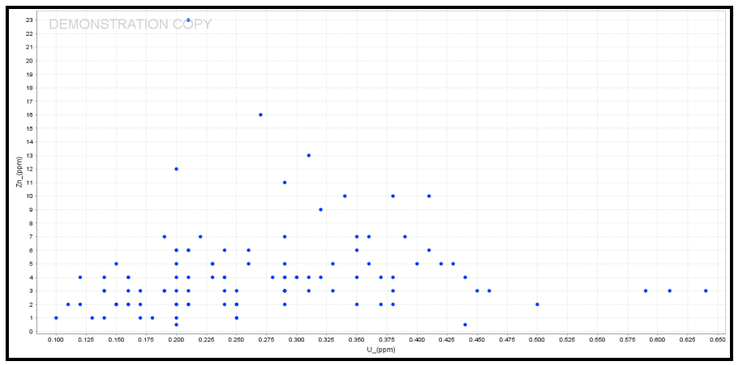

Appendix 4d: Normal Probability Plots of the 12 key elements, using IoGAS.

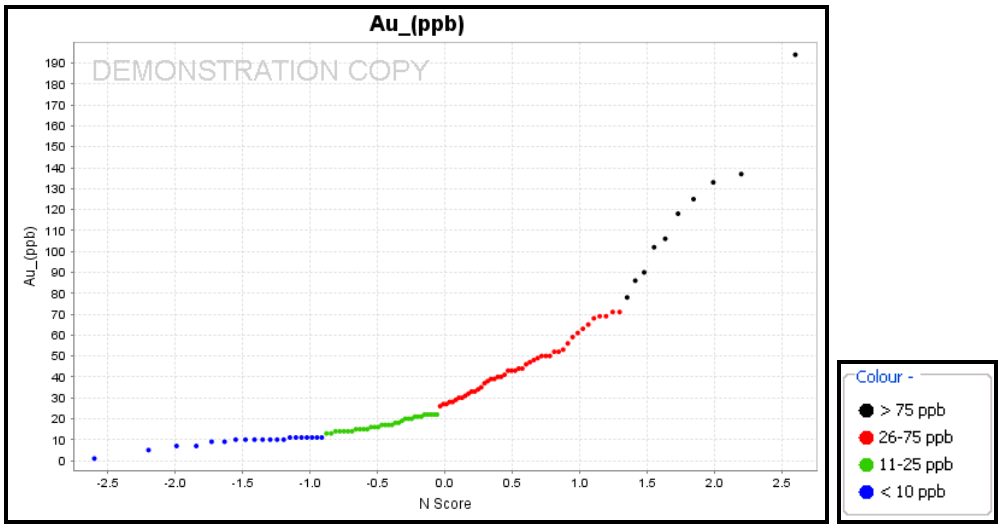

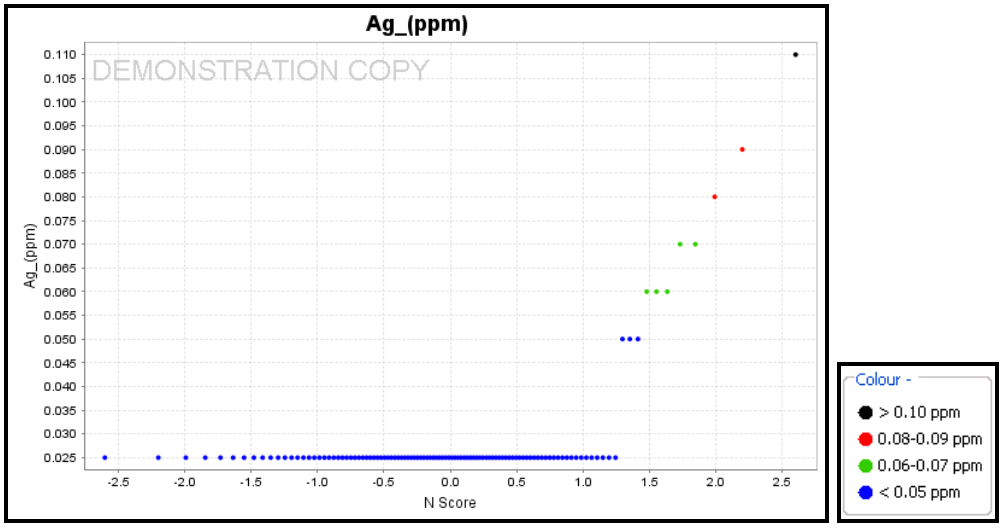

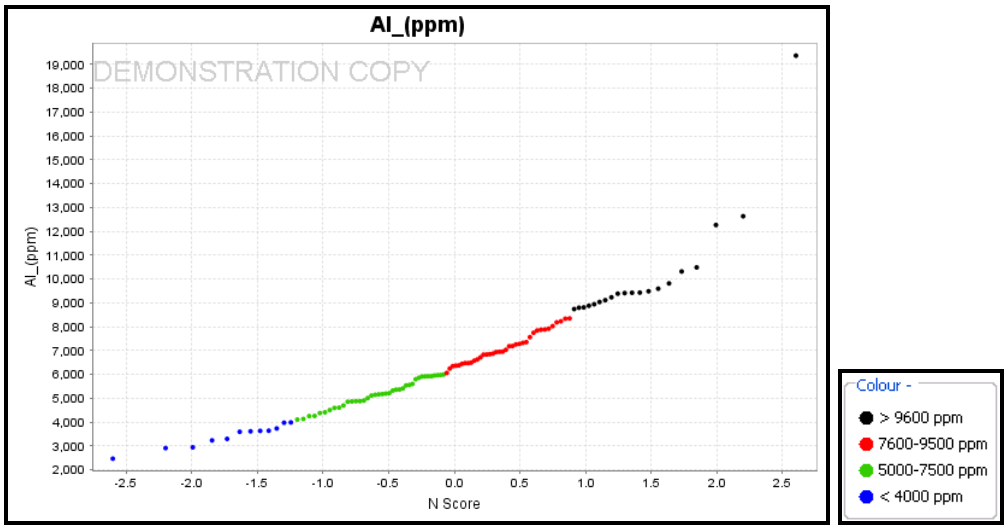

Appendix 4d: Normal Probability Plots of the 12 key elements, using IoGAS.

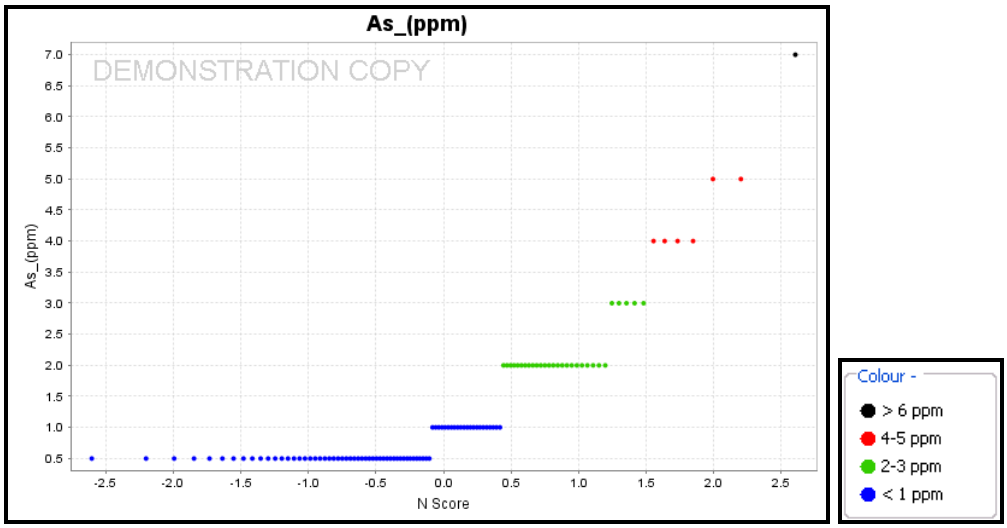

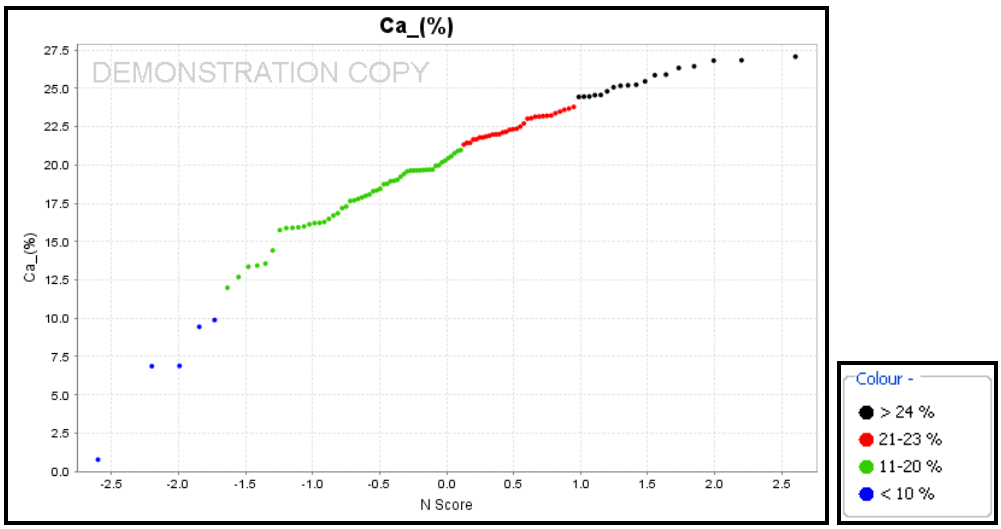

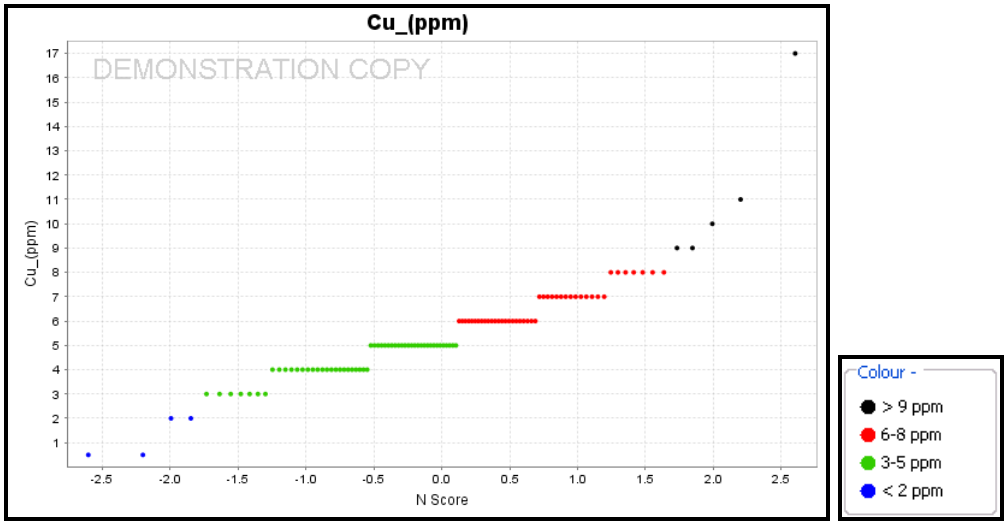

Appendix 4d: Normal Probability Plots of the 12 key elements, using IoGAS.

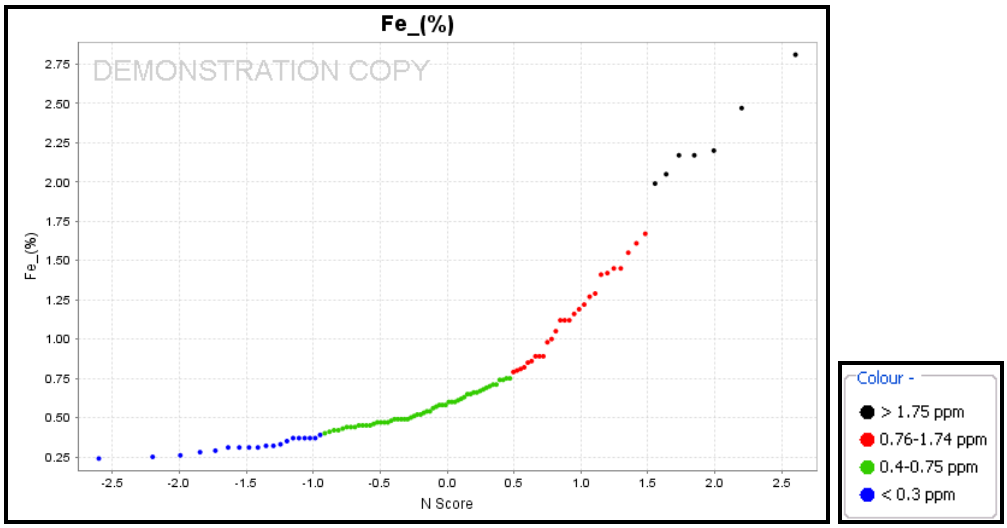

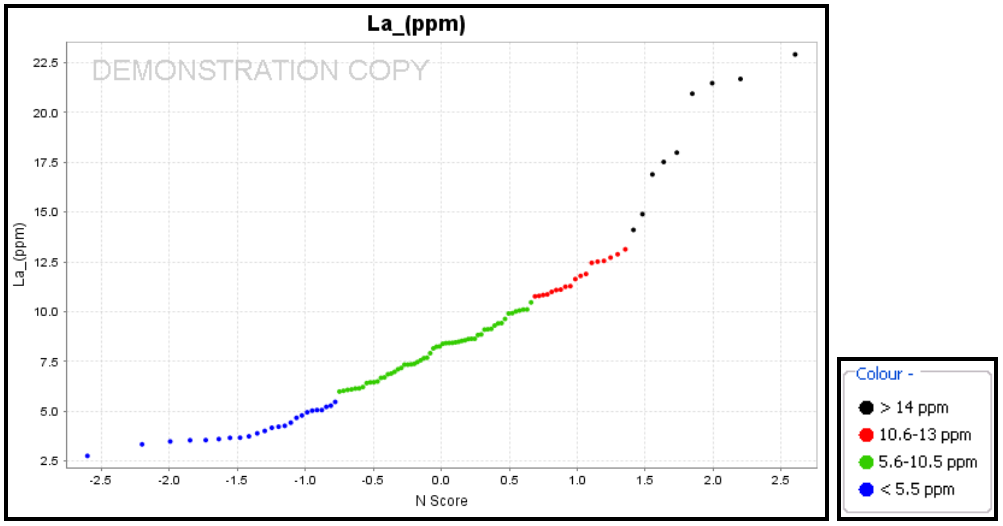

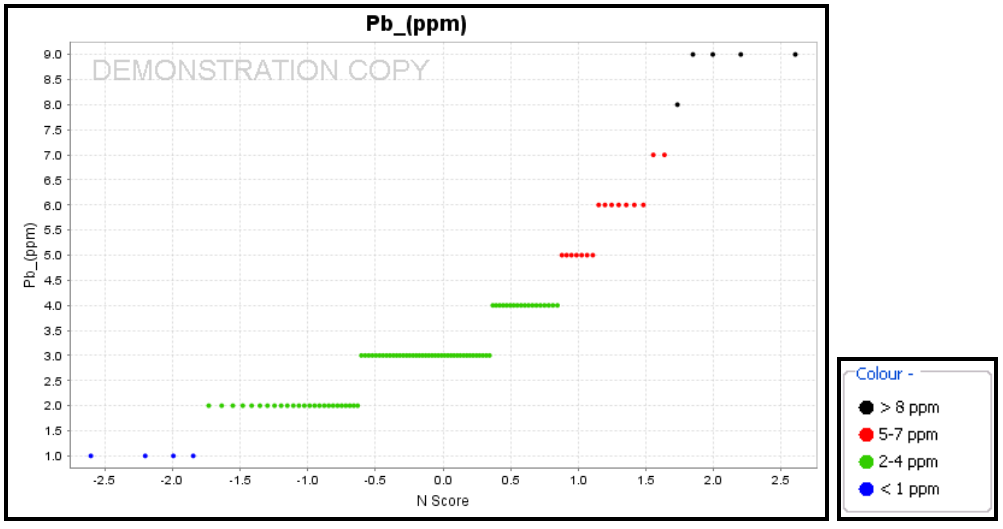

Appendix 4d: Normal Probability Plots of the 12 key elements, using IoGAS.

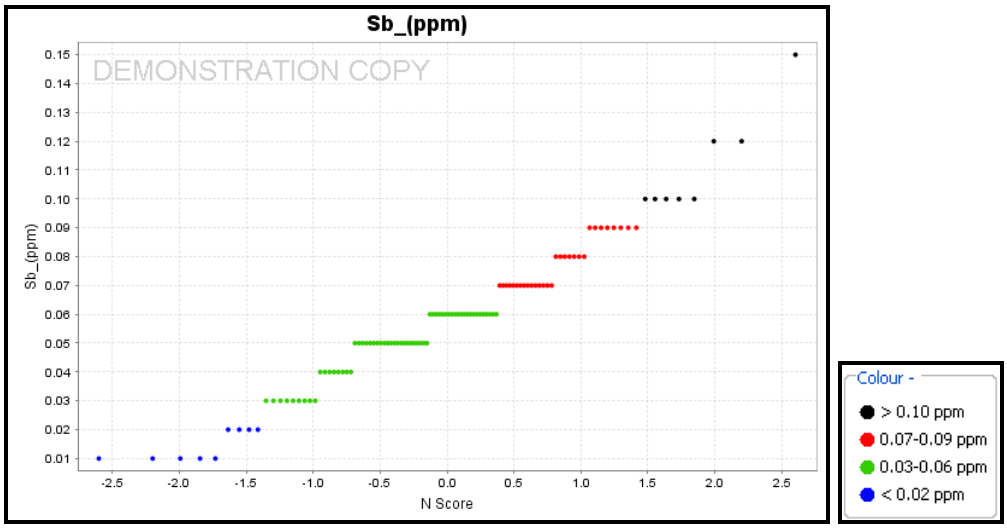

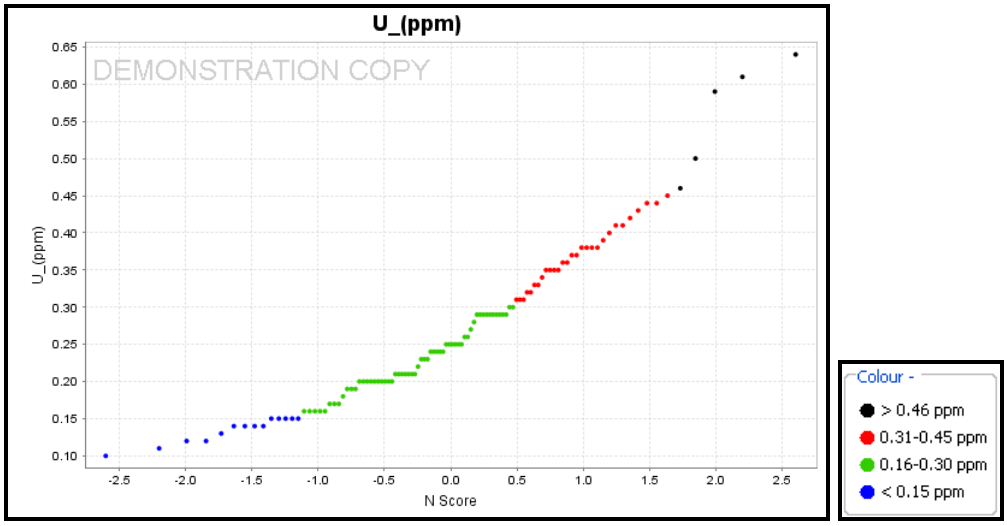

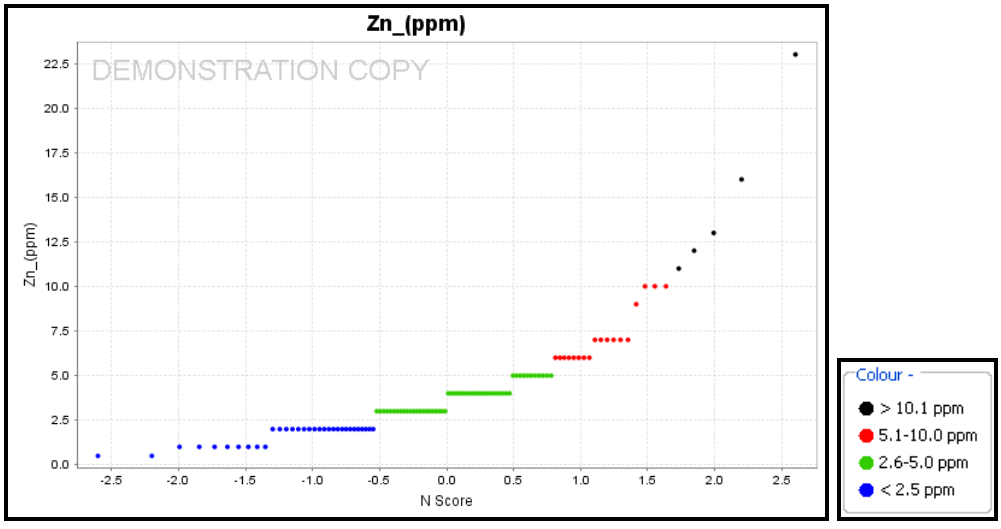

Appendix 4e: Spatial Plots of the 12 key elements, using IoGAS.

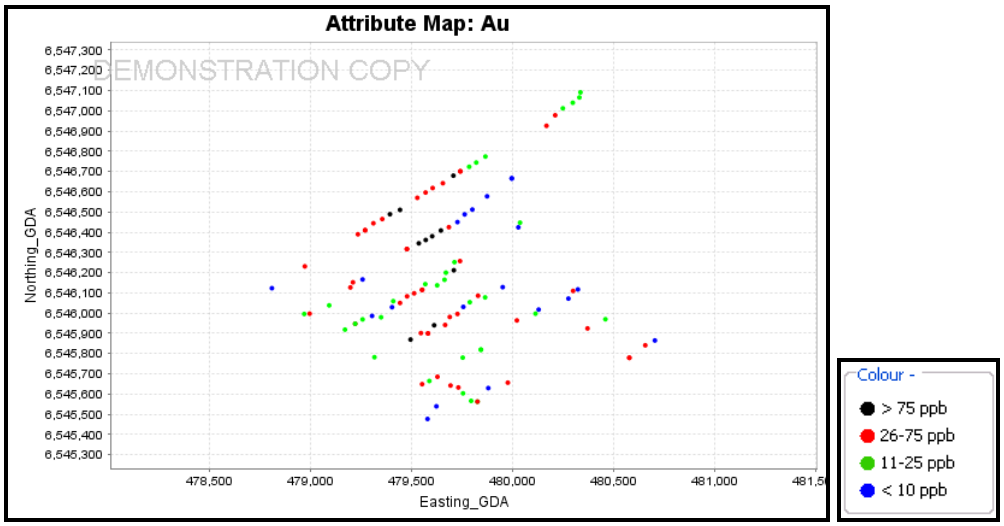

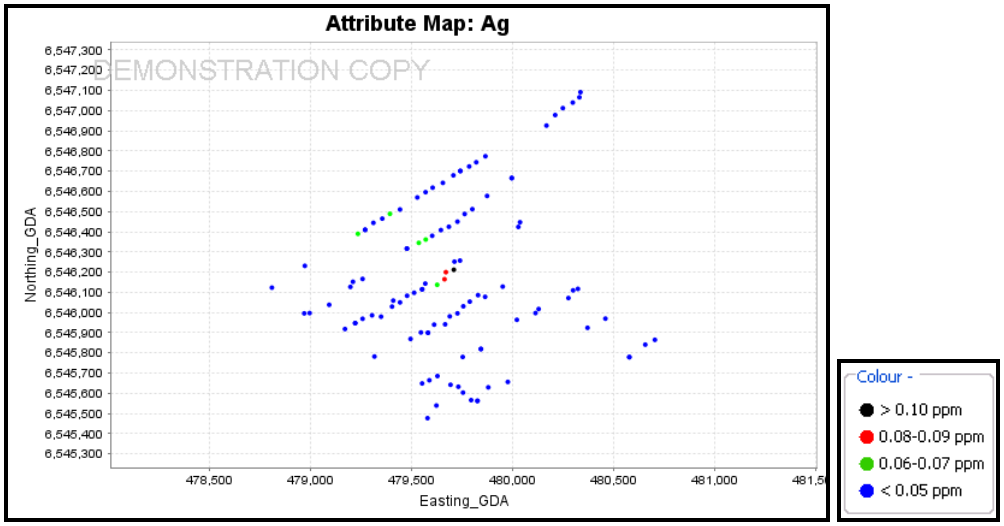

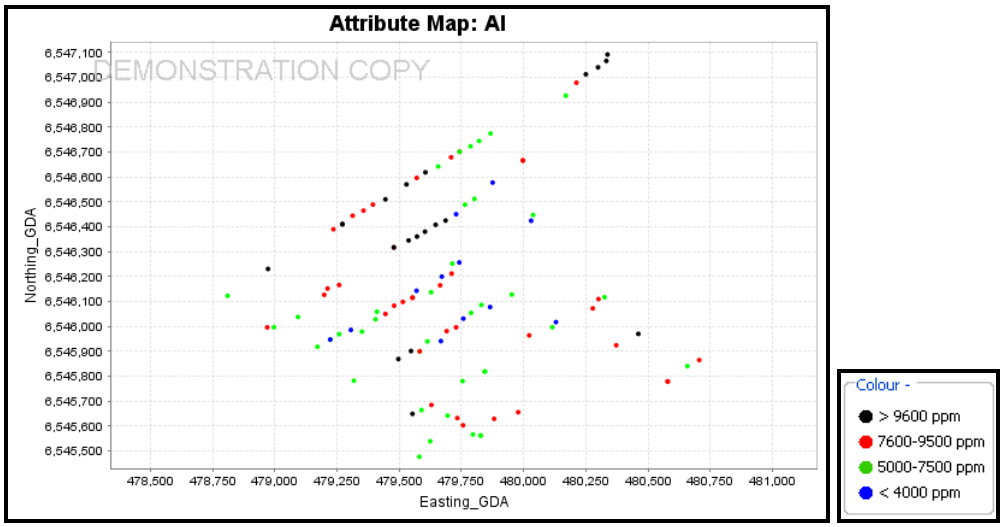

Appendix 4e: Spatial Plots of the 12 key elements, using IoGAS.

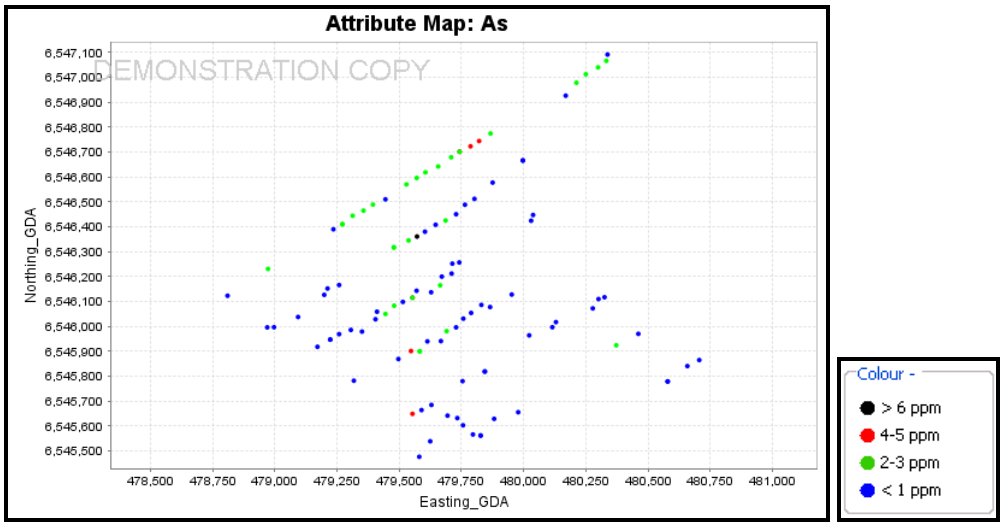

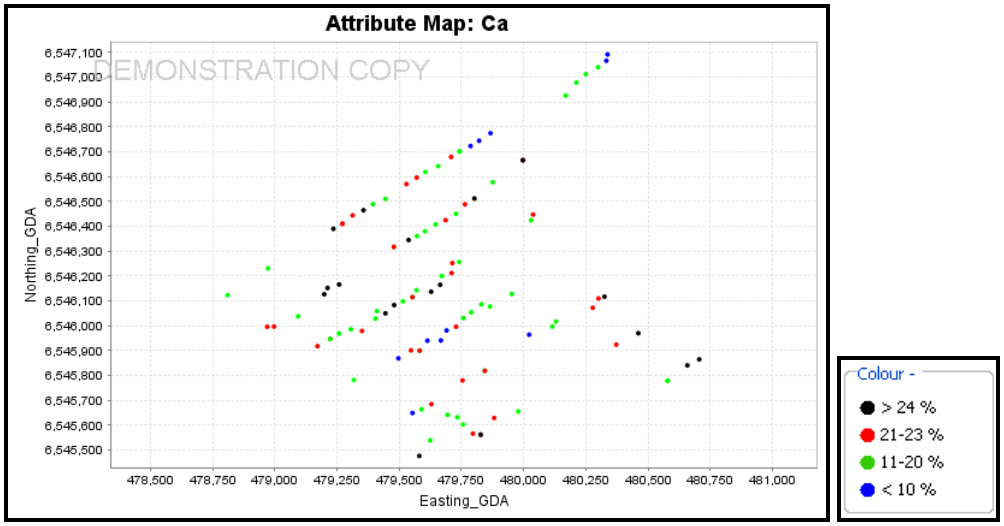

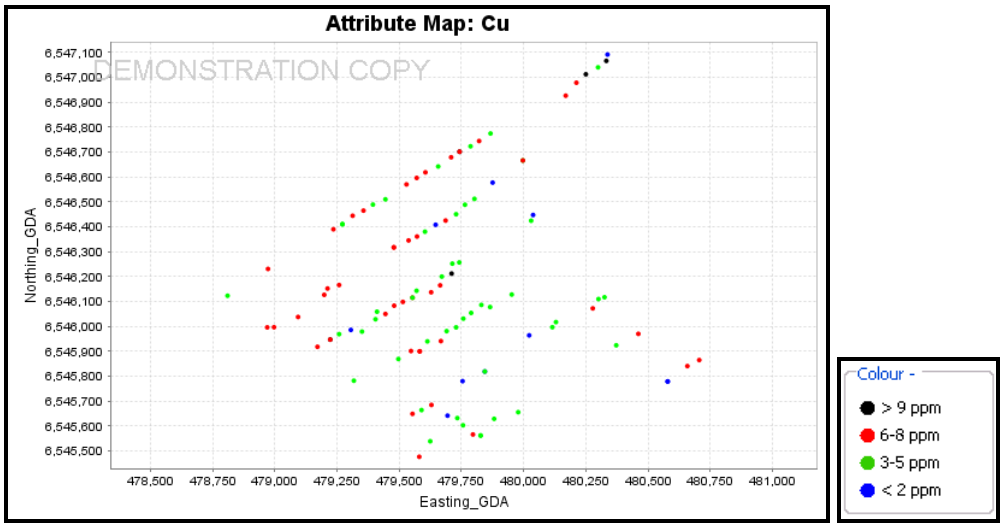

Appendix 4e: Spatial Plots of the 12 key elements, using IoGAS.

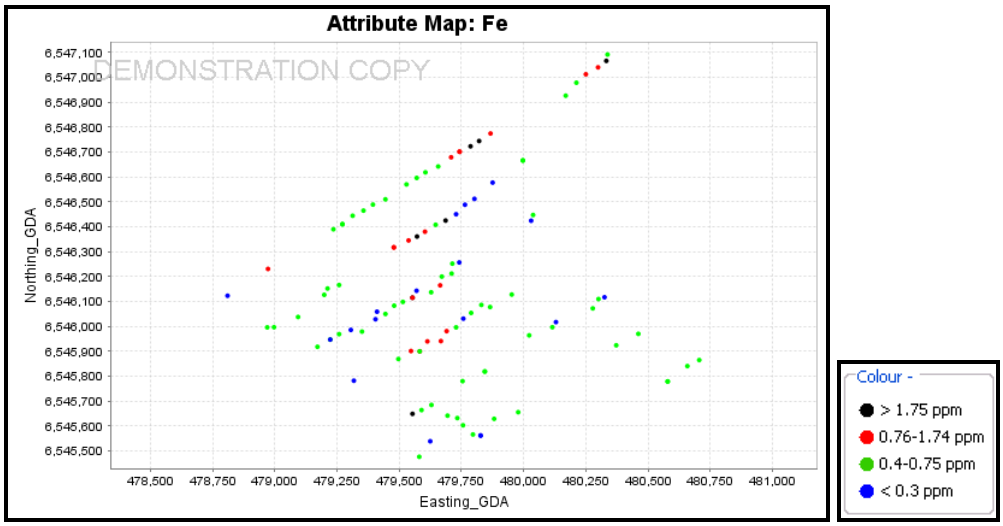

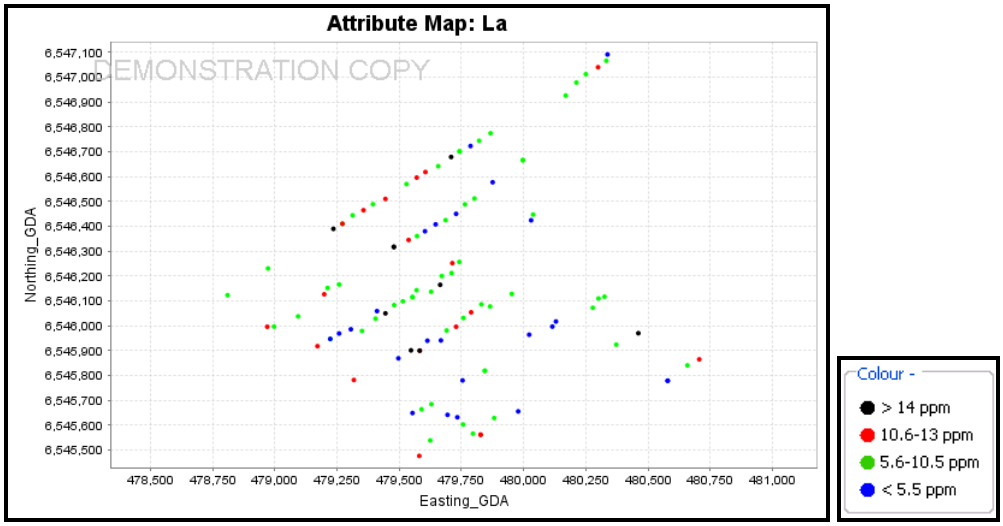

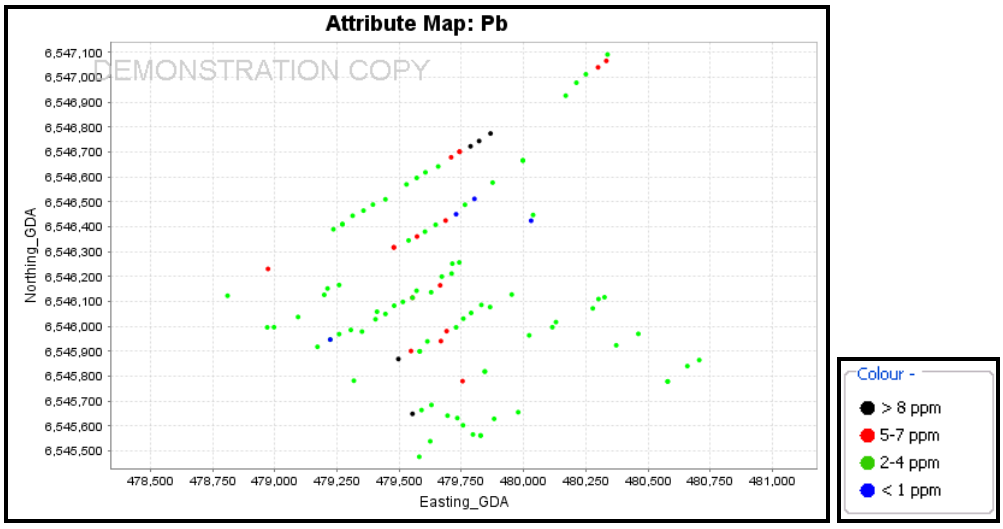

Appendix 4e: Spatial Plots of the 12 key elements, using IoGAS.

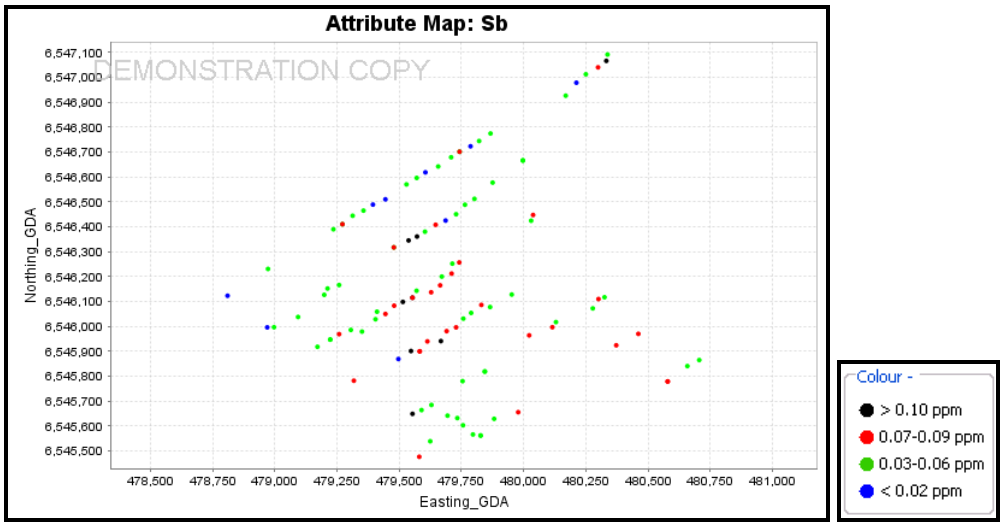

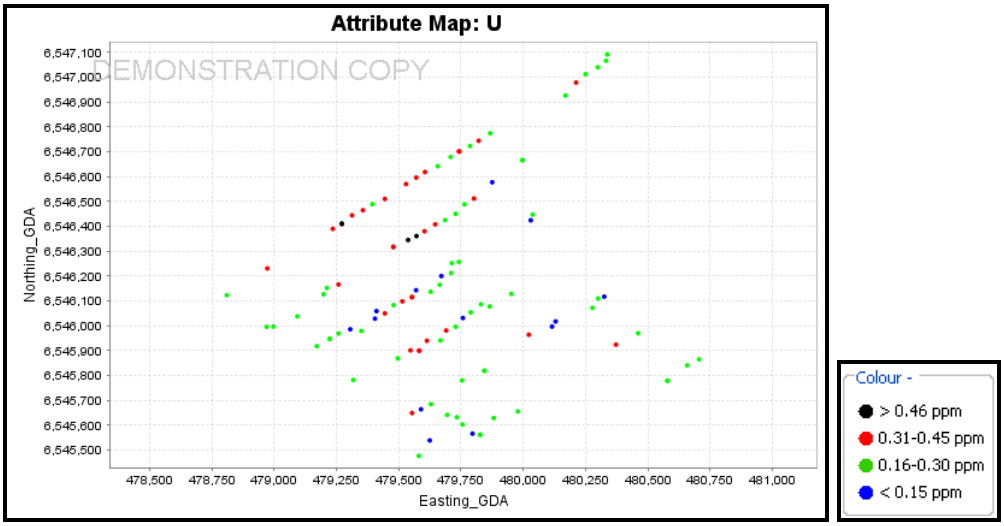

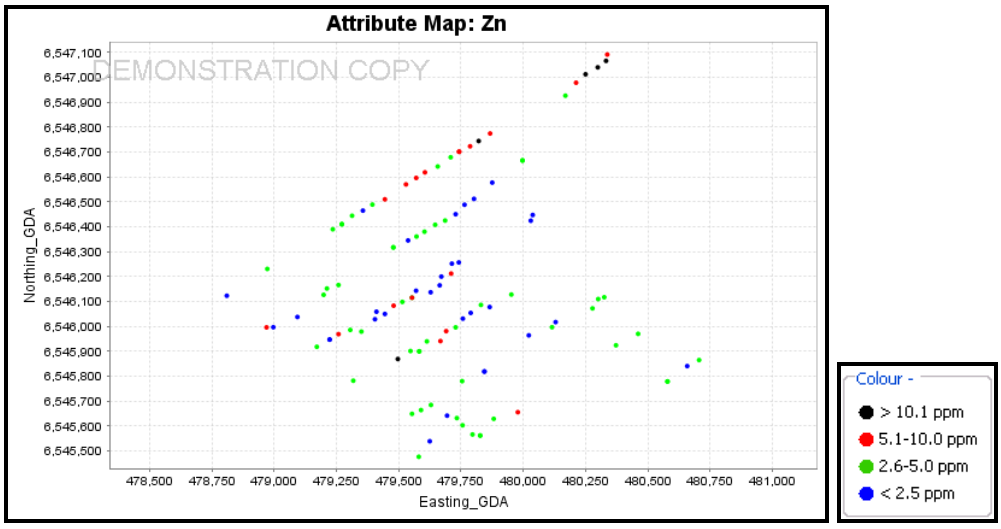

APPENDIX 5

Derivative Map of the ‘Tomahawk’ study area

Appendix 5a: Symbolic overview of the drainage pathways at Tunkillia, as produced by (Dart 2009).

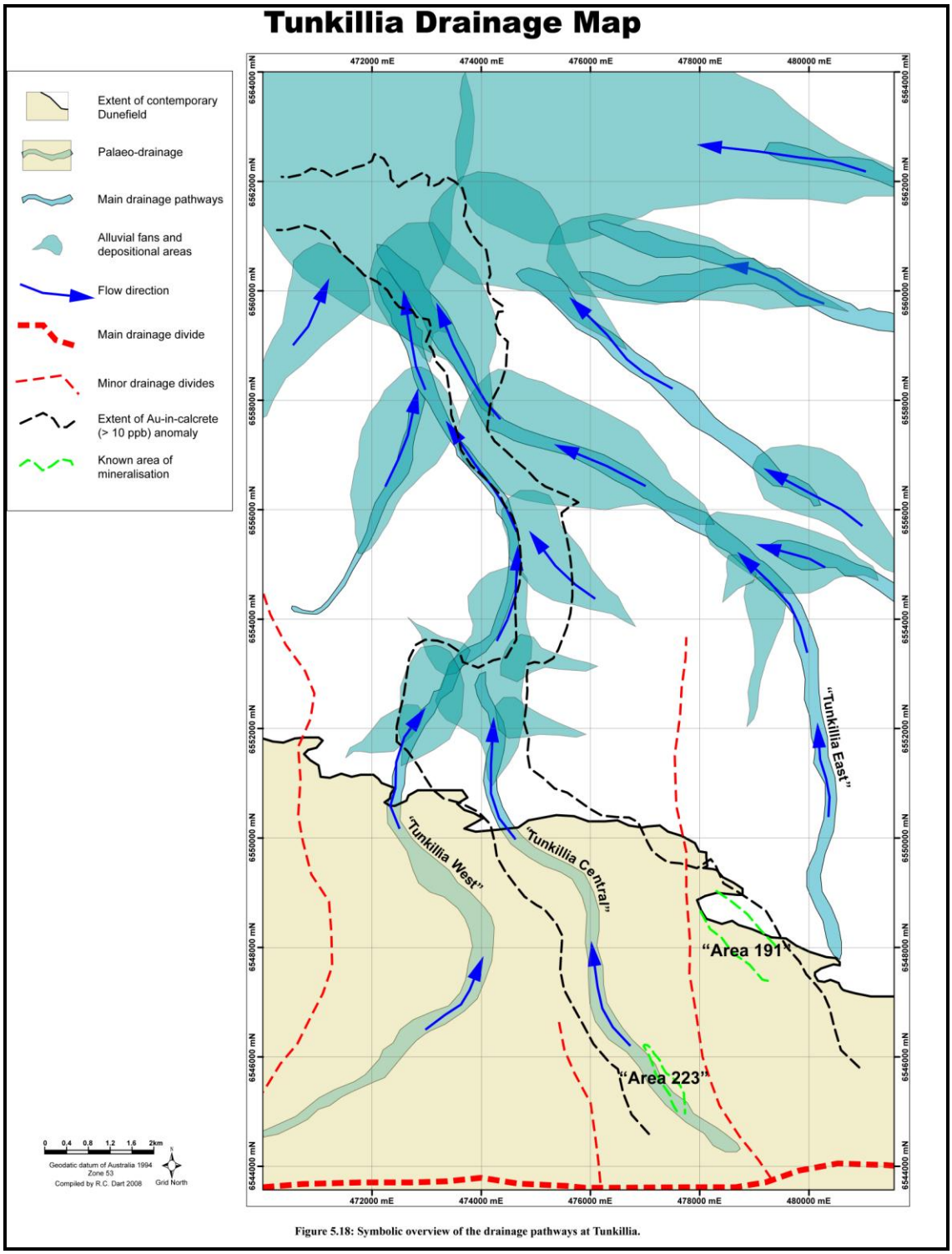

Figure 5.18: Symbolic overview of the drainage pathways at Tunkillia.

11.0 FIGURES

Figure 1

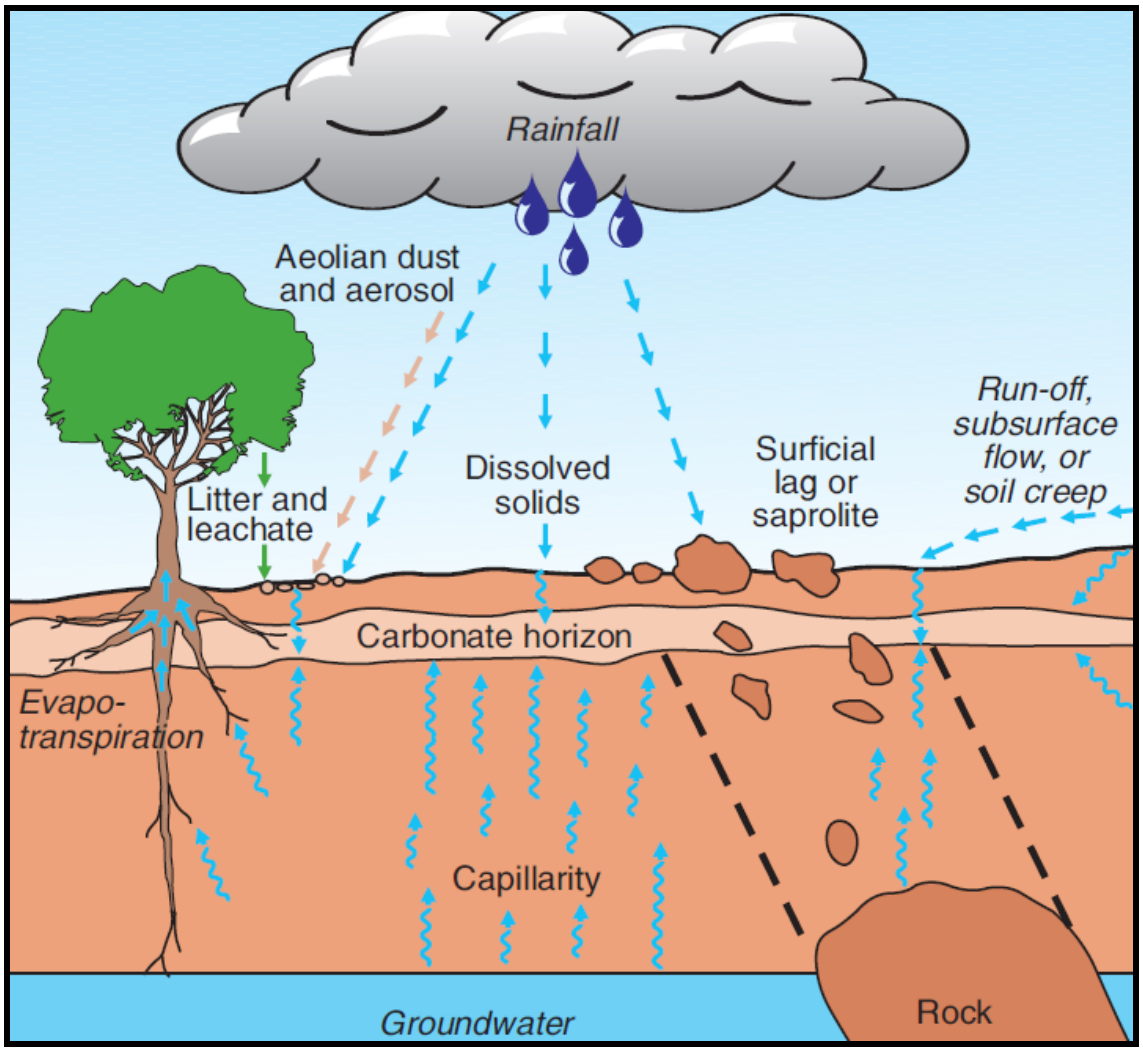
Rainfall
Aeolian dust and aerosol
Litter and leachate
Dissolved solids
Surficial lag or saprolite
Run-off, subsurface flow, or soil creep
Carbonate horizon
Evapo-transpiration
Capillarity
Groundwater
Rock

Figure 2

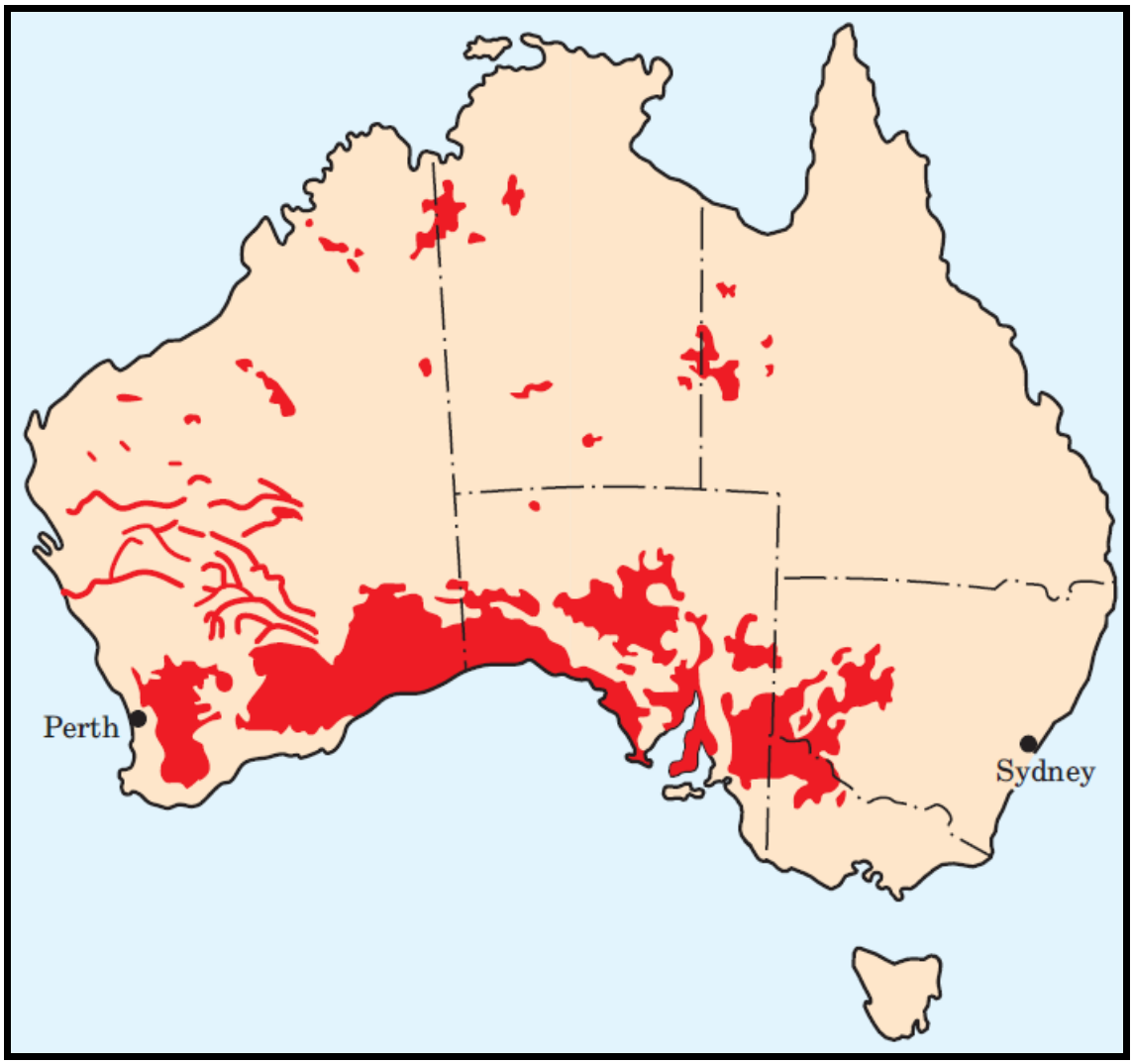

Figure 3

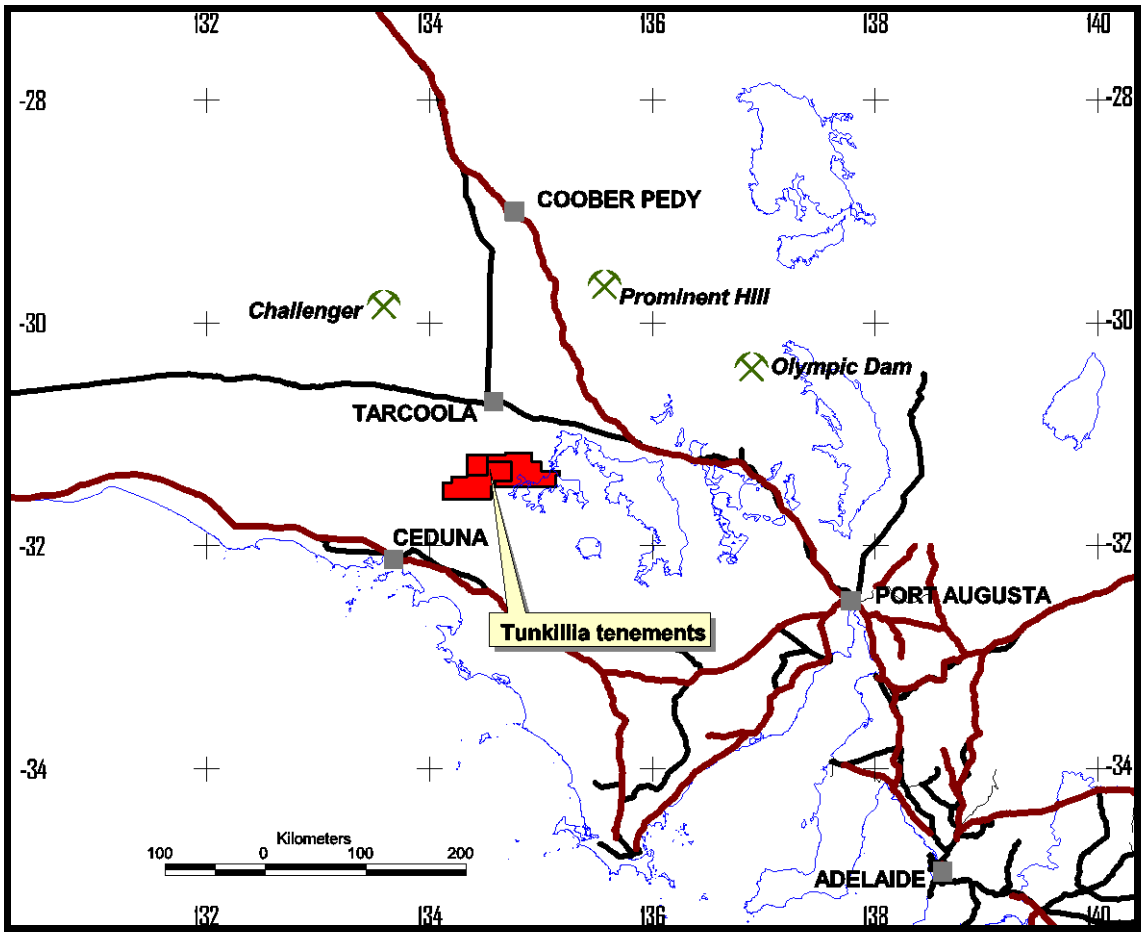
132
134
136
138
140
-28
-30
-32
-34
COOBER PEDY
Challenger
Prominent Hill
Olympic Dam
TARCOOLA
CEDUNA
PORT AUGUSTA
Tunkillia tenements
ADELAIDE
Kilometers
100
0
100
200

Figure 4

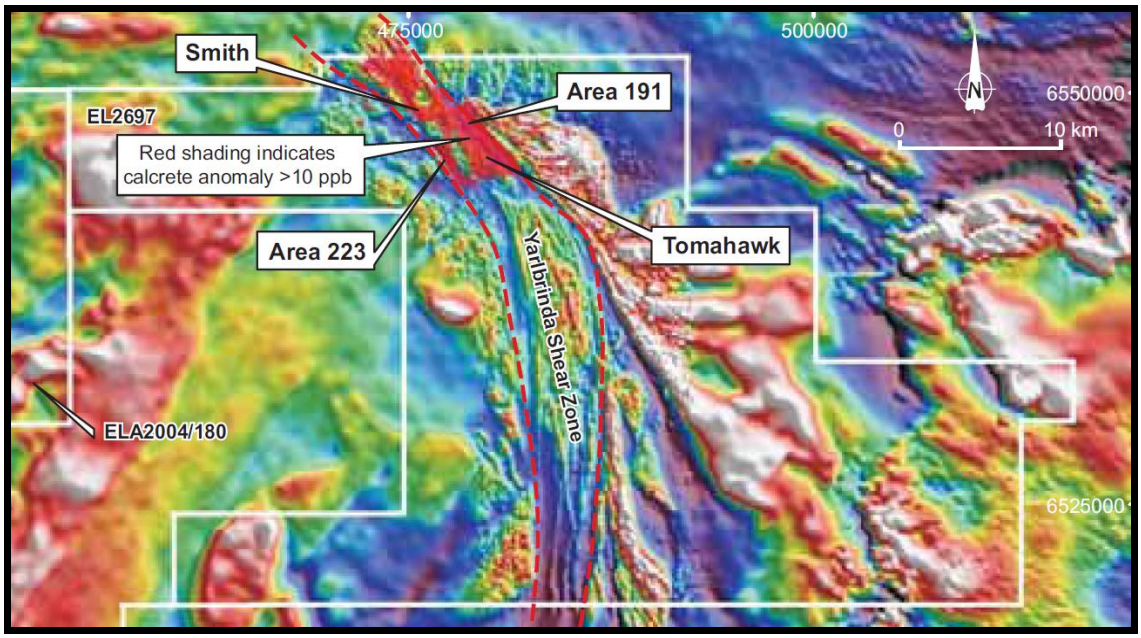
475000
500000
N
6550000
0
10 km
Smith
Area 191
EL2697
Red shading indicates
calcrete anomaly >10 ppb
Area 223
Tomahawk
Yarlbrinda Shear Zone
ELA2004/180
6525000

Figure 5

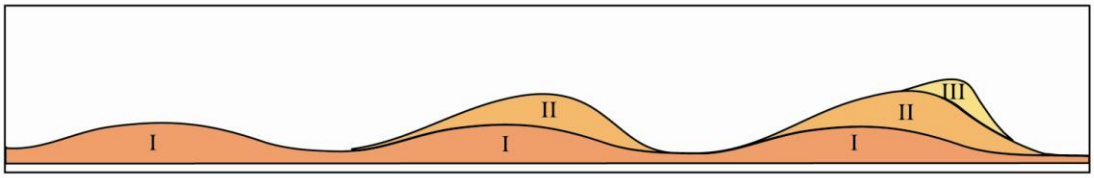

Phase I (ISu$_1$): Red-brown, well-sorted, fine to medium-grained quartzose sand with iron-oxide and clay cutans. Tall, open woodland dominated by *Acacia aneura*, *Acacia ramulosa*, and *Bossiaea walkeri*, typically with an extensive cryptogam crust on the soil surface.

Phase II (ISu$_2$): Yellow-brown to light red-brown, well-sorted, fine to medium-grained quartzose sand with iron-oxide and clay cutans. Tall, open woodland dominated by *Eucalyptus socialis*, *Acacia ramulosa*, *Bossiaea walkeri* and Triodia hummock-grass.

Phase III (ISu$_3$): Yellow-brown to light red-brown, well-sorted, fine to medium-grained quartzose sand with iron-oxide and clay cutans. These dunes have mobile crests that typically encroach over Phase I and II dunes. Vegetation is dominated by the vegetation of the previous underlying dune phases, but at least partially covered by sand.

Figure 6

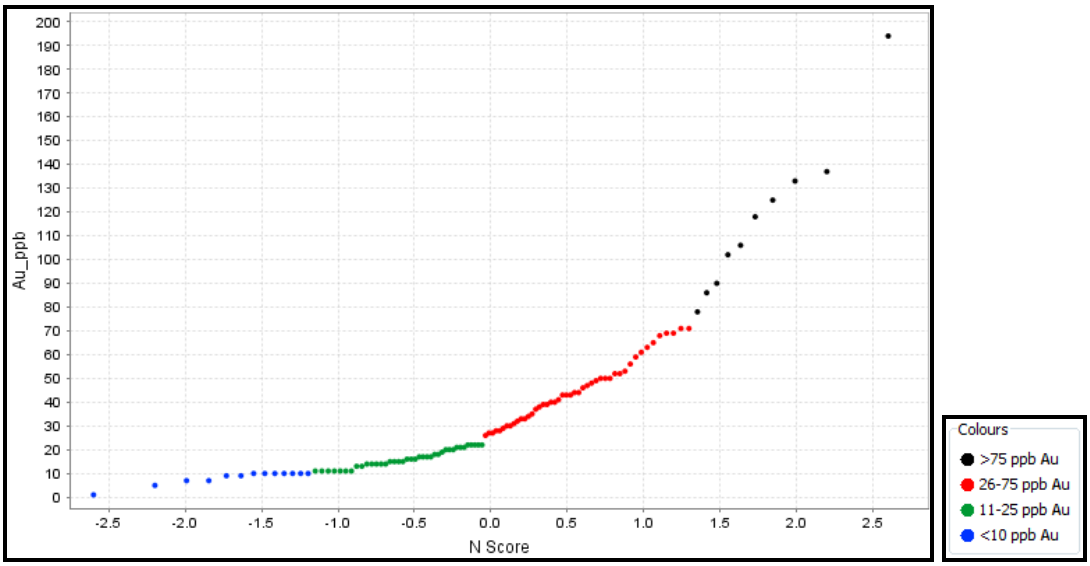

Figure 7

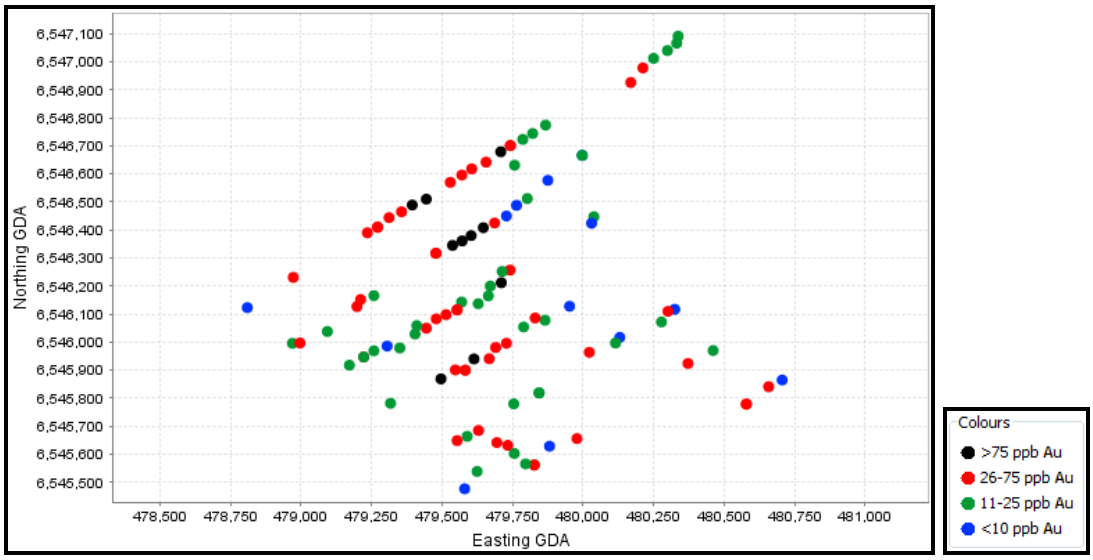

Figure 8

‘Tomahawk’ Regolith-Landform Map, Tunkillia, South Australia.

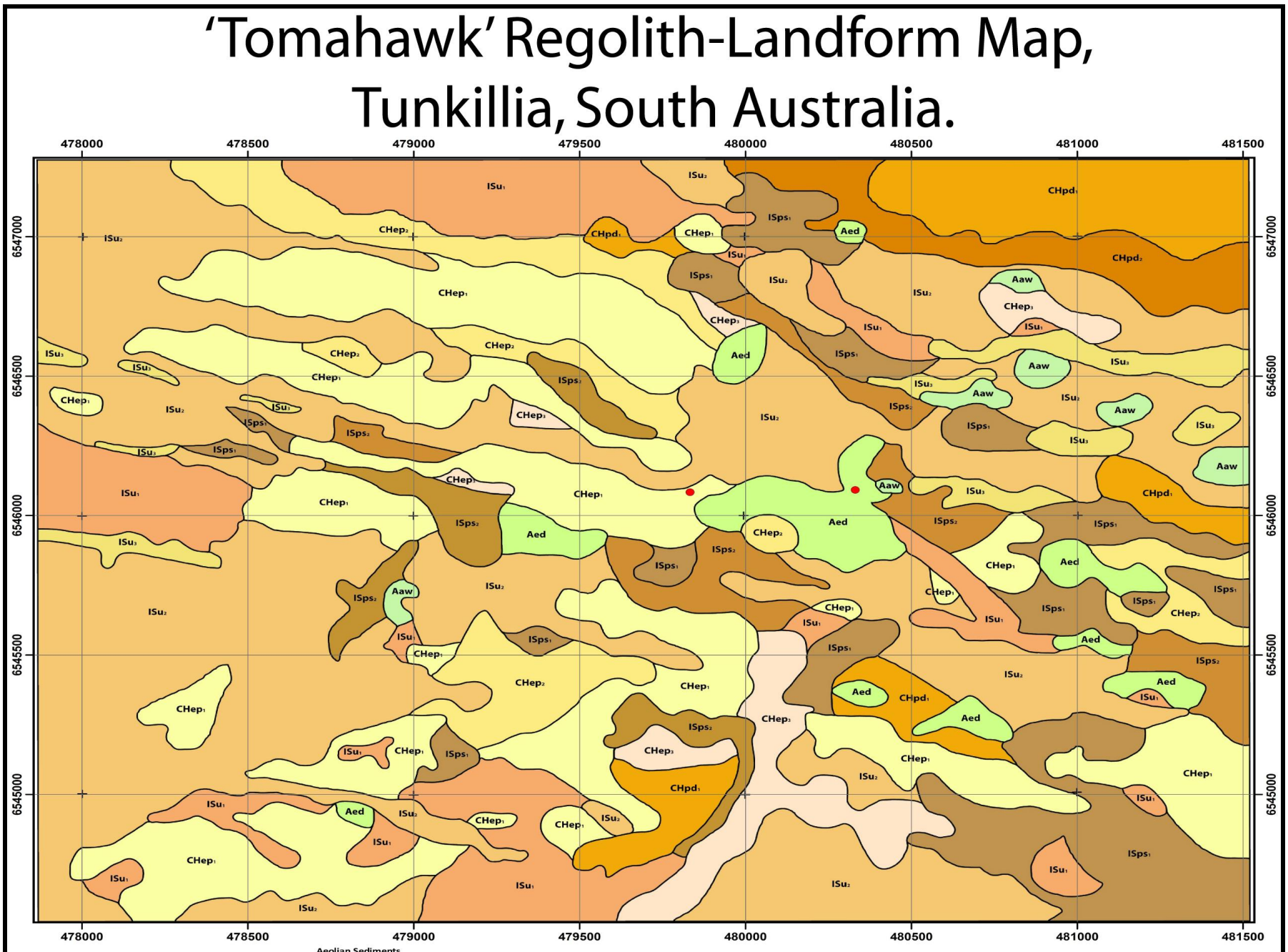

Aeolian Sediments

ISu_1	Red-brown, well sorted, fine to medium-grained quartzose sands with iron-oxide and clay cutans on a low relief, longitudinal dune. Open woodland dominated by *Acacia anuera, Eucalyptus socialis, Acacia ramulosa* and *Acacia ligulata* . Occasional *Eucalyptus concinnia* and *Casuarina pauper* with extensive, well developed surficial cryptogram crust on the soil surface.
ISu_2	Light red-brown, well sorted, fine to medium-grained, quartzose sands with iron-oxide and clay cutans on a moderate relief, longitudinal dune. Open woodland dominated by *Eucalyptus socialis, Triodia irritans, Acacia ramulosa, Bossiaea walkeri* and *Triodia scariosa, Acacia ligulata* and *Acacia burkittii*. Moderate cover of surficial cryptogram crust on the soil surface.
ISu_3	Brown to light red-brown, well sorted, fine to medium-grained quartzose sand with iron-oxide and clay cutans on a high relief, longitudinal dune. Mobile crests impinge on older ISu_1 and ISu_2 landforms, and therefore vegetation is partially covered by sand and characterises older landforms: Open woodland dominated by *Acacia ramulosa, Casuarina pauper, Bossiaea walkeri, Acacia aneura* and *herbs and tussock grasses.*
$ISps_1$	Red-brown, moderate to poorly-sorted, fine to medium-grained, quartzose sand with iron-oxide cutans on a low-relief sand plain/dune swale. well developed cover of cryptogram crust on the soil surface. Open woodland dominated by *Eucalyptus concinnia , Maireana sedifolia* and *Cratystylis conocephala* . Occasional *Casuarina pauper , Acacia anuera* and *Acacia ligulata* .
$ISps_2$	Red-brown, moderately to well-sorted, fine to medium-grained, quartzose sand with iron-oxide cutans on a low-relief sand plain/dune swale. Iron-oxide, lithic and quartz lag of <0.2cm. Open woodland dominated by *Casuarina pauper, Maireana sedifolia and Cratystylis conocephala.* Occasional *Eucalyptus concinnia, Acacia birkittii* and *Acacia ligulata.*
Aed	Red-brown, very fine to fine-grained, well sorted and well rounded consolidated clayey/silty soils, on a flat lying erosional drainage area. Minor medium-grained quartz and very high cover of cryptogram crust on the soil surface. Occasional minor calcrete and silcrete nodules, well rounded-sub rounded <2.0cm. Open woodland of dense thickets of *Acacia aneura* with occasional *Casuarina pauper* . Chenopod understorey of *Maireana sedifolia* , and *Acacia ligulata* .
Aaw	Red-brown, very fine to fine-grained, well sorted consolidated clayey soils with very well developed cryptogram crust on the soil surface. Occasional rounded to sub-rounded calcrete and silcrete nodules <3.0cm. Chenopod shrubland of *Casuarina pauper* and *Acacia ligulata* , occasional *Acacia anuera* , *Maireana sedifolia* and well developed cover of cryptogram crust on the soil surface.

Sheetflow Sediments

$CHep_1$	Light brown to red, moderately sorted, fine to medium-grained quartzose sand with medium-grained sub-rounded quartz, iron-oxide <1.0cm and silcrete <2.0cm. High occurrence of sub-rounded to rounded 0.5-8.0cm nodular calcrete lag on a low relief landform dominated by sheetflow sedimentary transport and well developed cover of cryptogram crust on the soil surface. Open woodland dominated by *Casuarina pauper* and occasional *Eucalyptus concinnia* and *Acacia aneura* thickets, with chenopod shrubland understorey dominated by *Maireana sedifolia* , *Cratystylis conocephala* and *Senna artesmaides* .
$CHep_2$	Red-brown to brown, moderately sorted, fine to medium-grained quartzose sand with angular to rounded silcrete lag <8.0cm on a low relief landform dominated by sheetflow sedimentary transport. Sub-rounded to rounded nodular calcrete lag <5.0cm, iron-oxides <2.0cm and a moderate cover of cryptogram crust on the soil surface. Chenopod shrubland dominated by *Maireana sedifolia, Cratystylis conocephala* and occasional *Casuarina pauper, Senna artesmaides* and *Acacia anuera*.
$CHep_3$	Brown-red, well sorted, fine to medium-grained quartzose sand. Low relief landform dominated by sheetflow sedimentary transport with a well developed cover of cryptogram crust on the soil surface. Angular to sub-angular calcrete <5.0cm and shallow <50cm hardpan carbonates. Rounded iron-oxide and sub-angular to sub-rounded silcrete grains <1.0 to 6.0cm cm and sub-angular to sub-rounded vein quartz <3.0cm. Chenopod shrubland dominated by *Maireana sedifolia* , *Cratystylis conocephala, Casuarina pauper* , *Senna artesmaides* and *Acacia anuera* .
$CHpd_1$	Brown-red, well sorted, very fine to fine-grained, quartzose sand with coarse sand sized grains of sub-angular to rounded quartz, iron-oxide, lithic and carbonates on a colluvial sheetflow depositional plain. Occasional angular to sub-rounded carbonates from 1-5cm. Very well developed cover of cryptogram crust on the soil surface. Open woodland dominated by *Casuarina pauper* with occasional *Eucalyptus concinnia* . Chenopod understorey of *Maireana sedifolia , Cratystylis conocephala , Acacia ligulata* and *Senna artesmaides* .
$CHpd_2$	Light brown to red, moderate to well sorted, very fine to fine-grained quartzose sand with medium sized grains of iron-oxide, quartz and sub-angular carbonates on a colluvial sheetflow depositional plain. Medium cover of cryptogram crust on the soil surface. Open woodland dominated by *Eucalyptus concinnia, Acacia ligulata, Senna artesmaides* and *Cratystylis conocephala* . Occasional *Eucalyptus socialis , Casuarina pauper* and *Maireana sedifolia* . More dense low lying vegetation than $CHpd_1$.

Saprolith

SMep	Small exposures of moderately weathered, *in situ* Quartz vein.

N

0 0.25 0.5 0.75 1 km

Geodatic datum of Australia 1994
Zone 53
Compiled by L.L.Klingberg 2009

KEY	
Regolith	
A	Alluvial sediments
CH	Colluvial sheetflow sediments
IS	Aeolian sediments
Landforms	
ed	Drainage depression
aw	Swampland
ep	Erosional plain
pd	Depositional plain
ps	Sandplain
u	Dunefield

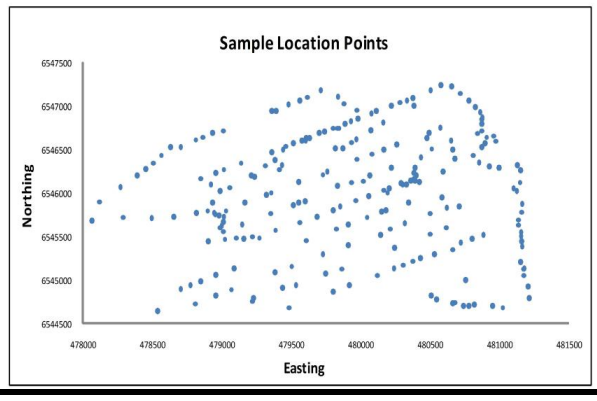

Figure 9

Approx. Depth (m)				Description
0.0	**Transported Regolith**	Cover	**Unconsolidated**	Brown-red matrix of very-fine to fine-grained, well-sorted and well-rounded quartzose sands, with strong dark-brown red 0.2-gravel sized sub-angular to sub-rounded silcrete, quartz and minor calcrete, all which have undergone substantial goethite weathering.
2 ± 2				
>4			**Consolidated / Cemented**	Either cream, 0.2-2.0cm sized well-sorted, well rounded nodular calcrete; or Orange-brown, sub-round to sub-angular gravel sized silcrete with and strong goethite weathering.
6 ± 3	***In Situ* Regolith**	Saprolite	**Plasmic Zone**	Yellow, very fine-grained, well-sorted and well-rounded matrix, with sub-angular <2cm sized silcrete and quartz grains. Goethite weathering visible.
18 ± 9			**Kaolinised Plasmic Zone**	White, kaolinitic zone with very fine-grained, well-sorted matrix of clay/powder texture. Medium-grained, sub-round quartz and minor plagioclase feldspar grains.
34 ± 15			**Plasmic Zone**	Cream, to grey-brown kaolinitic zone with very fine-grained, well-sorted matrix of clay/powder texture. Mineralogy includes sub-round quartz and minor plagioclase feldspar. Minor goethite weathering.
44 ± 23		Saprock	**Saprock**	Cream to brown, gravel sized, sub-angular to sub-round k-feldspar, quartz and plagioclase feldspar grains and occasional mica, with notable chlorite alteration; minor weathering of goethite, and down profile strength in weathering decreases. Approaching fresh rock at base of hole however has not been fully reached.
56 ± 2		Basement	**Fresh Rock**	Grey, gravel sized sub-angular to sub-round fresh bedrock with visible gneissic fabric and mineralogy of mica, k-feldspar, quartz, plagioclase feldspar. No chlorite alteration visible.

Figure 10

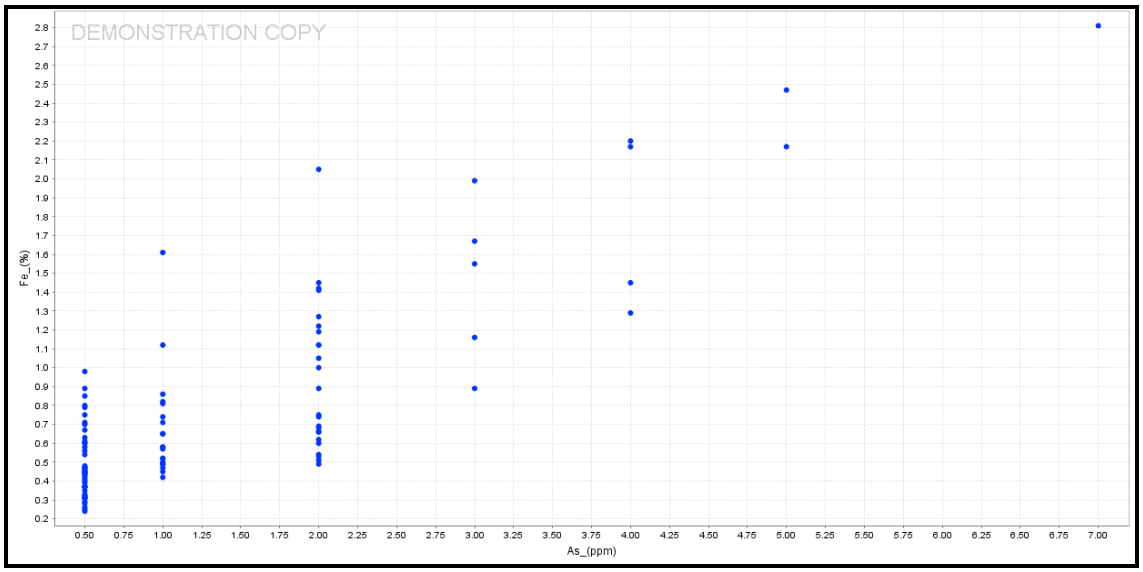

Figure 11

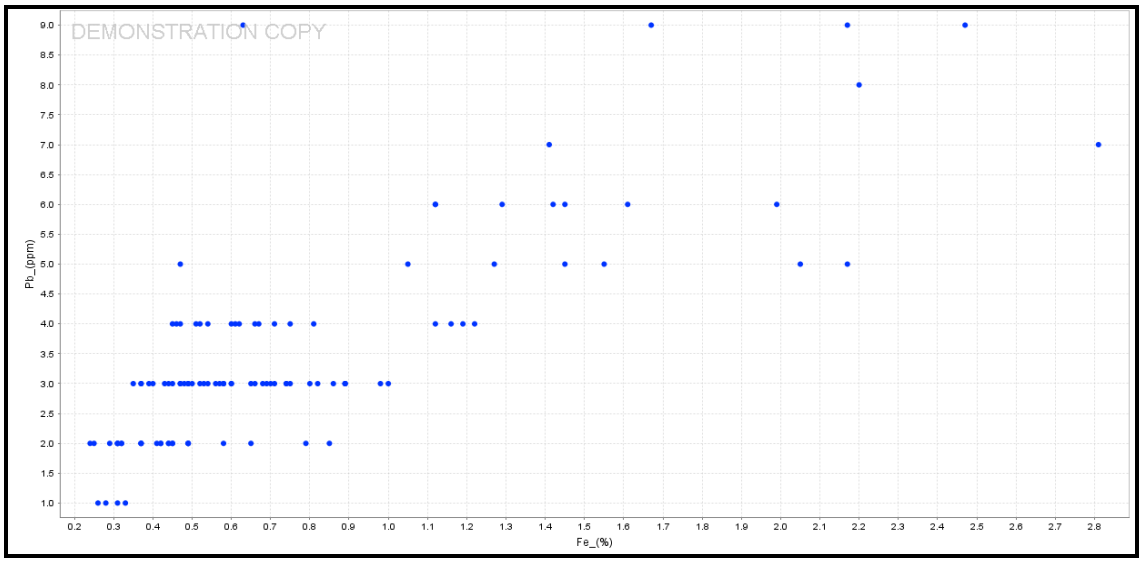

Figure 12

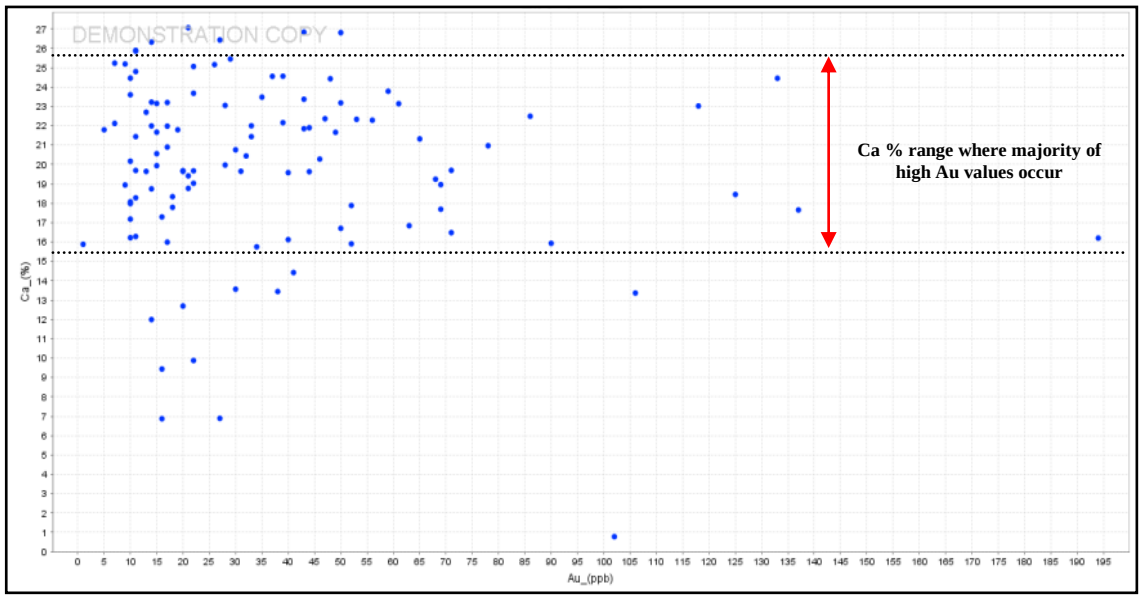

Figure 13

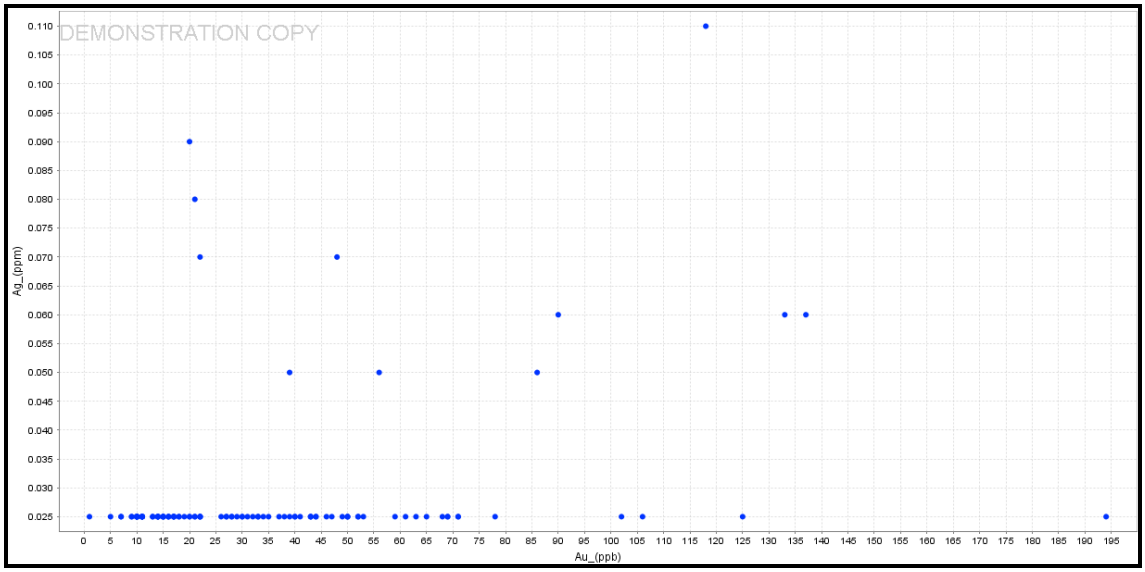

Figure 14.1

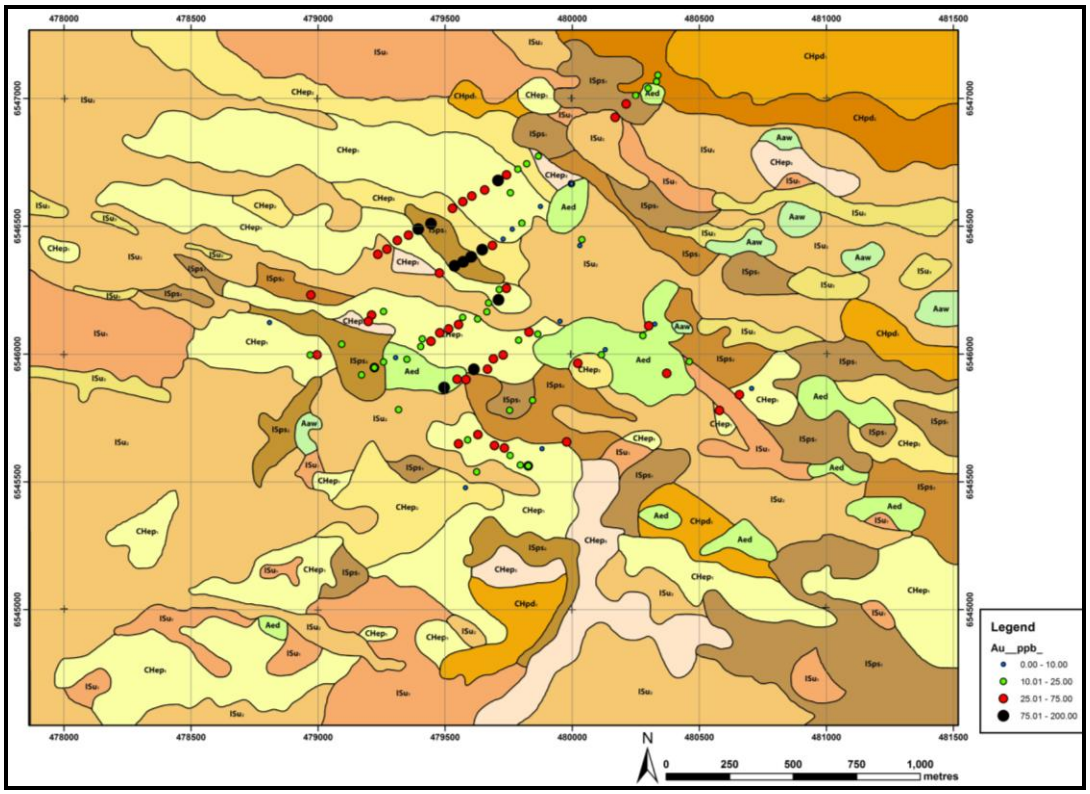

Figure 14.2

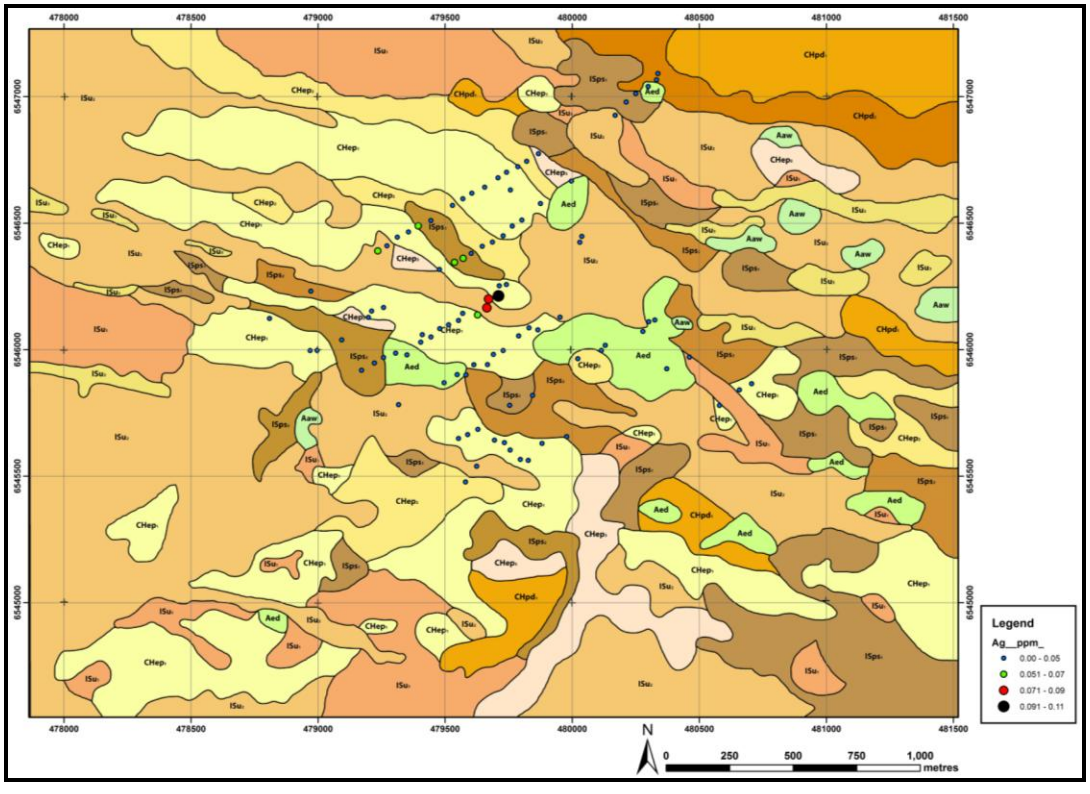

Figure 14.3

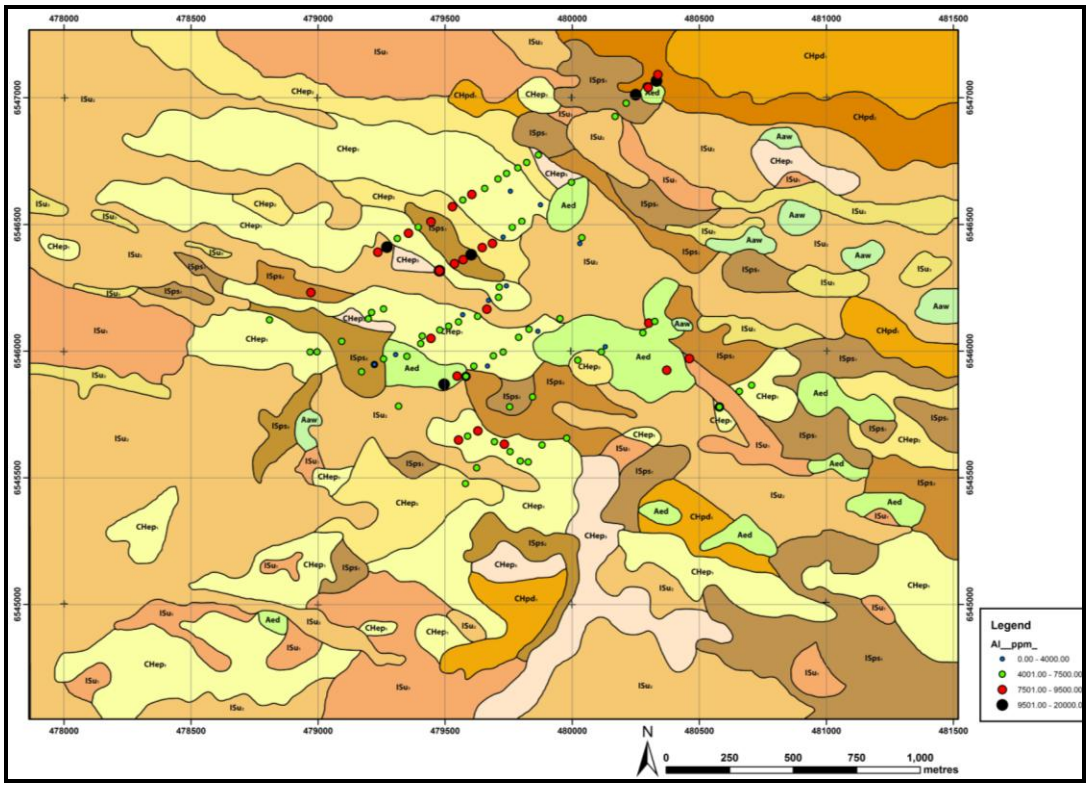

Figure 14.4

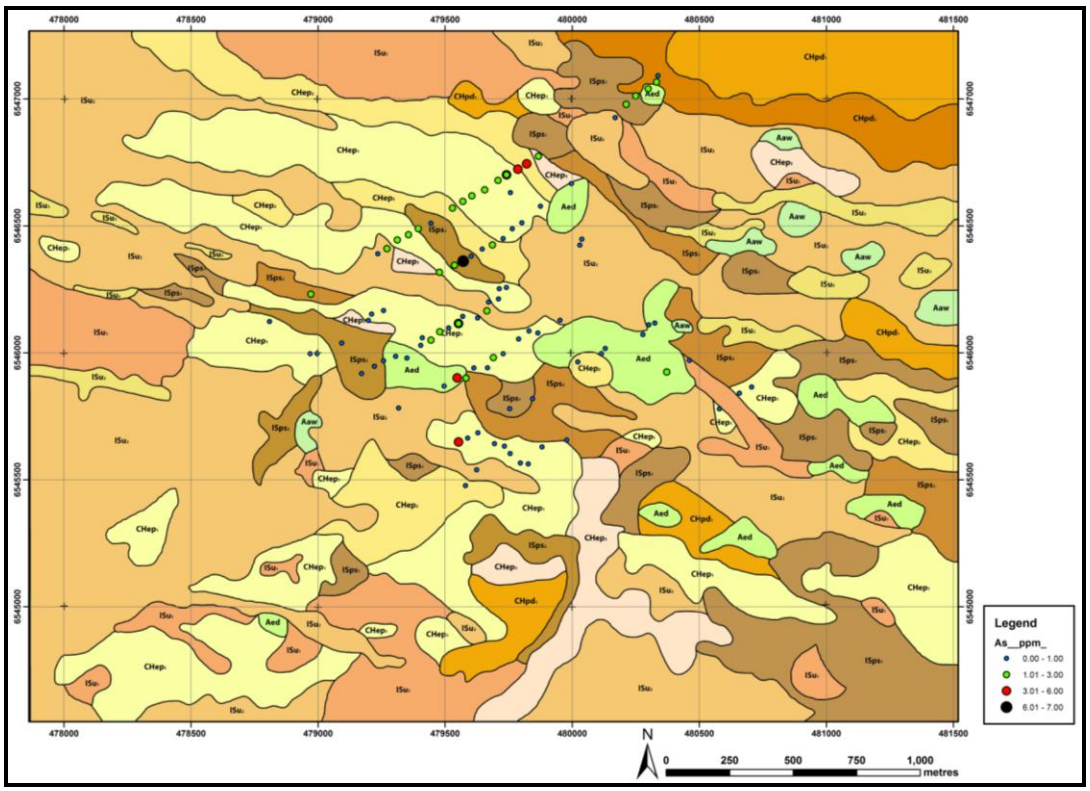

Figure 14.5

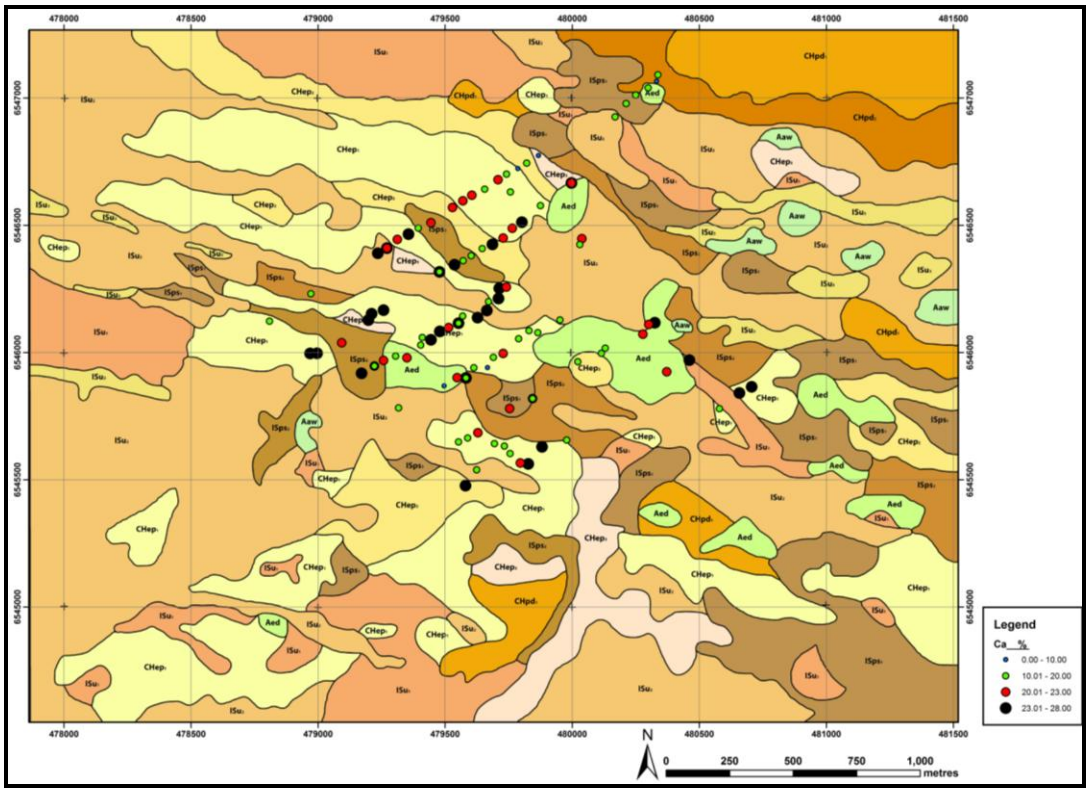

Figure 14.6

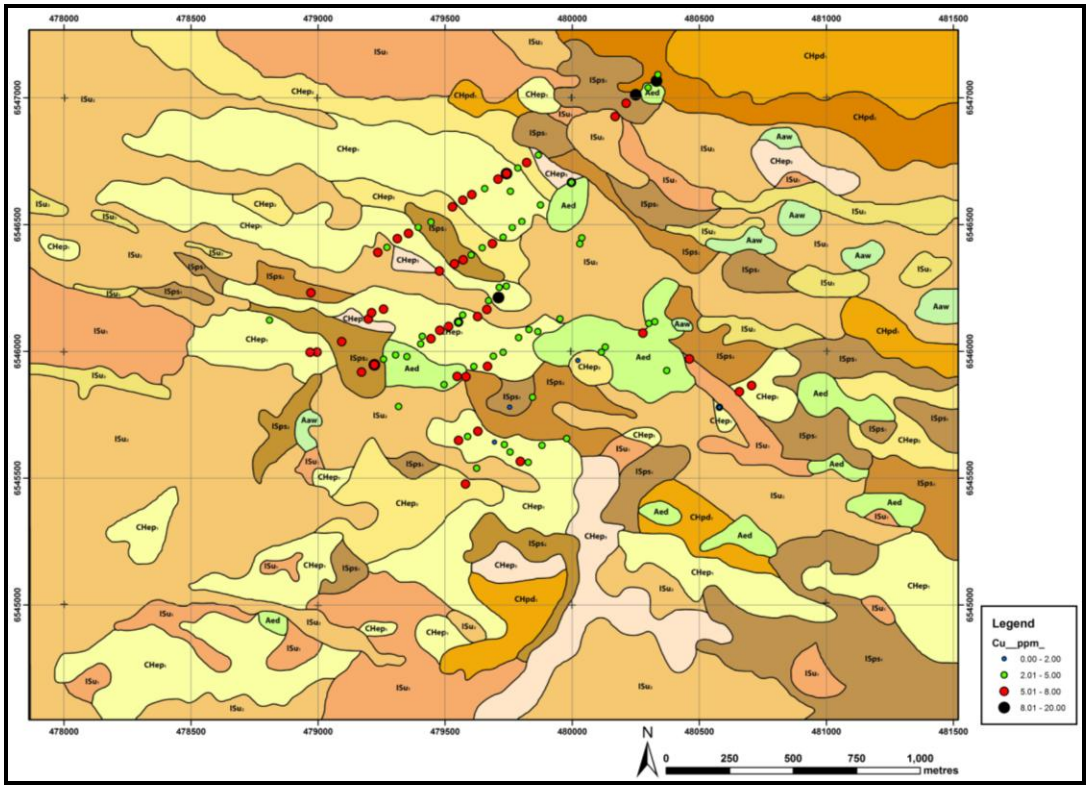

Figure 14.7

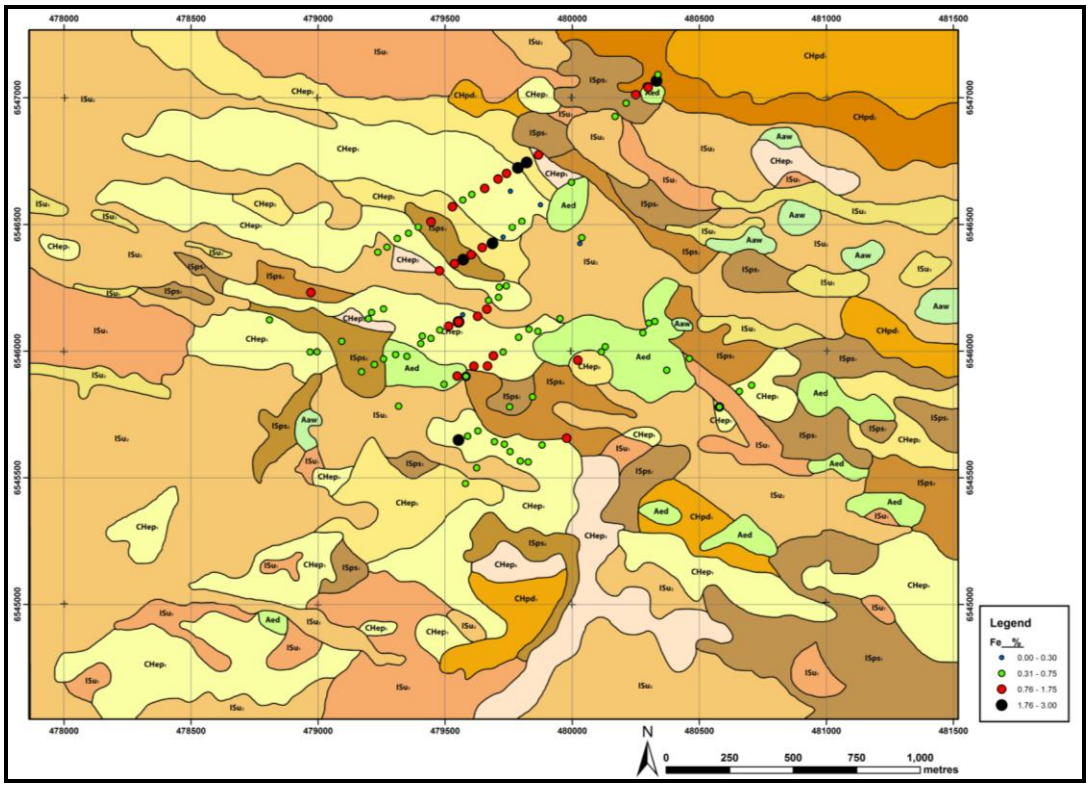

Figure 14.8

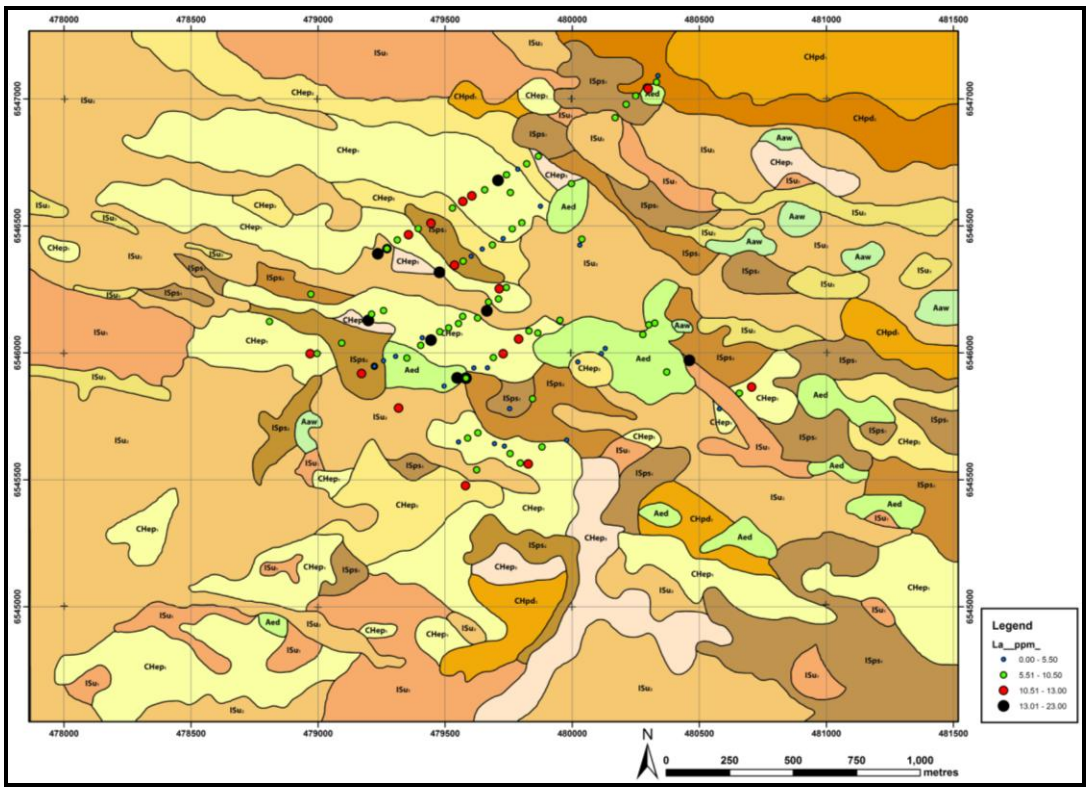

Figure 14.9

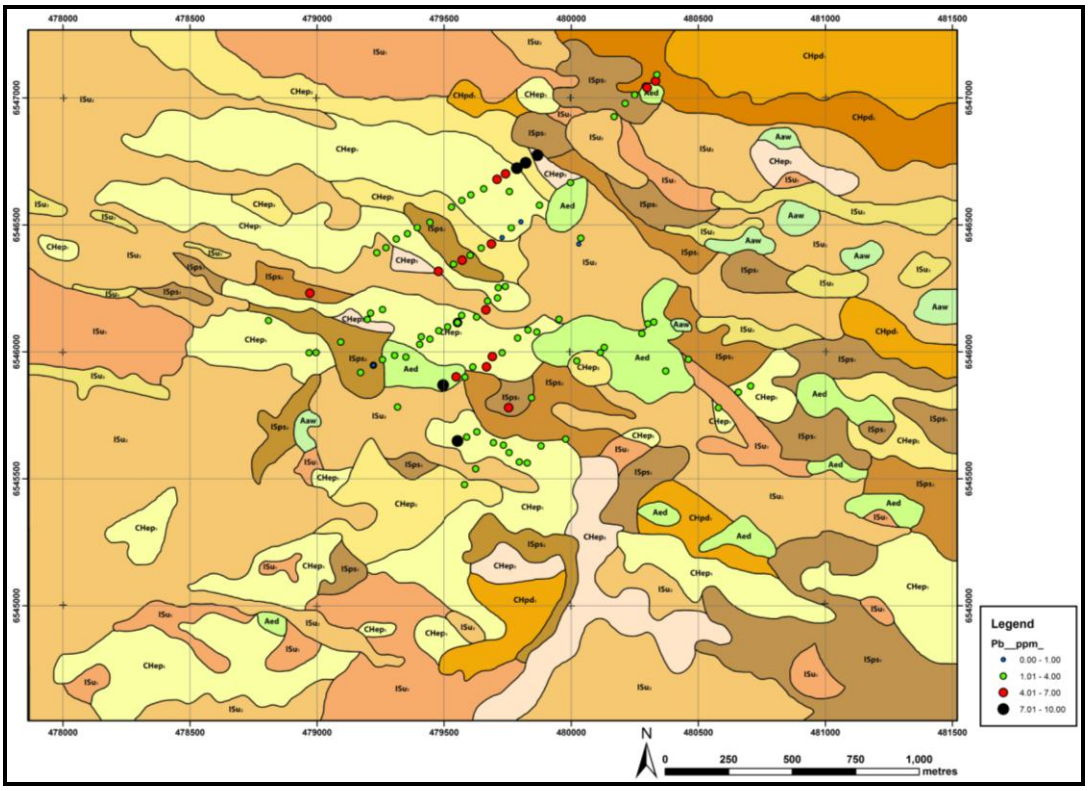

Figure 14.10

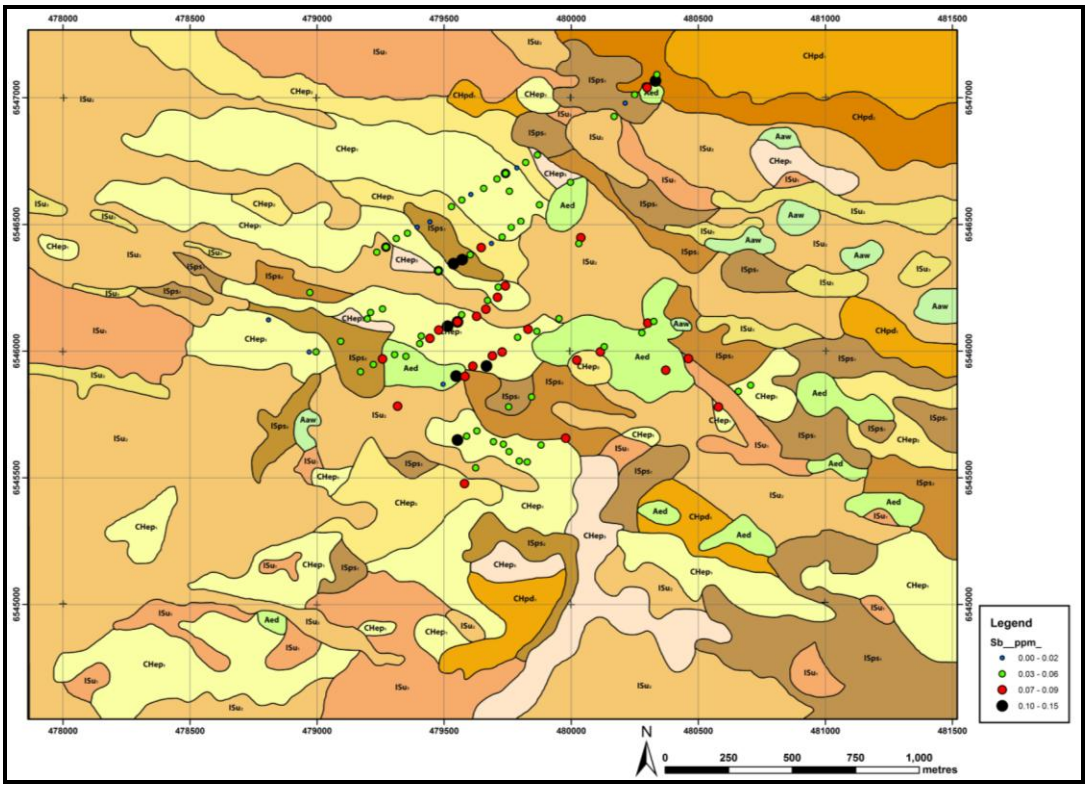

Figure 14.11

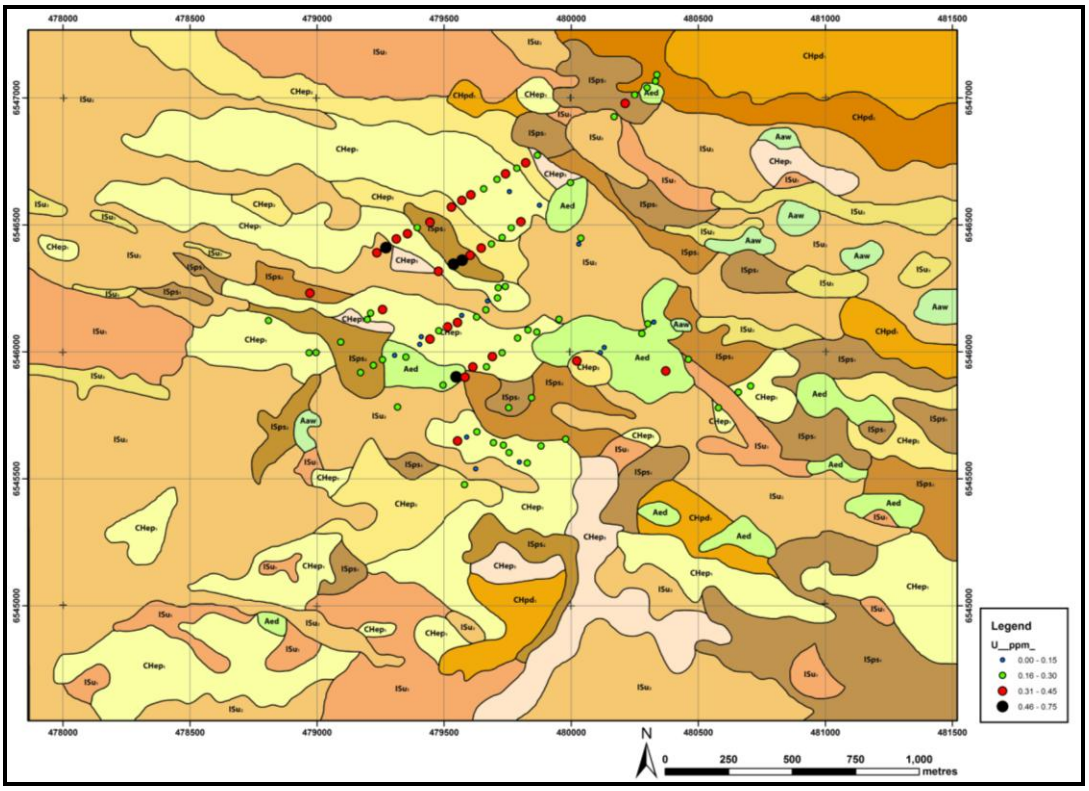

Figure 14.12

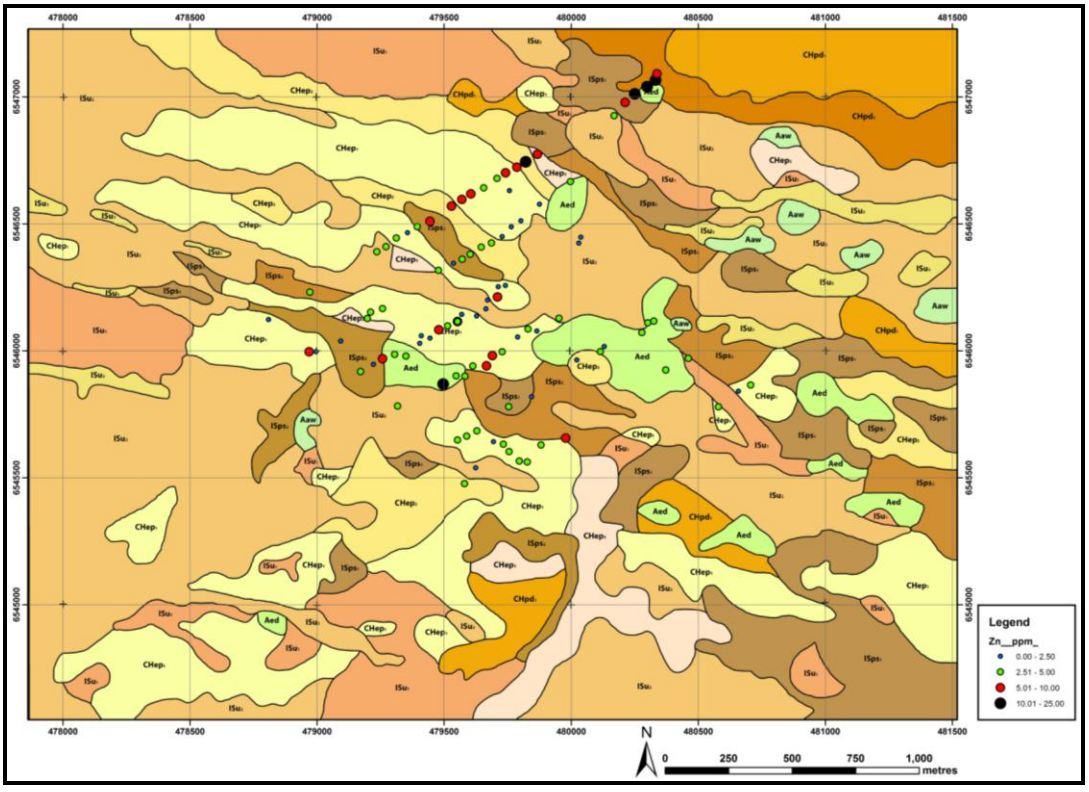

Figure 15

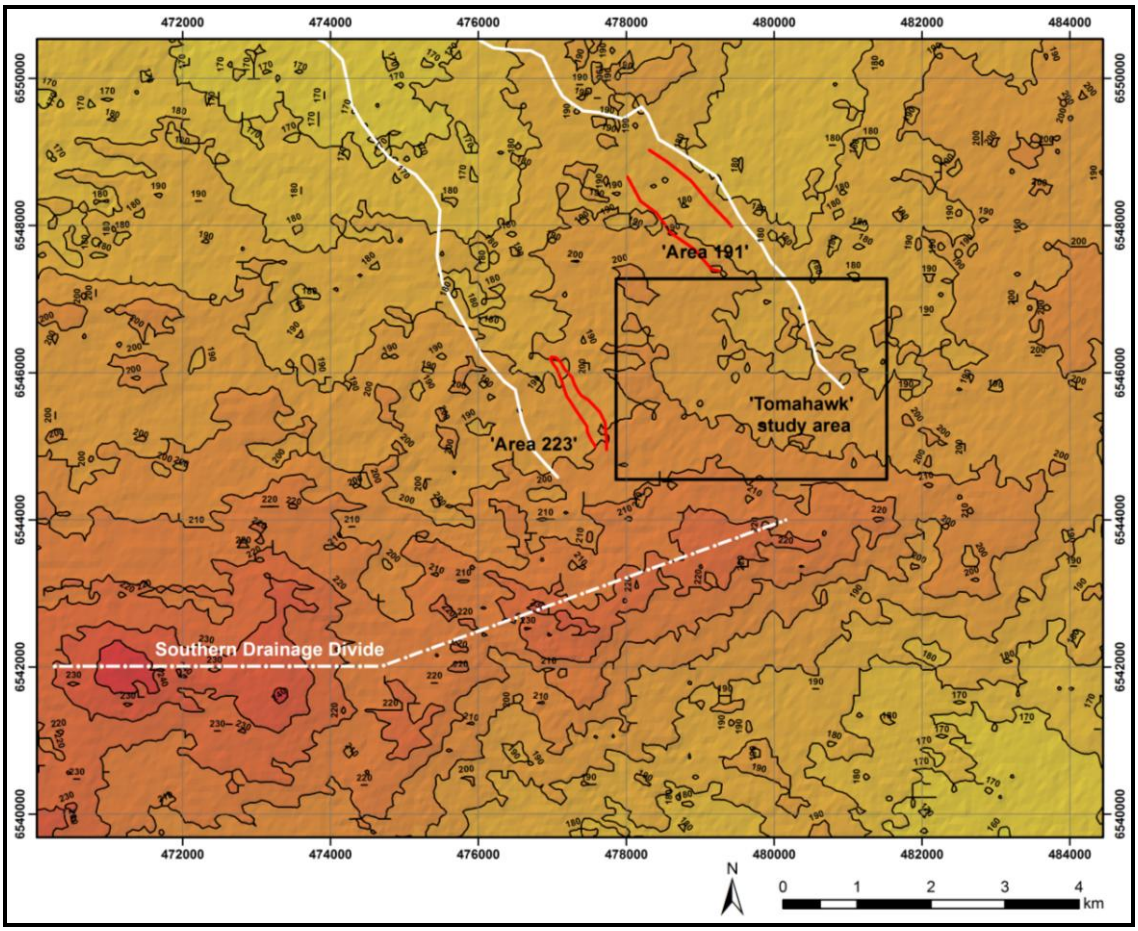
472000
474000
476000
478000
480000
482000
484000
6550000
6548000
6546000
6544000
6542000
6540000
'Area 191'
'Tomahawk'
study area
'Area 223'
Southern Drainage Divide
N
0
1
2
3
4
km

Figure 16

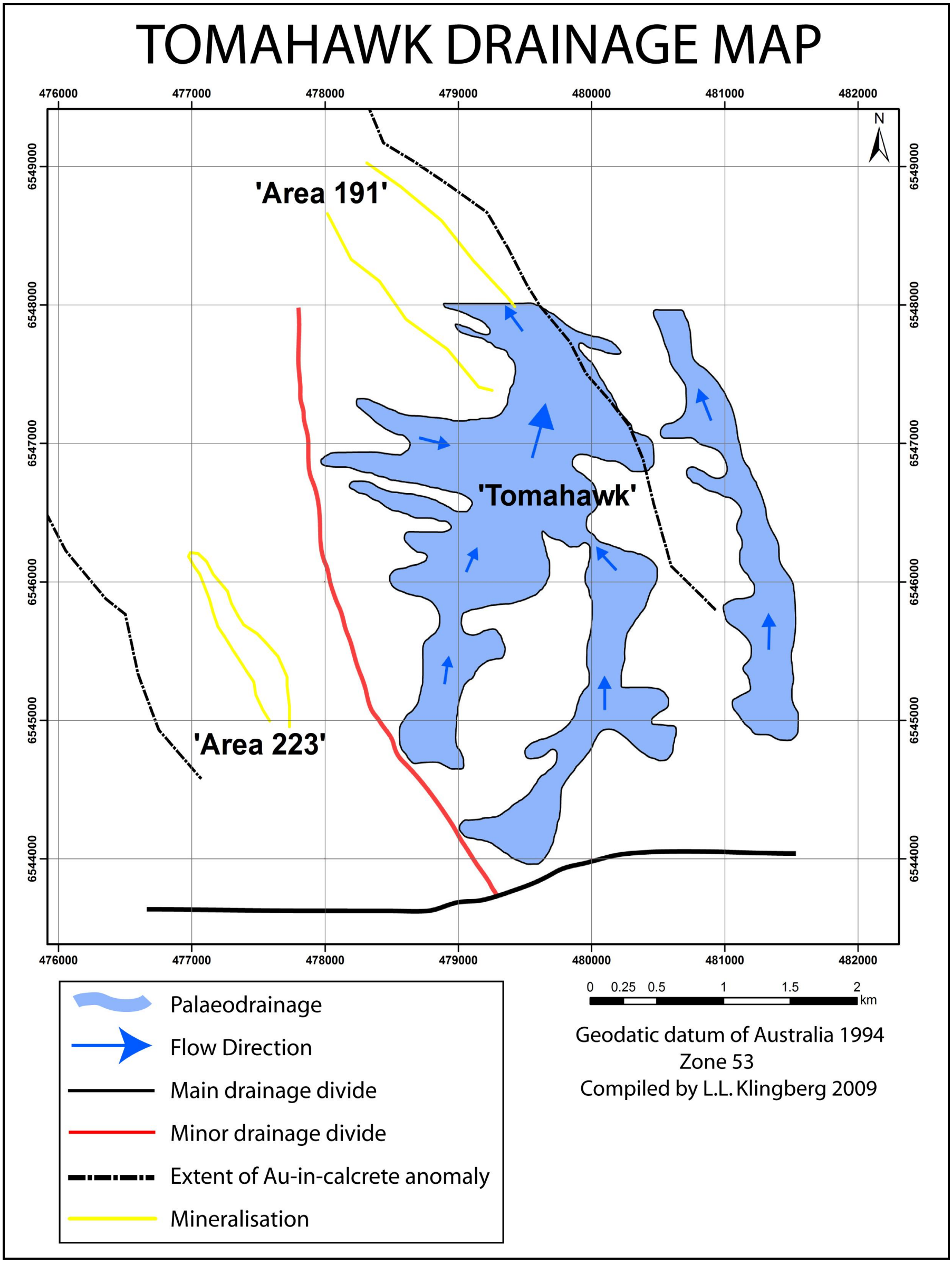
TOMAHAWK DRAINAGE MAP
476000
477000
478000
479000
480000
481000
482000
6549000
6548000
6547000
6546000
6545000
6544000
N
'Area 191'
'Tomahawk'
'Area 223'
Palaeodrainage
Flow Direction
Main drainage divide
Minor drainage divide
Extent of Au-in-calcrete anomaly
Mineralisation
0 0.25 0.5 1 1.5 2
km
Geodatic datum of Australia 1994
Zone 53
Compiled by L.L. Klingberg 2009

Figure 17

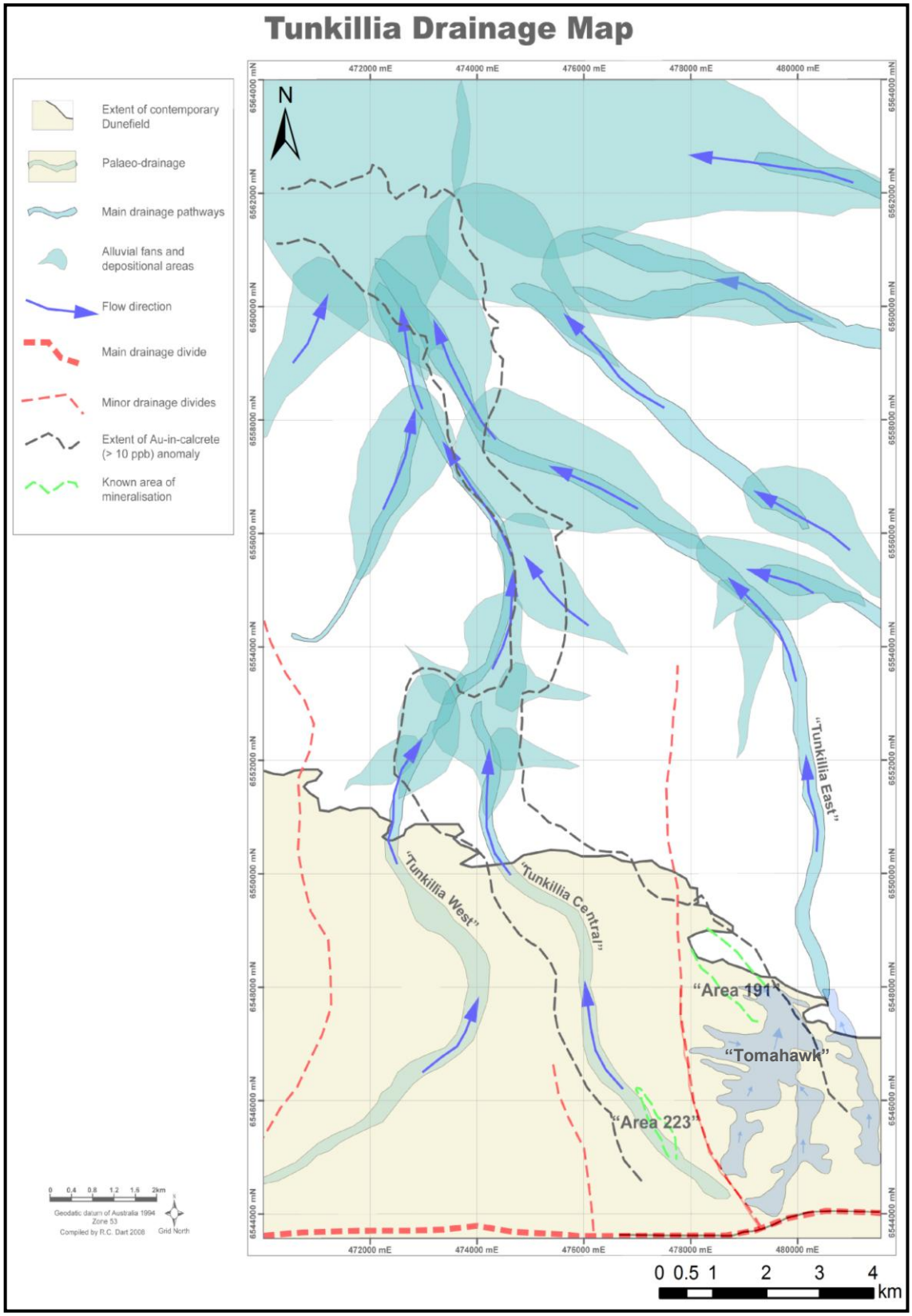
Tunkillia Drainage Map
Extent of contemporary Dunefield
Palaeo-drainage
Main drainage pathways
Alluvial fans and depositional areas
Flow direction
Main drainage divide
Minor drainage divides
Extent of Au-in-calcrete (> 10 ppb) anomaly
Known area of mineralisation
N
472000 mE
474000 mE
476000 mE
478000 mE
480000 mE
6564000 mN
6562000 mN
6560000 mN
6558000 mN
6556000 mN
6554000 mN
6552000 mN
6550000 mN
6548000 mN
6546000 mN
6544000 mN
"Tunkillia East"
"Tunkillia Central"
"Tunkillia West"
"Area 191"
"Tomahawk"
"Area 223"
0 0.4 0.8 1.2 1.6 2km
Geodatic datum of Australia 1994
Zone 53
Compiled by R.C. Dart 2008
Grid North
0 0.5 1 2 3 4
km

Figure 18

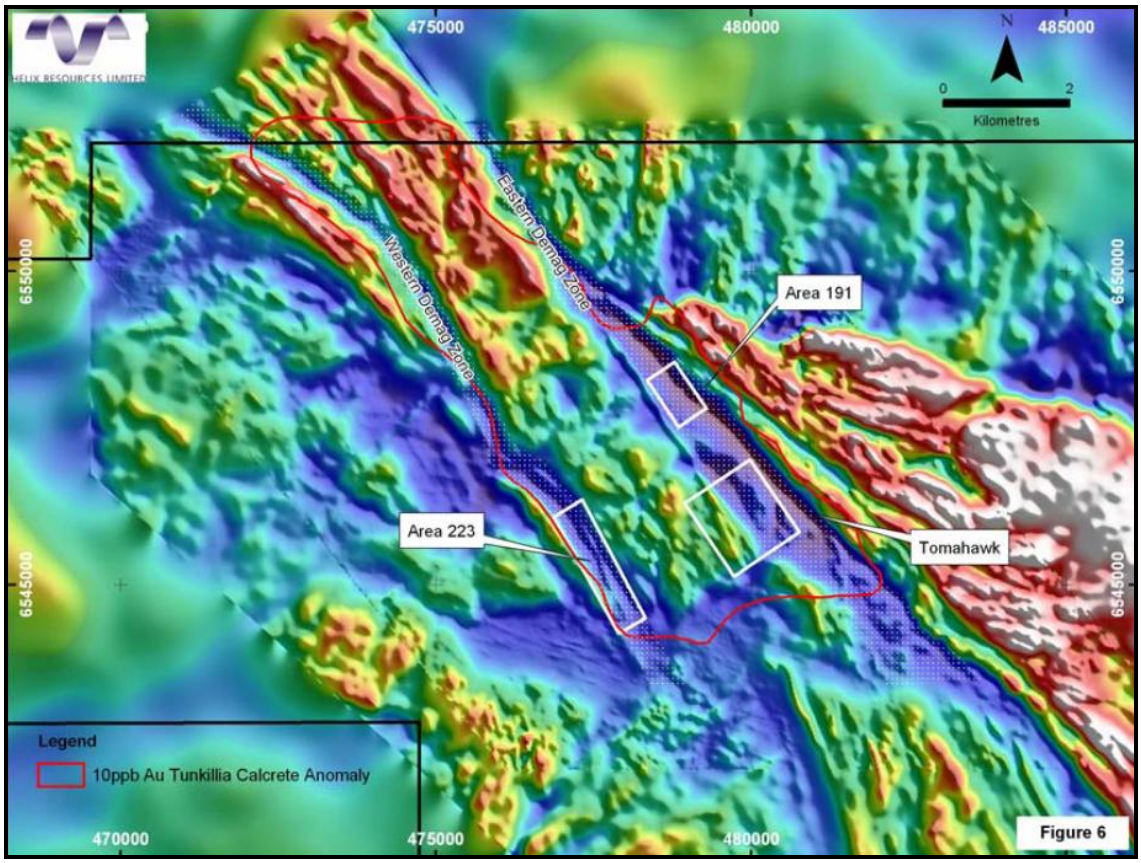
475000
480000
485000
N
0
2
Kilometres
6550000
6545000
Eastern Demag Zone
Western Demag Zone
Area 191
Area 223
Tomahawk
Legend
10ppb Au Tunkillia Calcrete Anomaly
470000
475000
480000
Figure 6

Figure 19

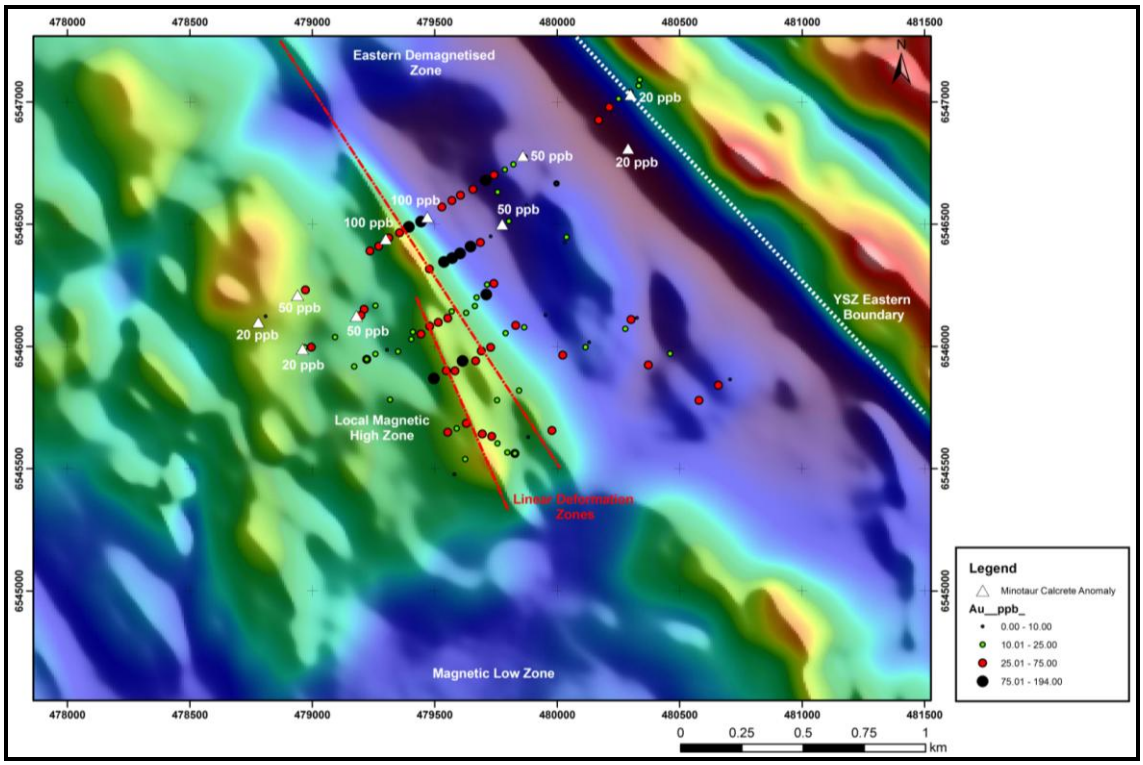
Eastern Demagnetised Zone
YSZ Eastern Boundary
Local Magnetic High Zone
Linear Deformation Zones
Magnetic Low Zone
20 ppb
50 ppb
100 ppb
Legend
Minotaur Calcrete Anomaly
Au__ppb_
0.00 - 10.00
10.01 - 25.00
25.01 - 75.00
75.01 - 194.00
0 0.25 0.5 0.75 1
km

Figure 20

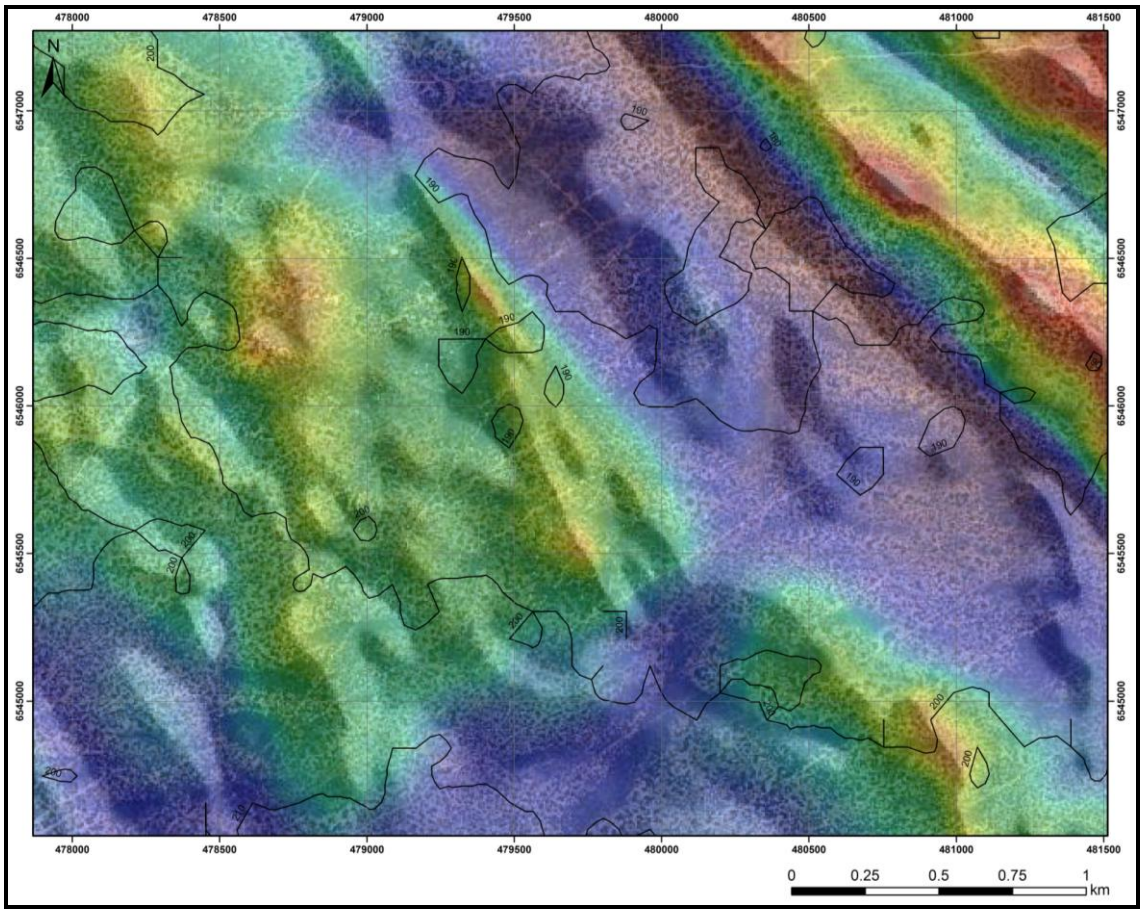
N
478000
478500
479000
479500
480000
480500
481000
481500
6547000
6546500
6546000
6545500
6545000
0
0.25
0.5
0.75
1
km